Intelligent Train Operation with On-Board Energy Storage Device: An Energy-Saving Perspective

Thesis submitted in accordance with the requirements of
the University of Liverpool for the degree of Doctor in Philosophy by

Chaoxian Wu

Department of Electrical Engineering & Electronics
School of Electrical Engineering, Electronics and Computer Science

August 2021

“科学是人类的荣光与庇护”

“*Scientia homines decus et tutamen*”

“*Scientific knowledge, the crowning glory and the safeguard of the humanity*”

Abstract

Railway transportation is applied extensively in urban transportation to satisfy the increasing travel demand as well as reduce CO_2 emission from the road transportation. However, energy consumption of the railway transportation is observed to increase due to its boosting construction and usage. In this case, energy efficiency of the railway transportation has become a popular research topic in the past few decades. At the same time, as an emerging technology, the on-board energy storage device (OESD) is utilised in many modern railway systems to help improve the energy efficiency. This thesis focuses on the investigation of the intelligent train operation with OESD, in which the optimal train operation strategy, OESD discharging/charging strategy, mutual influence between the train operation strategy and OESD, and study on different types of energy storage as OESD in train operation are given.

First, the intelligent train operation with OESD in single inter-station section is discussed. An integrated mathematical model to optimise the train speed trajectory with OESD to minimise the net energy consumption of the system for a single inter-station section is established. The influence of the OESD capacity, energy status of OESD and OESD degradation on optimal train operation solution is revealed based on the proposed model. The results show that with a general railway case, the net energy consumption can be significantly reduced by the intelligent management of both the train operation mode and OESD discharging/charging process.

Second, the intelligent train operation with OESD in a service cycle is discussed. The OESD is allowed to discharge/be charged when the train dwells at each station. A two-step method, which overcomes the drawbacks of the originally proposed mathematical programming model, is proposed to locate the optimal train speed trajectory, timetable and OESD discharging/charging strategy for both inter-station running and dwelling at stations with high computation efficiency. Beijing Yizhuang line as numerical experiment is given in this thesis, where the reduced energy consumption is observed when compared to other scenarios by using the optimised solution, showing the effectiveness of the

proposed method.

Third, the intelligent train operation with OESD in a network is investigated. By considering the train network and power network as the environment information, an agent-environment model for the train with OESD is proposed. In the model, the available regenerative braking energy from other trains in the railway power network is formulated into the time-variant expectation based on the stochastic running time distribution of the train network, which can be used by train and OESD during the running. This further utilises the OESD to receive as much as the regenerative braking energy in the environment to reduce the energy waste. The results shows that the proposed method is able to improve the utilisation of the regenerative braking energy in the power network, and also lead to the significantly reduced energy consumption.

Fourth, impact of the different types of energy storage as OESD on the optimal train operation strategy is studied. The dynamic discharging/charging power limits with respect to the energy status of each type of OESD, supercapacitors, flywheels and Li-ion batteries, are taken into account. In addition, the optimal sizing problems of the above three types of OESD are also investigated. The results show that the introduction of different type of OESD will lead to the change of the optimal train operation strategy and the resulted energy-saving performance. Using Beijing Changping line as numerical experiment, it is found that choosing the right type and right sized OESD are important due to the significantly different engineering characteristics, energy cost and monetary cost brought to the system when introducing different OESD.

In summary, this thesis gives a systematic discussion and exploration on the intelligent train operation with OESD in a perspective of energy saving from small operation scale to large operation scale, and the OESD is also studied as general/no specific type to multiple/specific type to ensure both of the academic and industrial value of the thesis.

Acknowledgements

I would like to extend my deepest gratitude for the effort made by my advisers, Dr. Shaofeng Lu from South China University of Technology, Dr. Fei Xue from Xi'an Jiaotong-Liverpool University, and Dr. Lin Jiang from the University of Liverpool, from my supervisory team.

I am extremely fortunate to be supervised by Dr. Shaofeng Lu during my PhD journey. Four years ago, he gave me the opportunity to pursue this PhD degree related to railway transportation research which I was eager to achieve. Without his constant support, encouragement, and patience during this journey, this thesis and the outcomes of these years would not have been possible. In addition, I also want to thank Dr. Fei Xue, for his constructive advice and continuous help in dealing with general affairs required by the university, and Dr. Lin Jiang, for his kind support on my research visit issue for offering me the strong academic justification.

I am grateful to the seniors in the research group, Dr. Bing Han and Dr. Xiaotong Xu, who shared their abundant research experiences and ideas during my PhD journey. Additionally, I would like to thank the juniors of the research group, Mr. Wenrui Zhang, Mr. Zhaoxiang Tan, Mr. Kai Bao, Ms. Rui Miao, Mr. Bin Xu, Mr. Kuan Zhu, Mr. Zheng Huang, Ms. Minling Feng, and Mr. Guangzhao Meng. Their hard work, motivations, and passion for research also deeply motivated me, driving me to explore more interesting problems in the field of study.

I would also like to thank my colleagues and friends, Mr. Xiaoyang Chen, Ms. Zhenzhen Jiang, Mr. Shufei Zhang, Mr. Chenru Jiang, Dr. Haochuan Jiang, Dr. Yujie Liu, and Mr. Yida Guo. It is they who make my whole PhD journey more colourful and happier by sharing the funny stuff in daily life and encouraging each other during work.

I would like to express my gratitude to Prof. Jeremy Smith and Dr. Cheng Zhang from my independent progress assessment panel for their constructive comments and evaluation of my work in each year's annual progress interview, which guaranteed the quality of my research as well as ensured that my research direction was on the right

track according to the requirements of the university.

Finally, I would like to express my sincere gratitude and dedicate this thesis to my parents, Mr. Guohui Wu and Mrs. Yuanzhen Chen, and my whole family, for their unconditional love and support throughout my life, not just during my PhD. In particular, I am deeply grateful to my dear wife, Mrs. Dong Liang, who has always supported and encouraged me in both life and work over the past four years, although she is already extremely busy with her own job.

The sea of stars, destination of my journey, and your love gives me the strength to hit the road. THANK ALL OF YOU.

Contents

List of Figures

List of Tables

List of Acronyms

AC	Alternating Current
ACO	Ant Colony Optimisation
ATO	Automatic Train Operation
DAS	Driver Advisory System
DC	Direct Current
DP	Dynamic Programming
EV	Electric Vehicle
GA	Genetic Algorithm
GHG	Greenhouse Gases
HVAC	Heating, Ventilation, and Air Conditioning
IABC	Improved Artificial Bee Colony
IGBT	Insulated Gate Bipolar Transistor
ILP	Integer Linear Programming
ISOE	Initial State Of Energy
LP	Linear Programming
LR	Lagrangian Relaxation
MG	Micro Grid

MILP	Mixed Integer Linear Programming
MRT	Mass Rapid Transit
NSGA	Non-dominated Sorting Genetic Algorithm
OECD	Organisation for Economic Co-operation and Development
OESD	On-Board Energy Storage Device
PMP	Pontryagin's Maximum Principle
SESD	Stationary Energy Storage Device
SOC	State Of Charge
SOE	State Of Energy
SOS2	Special Ordered Sets 2
SQP	Sequential Quadratic Programming
WESD	Wayside Energy Storage Device

Chapter 1

Introduction

This chapter provides an overview of the thesis. The background information of the research conducted in this thesis is provided at first. The rapid development of railway transportation around the world, energy consumption issues related to railway transportation and approaches already applied to reduce energy consumption resulting from the railway transportation are discussed. Then, the motivation for conducting this study is given, highlighting the research gaps and unsolved problems in the field of study as well as the meaning of the proposed research, followed by the objectives to be achieved in the research conducted in this thesis. The charpter also presents the thesis outline for a quick review of the entire thesis, in which the main contents and main outcomes of each chapter are briefly detailed.

1.1 Background

In modern society, railway transportation, especially the electrified railway system, has become an important transportation mode around the world to mitigate the traffic congestion in road transportation in mega or big cities, and satisfy the increasing travel demand in cities. Nearly all countries have seen growth in railway passenger movements in recent years. China and India each individually generated the most railway passenger movements in 2017 compared to all OECD countries (Organisation for Economic Co-operation and Development: 33 countries). China has experienced consistently strong growth in railway passenger traffic, with over 1.3 trillion passenger-kilometres travelled in 2017, which is 7% higher than that in 2016. Japan saw a 1.3% growth and European Union railway passenger-kilometres continued to grow at a modest pace between 2016 and 2017 with growth rate being 3.2% [1].

On the other hand, railway transportation is welcomed because it is regarded as "green transportation" for its relatively low energy and emission intensity. Energy demand from the transportation sector has risen significantly in the past decade, driven mostly by growth in Asia and by demand in road transport. Nevertheless, when expressed as final energy use per passenger-kilometre, the energy intensity of railway transportation generally significantly outperforms other transportation modes [2], as shown in Figure 1.1. In addition, as railway transportation is the only mode of transportation that is widely electrified today, for example, metro systems, high-speed rail, tram or maglev, it has the advantage of less consumption of the fossil fuels, because of which it has the lowest emission intensity among all transportation modes [3].

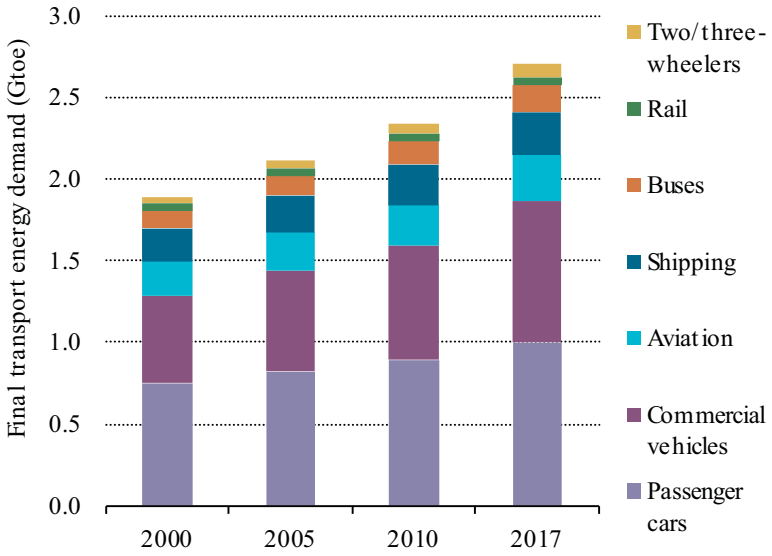

Figure 1.1: Final energy use in transportation by mode, 2000-2017 [2]

Both these characteristics make railway transportation the most promising and sustainable way to transport people and goods to cope with the energy exhaustion and global warming issues.

1.1.1 Fast Development of Railway Transportation

Railway transportation around the world is rapidly developing nowadays in multiple forms. According to the different usage types and rolling stocks, railway transportation can be grouped into numerous specific types:

- **Regional trains**, also known as local trains and stopping trains, are the passenger railway services that operate between towns and cities. Regional train services

operate beyond the limits of urban areas, and either connect smaller cities and towns, or cities and surrounding towns, outside or at the outer rim of a suburban belt.

- **Metro**, also known as rapid transit, mass rapid transit (MRT), heavy rail, subway, tube, or underground, is a type of high-capacity public transport generally found in urban areas.

- **High-speed rail** is a type of railway system that runs significantly faster than traditional railway traffic, using an integrated system of specialised rolling stock and dedicated tracks. No single standard for high-speed rails can be applied worldwide, and new lines in excess of 250 km/h and existing lines in excess of 200 km/h are widely considered to be high-speed rail.

- **Tram** is a railway vehicle that runs on a tramway track on public urban streets. It is usually lighter and shorter than the main line and rapid transit train. Today, most trams use electrical power, which is usually fed by a pantograph sliding on an overhead line (catenary).

- **Maglev** (derived from magnetic levitation) is a system of railway transportation that uses two sets of magnets: one set to repel and push the train up off the track, and another set to move the elevated train ahead, taking advantage of the lack of friction. Along certain "medium-range" routes (usually 320 to 640 km), maglev can compete favourably with high-speed rail and air planes.

- **Freight trains**, also known as cargo trains, or goods trains, are a group of freight cars (US) or goods wagons hauled by one or more locomotives on a railway, transporting cargo all or some of the way between the shipper and the intended destination as part of the logistics chain.

Among the different forms of railway transportation, the railway passenger transport activity significantly increased in the period from 1975 to 2015, soaring from the 1.8 trillion passenger-kilometres to more than 3 trillion passenger-kilometres around the world [4]. Moreover, all types of railway transportation activities have nearly maintained their pace with the global increase in demand for mobility, see Figure 1.2. In particular, the global high-speed rail is expected to expand to more than 80,000 km from 2020 [4], making it the fastest developing railway transportation mode.

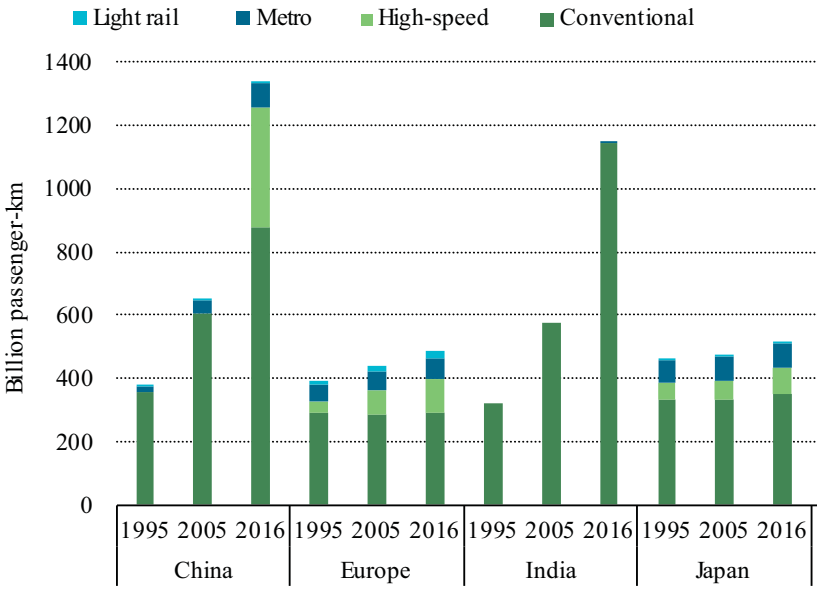

Figure 1.2: Passenger activity by railway transportation type [2]

1.1.2 Increasing Energy Consumption of Railway Transportation

Electricity and diesel are the two main energy sources for railway transportation. Electric power constitutes 47% of railway energy use, amounting to 290 TWh (or 25 million tonnes of oil equivalent [Mtoe]) today, whereas diesel accounts for 53%, roughly equivalent to 29 Mtoe. Approximately 55% of electricity use in railway transportation is for passenger services, and most of the diesel (85%) is for freight services [2].

Although the energy and carbon intensity of railway transportation outperform other transportation modes, its energy consumption has increased in Russia, China and India since 2000 with the extension of the railway systems and their extensive use. For instance, data from the Beijing subway show that the whole electricity consumption of all lines added to 1.71 billion kWh in 2016, nearly three times the amount in 2010 [5], which has given a serious cause for concern that the overall level of electricity consumption of the metro system will continue to increase as its network continues to expand. On the other hand, the wider electrification makes railway transportation the most green transportation mode, whereas more than 80% of the electricity consumption of it comes from fossil fuels, and less than 20% is from renewable, nuclear, and biofuel resources [2]. This indicates that with the increasing use of electricity, railway transportation will lead to more greenhouse gas (GHG) emissions and resource consumption, which in turns, will undermine its sustainability.

Figure 1.3 shows that the energy consumption of the global railway transportation for passenger service continuously dropped from 2000 to 2013 owing to the large scale of electrification to replace the diesel-driven mode, while it began to increase from 2013 due to the expansion of the worldwide railway networks. Accompanied by this, the CO_2 emissions of passenger service decreased from 2000 to 2013 as well, however, a significant increase also occurred since 2013.

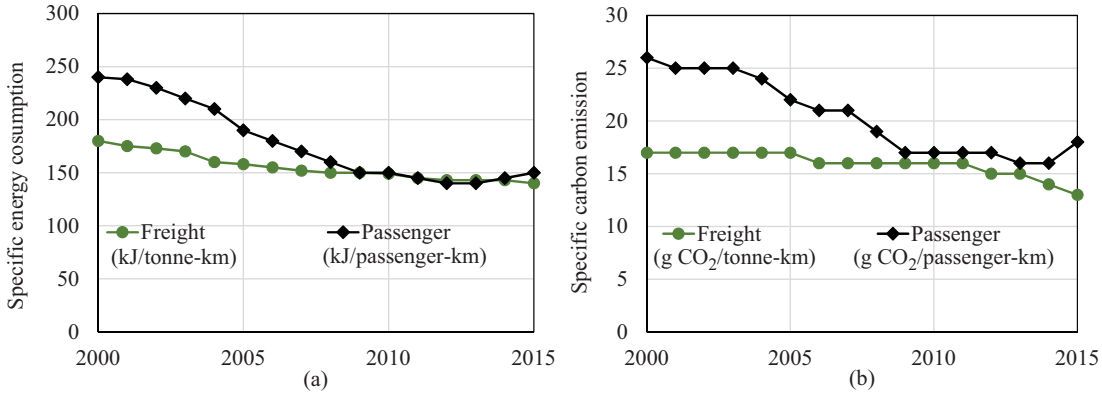

Figure 1.3: Railway transportation specific energy consumption (a) and CO_2 emission (b) from 2000 to 2015 [4]

1.1.3 Measures to Reduce Railway Energy Consumption

An Overview

To deal with the increasing energy consumption of railway transportation, several measures have been undertaken and both the industry and academia have provided advice to improve the energy efficiency of railway transportation. The commonly applied measures can be divided into four classes [6], with corresponding current applications detailed as follows:

- Measures related to the design of the infrastructure, installations, and rolling stock:
  - The design of an efficient infrastructure may reduce the use of the brake, which may lead to a reduction in losses.
  - The design of trains considering new train architectures that allow reducing drag resistance.
  - The introduction of new materials that allow decreasing, for example, the total weight of the rolling stock, which will help reduce energy consumption.

  - The use of renewable sources in non-traction loads, as workshops and stations, may have a significant impact on CO_2 emissions.

- Measures related to power traction:
  - Electrification of the railway lines that are not electrified can result in electric traction gross tons that currently are transported by diesel traction.
  - The use of more advanced technologies (such as AC asynchronous traction motors with IGBT inverters).
  - The inclusion of reversible substations in the power supply system, mainly in DC electrification lines, contributing to a higher use of the regenerative braking energy returned to the grid by trains.
  - Utilisation of alternative fuels (as liquid gas or hydrogen fuel cells)

- Measures related to ancillary systems:
  - Incorporation of new technologies that allow decreasing the energy consumption in both the ancillary systems on-board (as HVAC technologies or new lighting systems) and the ancillary system of the infrastructure.

- Measures related to intelligent energy management:
  - Measures related to operational procedures, such as load factors. Increasing the load factor may entail a significant reduction in energy consumption.
  - Measures related to the operation of trains (timetables, stops, traffic control, driving techniques, etc.)., by either the introduction of eco-driving Systems or drivers' knowledge of the existing differences of the driving techniques, or by using optimised timetable and train dispatch plans.
  - Introducing energy storage systems in the power network, and provide them with "intelligence" in order to manage the use of the energy.
  - Introducing smart grid technologies that allow greater controllability of electric loads (trains, auxiliaries, etc.).

The average ratio of the investment increment and energy efficiency enhancement of each type of measure is shown in Figure 1.4. The measures related to ancillary systems and intelligent energy management are with the highest cost efficiency because they both lead to the largest energy efficiency improvement with the lowest investment increase, due to which they are welcomed by operators and are more practical and realistic in real applications.

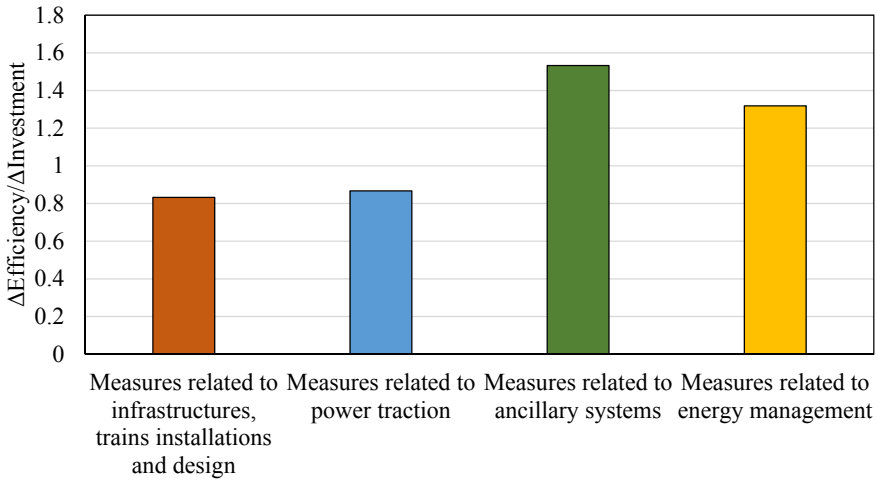

Figure 1.4: Comparison between the different technologies according to their relationship with the efficiency and increase in investment [6]

Energy-Efficient Train Operation and Energy Storage Applications

Energy management of the railway system can significantly reduce the energy use, and proper train operations and introduction of energy storage devices lead to the greatest contribution in reducing energy cost among the other energy management strategies [6].

- **Energy-Efficient Train Operations** aim to find the train speed trajectory to be traced by the driver or Automatic Train Operation (ATO) system or the timetable plan to be followed by the operator to achieve a more energy-saving system operation. It is known that 80% of the energy use of the train operation is consumed by the traction and more than 60% of the regenerative braking energy is wasted due to the improper driving strategy and the timetable which fails to properly allocate the running time, dwell time, or headway and coordinate the trains in the network [7]. By managing the train operation with an optimised driving strategy (Figure 1.5-(a)) or scheduling (Figure 1.5-(b)), significant energy reduction can be achieved without changing any infrastructure.

- **Application of Energy Storage Devices** aims to recover the regenerative braking energy in the network to reduce energy waste. There are mainly two forms of utilisation of energy storage devices: wayside/stationary energy storage devices (WESD/SESD), see Figure 1.6-(a), and on-board energy storage devices (OESDs), see Figure 1.6-(b). From the existing literature and industry reports, it can be concluded that energy savings between 15% and 30% can be achieved

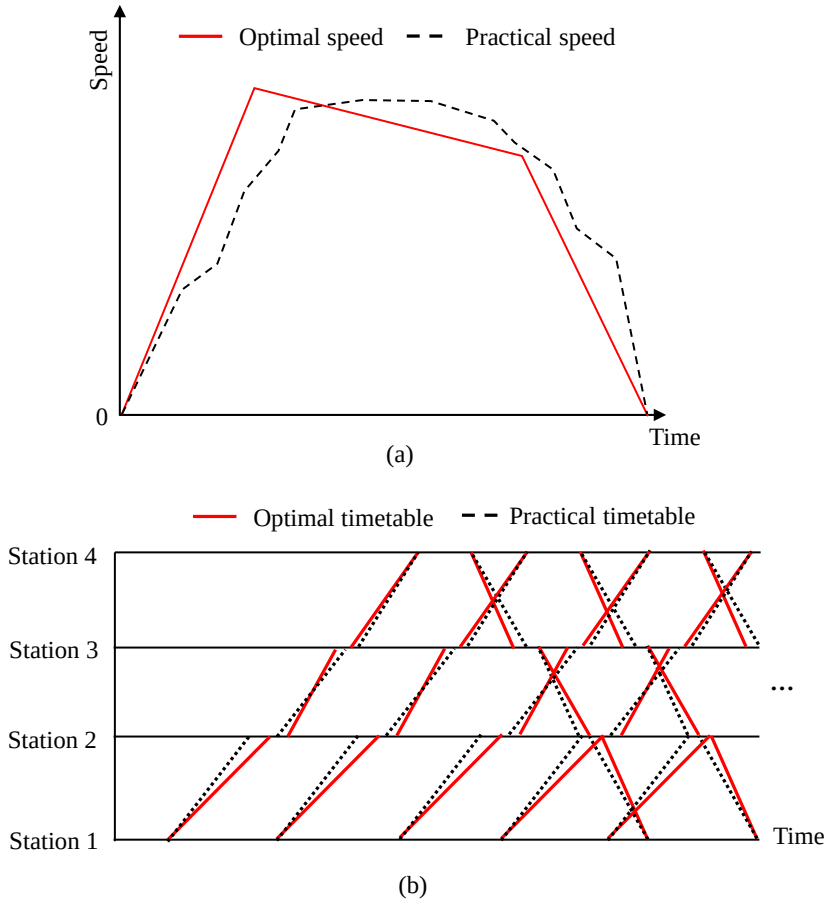

Figure 1.5: Difference between the (a) optimal speed trajectory and non-optimal speed trajectory and (b) optimal timetable and non-optimal timetable

by utilising energy storage devices [8]. Different from the wayside energy storage devices installed in substations or near stations that focus more on the energy recovery of all the trains in the same power supply sections, OESDs have the following advantages:

- Lower investment cost of the installation of the OESD than wayside solutions is observed due to its smaller size and volume, which requires no complicated reconfiguration of the electrical devices onsite in substations or stations.
- Shaving of power peaks demanded in the supply line during acceleration of the train, which leads to reduced energy costs and minimum resistive losses.
- Operating with higher efficiency due to the absence of line losses.
- The energy recovered and stored during the braking process can be used

directly to power the train itself during the next acceleration.

– Operating for certain power autonomy, for instance in emergency situations, in depot operations or in catenary-free applications such as lines going through historical city centres with visual impact restrictions.

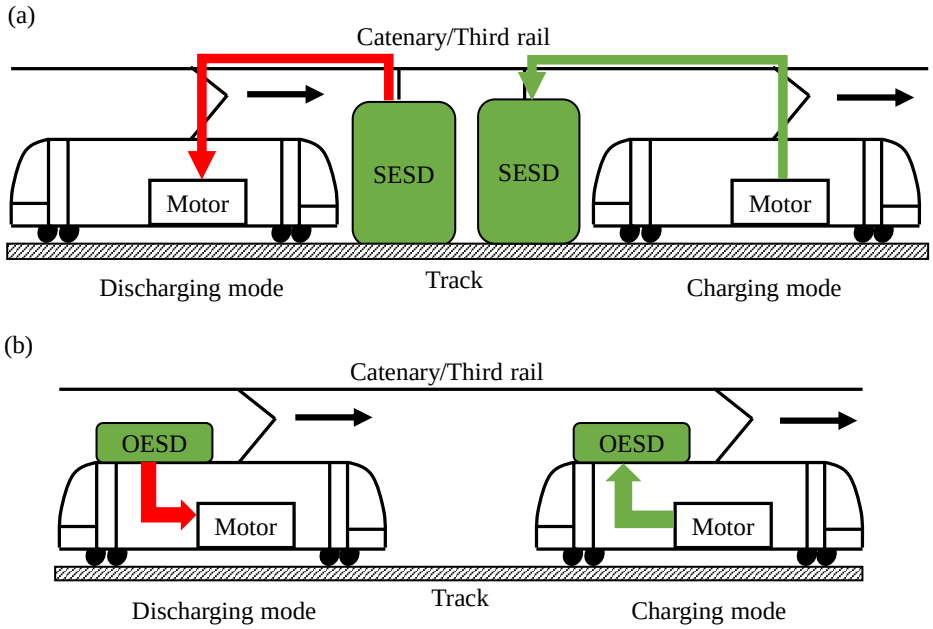

Figure 1.6: Schematic of the discharging/charging process of (a) the wayside/stationary energy storage device and (b) on-board energy storage device

1.2 Motivations

Section 1.1.3 states that intelligent train operations and energy storage utilisation in railway systems both contribute significantly to the improvement of the energy efficiency, and the utilisation of the OESD is promising in many aspects when compared to the use od WESD/SESD. Nevertheless, with the rapid development of the railway system as a type of green transportation mode around the world and the increasing utilisation of energy storage technologies in modern railway transportation systems, focusing on OESD, this more promising specific form of energy storage utilisation, still leads to many questions posed by scholars in existing works, which are summarised as follows:

- *How can the OESD be fully utilised to reduce energy consumption when integrated with railway systems because it has more restricted capacity, power, and space*

limits than wayside solutions? [8–10]

- *Does the installed OESD have significant influence or no influence on train operations due to the changes in the system, is the cooperation of the train and OESD necessary, and can it be achieved?* [10, 11]
- *There are many types of energy storage technologies and the corresponding specific products with different characteristics, how the railway operator chooses the best type and size to save both energy and monetary cost?* [9, 11]

The above questions show that systematic investigations on train operation with OESD are necessary to fill the gap in academia and industry when the OESD is widely introduced into the railway system. The changes that might be caused by the integration of both subsystems (train and OESD) requires detailed exploration.

1.3 Objectives

Focusing on the train operation with OESD utilisation, to answer the questions in Section 1.2, the objectives of the thesis are summarised as follows:

- This thesis aims to establish mathematical models to integrate both the train operation and OESD, from a small operation scale (single inter-station section) to a large operation scale (train network and power network), to optimise both the train and OESD operations with the objective of minimising the energy consumption of the system.
- This thesis aims to use the proposed mathematical models to provide insightful discussions and investigations on the mutual influence between the OESD discharging/charging strategy and train operation strategy. The intelligent energy management of the train operation and full utilisation of the OESD considering their respective engineering constraints are explored.
- This thesis also aims to explore the influence of the dynamic characteristics of different types of energy storage as OESD used in railway systems. The impact of these dynamic characteristics on the optimal train operation mode, selection of the optimal size of OESD, system energy cost, and monetary cost is discussed.

1.4 Thesis Outline

The thesis outline is shown in Figure 1.7.

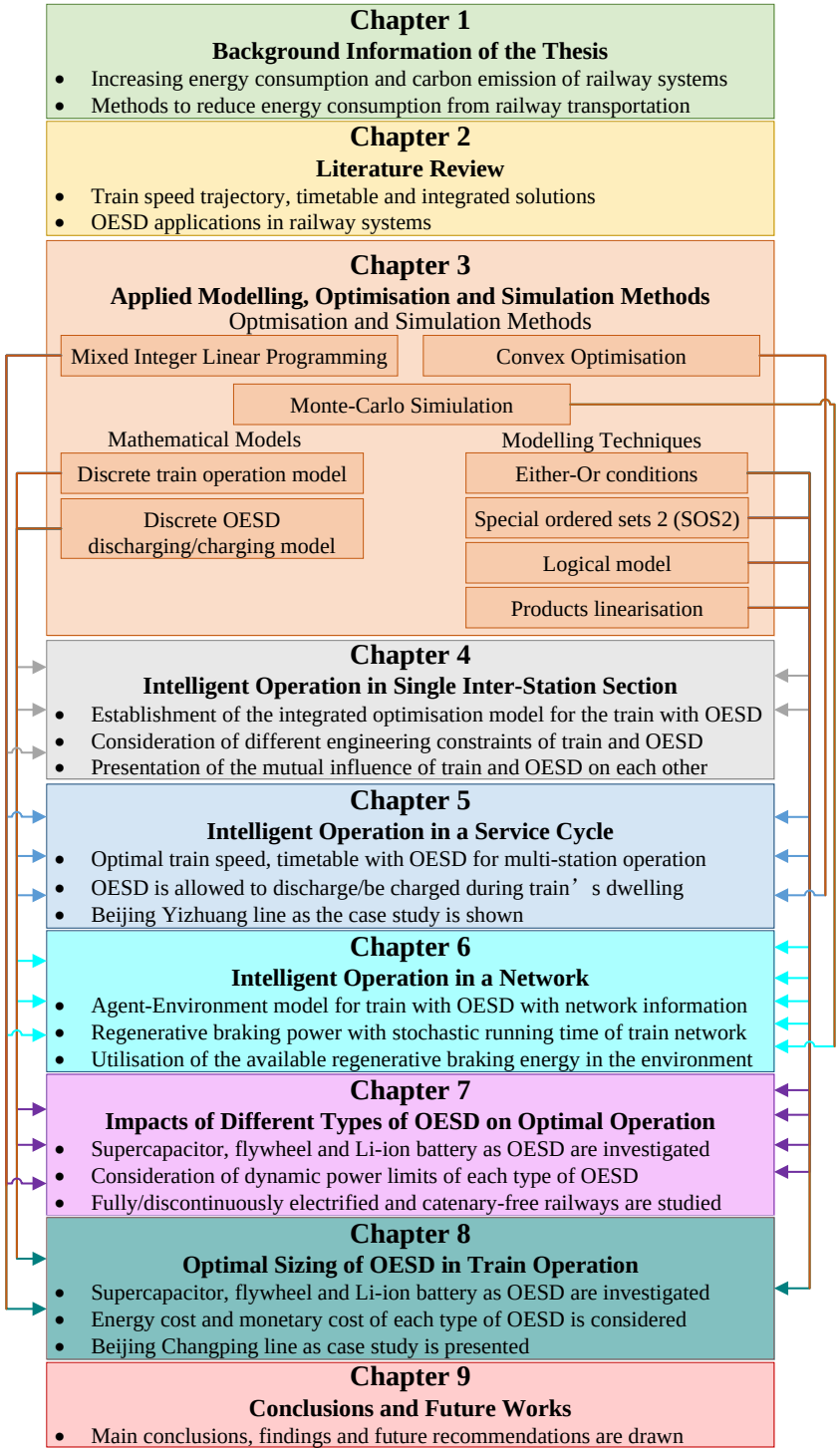

Figure 1.7: The outline of this thesis

- Chapter 1 introduces the background of the research, where the current status of energy use and carbon emissions from railway transportation is given, followed by an introduction of existing methods to reduce energy consumption in modern railway systems. Moreover, the research motivations, objectives, and thesis outline are presented.

- Chapter 2 provides the literature review regarding optimal train speed trajectory, timetabling, applications of different types of OESD in railway systems, and the integrated optimisation of trains with OESD.

- Chapter 3 introduces the traditional energy-efficient train control models in existing works and the proposed discrete distance-based train operation model. Then, the utilised modelling, optimisation, and simulation methods are shown. The main contents of the discrete train operation model in this chapter have been published in the following journal article:

  – Z. Tan, S. Lu, K. Bao, S. Zhang, **C. Wu**, J. Yang and F. Xue, "Adaptive Partial Train Speed Trajectory Optimization," *Energies*, vol. 11, no. 12, p. 3302, 2018.

- Chapter 4 proposes an integrated mathematical model to optimise the train speed trajectory and OESD discharging/charging strategy from the viewpoint of a single inter-station section. Mixed integer linear programming (MILP) is applied in this chapter to determine the optimal solution, based on which the influence of the OESD capacity, initial energy status, and degradation of the OESD on optimal train operation are presented. The main contents of this chapter have been published as a journal article:

  – **C. Wu**, W. Zhang, S. Lu, Z. Tan, F. Xue and J. Yang, "Train Speed Trajectory Optimization with On-Board Energy Storage Device," *IEEE Transactions on Intelligent Transportation Systems*, vol. 20, no. 11, pp. 4092-4102, 2019.

- Chapter 5 firstly extends the MILP model in Chapter 4 to optimise the train speed trajectory, running time, and OESD discharging/charging strategy (for both inter-station running and dwelling at stations) in the scope of service cycles with multiple inter-station sections. Then, a two-step method is proposed to solve the problem with much higher computation efficiency by combining the MILP model and convex optimisation together. Beijing Yizhuang line is adopted as the

numerical experiment in this chapter. The main contents of this chapter have been published as a conference paper and a journal article:

  - **C. Wu**, S. Lu, F. Xue, L. Jiang, and J. Yang, "Optimization of Speed Profile and Energy Interaction at Stations for a Train Vehicle with On-board Energy Storage Device," in *2018 IEEE Intelligent Vehicles Symposium (IV)*, 2018, pp. 1-6.
  - **C. Wu**, S. Lu, F. Xue, L. Jiang, M. Chen and J. Yang, "A Two-Step Method for Energy-Efficient Train Operation, Timetabling, and On-Board Energy Storage Device Management," *IEEE Transactions on Transportation Electrification*, Early Access, 2021.

- Chapter 6 proposes an agent-environment optimisation model to optimise the train speed trajectory with OESD within the scope of the network by considering the stochastic train network and power network information. The stochastic regenerative braking energy from other trains in the network, formed as the expected parameters using the Monte-Carlo simulation based on the MILP model in Chapter 4, can be utilised further by employing the optimised solution. The main contents of this chapter have been submitted as a journal article for consideration to be published:

  - **C. Wu**, S. Lu, Z. Tian, F. Xue and L. Jiang "Energy-Efficient Train Operation with Onboard Energy Storage Device considering Stochastic Regenerative Braking Energy," *under review.*

- Chapter 7 discusses the impact of the three popular types of energy storage, supercapacitors, flywheels, and Li-ion batteries, as OESD in train operation optimisation. A MILP model is proposed considering the dynamic power characteristics of each type of OESD, and the comparisons are conducted on fully electrified railways, discontinuously electrified railways and catenary-free railways to show the difference of energy-efficient operation strategies and their corresponding energy-saving performance. The main contents of this chapter have been published as a journal article:

  - **C. Wu**, B. Xu, S. Lu, F. Xue, L. Jiang and M. Chen, "Adaptive Eco-Driving Strategy and Feasibility Analysis for Electric Trains with On-Board Energy Storage Devices," *IEEE Transactions on Transportation Electrification*, Early Access, 2021.

- Chapter 8 discusses the optimal sizing problem of each type of energy storage as OESD in train operations to minimise energy consumption. The sizing problems of the the supercapacitors, flywheels, and Li-ion batteries are explored using the data-based method proposed in this chapter. Beijing Changping line as a real-world case study is investigated in this chapter, in which an insightful comparison of energy-saving and cost-saving performance of these three types of OESD is presented. The main contents of this chapter have been published as a journal article:

  – **C. Wu**, S. Lu, F. Xue, L. Jiang and M. Chen, "Optimal Sizing of On-Board Energy Storage Devices for Electrified Railway Systems," *IEEE Transactions on Transportation Electrification*, vol. 6, no. 3, pp. 1301-1311, 2020.

- Chapter 9 draws the main conclusions of this thesis, in which the outcomes and findings are elaborated. The recommendations formulated based on this thesis are also identified as future research directions.

In addition, from the perspective of the train operation scale to be studied and the OESD types involved in the research, the outline of this thesis is presented in Figure 1.8.

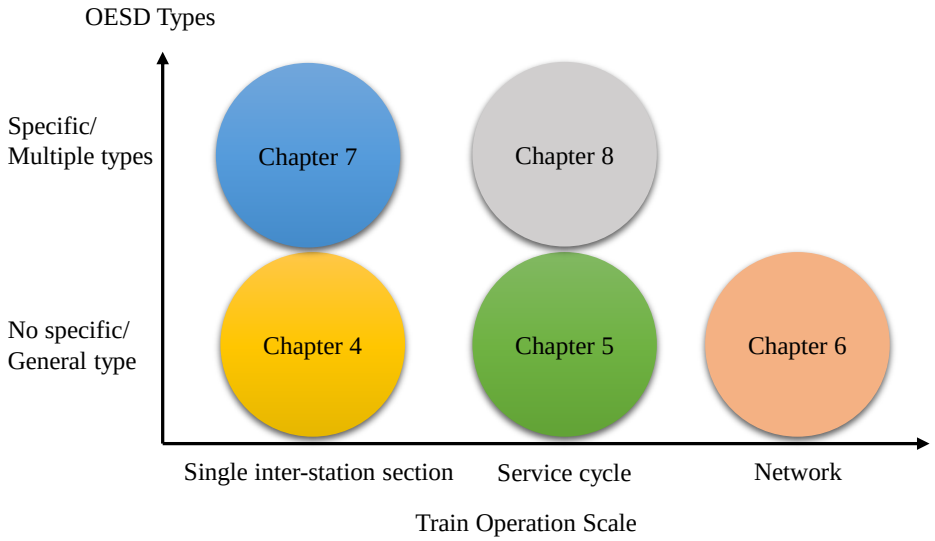

Figure 1.8: Outline of this thesis in terms of train operation scale and OESD types studied

1.5 Summary

This chapter first introduces the background information of the thesis, where the current status of worldwide railway transportation is discussed based on the open data of growing passenger demand for railway transportation and its lowest energy and carbon intensity. Railway transportation has rapidly advanced recently in terms of multiple forms of systems, and the expansion of worldwide railway systems is given. The extensive use and construction of railway systems have led to the increasing energy consumption and carbon emissions of railway transportation, which undermines its sustainability. Many measures have been taken to reduce the energy consumption of railway systems, among which intelligent energy management by optimising train operation and applying energy storage technologies outperforms the other methods.

Focusing on OESD, the motivations and objectives of the thesis are provided in this chapter, followed by the thesis outline. The outline explains the entire thesis in a chapter-by-chapter form in Figure 1.7 and a scale-oriented form in Figure 1.8, to make the structure of this thesis more easier to follow and the contributions clearer.

Chapter 2

Review of Train Operation Optimisation and OESD Applications

2.1 Introduction

With the rapid development of railway transportation, intelligent energy management is indispensable for saving energy consumed by increasing travel demand [7]. To improve the energy efficiency of railway systems, train speed trajectory and train timetable optimisation have become two popular and direct approaches to help reduce energy consumption without changing the existing infrastructure [12]. On the other hand, in the railway industry, regenerative energy has been utilised and usually consumed by another accelerating trains around, or stored by energy storage devices. Therefore, the application of energy storage devices, OESDs and WESDs/SESDs, have become popular in recent years [10, 13]. This chapter discusses the existing work regarding both train operation optimisation (including train speed trajectory optimisation, train timetable optimisation and their integrated study), OESD applications in railway transportation, and train operation with OESD.

2.2 Train Operation Optimisation for Energy Saving

Train operation normally consists of two main aspects: train speed trajectory and train timetable. The train speed trajectory determines how fast the train should run between two adjacent stations at each time instant or position, which is always controlled by the

driver relying on the driver's own experience/under assistance of Driver Advisory System (DAS) or ATO system. The train timetable determines the time required to travel between two adjacent stations, that is, running time, the time required for dwelling at a station, that is, dwell time, and the time between two adjacent train services, that is, departure/arrival headway. In this section, existing works related to train speed trajectory optimisation, train timetable optimisation, and their integrated optimisation are reviewed.

2.2.1 Speed Trajectory Optimisation

Optimal Control Theory

As early as 1968, Ichikawa applied the modern optimal train control theory based on Pontryagin's Maximum Principle (PMP) in railway systems to optimise the train control strategy [14]. Many similar studies in this area were conducted from 1970 to 2000. Some earlier works on the significance can be found in papers by [15–18]. Since 1990, the Scheduling and Control Group (SCG) at the University of South Australia developed modern theory of train control in a collection of publications [19–25]. It can be seen from these early works that the train speed trajectory optimisation problem can involve practical considerations on the speed limit, travel time and gradient etc. and targets different train systems such as diesel freight trains and electric passenger trains.

In 2000, Howlett applied PMP to study the optimal control for both continuous and discrete control cases [26]. Taking time as the independent variable in the model, this study developed key equations to determine the optimal switch points based on the necessary conditions for an optimal strategy. Khmelnitsky proposed a linking function to find the optimal trajectory and presented a numerical algorithm to solve the optimal train control problem with varying gradients and speed limits [27]. [28] proposed an analysis method to deal with the switching point between each control strategy and using a complementary variable to meet the speed limits constraints. In [29], the authors proposed a new local energy minimisation principle to locate the critical switching points for a global optimal strategy on a track with steep gradients. Based on the work [27], in [30] the application of a numerical is to optimise the trajectory by considering both varying gradients and speed limits. [31] studied the control operation during the varying gradient and the coasting operation on the slope and analysed a new local optimisation principle. [32, 33] summarised the key principles of the optimal train control developed in the past few decades, in which different aspects of optimal train control problem are summarised and discussed. These two papers focus on the classic two-station train

optimal control problem, where it is proven that the optimal strategy always exists in the proposed optimal train control model, and perturbation analysis is used to show that the strategy is unique.

On the other hand, by modelling the train operations as a standard optimal control problem, researchers from Delft University of Technology and University of Leeds proposed the application of pseudospectral algorithm and non-linear programming as a direct method in comparison to indirect methods such as PMP to solve the train speed trajectory optimisation problem under various engineering constraints. The studied cases can be well extended to multi-train problems and can consider more complex signalling and operational constraints [34–38]. [34] applied both the pseudospectral algorithm and MILP to solve the speed trajectory optimisation problem considering passenger riding comfort. The problem was formulated as an optimal control problem and a comparative study was conducted between the two proposed methods. [36] presented a multiple-phase optimal control model for train trajectory optimisation to be solved using a pseudospectral algorithm. This paper put a particular consideration on the operational (time and speed restrictions) and signal (signal aspects and automatic train protection) constraints for the trajectory optimisation under delay and no-delay situations. [37] applied a pseudospectral method to optimise multi-train optimisation by formulating the problem as a multiple-phase optimal control problem. Multiple objectives, including minimisation of energy consumption and train delays, exist for optimisation to locate the proper driving strategies. By modelling train operation in a closed-form model, [38] applied non-linear programming to address the train optimal control problem and the proposed methods were further applied to formulate a more complex optimal train control problem for scheduling and train following. In the above studies [36–38], undesirable fluctuations in the speed trajectory and operations spanning short durations are presented which may hinder the direct application of these methods if not properly addressed.

Heuristic Algorithms

In addition to the optimal train control algorithm, the speed trajectory optimisation problem has also been solved by using different heuristic algorithms. As discussed in [39], this is usually due to the fact that with more practical constraints considered, many practical problems such as the speed trajectory optimisation becomes an "NP-complete" problem. Heuristic algorithms, usually regarded as approximate algorithms, are applied to achieve near-optimal solutions with reduced computation time. Typical heuristic

algorithms include the Ant Colony algorithm (ACO), Genetic Algorithm (GA), and particle swarm algorithm etc. These algorithms can find the available solution at an acceptable cost arising from the consumed energy and elapsed time. GA is one of the most widely used methods in speed trajectory optimisation [40–45]. GA was applied to design a formal method to optimise traction energy and to investigate the relationship between the journey time and energy consumption [40]. [41] applied GA to solve an optimisation model targeting the minimisation of net energy. In this model, both train operation and time tabling are considered so that the integrated model can take advantage of regenerative braking and speed trajectory optimisation during the multi-train operations. As one of the advantages, different heuristic methods can be easily applied to solve the same optimisation problem and conduct comparative studies on each algorithm.

[43] used GA to solve the speed trajectory optimisation problem with a special consideration of regenerative braking so that the net energy can be reduced. [44] investigated the influence of the error in train positioning in the optimal speed trajectory obtained using GA. Speed trajectory optimisation is based on a simple case with a single speed limit and assumes that the operations of the train are designed in a preset sequence. In a recent study [45], a simulation-based GA was applied to solve a two-phase stochastic model considering the uncertain train mass to optimise the timetable and train speed profile. The optimisation of the train speed profile is based on a simple assumption that the optimal train trajectory comprises maximum acceleration, coasting and maximum deceleration. [46] proposed an integrated optimisation model to simultaneously consider both timetabling and train trajectories for minimum energy consumption using GA and brute force methods. Based on Monte-Carlo simulation, [47] presented an integrated optimisation method to incorporate the train operation and electric network power flow.

Mathematical Programming

Compared with heuristic algorithms arising from advances in computational intelligence, mathematical programming is a more traditional optimisation method that heavily relies on numerical iterations and mathematical modelling. With proper linearisation and modelling of practical problems, such a method can also be robust and adaptive with guaranteed global optimum in convex cases. Numerous studies have also utilised mathematical programming to locate the optimal speed trajectory in different scenarios. [48] achieved the optimal train speed trajectory in a discrete search space for a single train using GA, ACO, and Dynamic Programming (DP) using a distance-time-speed

model which has become a popular method of modelling problems dealing with integrated optimisation for both speed profiles and timetabling [49]. [50] proposed an integrated model to minimise the energy in dynamic train scheduling and control in metro rail operations. In this study, a convex optimisation model was built to consider train operation in terms of curve planning and scheduling in terms of journey time allocations simultaneously. The Kuhn-Tucker conditions were applied to solve the optimisation model to achieve a significant energy reduction. [51] applied an approximate DP to solve the train rescheduling problem in which the speed trajectory was optimised in a discrete search space. [52] proposed a DP method to solve speed trajectory optimisation using an event-based decomposition to reduce the search space leading to significant computational time reduction. [49] proposed a unified modelling approach using space-time-speed to address the joint optimisation problem for high-speed train timetables and speed profiles. Lagrangian Relaxation (LR) were applied to address the power supply and safety constraints.

Since 2014, [53–55] conducted a series of studies focused on the partial speed trajectory optimisation problem. This problem arises from the question of "how much regenerative braking energy can be obtained from a braking procedure of train with given travel distance and elapsed time". The problem was first studied by [53] using the Bellman-Ford algorithm, that is, a DP-based graphical searching method, by modelling the braking speed trajectory in a discrete manner and an optimum analysis based on PMP was conducted; they demonstrated high-level agreements between the analysis and optimisation results. [54] and [55] proposed the application of linear programming to solve the monotonous speed trajectory problem during the regenerative braking process. [55] applied the MILP to address non-linear constraints arising from varying gradients along the braking route for partial speed trajectory optimisation problems. By formulating the speed trajectory optimisation as an MILP model, [56] attempted to optimise the speed trajectory to achieve the minimum net energy.

The selected publications for train speed trajectory optimisation in the categorisation of the methods are tabulated in Table 2.1.

Table 2.1: Selected publications on train speed trajectory optimisation

Publication(s)	Algorithm(s)	Transport mode(s)	Contribution
	Optimal Control		
[26]	PMP	R; F; M	Theory proof

H=high-speed trains, R= regional trains, F=freight trains, M=metro trains.

(Continued table from last page)

Publication(s)	Algorithm(s)	Transport Mode(s)	Contribution
[27]	PMP	R; M	Theory proof
[28]	PMP	R; M	Theory proof
[30]	PMP	H	22.2% to 44.2% energy saving compared with flat-out operation
[32, 33]	PMP	H	Theory proof
	Heuristic Algorithm		
[40]	GA	R	10.59 % energy saving for a 4.95% increase in journey time
[48]	[1]GA [2]ACO [3]DP	M	Train speed trajectories with minimised energy consumption using three methods are achieved and compared
[42]	[1]Brute force algorithm [2]ACO [3]GA	H	17.9% energy saving compared with flat-out operation
[43]	GA	M	3.3% energy saving in Beijing Metro
	Mathematical Programming		
[34]	[1]Pseudospectral method [2]MILP	/	Train speed trajectories with minimised energy consumption using two methods are achieved and compared
[53]	Bellman-Ford algorithm	M	17.23% regenerative braking energy increment
[55]	MILP	R	Regenerative braking energy is maximised
[52]	DP	R	3.3% energy saving compared to commercial solver
[36]	Pseudospectral method	R	Signalling systems and delay recovery are considered

H=high-speed trains, R= regional trains, F=freight trains, M=metro trains.

(Continued table from last page)

Publication(s)	Algorithm(s)	Transport Mode(s)	Contribution
[37]	Pseudospectral method	R	Multiple trains are considered

H=high-speed trains, R= regional trains, F=freight trains, M=metro trains.

2.2.2 Timetable Optimisation

Timetable is an indispensable part of train operation, and it determines the departure and arrival time for all trains at stations which ensures both the safety constraints of operation and travel demand.

Reducing Traction Energy Consumption

Energy consumption and service quality are two important concerns of the railway operator that directly influence the operating cost of the railway system and the passenger satisfaction by taking railway transportation. Improving service quality by finding the optimal timetable under the constraints of energy consumption has always been an important research problem. Yang *et al.* [57] proposed a two-objective integer programming model to increase the reproducible utilisation of energy sources and minimise the total waiting time of passengers. Xu *et al.* [58] proposed a multi-objective approach to minimise the passenger time and energy consumption by controlling the travel time at each interval and dwelling time at each platform, where an ideal-point compromise approach and a linearly weighted compromise approach were respectively employed via GA. Binder *et al.* [59] integrated passenger satisfaction, operational costs, and deviation to generate a disposition timetable and formulated it as an Integer Linear Programming (ILP) model. A three-dimensional Pareto frontier was explored to study the relationship and trade-offs among the three objectives. Yin *et al.* [60] proposed an integrated approach for solving the train timetabling problem on two-way urban metro lines to simultaneously minimise the energy consumption and passenger waiting time. Sun *et al.* [61] developed a bi-objective timetable optimisation model to minimise total passenger waiting time and net energy consumption without ignoring time-variant characteristics of passenger demand at each station. Mo *et al.* [62] developed a flexible model to minimise energy cost and passenger waiting time, considering a variety of system constraints such as inventory train constraints, train loading capacity constraints and train type constraints, etc.

Improving Regenerative Braking Energy Utilisation

In addition to setting the constraints on the traction energy consumption, timetable optimisation also focuses on improving the regenerative braking energy utilisation in the network. Yang *et al.* [57] developed a scheduling method to coordinate the arrival and departure times of all trains that in the same power supply section to improve the utilisation of regenerative braking energy . Tian *et al.* [47] demonstrated a traction power network modelling method for multi-trains to determine the energy flow of regenerative braking train systems. Considering the total travel time and operation energy consumption, Huang *et al.* [63] proposed a multi-objective optimisation model to adjust the headway in different lines from the perspective of system optimisation. A multi-objective integer programming model was developed by Yanget *et al.* [64] to optimise the departure and arrival times of trains at each station, which considers energy consumption, passenger waiting time, and robustness. Liao *et al.* [65] proposed an energy-saving optimisation strategy for multi-train metro timetables to minimise the difference between the traction energy consumption and feedback energy by applying GA. Liu *et al.* [66] proposed a timetable optimisation problem by considering realistic constraints with headway time and dwell time to further utilise the regenerative braking energy. By controlling the headway and dwell time, Liu *et al.* [67] proposed a timetable optimisation model to maximise the regenerative braking energy utilisation, which coordinates the traction and braking trains supplied by each substation. To increase the utilisation rate of regenerative braking energy as much as possible, Mo *et al.* [68] proposed an integrated model to simultaneously obtain the optimal train timetable and rolling stock circulation plan, thus maximising the brake-traction overlapping time at stations. Su *et al.* [69] proposed an integrated train operation method that combines driving strategies and train timetable to minimise the systematic net energy consumption, namely the difference between the traction energy consumption and the regenerative braking energy.

The selected publications for train timetable optimisation in the categorisation of the methods are tabulated in Table 2.2.

Table 2.2: Selected publications on train timetable optimisation

Publication(s)	Algorithm(s)	Transport mode(s)	Contribution
Heuristic Algorithm			

H=high-speed trains, R= regional trains, F=freight trains, M=metro trains.

(Continued table from last page)

Publication(s)	Algorithm(s)	Transport Mode(s)	Contribution
[57]	GA	M	Saved energy by 8.86% and reduced passenger waiting time by 3.22% in comparison with the current timetable.
[58]	GA	M	Reduced passenger waiting time and energy consumption during peak hours and passenger travelling time during off-peak hours
[60]	LR-based algorithm	M	Reduced the total passenger waiting time, especially in peak-hours, and kept relatively low energy consumption in comparison with fixed-headway timetables.
[61]	GA	M	Reduced the total energy consumption by 9.67% and the total passenger waiting time by 4.72% using the Beijing Yizhuang line as a case study
[62]	[1]GA [2] Prior enumeration method [3] Modified tabu search algorithm	M	Energy cost of the optimised solution is drastically reduced by 49.3% with a 15% increase in total waiting time using the Beijing Yizhuang line as an example
[57]	GA	M	Reduced energy consumption by 6.97% and saved approximately 1,054,388 CNY (or 169,223 USD) each year
[47]	Monte-Carlo simulation	M	Reduced the substation energy consumption by 38.6%

H=high-speed trains, R= regional trains, F=freight trains, M=metro trains.

(Continued table from last page)

Publication(s)	Algorithm(s)	Transport Mode(s)	Contribution
[63]	Tabu search algorithm	M	22.0% reduction of energy consumption and 12.2% reduction of the total waiting time with uneven headway, 13.7% reduction of energy consumption and 8.7% reduction of total waiting time with even headway
[64]	Non-dominated sorting genetic algorithm II (NSGA-II)	M	Improve the performance of the total energy consumption, total passenger waiting time and robustness value by 2.10%, 15.80% and 24.81%, respectively
[65]	GA	M	Energy consumption was reduced by 23.28% using the Shanghai Metro line 1 as a case study
[66, 67]	Improved artificial bee colony (IABC) algorithm	M	Largest regenerative braking energy utilisation improvement ratio of 34.7%
	Mathematical Programming		
[59]	ILP	R	Pareto frontier for the trade-off between operational cost and passenger satisfaction is obtained
[68]	MILP	M	Brake-traction overlapping regions reach up to 64.42% to 89.42% using the Beijing Yizhuang line as an example
[69]	DP	M	Net energy consumption can be reduced by 2.4% and 2.8%

H=high-speed trains, R= regional trains, F=freight trains, M=metro trains.

2.2.3 Integrated Optimisation

Some researchers found that only optimising the train speed trajectory or timetable is not sufficient; thus, integrated approaches that considers both speed control and timetabling has become the a new research direction in recent years.

An iterative method is proposed to optimise both the running time and train speed profile together to reduce the total traction energy consumption of the entire metro line [70]. Regenerative braking energy is also considered in the integrated approach, and in [41], the integrated optimisation of the train operation timetable was investigated by maximising the overlapped time for traction and braking events to take advantage of the regenerative braking energy to reduce the net energy consumption.

The analytical method is also used to deal with this combined problem. This method is used to optimise the train speed trajectory, that is, the speed between switching points, and schedule, that is, the departure and arrival time of each station is optimised to save more net energy consumption [50]. High-speed railway corridor was also studied, and a DP solution was provided. The algorithm was proposed to find the speed/acceleration profile solutions with dualised train headway and power supply constraints [49]. A three-dimensional space-time-speed grid networks was established to characterise both second-by-second train speed trajectory and segment-based timetables at different space and time resolutions. Recently, the optimal multi-train speed profile optimisation and timetable design were considered in [71] to reduce traction energy consumption based on a real-world case study. In addition to the DC railway systems, the integrated train speed trajectory and timetable optimisation for AC railway systems were also explored in [72] to achieve the minimum electrical energy consumption.

2.3 OESD Applications in Railway Systems

Energy storage devices have been utilised in modern railway systems, some of which are used as the wayside/stationary energy storage, and the remaining are used as OESDs on trains. There are three main types of OESD that have been tested or are utilised nowadays, which are supercapacitors, flywheels, and batteries.

2.3.1 Supercapacitors

A supercapacitor, also called an ultracapacitor, is a high-capacity capacitor with a capacitance value much higher than that of other capacitors, but with lower voltage limits, which bridges the gap between electrolytic capacitors and rechargeable batteries [73].

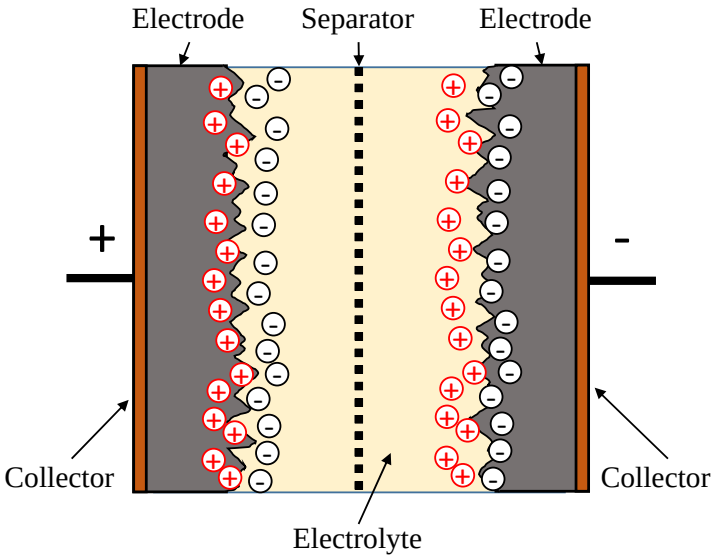

Figure 2.1: The structure of a typical supercapacitor

It consists of two electrodes (coated with collectors) separated by an ion-permeable membrane (separator) and an electrolyte, which iconically connects both electrodes. When the electrodes are polarised by an applied voltage, ions in the electrolyte form electric double layers of opposite polarity to the polarity of the electrode, as shown in Figure 2.1. Rather than long-term compact energy storage, supercapacitors are used in applications requiring many rapid charging/discharging cycles, for example, in automobiles, buses, trains, cranes, and elevators, where they are used for regenerative braking, short-term energy storage, or burst-mode power delivery [74].

In real applications, supercapacitors are the most popular type of energy storage device used in railway systems. Bombardier produced the MITRAC^{TM} Energy Saver and installed it as an OESD for a prototype of a light rail vehicle (LRV) for public transport by the German operator Rhein-Neckar-Verkehr Gmbh in Mannheim, Germany from 2003 to 2008 [75, 76]. The test onsite showed that the traction energy consumption can be reduced by 30% and the line current peak decreases by 50%. Siemens developed a type of OESD called Sitras® MES (Mobile Energy Storage) and installed it on Innsbruck tramway for energy reduction [77]. The CAF company produced a type of OESD called ACR in 2012, and it is now still in service in Seville, Saragossa and Granada tramway systems [8]. Alstom produced a type of supercapacitor-based OESD called STEEM which was used in the Paris tramway from 2009 to 2010 [78], which reduced the average daily energy consumption by 13%, with a minimum and maximum energy consumption

of 10% and 18%, respectively.

2.3.2 Flywheels

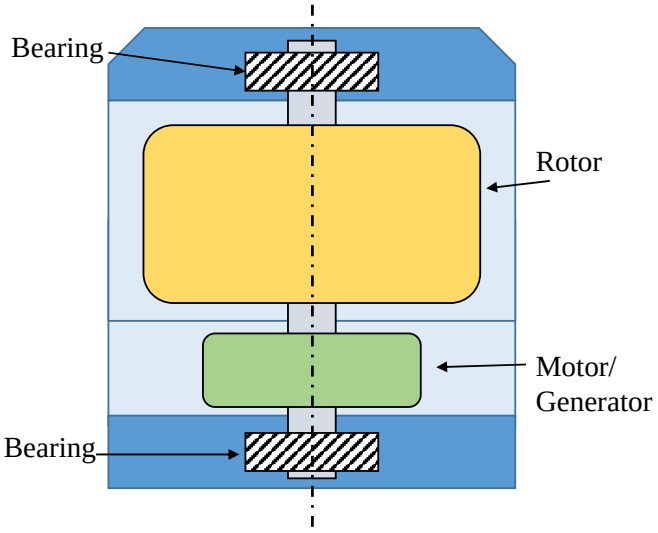

Figure 2.2: The structure of a typical flywheel

A flywheel is a mechanical device specifically designed to use the conservation of angular momentum to efficiently store rotational energy. The flywheel system is typically supported by a rolling-element bearing, and its rotor is connected to an electrical machine that can operate either as a motor or as a generator (Figure 2.2). It acts as a motor in the charging process when an electrical supply is used to increase the kinetic energy of the flywheel by speeding up its rotational speed [8]. The flywheel and sometimes the motor–generator may be enclosed in a vacuum chamber to reduce friction and energy loss.

Flywheels have already been reported as OESDs in railway systems but and are still in an early stage of development. Only the study by [79] reported the construction of a prototype for hybrid light rail vehicles within the "Ultra Low Emission Vehicle – Transport Advanced Propulsion 2 (ULEV–TAP2)" project. Developed by the Centre for Concepts in Mechatronics (CCM), this OESD consisted of a 250-kW high-speed carbon-fibre flywheel with an effective energy storage capacity of 4 kWh. On the other hand, CCM has collaborated with Alstom to integrate a flywheel-based OESD in their Citadis tramway [80]. In addition, flywheels were installed on the roof of trams for catenary-free operations in Rotterdam in the Netherlands. The energy, power capacity, and speed of the flywheel were 4 kWh, 325 kW and 20000 rpm, respectively [81].

2.3.3 Batteries

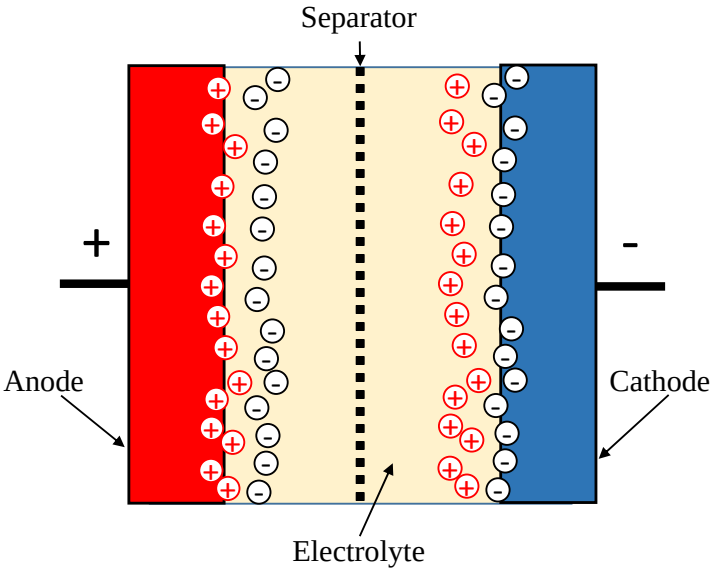

Figure 2.3: The structure of a typical battery

A battery is a device comprising one or more electrochemical cells with external connections for powering electrical devices such as flashlights, mobile phones, and electric cars. It stores and delivers energy via reversible electrochemical reaction occurring between two different materials (electrodes) immersed in an electrolyte solution (Figure 2.3). Conventional lead-acid batteries have been studied and designed since a long time. Lithium-ion (Li-ion) and nickel-metal hydride (Ni-MH) batteries are the emerging technologies for transport applications because their energy densities are higher than that those of lead-acid batteries [11].

Alstom developed a type of OESD based on Ni-MH batteries, called Alstom-Saft, and it has been applied in the Citadis tramway in Nice since 2007 [78, 80]. This tram had a maximum speed of 30 km/h and was able to run catenary free over a length of 1 km [82]. Kawasali also produced a Ni-MH battery-based OESD which was installed on a prototype vehicle called 'SWIMO' developed by Sapporo Municipal Transport and Kawasaki Heavy Industry with operating voltage of 600 V from December 2007 to March 2008 [80, 83]. A type of Li-ion battery-based OESD, called LFX-300 streetcar, from Kinki Shayro has been applied by the MTS light rail system in south Lisbon since 2008 [84]. The on-board Li-ion battery unit was composed of 168 cells in series and a rated capacity of 33 kWh, which was operated in public service from 2003 to 2005 in Japan [85, 86]. In February 2020, the core Merseyrail network in Liverpool,

UK, was electrified at 750 V DC third rail, where the Class 777s have a dual voltage capability to use 25 kV 50 Hz electrification on any extension [87]. Options also exist for a battery-electric variant, and it is anticipated that one of the initial builds will be equipped with on-board energy storage for evaluation. There is a space under one vehicle to house a battery weighing up to 5 tonnes within the axle load limit. All Class 777s will be fitted with small batteries to allow independent movement around the workshop and maintenance facilities.

2.3.4 Hybrid Systems

A combination of batteries and supercapacitors or flywheels, known as the hybrid energy storage device (HESD), exhibits better performance than a single energy storage device [11] owing to the mutual assistance of each type of energy storage to reconfigure the power and energy during the operation according to each other's specific characteristics.

Hybrid system have rarely been studied and applied in technical or academic works. One application was proposed by Siemens, wherein a hybrid system known as Sitras® HES was developed. The system consists of a Sitras® MES mobile energy storage unit (supercapacitors) and a traction battery made of Ni-MH batteries provided by Alstom-Saft [84]. This solution has been tested in passenger operation at the MTS network (Metro Ligeiro da Margem Suldo Tejo) since 2008 and has shown very promising results. On 28 December 2020, Guangzhou Huangpu Tram Line 1, designed by the Fourth Railway Institute, was put into operation [88]. This is the first Chinese domestic tram powered by the hybrid energy storage system, supercapacitors and lithium-titanate batteries, without energy supply from the catenary or third rail during operation.

Figure 2.4 illustrates the current conditions of the utilisation of OESD with respect to different energy storage types and countries. It can be found that supercapacitors are the most popular types in real operations, and batteries rank the second. Flywheels and hybrid systems, as mentioned in the above review, are both still in the early developing stages, but their utilisation is still observed. European countries have almost the highest utilisation of OESDs in railway systems in the world, except for Japan which has employed batteries in operations, and China, where trams are equipped with hybrid energy storage systems in operation since 2020.

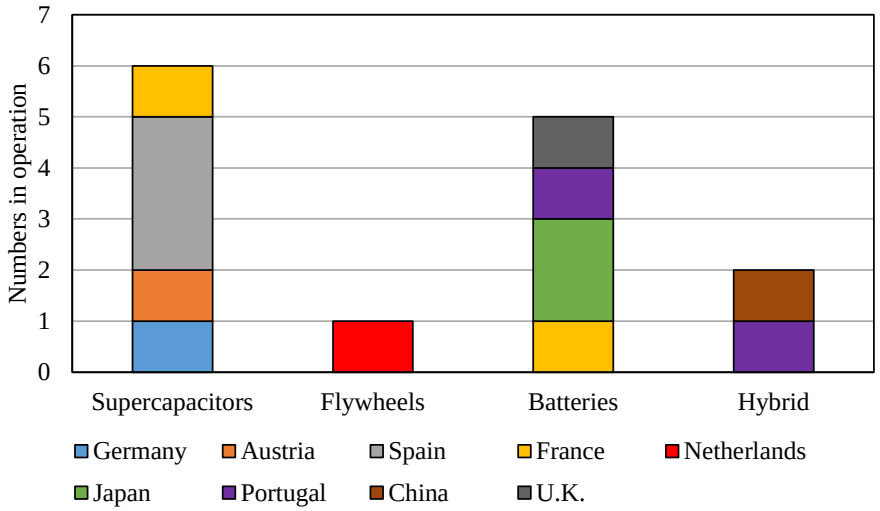

Figure 2.4: OESD utilisation in operations with respect to energy storage types and countries

2.4 Train Operation Optimisation with OESD

Since OESDs have been put into use or tested in railway industries, it is necessary to explore the integrated train operation with OESD considering their engineering properties. Some researchers have conducted some early studies related to this topic.

Miyatake *et al.* from Sophia University, Japan, investigated the optimal train speed trajectory with supercapacitor as OESD [89]. In this paper, the optimal train speed trajectory was found with the modelled circuits of the supercapacitor and the application of the Sequential Quadratic Programming (SQP). The train speed, time instant, and state of charge (SOC) of the OESD are formulated into a mathematical programming model to be optimised as an optimal control problem. A specific type of supercapacitor was adopted in the case study, and the results show the effectiveness of the proposed method. This indicates that with the initial and terminal control of the SOC of the OESD, the utilisation of OESD has little influence on the optimal driving strategy of trains. The work was extended in [90] to investigate the catenary-free tram operation with OESD, where the train speed trajectory and timetable with a supercapacitor as OESD is studied. In the research, DP was applied to solve the problem with train speed and time instant, and SOC of OESD are regarded as the state variables to be optimised. A 3-station route was studied in the case study, and the results show that the OESD can be quickly charged at intermediate stations. The running time at each inter-station section can be obtained by using the proposed method. In addition to supercapacitors,

Miyatake *et al.* also proposed an MILP model to optimise the train control strategy and timetable for a Li-ion battery-driven train [91]. In the study, the relationship among the energy status of the OESD, running time and energy consumption of the train operation was approximated using integer variables.

Kampeerawar *et al.* from the University of Tokyo, Japan, proposed an integrated optimisation model solved by GA to design optimal train control and timetable considering the batteries as the OESD [92]. The Bangkok metro system, Thailand, and the Jinan metro system, China, are both adopted as cases, and the results show that the proposed integrated design can provide up to 16% energy-saving performance in the case of the Jinan metro system and 27% energy-saving performance in the case of the Bangkok metro system.

Using DP, Huang *et al.* [93] from Beijing Jiaotong University, China, explored the energy-saving potential of supercapacitors by optimising the train speed trajectory and running time from the viewpoint of energy flow modelling. The Beijing Yizhaung line was the research object in this study, and the results show that the proposed method can significantly save energy.

Ghaviha *et al.* [94] proposed a DP-based model to find the optimal speed trajectory for Li-ion battery-driven trains. Unlike previous approaches, the control variable was the speed change instead of the applied traction force in the problem.

In [95], the optimal power split and speed trajectory of a catenary-free tram equipped with suprecapacitors were studied. A DP algorithm was presented to determine the voltage trajectories of supercapacitors with power plant voltage limitations and dynamic power losses. The performance of the proposed integrated method was evaluated by numerical simulation based on the actual route of Chengdu Tramway Line 2, China.

2.5 Summary

In this chapter, a literature review of the train operation optimisation is provided at the beginning, where methods for train speed trajectory optimisation and train timetable optimisation are categorised. Notably, the attention on speed and timetable optimisation has shifted from only minimising traction energy consumption to concurrently maximising the utilisation rate of the regenerative braking energy. Furthermore, a rising trend of use of the heuristic algorithm is observed, which is the most popular method to solve problems, and mathematical programming is relatively less applied.

Current OESD applications in railway systems around the world are presented. Supercapacitors, flywheels, batteries, and hybrid systems are elaborated using the real

applications from technical reports and academic papers, showing the energy-saving potential and fast developing trend of OESDs. Finally, the current status of the research related to the optimisation of train operation with OESD is shown. Only a few works in the field could be found, which indicates that there is a gap in the field, and the systematic investigation of the integrated optimisation considering both trains and OESDs in combination is necessary and promising.

OESDs are one of then emerging technologies that will help enhance the sustainability of modern railway systems. They will be utilised increasingly in the foreseeable future. The relevant works related to the integrated optimisation of train operation with OESD still focus on solving the optimisation problem whereas the mechanism of the mutual influence and further cooperation of both train control and OESD discharging/charging strategies, which are also highlighted in Section 1.2, are not discussed.

Chapter 3

Modelling, Optimisation, and Simulation Methods

The content of this chapter, especially the proposed discrete energy-efficient train control model (Section 3.3), is from the author's published article in a modified and restructured version to fit the context of this thesis. The published article is:

Z. Tan, S. Lu, K. Bao, S. Zhang, **C. Wu**, J. Yang and F. Xue "Adaptive Partial Train Speed Trajectory Optimization," *Energies*, vol. 11, no. 12, p. 3302, 2018.

3.1 Introduction

This chapter introduces the mathematical modelling and optimisation methods applied in this thesis. First, the basic energy-efficient train control models proposed in the existing works are introduced, followed by the train control model proposed in this thesis. Second, the OESD charging/discharging model established in this study is introduced. Then, the linearisation techniques adopted in the thesis are presented using simple examples. In addition, a brief discussion on the optimisation methods, MILP and convex optimisation, is provided. Finally, the Monte-Carlo simulation used to build the railway environment in this thesis is introduced.

3.2 Existing Energy-Efficient Train Control Models

Train movement and control modelling have been studied by numerous researchers, especially from the perspective of energy efficiency. This section introduces the basic energy-efficient train control models in previous works and the proposed modified model used in this thesis.

3.2.1 Time-Based Model

The train control problem was first analysed in a mathmatical form by Milroy [17] in his PhD thesis in 1980. The mathematical form described a train running between two adjacent stations with minimised energy consumption, as shown in (3.1)-(3.5).

$$J = \min \int_0^T F^+(t)v(t)\,dt \tag{3.1}$$

$$\text{s.t.} \quad \dot{x}(t) = v(t) \tag{3.2}$$

$$\dot{v}(t) = F(t) - R(v(t)) \tag{3.3}$$

$$x(0) = 0, x(T) = X, v(0) = 0, v(T) = 0 \tag{3.4}$$

$$v(t) \geq 0, F(t) \in [-F_{min}(v(t)), F_{max}(v(t))] \tag{3.5}$$

In the model, t is the time instant, T is the given running time between two adjacent stations, $F(t)$ is the traction force over time t, and $v(t)$ is the train speed over time t. $F^+ = \max(F(t), 0)$ is used to represent the positive value of the traction force because it is assumed that braking does not cost or generate energy. $x(t)$ is the distance travelled over time t, and X is the total distance between two adjacent stations. $R(v(t)) = R_0 + R_1 v + R_2 v^2$ is the drag force given by the Davis equation [96], where the constant and linear terms are rolling resistances and quadratic term is the air resistance. F_{min} and F_{max} are the maximum braking and traction forces, respectively, which depend on the train speed $v(t)$.

3.2.2 Distance-Based Model

To consider the varying gradients and speed limits along the route, in 1995, Howlett and Pudney [22] transformed the basic time-based model into the distance-based form,

as follows (3.6)-(3.10):

$$J = \min \int_0^X F^+(x)\, dx \tag{3.6}$$

$$\text{s.t.} \quad \dot{t}(x) = 1/v(x) \tag{3.7}$$

$$\dot{v}(x) = (F(x) - R(v(x)) - G(x))/v(x) \tag{3.8}$$

$$t(0) = 0, t(X) = T, v(0) = 0, v(X) = 0 \tag{3.9}$$

$$v(x) \in [0, v_{max}(x)], F(x) \in [-F_{min}(v(x)), F_{max}(v(x))] \tag{3.10}$$

In the distance-based model, the external force $G(x)$ due to the track gradient or curvature is introduced, and $v_{max}(x)$ is the speed limit in terms of the distance travelled. Incorporating the gradient and speed limit information into the model is a practical approach for actual industrial applications.

3.2.3 With Regenerative Braking

The introduction of the regenerative braking system in the railway system is a new energy-saving option to maximise the generation of regenerative braking energy. This energy can be used by other trains or stored by the energy storage device to support the running later, and reduce the overall energy consumption of the system. In 1985, Asnis [97] combined regenerative braking into a time-based model (3.1)-(3.5) with an adjusted form to minimise the difference of the traction energy consumption and regenerative braking energy generation. In 2000, Khmelnitsky [27] transformed this time-based model into distance-based form, and the objective function of the model is shown as follows:

$$J = \min \int_0^X (F^+(x) - \eta F^-(x))\, dx \tag{3.11}$$

$$\text{s.t.} \quad (3.7) - (3.10)$$

where η is the recuperation efficiency of the regenerative braking energy based on the characteristics of the braking system. $F^- = -\min(F(t), 0)$ is used to represent the specific braking force.

3.3 Proposed Discrete Train Control Model

In this thesis, in contrast to the basic model in the continuous form proposed in existing studies, the train control model in the discrete and distance-based form is proposed to locate the optimal speed trajectory.

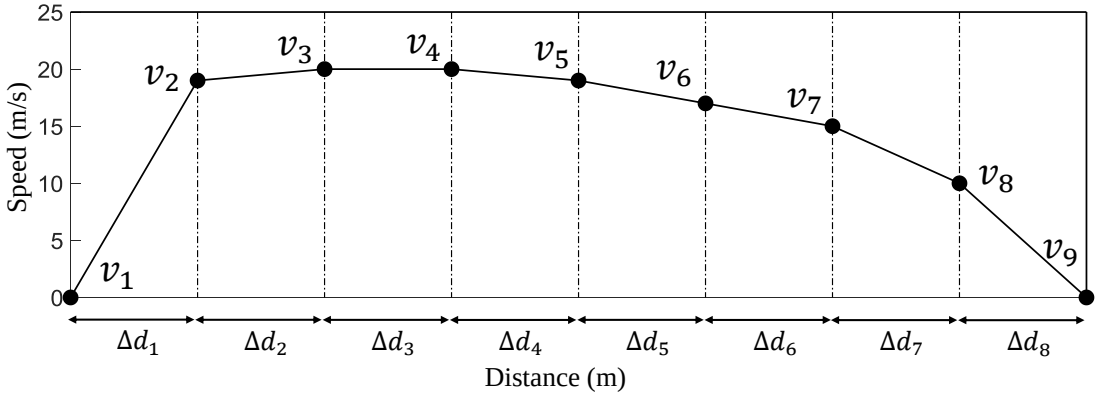

Figure 3.1: An example of the discretisation of the track length in the proposed method. The number of Δd_i, denoted by N, is 8; thus, there are 9 determinant speed points, each of which is denoted by v_i, i=1,2,...,9

The entire route is discretised into a series of sections with a distance of Δd_i. Δd_i is present and can be modified to be sufficiently small to ensure high calculation precision, as shown in Figure 3.1. Each of the sections represents a part of the trajectory that contains the travelled distance, elapsed time and consumed energy. N is used to represent the number of sections. The products in (3.11), $F^+(x)dx$ and $\eta F^-(x)dx$, represent the work done by the motor in both the traction and braking modes. These values are changed to be a set of variables. The energy consumed or generated by the motor in each Δd_i is referred to as $\Delta E_1, \Delta E_2, \cdots, \Delta E_i, \cdots, \Delta E_N$ in the proposed model.

In this case, the continuous form of the objective function (3.11) of the model can be transformed into a discrete form, as shown in (3.12).

$$J = \min \sum_{i=1}^{N} \Delta E_i \tag{3.12}$$

Because the route is discretised into N distance segments, there are $N+1$ speed points $v_1, v_2, v_3, \cdots, v_i, \cdots, v_{N+1}$, and N average speeds $v_{i,ave} = (v_i + v_{i+1})/2$. Thus, constraint (3.7) can be transformed into a discrete form, i.e., $\dot{t}(x) = \Delta t_i / \Delta d_i$, as shown

in (3.13).

$$\frac{\Delta t_i}{\Delta d_i} = \frac{1}{v_{i,ave}}, \quad \forall i = 1, 2, 3, ..., N \tag{3.13}$$

where Δt_i is the elapsed time of Δd_i.

In each Δd_i, the train runs with a constant acceleration a_i between two adjacent speed points v_i and v_{i+1}. Thus, the constraint (3.8) can be transformed into the discrete form, i.e., $\dot{v}(x) = \Delta v_i/\Delta t_i \cdot \Delta t_i/\Delta d_i = a_i/v_{i,ave}$, without term $1/v_{i,ave}$, as shown in (3.14).

$$a_i = \frac{v_{i+1}^2 - {v_i}^2}{2\Delta d_i}, \quad \forall i = 1, 2, 3, ..., N \tag{3.14}$$

Assume that the maximum acceleration rate and deceleration rate that passengers can tolerate are $\overline{a_a}$ and $\overline{a_d}$, respectively. Thus, riding comfort can be ensured by imposing equation (3.15).

$$-\overline{a_d} \le a_i \le \overline{a_a}, \quad \forall i = 1, 2, 3, ..., N \tag{3.15}$$

The drag force $R(x)$ and external force $G(x)$ are also transformed into discrete forms in each Δd_i, as shown in (3.16) and (3.17), respetively.

$$R_i = R_0 + R_1 v_{i,ave} + R_2 v_{i,ave}^2, \quad \forall i = 1, 2, 3, ..., N \tag{3.16}$$

$$G_i = Mg\theta_i, \quad \forall i = 1, 2, 3, ..., N \tag{3.17}$$

where M_t is the mass of the train and θ_i is the gradient of each Δd_i.

Similar to constraint (3.9), in the discrete model, the initial and terminal conditions of the speed and running time constraints also need to be added, as shown in (3.18) and (3.19).

$$\sum_{i=1}^{N} \Delta t_i = \sum_{i=1}^{N} \frac{\Delta d_i}{v_{i,ave}} = T \tag{3.18}$$

$$v_1 = 0, \quad v_{N+1} = 0 \tag{3.19}$$

The speed limit along the route and the maximum traction/braking force limits in constraint (3.10) are also transformed into their discrete forms (3.20) and (3.21), respectively.

$$0 \le v_i \le \overline{V_i}, \quad \forall i = 1, 2, 3, ..., N \tag{3.20}$$

$$-\eta_b \overline{F_b} \Delta d_i \le \Delta E_i \le \frac{1}{\eta_t} \overline{F_t} \Delta d_i, \quad -\eta_b \overline{P_b} \Delta t_i \le \Delta E_i \le \frac{1}{\eta_t} \overline{P_t} \Delta t_i, \quad \forall i = 1, 2, 3, ..., N \tag{3.21}$$

where $\overline{V_i}$ is the speed limit in each Δd_i, $\overline{F_t}$ and $\overline{F_b}$ are the maximum traction/braking force of the motor, respectively, $\overline{P_t}$ and $\overline{P_b}$ are the maximum traction/braking power of the motor, respectively, and η_t and η_b are the motor efficiency in traction and braking modes, respectively.

The objective and constraints in the continuous form of the basic distance-based model have been transformed into a model with discrete forms (3.12) - (3.21). The proposed model will be modified to satisfy different problems integrated with OESD model in later chapters.

3.4 OESD Charging/Discharging Model

The charging/discharging process of OESD is normally affected by the charging/discharging power and charging/discharging time. The energy released or received by the OESD from time instant t_i to t_j can be expressed in (3.22).

$$E(t_j) - E(t_i) = \int_{t_i}^{t_j} p(t)dt, \quad p(t) \in [-\overline{P_d}, \overline{P_c}] \tag{3.22}$$

where $E(t_i)$ and $E(t_j)$ are the stored energies of OESD at time t_i and t_j, $p(t)$ is the charging/discharging power of the OESD at time instant t, and $\overline{P_d}$ and $\overline{P_c}$ are the maximum discharging and charging power of the OESD, respectively. It can be seen that if $E(t_j) - E(t_i) < 0$, OESD discharges from t_i to t_j; otherwise, OESD is charged.

Here the state of energy (SOE) is introduced to represent the energy status of OESD at time t, and it is defined as (3.23).

$$SOE(t) = \frac{E(t)}{E_{cap}} \tag{3.23}$$

where $SOE(t)$ is the SOE of the OESD at time t, and E_{cap} is the capacity of the OESD. Thus, the energy status of the OESD at time t_j can be expressed in (3.24).

$$SOE(t_j) = \frac{E(t_i)}{E_{cap}} + \frac{1}{E_{cap}} \int_{t_i}^{t_j} p(t)dt \tag{3.24}$$

In this thesis, both the charging/discharging process of the OESD are discretised, as shown in Figure 3.2. Therefore, (3.22) can be transformed into equation (3.25).

$$E_j - E_i = \sum_{t=i}^{j} p_t \Delta t_i, \quad -\overline{P_d} \leq p_t \leq \overline{P_c} \tag{3.25}$$

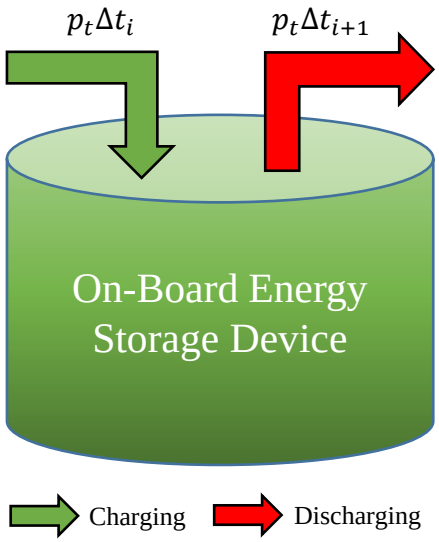

Figure 3.2: The discrete discharging/charging process of OESD

Similarly, the energy status of the OESD in the discrete form can also be obtained as (3.26)

$$SOE_j = \frac{E_i}{E_{cap}} + \frac{1}{E_{cap}} \sum_{t=i}^{j} p_t \Delta t_i \tag{3.26}$$

The continuous charging/discharging model of the OESD is transformed into the discrete form (3.25) and (3.26), respectively.These equations will be integrated with the discrete energy-efficient train control model in this thesis to solve different type of problems.

3.5 Linearisation Techniques

When dealing with complex and nonlinear systems or problems, linearisation is often used to simplify and approximate the system with acceptable accuracy or to model the conditions selected that cannot be expressed in an analytical form. In this thesis, linearisation of the discrete train control and OESD charging/discharging model are conducted by applying and modifying the well-established modelling techniques.

3.5.1 Either-Or Conditions

Consider two conditions (3.27) and (3.28) in the problem:

$$\sum_{j=1}^{J} a_{1j}x_j \leq b_1 \tag{3.27}$$

$$\sum_{j=1}^{J} a_{2j}x_j \leq b_2 \tag{3.28}$$

Where at least one of the conditions (3.27) or (3.28) is satisfied

To realise this logical determination in the modelling, a binary variable y, and sufficiently large upper bounds M_1 and M_2, which are upper bounds on the activity of the constraints, are introduced. The bounds are chosen such that they are as tight as possible, while still guaranteeing that the left-hand side of constraint i is always smaller than $b_i + M_i$. The constraints can be rewritten as in (3.29) and (3.30).

$$\sum_{j=1}^{J} a_{1j}x_j \leq b_1 + M_1 y \tag{3.29}$$

$$\sum_{j=1}^{J} a_{2j}x_j \leq b_2 + M_2(1 - y) \tag{3.30}$$

When $y = 0$, constraint (3.29) is imposed, and constraint (3.30) is weakened to the following: $\sum_{j=1}^{J} a_{2j}x_j \leq b_2 + M_2(1 - y)$, which will always be non-binding. Constraint (3.30) may still be satisfied. When $y = 1$, the situation is reversed. Thus, in all cases one of the constraints is imposed, and the other constraint may also hold.

3.5.2 Piecewise Linearisation

Consider a simple example with only one nonlinear term to be approximated. Figure 3.3 shows the curve divided into three pieces that are approximated by straight lines. This approximation is known as piecewise linearisation. The points where the slope of the piecewise linear function changes (or its domain ends) are referred to as breakpoints. This approximation can be mathematically expressed in several ways. Two approximation methods are used in this thesis: Special Ordered Sets 2 (SOS2) and Logical Model [98].

Special Ordered Sets 2 (SOS2)

Special Ordered Sets 2 (SOS2) is a set of non-negative variables, in which at most two variables can be nonzero. In addition, the two variables must be adjacent to each other in the fixed-order list.

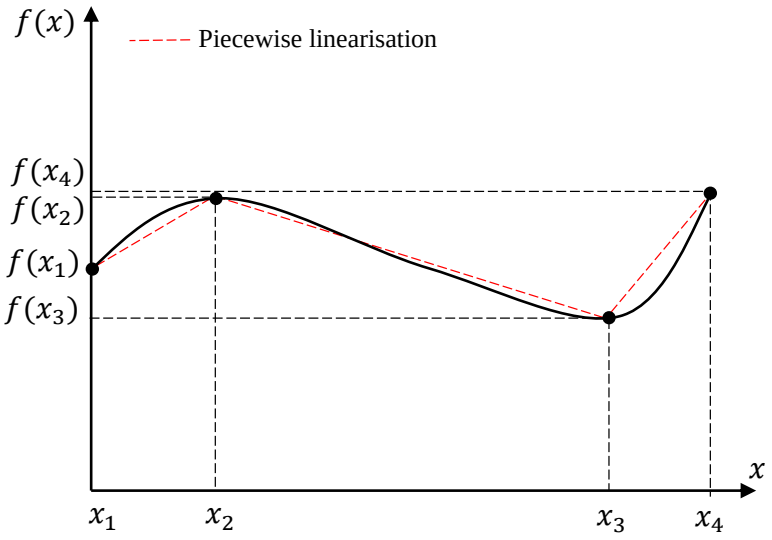

Figure 3.3: Schematic of use of SOS2 for linearisation

As shown in Figure 3.3, let x_1, x_2, x_3 and x_4 denote the four breakpoints along the x-axis, and let $f(x_1)$, $f(x_2)$, $f(x_3)$ and $f(x_4)$ denote the corresponding function values. Note that any point between two breakpoints is a weighted sum of these two breakpoints.

Let α_1, α_2, α_3 and α_4 denote the four non-negative weights such that their sum is 1. Then the piecewise linear approximation of $f(x)$ in Figure can be written as (3.31) - (3.35).

$$f'(x) = \alpha_1 f(x_1) + \alpha_2 f(x_2) + \alpha_3 f(x_3) + \alpha_4 f(x_4) \tag{3.31}$$

$$\alpha_1 x_1 + \alpha_2 x_2 + \alpha_3 x_3 + \alpha_4 x_4 = x \tag{3.32}$$

$$\alpha_1 + \alpha_2 + \alpha_3 + \alpha_4 = 1 \tag{3.33}$$

$$\alpha_1 + \alpha_2 - \epsilon_1 \geq 0, \quad \alpha_2 + \alpha_3 - \epsilon_2 \geq 0, \quad \alpha_3 + \alpha_4 - \epsilon_3 \geq 0 \tag{3.34}$$

$$\epsilon_1 + \epsilon_2 + \epsilon_3 = 1, \quad \epsilon_1, \epsilon_2, \epsilon_3 \quad \text{binary} \tag{3.35}$$

where ϵ_1, ϵ_2 and ϵ_3 are the binary variables, and (3.34) and (3.35) are imposed to ensure that that at most two adjacent α's are greater than zero. The SOS2 constraints for all separable functions together guarantee that the points $(x, f'(x))$ always lie on the approximating line segments.

Logical Model

A logical model can be used to build the piecewise linear functions. Similarly, as shown in Figure 3.4, let x_1, x_2, x_3 and x_4 denote the four breakpoints along the x-axis, let $f(x_1)$, $f(x_2)$, $f(x_3)$ and $f(x_4)$ denote the corresponding function values, and let k_1x+c_1, k_2x+c_2 and k_3x+c_3 denote the corresponding piecewise linear functions. In contrast to SOS2, the linear coefficients k_1, k_2 and k_3 and constants c_1, c_2 and c_3 of each line segment need to be calibrated based on the x and $f(x)$ values.

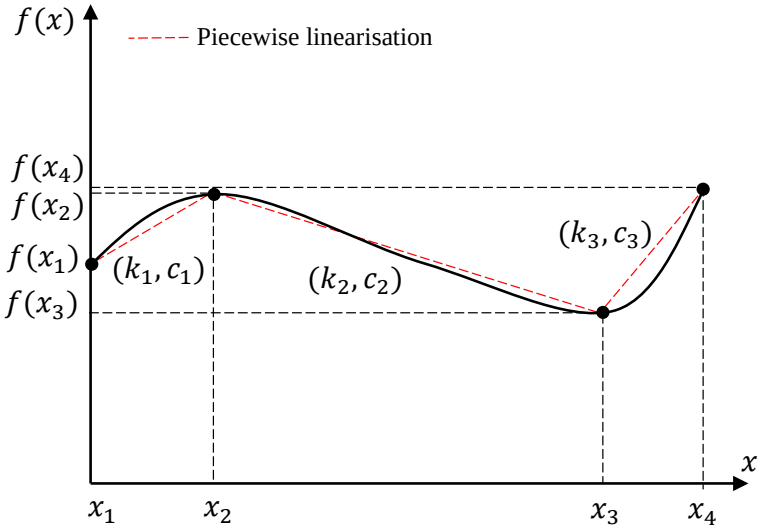

Figure 3.4: Schematic of the use of a logical model for linearisation

Using binary variables λ_1, λ_2, and λ_3, and auxiliary variables x'_1, x'_2 and x'_3, the piecewise linear approximation of $f(x)$ in the figure can be written as (3.36) - (3.39).

$$f'(x) = k_1x'_1 + c_1\lambda_1 + k_2x'_2 + c_2\lambda_2 + k_3x'_3 + c_3\lambda_3 \tag{3.36}$$

$$x'_1 + x'_2 + x'_3 = x \tag{3.37}$$

$$\lambda_1x_1 \leq x'_1 \leq \lambda_1x_2, \quad \lambda_2x_2 \leq x'_2 \leq \lambda_2x_3, \quad \lambda_3x_3 \leq x'_3 \leq \lambda_3x_4, \tag{3.38}$$

$$\lambda_1 + \lambda_2 + \lambda_3 = 1 \tag{3.39}$$

It can be observed that when $\lambda_1 = 1$, then $\lambda_2 = \lambda_3 = 0$. $x = x_1'$ in the range of $[x_1, x_2]$, and the approximating function is selected as $f'(x) = k_1 x + c_1$. The logical model formulates the selection of piecewise linear functions by adjusting the value of different λ.

3.5.3 Linearising Products of Variables

This section details a method for linearising the products of variables that are incorporated in the modelling [98]. In general, a product of two variables can be replaced by a new variable, on which a number of constraints are imposed. The extension to products of more than two variables is straightforward, and because the lineraisation process of products of more than three variables is not applied in the thesis, this part mainly demonstrates the basic linearisation techniques based on two variables.

Two Binary Variables

First, we consider the binary variables x_1 and x_2. Their product, $x_1 x_2$, can be replaced by an additional binary variable y. The following constraints (3.40) -(3.42) force y to take the value of $x_1 x_2$.

$$y \leq x_1 \tag{3.40}$$

$$y \leq x_2 \tag{3.41}$$

$$y \geq x_1 + x_2 - 1 \tag{3.42}$$

Two Continuous Variables

Second, the product of two continuous variables can be converted into a separable form. Suppose the product $x_1 x_2$, where $x_1 \in [l_1, u_1]$ and $x_2 \in [l_2, u_2]$, must be transformed. Two additional continuous variables y_1 and y_2 need to be introduced in the modelling, and the following constraints (3.43) -(3.45) need to be imposed.

$$y_1 = \frac{1}{2}(x_1 + x_2) \tag{3.43}$$

$$y_2 = \frac{1}{2}(x_1 - x_2) \tag{3.44}$$

$$\frac{1}{2}(l_1 + l_2) \leq y_1 \leq \frac{1}{2}(u_1 + u_2), \quad \frac{1}{2}(l_1 - u_2) \leq y_2 \leq \frac{1}{2}(u_1 - l_2) \tag{3.45}$$

In this case, the term $x_1 x_2$ can be represented by the separable function $y_1^2 - y_2^2$,

which can be approximated by using SOS2 or logical model detailed in the previous section.

3.6 Mixed Integer Linear Programming

MILP problem has an objective function and constraints that are linear with integer variables presented [99]. Different from the linear optimization problems, at least some of the variables in MILP problems are constrained to take on integer values. The general form of the MILP problem is shown in (3.46).

$$\begin{aligned}
\min \quad & c_0 + \sum_{i=1}^{n} c_i x_i \\
\text{s.t.} \quad & \sum_{i=1}^{n} A_j^e x_i = b_j^e, && \forall j = 1, ..., l_e \\
& \sum_{i=1}^{n} A_j^{ine} x_i \leq b_j^{ine}, && \forall j = 1, ..., l_{ine} \\
& x_i \in \mathbb{Z}, && \text{for some} \quad i = 1, ..., n \\
& x_i \in \mathbb{R}, && \text{for the remaining} \quad i = 1, ..., n,
\end{aligned} \tag{3.46}$$

where $x_1, ..., x_n$ are the decision variables to be optimised. l_e and l_{ine} are the numbers of equality and inequality constraints, respectively. Thus, l_e+l_{ine} represents the total number of constraints. The coefficients, A_j^e, A_j^{ine}, l_e and l_{ine}, the terms on the right-hand sides of the constraints, b_j^e and b_j^{ine} and the coefficients, $c_o, ..., c_n$, in the objective function are all constants. Because the optimal train driving strategy with OESD for electrified railway systems is formulated into an MILP problem, the constraints and objective of the model need to be adjusted according to the specific problem.

3.7 Convex Optimisation

Different from the objective function and constraints that are linear in MILP problem shown in the previous section, for some complex and real systems, only the nonlinear relationships (functions) between each variable can be found. One of the nonlinear functions, the convex function, is well known and studied among various optimisation methods owing to convex optimisation problems.

The standard form of a convex optimisation problem is shown in (3.47)

$$\begin{aligned} \min \quad & f_0(x) \\ \text{s.t.} \quad & f_i(x) \leq 0, \qquad \forall i = 1, ..., m \\ & a_i^T x = b_i, \qquad \forall i = 1, ..., p \end{aligned} \tag{3.47}$$

where the objective function is $f_0(x)$, the inequality constraint $f_1, \cdots, f_m$ must be convex, and the equality constraint function $h_i(x) = a_i^T = b_i$ must be affine.

Convex functions and convex optimisation have many fundamental properties [100], and three of which are used in this thesis, and listed as follows:

1. A function $f(x)$ is convex if and only if its second-order derivative $f''(x) \geq 0$ or its Hessian matrix $\mathbf{H} \geq 0$ (positive semi-definite) in the domain.

2. If $f(x)$ and $g(x)$ are both convex, then $h(x) = f(x) + g(x)$ is also convex. This property can be extended to the sum of a limited number of convex functions.

3. For the convex optimisation problem, its local optimal point is also its global optimal point.

Property 1 can be used to check whether the functions (including the objective function and constraints) in the optimisation problem are convex. Based on Property 2, the combination of different functions to fit a specific problem with the convexity remaining can be adopted. For most nonlinear optimisation problems, commercial solvers can only find the local optimal point but not the global one. However, Property 3 offers the proof that the global optimum can be located, and the nonlinear optimisation problem belongs to convex optimisation problems.

3.8 Monte-Carlo Simulation

Monte-Carlo simulation, also known as the Monte-Carlo Method or multiple probability simulation, is a mathematical technique that is used to estimate the possible outcomes of an uncertain event [101, 102]. Unlike a normal forecasting model, Monte-Carlo simulation predicts a set of outcomes based on an estimated range of values versus a set of fixed input values. In other words, a Monte-Carlo Simulation builds a model of possible results by leveraging a probability distribution, such as a uniform or normal distribution, for any variable that has inherent uncertainty. Then it recalculates the results over and over, each time using a different set of random numbers between the

minimum and maximum values. In a typical Monte-Carlo experiment, this exercise can be repeated thousands of times to produce a large number of likely outcomes.

Normally, the Monte-Carlo techniques involves three basic steps:

- Set up a predictive model, identifying both the dependent variable to be predicted and the independent variables (also known as the input, risk or predictor variables) that will drive the prediction.
- Specify the probability distributions of independent variables. Use historical data and/or the analyst's subjective judgement to define a range of likely values and assign probability weights for each value.
- Run simulations repeatedly to generate random values of the independent variables. This is done until sufficient results are gathered to make up a representative sample of the near infinite number of possible combinations.

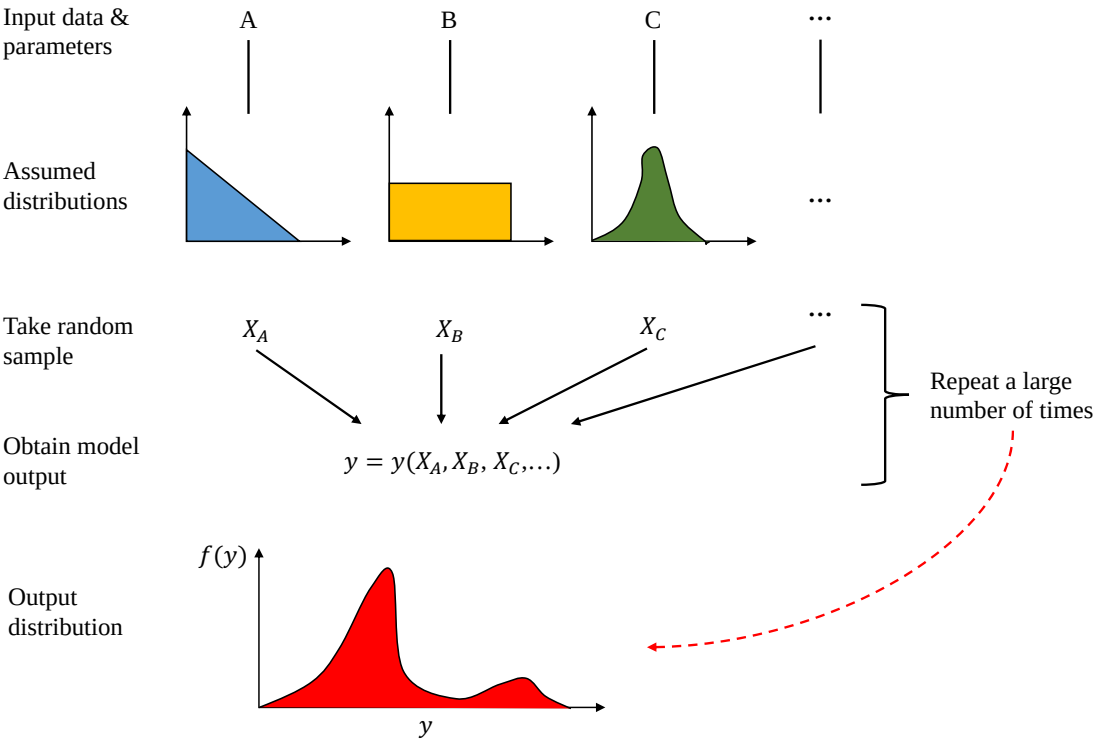

Figure 3.5: Schematic of the Monte-Carlo simulation process

Overall, Monte-Carlo methods offer a common statistical model for simulating physical systems and are especially useful for modelling systems with variable and uncertain inputs, as shown in Figure 3.5.

3.9 Summary

In this chapter, the applied modelling, optimisation and simulation methods are introduced. Traditional continuous energy-efficient train control models, discrete train control model and discrete OESD discharging/charging model are elaborated. Then, the linearisation techniques, MILP, convex optimisation and Monte-Carlo simulation are detailed upon.

It should be noted that the suitable application scenarios for time-based and distance-based model rely on the specific problems to be solved, and in different scenarios they have their own advantages and disadvantages. Time-based model is normally used in solving the the train control optimisation problem considering temporal constraints or variables, for example, the signalling system constraints, running time constraints or constraints of coordination with other trains etc., which is not easy when using distance-based model. In contrast, time-based model is difficult to model spatial constraints or variables, such as gradient constraints, speed limit constraints and the constraints related to the power supply section etc. whereas distance-based model is applied widely when these constraints are considered. In this thesis, since more spatial constraints and conditions are involved, the distance-based discrete model is employed to conduct the studies.

Chapter 4

Intelligent Train Operation with OESD in an Inter-Station Section

The main content of this chapter is from the author's published article in a version with minor reconfiguration to fit the structure and context of this thesis. The published article is:

C. Wu, W. Zhang, S. Lu, Z. Tan, F. Xue and J. Yang, "Train Speed Trajectory Optimization with On-Board Energy Storage Device," *IEEE Transactions on Intelligent Transportation Systems*, vol. 20, no. 11, pp. 4092-4102, 2019.

4.1 Introduction

In this chapter, an integrated model to optimise the train speed trajectory with OESD is established by using the MILP with the objective to reduce the net energy consumption of the system. Based on the model, the influence of the OESD on optimal train operation is also shown with case studies for comparisons in this chapter.

With the development of the energy storage technologies, increasing number of OESD have been applied in the modern railway systems [10]. Some studies have been conducted to manage the OESD system to enhance the efficiency of battery [103–105], where the recovery rate of regenerative braking energy is increased. Some studies indicate that OESD has evident effect on reducing energy consumption [106–108]. In addition, Miyatake *et al.* investigate the optimal control with OESD in several papers [89, 90, 109, 110]. In these papers, the objective is to minimise the energy

consumed by the substations considering state of charge (SOC) and [89] and [106] conclude that the introduction of the OESD has insignificant impact on train speed trajectory. However, the influence of OESD properties (capacity, initial SOE and degradation) on optimal speed trajectory are not investigated. Meanwhile, the optimal discharging/charging strategy of OESD operation is not analysed in the existing works, which weakens the understanding of the energy-saving potential and possible impact of the OESD on the railway systems.

In this chapter, from the perspective of the energy conversion and the law of conversion of energy, the train operation and OESD are combined together in a general mathematical model to achieve the energy-saving system operation. The contributions of this chapter are listed as follows:

- The optimisation problem on train speed trajectory with OESD is solved by applying MILP. The train motion, energy conversion and OESD discharging/charging process are linearised in an integrated mathematical form with objective to minimise the net energy consumption of the system.
- The influence of the OESD capacity, initial SOE and degradation on the optimal train operation are presented based on the proposed model. The insightful comparisons are given by the case studies with several typical scenarios.
- From a general scenario, the proposed method can bring a more than 11.6% energy-saving rate when compared with the train without OESD. Showing the energy-saving potential of the OESD as well as the proposed method.

4.2 Integrated Model for Train with OESD

Notation of variables	
v_i^2	Square of train speed in the position of $\sum_1^{i-1} \Delta d_i$ [m^2/s^2]
$\Delta E_{i,s}$	Energy from the substation in Δd_i [kJ]
$\Delta E_{i,dch}$	Energy discharged from the OESD in Δd_i [kJ]
$\Delta E_{i,ch}$	Energy charged to the OESD in Δd_i [kJ]
$\Delta E_{i,r}$	Energy transmitted to the resistor from the motor in Δd_i [kJ]
λ_i	Binary variables to determine the train operation mode in Δd_i
$\alpha_{i,j} \in [0,1]$	SOS2 variable set for linearisation of nonlinear speed-related constraints

(Continued from last page)	
$\beta_{i,j} \in [0,1]$	SOS2 variable set for linearisation of nonlinear speed-related constraints
$\mu_{i,j}^{\alpha}$	Binary variables in SOS2 variable set
$\mu_{i,j}^{\beta}$	Binary variables in SOS2 variable set
Assumption	
	The regenerative braking energy can only be recovered by OESD or dissipated by resistors but cannot be fed back to the substation or used by other trains.

4.2.1 Energy Flow among Train, OESD and Substation

From Section 3.3, it can be seen that the proposed discrete train control model is distance-based, thus the train model and OESD model both need to be modified to fit in each step of Δd_i in the integration process. For the train itself, due to the split of the energy supply (from both substation and OESD), original ΔE_i needs to be replaced by different variables in different situations. For the OESD, the discrete time-based charging/discharging model in Section 3.4 also needs transformation, as shown in Figure 4.1 where the train and OESD operation are both discretised based on distance.

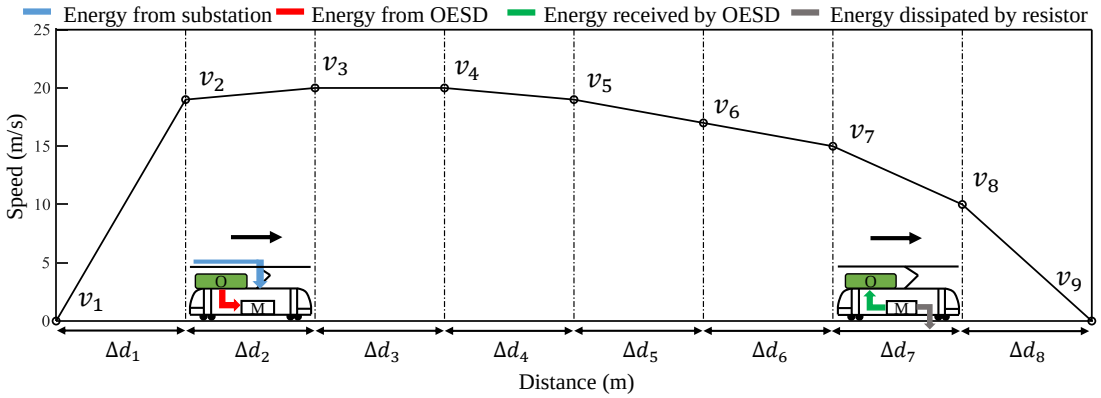

Figure 4.1: A schematic of the speed trajectory and energy flow of the train with OESD on a discretised track. The number of Δd_i, denoted by N, is 8 thus there are 9 v_i in total. "O" is the OESD and "M" is the motor

Here $\Delta E_{i,m}^{+}$ is denoted as the traction energy supplied by motor in distance segment Δd_i, and $\Delta E_{i,m}^{-}$ is used to represent the energy generated by the motor in braking mode. When the train conducts traction operation, $\Delta E_{i,m}^{+}$ can be expressed as (4.1), and the motor consumes both the energy from the traction substation, $E_{i,s}$, through

catenary/third rail with efficiency η_s and the energy from the OESD, $E_{i,dch}$, with efficiency η_o. When the train conducts braking, the regenerative braking energy $\Delta E^-_{i,m}$ would be recovered by OESD with efficiency η_o or dissipated by resistor, which can be expressed by using (4.2)

$$\Delta E^+_{i,m} = \Delta E_{i,s} \cdot \eta_s + \Delta E_{i,dch} \cdot \eta_o, \quad \forall i = 1, 2, ..., N \tag{4.1}$$

$$\Delta E^-_{i,m} = \frac{\Delta E_{i,ch}}{\eta_o} + \Delta E_{i,r}, \quad \forall i = 1, 2, ..., N \tag{4.2}$$

where the η_s is to specify the total efficiency for the motor with the driving system and energy transmission from substation to the motor through the grid; similarly, η_o here is to specify the total efficiency for the motor with the driving system and energy conversion from the OESD.

For OESD, its SOE can be expressed by using (4.3) based on the proposed model.

$$0 \leq SOE_i = \frac{E_{ini} - \sum_1^{i-1} \Delta E_{i,dch} + \sum_1^{i-1} \Delta E_{i,ch}}{E_{cap}} \times 100\% \leq 100\%, \quad \forall i = 1, 2, ..., N \tag{4.3}$$

where E_{ini} is the initial available energy in the OESD when the train departs, and a [0,100%] range needs to be imposed to ensure a valid SOE in real applications. E_{cap} is the capacity of the adopted OESD.

For the train motor, (4.4) and (4.5) are used to ensure the force and power that the motor supplies in both traction mode and braking mode does not exceed the maximum traction force $\overline{F_t}$ and maximum braking force $\overline{F_b}$, and maximum traction power $\overline{P_t}$ and maximum braking power $\overline{P_b}$.

$$\Delta E^+_{i,m} \leq \overline{F_t} \Delta d_i, \quad \Delta E^-_{i,m} \leq \overline{F_b} \Delta d_i, \quad \forall i = 1, 2, ..., N \tag{4.4}$$

$$\Delta E^+_{i,m} \leq \overline{P_t} \Delta t_i, \quad \Delta E^-_{i,m} \leq \overline{P_b} \Delta t_i, \quad \forall i = 1, 2, ..., N \tag{4.5}$$

For the OESD, the power for the input and output energy cannot exceed the maximum charging and discharging power, as shown in (4.6).

$$\Delta E_{i,dch} \leq \overline{P_o} \Delta t_i, \quad \Delta E_{i,ch} \leq \overline{P_o} \Delta t_i, \quad \forall i = 1, 2, ..., N \tag{4.6}$$

According to the law of the conservation of energy, if the train is in traction mode,

in each Δd_i the transformation of the energy can be expressed as in (4.7).

$$\Delta E^{+}_{i,m} - \frac{1}{2}(M_t + M_o)(v^2_{i+1} - v^2_i) - R_i \Delta d_i - (M_t + M_o) g \theta_i \Delta d_i - \Delta E_{i,r} = 0, \quad \forall i = 1, 2, ..., N \tag{4.7}$$

Similarly, when the train is braking, in each Δd_i the transformation of the energy can be expressed as in (4.8).

$$-\Delta E^{-}_{i,m} - \frac{1}{2}(M_t + M_o)(v^2_{i+1} - v^2_i) - R_i \Delta d_i - (M_t + M_o) g \theta_i \Delta d_i - \Delta E_{i,r} = 0, \quad \forall i = 1, 2, ..., N \tag{4.8}$$

where M_t is the mass of the train and M_o is the mass of OESD, R_i is the drag force, g is the gravitational constant and θ_i is the gradient of Δd_i.

4.2.2 Selection of Operation Modes of Train and OESD

As shown in Figure 4.2, it can be easily observed that when the train is in traction mode, $\Delta E^{+}_{i,m} \geq 0$, the energy from both the substation and the OESD are used by the motor and transformed into kinetic energy, heat and potential energy; when the train conducts braking, $-\Delta E^{-}_{i,m} \leq 0$, the kinetic energy is transformed into heat, potential energy and energy recovered by the OESD.

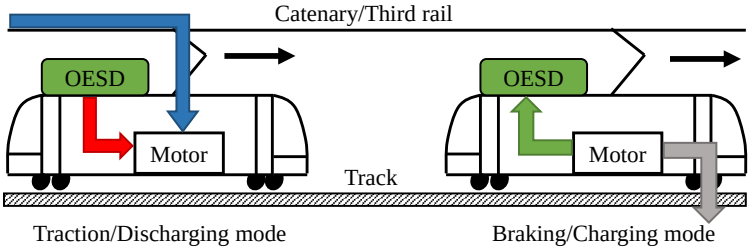

Figure 4.2: Schematic of different operation mode for a typical train with OESD in each Δd_i

However, it should be noted that $\Delta E^{+}_{i,m}$ and $-\Delta E^{-}_{i,m}$ cannot exist at the same time since the train is unable to conduct traction and braking simultaneously, and the OESD is unable to be charged or discharge simultaneously as well. This also means that when there are $\Delta E_{i,s}$ and $\Delta E_{i,dch}$, there are no $\Delta E_{i,ch}$ and $\Delta E_{i,r}$ existing at the same time, and vice versa. In this case, the binary variables λ_i are introduced to determine the train and OESD operation modes in each Δd_i. Thus, (4.7) and (4.8) are formulated as

the Either-or conditions (see Section 3.5.1), as shown in (4.9)and (4.10).

$$\Delta E_{i,s} \leq \lambda_i L_1, \quad \Delta E_{i,dch} \leq \lambda_i L_1, \quad \forall i = 1, 2, ..., N \tag{4.9}$$

$$\Delta E_{i,ch} \leq (1 - \lambda_i) L_2, \quad \Delta E_{i,r} \leq (1 - \lambda_i) L_2, \quad \forall i = 1, 2, ..., N \tag{4.10}$$

where L_1 and L_2 are two sufficiently large numbers.

It can be seen that when λ_i is 1, (4.7) is imposed and (4.8) is relaxed, the train is in traction mode, and the OESD and substation are able to jointly support the train's running. In contrast, when λ_i is 0, (4.8) is imposed and (4.7) is relaxed, the train is braking, and the OESD can be charged to receive the regenerative braking energy.

4.2.3 Linearisaiton of Nonlinear Speed-Related Constraints

In the model, the square of train speed v_i^2 are regarded as the variables to be optimised, this is convenient for establishing the linear relationship between the speed and energy variables, while leads to the nonlinear relationships as shown in the elapsed time Δt_i (3.13) and discrete drag force constraint (3.16) due to the nonlinear relationship among v_i^2, v_i, $v_{i,ave}^2$ and $\frac{1}{v_{i,ave}}$. For transferring the nonlinear constraints in (3.13) and (3.16), the SOS2 method is used (see Section 3.5.2).

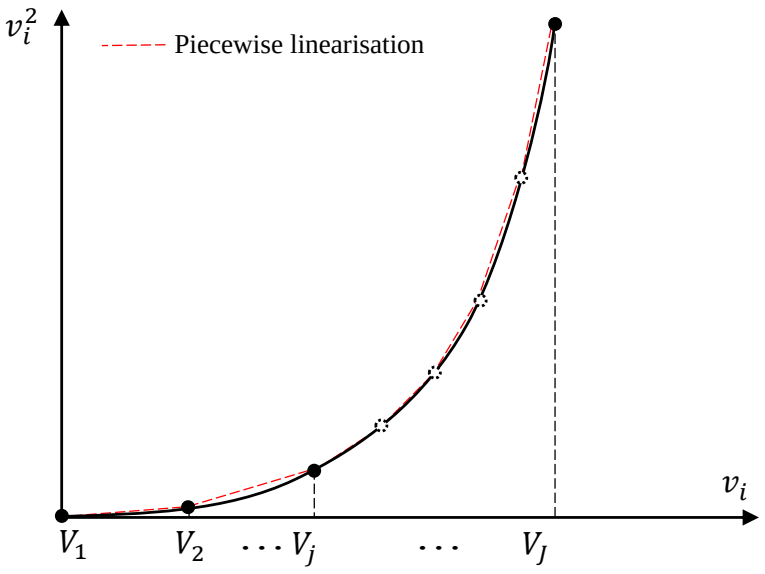

Figure 4.3: An example to show the piecewise linearisation of the v_i^2 and v_i using SOS2

To linearise these relationships, the speed value range is divided into J sections and a series of breakpoints are chosen to represent the speed within the range from V_1 to

V_J, as shown in Figure 4.3 which demonstrates the linearisation between v_i^2 and v_i. In this case, two sets of SOS2 α_i and β_i are applied, as shown in (4.11) - (4.13).

$$v_i^2 = \sum_{j=1}^{J_1} V_j^2 \alpha_{i,j}, \quad v_i^{'} = \sum_{j=1}^{J} V_j \alpha_{i,j}, \quad \forall i = 1, 2, ..., N \tag{4.11}$$

$$v_{i,ave}^{'} = \frac{v_i^{'} + v_{i+1}^{'}}{2} = \sum_{j=1}^{J} V_j \beta_{i,j}, \quad \forall i = 1, 2, ..., N \tag{4.12}$$

$$v_{i,ave}^{'2} = \sum_{j=1}^{J} V_j^2 \beta_{i,j}, \quad \frac{1}{v_{i,ave}^{'}} = \sum_{j=1}^{J} \frac{1}{V_j} \beta_{i,j}, \quad \forall i = 1, 2, ..., N \tag{4.13}$$

The SOS2 series also need to satisfy (4.14) and (4.15).

$$\sum_{j=1}^{J} \alpha_{i,j} = 1, \quad \sum_{j=1}^{J} \beta_{i,j} = 1, \quad \forall i = 1, 2, ..., N \tag{4.14}$$

$$0 \leq \alpha_{i,j} \leq 1, \quad 0 \leq \beta_{i,j} \leq 1, \quad \forall i = 1, 2, ..., N \tag{4.15}$$

To ensure that only the adjacent $\alpha_{i,j}$ and $\beta_{i,j}$ can be nonzero and their sum being 1, additional binary variables $\mu_{i,j}^{\alpha}$ and $\mu_{i,j}^{\beta}$ need to be imposed, as shown in (4.16) to (4.17).

$$\alpha_{i,j} + \alpha_{i,j+1} - \mu_{i,j}^{\alpha} \geq 0, \quad \beta_{i,j} + \beta_{i,j+1} - \mu_{i,j}^{\beta} \geq 0, \quad \forall i = 1, 2, ..., N \tag{4.16}$$

$$\sum_{j=1}^{J-1} \mu_{i,j}^{\alpha} = 1, \quad \sum_{j=1}^{J-1} \mu_{i,j}^{\beta} = 1, \quad \forall i = 1, 2, ..., N \tag{4.17}$$

As a result, the nonlinear constraints (3.13) and (3.16) are linearised by replacing $v_{i,ave}$, $v_{i,ave}^2$ and $1/v_{i,ave}$ with their respective linearly approximated value $v_{i,avg}^{'}$, $v_{i,ave}^{'2}$ and $1/v_{i,ave}^{'}$ respectively, and can be rewritten as (4.18) and (4.19).

$$\Delta t_i = \frac{\Delta d_i}{v_{i,ave}^{'}}, \quad \forall i = 1, 2, ..., N \tag{4.18}$$

$$R_i = R_0 + R_1 v_{i,ave}^{'} + R_2 v_{i,ave}^{'2}, \quad \forall i = 1, 2, ..., N \tag{4.19}$$

4.2.4 Objective: Net Energy Consumption Minimisation

In the model, it is assumed that the regenerative braking energy cannot be fed back to the substation. The energy recovered by the OESD can be used in the next journey, which helps reduce the traction energy consumption. Thus, similar as the existing continuous model (3.11), the objective function of the integrated model is the difference of the traction energy consumption and regenerative braking energy recovered by the OESD, which can also be called as net energy consumption, as shown in (4.20).

$$\min \quad \sum_{i=1}^{N} \underbrace{(\Delta E_{i,s} + \Delta E_{i,dch}}_{\text{Traction energy consumption}} - \underbrace{\Delta E_{i,ch})}_{\text{Energy recovered by the OESD}} \tag{4.20}$$

By solving this model, the optimal solution v_1^2, v_2^2, v_3^2,...,v_{N+1}^2 can be found, and each v_i, namely the optimal speed points, can be obtained easily. By linking them together, the optimal train speed trajectory shown can be presented. The MILP algorithm exploits the solution space to find the minimum net energy consumption. For achieving the objective of minimising the traction energy and maximising the recovered energy, the model integrates both of the train and OESD's properties together to optimise the train operation and the discharging/charging strategy of the OESD.

4.3 Numerical Experiments

In this section, the numerical experiments are conducted to show the effectiveness of the proposed model in finding the optimal train and OESD operation concurrently. They are all based on the general cases but not real-world systems in order to present the generality of the model, in which the capacity, initial SOE, degradation of the OESD as well as the complex route conditions are introduced to test the robustness of the model. The experiments also give a comparison of influence of the OESD on optimal train operation. Noted that the model is solved by using CPLEX 12.8.0 on a PC with Intel Core i5-6500 processor (3.20 GHz) and 8-GB RAM.

4.3.1 Parameters Set-Up and Performance Test

Parameters Adopted in Experiments

As shown in Table 4.1, the running time is set to be 100 s and initial SOE and capacity of the OESD are 0% and 8.33 kWh (30 MJ) respectively in the performance test and without any speed limits and gradients variation. The mass of the OESD needs to be

obtained, and a supercapacitor is assumed to be adopted thus specific energy, which is also called energy density, can be known as in the range of 0.72-18 kJ/kg [10]. Therefore, a specific value e.g. 18 kJ/kg is selected then the mass of the adopted OESD M_o can be calculated as $8.3 \times 3600/18/1000$ =1.7 t. The mass of the train M_t is assumed to be 176.3 t, thus the total mass $M_t + M_o$ of the train with OESD is 176.3+1.7=178 t. Noted that the room for passengers and that for the OESD are separate. In the existing applications, the OESD can be installed on the roof of the car/under the car, or can be separated into several packs installed in the places that will not influence passenger space and riding comfort or reduce the train capacity.

Table 4.1: Parameters adopted in a journey for a typical train with OESD

$M_t + M_o$ (t)	$\overline{P_t}$ (kW)	$\overline{P_b}$ (kW)	$\overline{a_a}$ (m/s^2)	$\overline{a_d}$ (m/s^2)	$\overline{P_o}$ (kW)	D (m)
178	5000	5000	1.2	1.2	500	1800
η_s	η_o	$\overline{F_t}$ (kN)	$\overline{F_b}$ (kN)	R_0 (kN)	R_1 (kN $\cdot$ s/m)	R_2 (kN $\cdot$ s^2/m^2)
0.81	0.88	200	200	2.0895	0.0098	0.0065

As for the values of η_s and η_o in Table 4.1, in general, η_o is greater than η_s due to its absence of line losses and the higher transmission losses of the grid [111] based on the data from the current research. The energy from substation needs to be transmitted to the train motor via the catenary/third rail with a transmission efficiency and this value is normally to be 90% due to a 10% average energy loss [111]. It is known that the state-of-the-art train motor can reach a 97% high traction efficiency [111] thus can locate the approximate transmission efficiency of the train motor in the numerical experiment to be about 90%. Therefore, an approximate value for η_s, $90\% \times 90\% = 81\%$, can be obtained. For the OESD, the motor can use the energy from it directly with its traction efficiency but no transmission line loss. Normally the discharging and charging efficiency of the ESD is relatively high e.g. 90%-100% for supercapacitor [8]. Therefore, the value for η_o is $90\% \times 98\% = 88\%$, and it is chosen to be approximately 0.9. Both values can be modified according to the field data collected from different types of railway power supply system, different rolling stocks and different types of OESD. The values for maximum traction/braking power in the performance test and case studies are set to be same. The same thing to maximum traction/braking force as well as the maximum allowed acceleration and deceleration. All of these parameters in Table 4.1 can be modified when this model is applied in the train operation optimisation for real-world systems.

Model Performance

The model performances are shown in Table 4.2 and Table 4.3. The Δd_i can be modified in the model and the shorter one can bring a more accurate result. In addition, the total number of the breakpoint J in SOS2 also influences the precision of the results and larger ones bring more precise results. It can bee seen that from $\Delta d_i = 200$ m to $\Delta d_i = 100$ m, the net energy consumption sees a notable decrease because the model becomes more precise to reflect the actual optimal train operation. From $\Delta d_i = 100$ m to $\Delta d_i = 10$ m, net energy consumption has no significant change while the computation time rises noticeably due to much more variables. Table 4.3 is obtained with $\Delta d_i = 100$ m in the test to check the influence of change of J on the precision of net energy consumption. The net energy consumption sees a significant drop from $J = 5$ to$J = 10$ while from $J = 10$ to $J = 45$ the reduction of the net energy consumption is not significant.

Table 4.2: Performance comparison with different value of Δd_i

Δd_i (m)	Problem Size*	Net Energy Consumption (kWh)	Computation Time (s)
200	788 / 370 / 2124	14.73	0.07
100	1535 / 721 / 4140	13.58	0.15
50	3029 / 1423 / 8172	13.60	0.88
20	7511 / 3529 / 20268	13.46	10.27
10	14981 / 7039 / 40428	13.49	25.94

* The number n_1 in the notation $n_1/n_2/n_3$ is the total variables, n_2 is the integer-valued variables, and n_3 is the number of constraints.

Table 4.3: Performance comparison with different J when Δd_i=100 m

J	Net Energy Consumption (kWh)	Computation Time (s)
5	19.25	0.06
10	13.58	0.15
15	13.45	0.20
20	13.16	0.20
45	13.16	0.26

Therefore, the more specific experiments below are all based on $\Delta d_i = 100$ m and $J = 10$ due to a good balance between computational efficiency and model precision. For real railway systems, both values can be set according to the different track conditions e.g. gradients or block sections and running constraints e.g. speed limits.

4.3.2 Optimal Operation with Different OESD Capacities

This section shows the optimal train speed trajectory given by the proposed model under the varying OESD capacities, where the influence of the OESD capacity on train operation and speed trajectory are investigated. 3 scenarios are given, where the capacity of the OESD is set to be 0 (Scenario 1), 5.55 kWh (20 MJ) (Scenario 2) and 8.33 kWh (30 MJ) (Scenario 3) respectively with same specific energy 18 kJ/kg and the initial SOE of the OESD are 0 for all the scenarios.

As shown in Figure 4.4 and Figure 4.5, the speed trajectories and discharging/charging operations see substantial differences when OESD's capacity is different. When the train runs with the OESD capacity being 0, which means that the train is without the OESD, there is no regenerative braking energy recovered, and only resistor is available to receive the energy in braking mode. In this situation, the train operation regimes is similar as the results brought by the optimal control theory (acceleration with maximum traction force, coasting and deceleration with maximum braking force [12]) and it has the longest coasting distance, which is from 300 m to 1600 m among the 3 scenarios, to reduce energy loss due to absence of regenerative braking energy recovery.

The optimal solution is affected when the OESD is introduced to this optimisation model. For the train with OESD capacity of 5.55 kWh, the initial speed of the coasting operation is raised to be slightly higher than that of the train without OESD. Additionally, the coasting distance is shortened while the braking distance is longer. Similarly, the speed trajectory for the train with OESD capacity of 8.33 kWh changes and the highest operation speed of the train is raised again with the much shorter coasting distance and longer braking distance.

Table 4.4: Results of Scenario 1-3

Scenario	$M_t + M_o$ (t)	E_{cap} (kWh)	Coasting Distance (m)	Braking Distance (m)	Largest Speed (m/s)	Net Energy Consumption (kWh)
1	176.3	0	1300	200	24.0	18.26
2	177.4	5.55	800	700	24.7	13.94
3	178	8.33	400	1000	25.5	13.59

The numerical results can be found in Table 4.4. Based on the outcomes of Scenario 1-3, it implies that when there is no OESD, the optimal solution is the operation with the longest coasting to reduce energy loss due to braking. If there is an OESD and an increase in OESD capacity, the optimisation model will choose to shorten the train's coasting distance and lengthened its braking distance because the regenerative braking

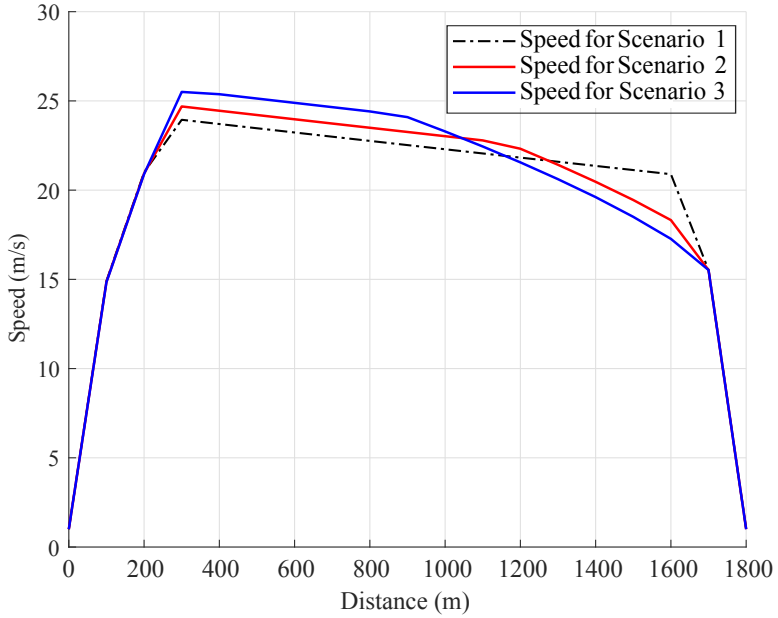

Figure 4.4: Optimal train speed trajectories for Scenario 1-3

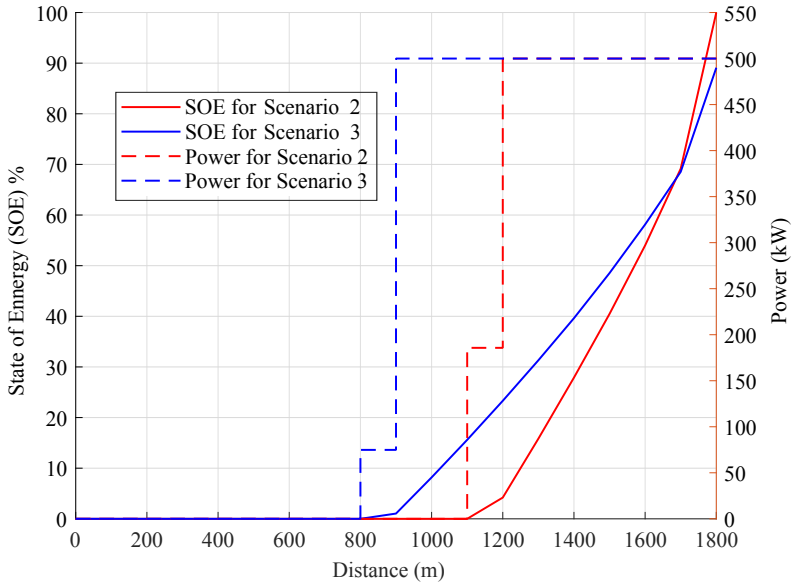

Figure 4.5: Optimal discharging and charging curves for Scenario 2-3

energy can be recovered by the OESD to achieve a more energy-saving operation rather than just depends on the coasting operation. It should be noted that with an increase of the OESD capacity, raising largest speed of the train will be observed, and the reason might be that higher speed can result in more recovery of the energy converted from

kinetic energy to compensate the traction energy supplied by the substation.

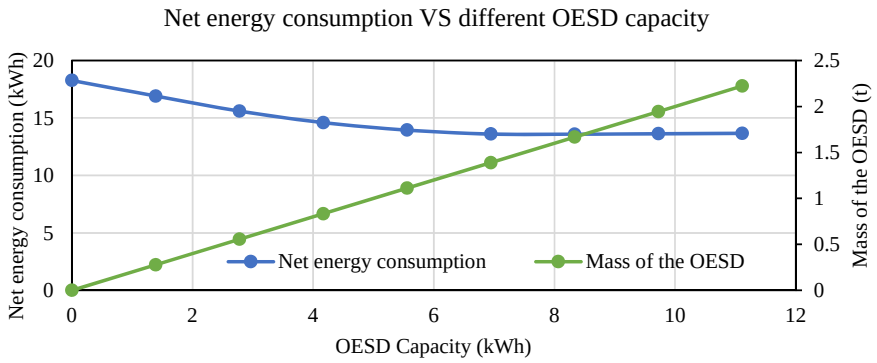

Figure 4.6: Relationship between net energy consumption and OESD capacity

Figure 4.6 illustrates the detailed trend in how the OESD capacity influences the net energy consumption of the train operation. It is easily observed that with the increase of OESD capacity, the net energy consumption decreases with a gradually-reduced changing rate. This implies that when the OESD capacity reaches a certain value, the net energy consumption also reaches the minimum value that cannot be reduced anymore. If the capacity of the OESD increases continually, the net energy consumption even raises slightly due to the increase of the total mass resulted from the heavier OESD. This clearly indicates that with the given running time and travel distance, the optimal OESD capacity which brings the minimum net energy consumption is unique. Locating this value of capacity will help reduce the unnecessary waste of OESD capacity i.e. the capital cost of railway operators.

4.3.3 Optimal Operation with Different OESD Initial SOE

This section is aimed at exploring more on the impact of the different initial SOE, which is another important engineering property of the OESD, on the optimal train operation. Another three scenarios, Scenario 4 (Initial SOE=16.7%), 5 (Initial SOE=66.7%) and 6 (Initial SOE100%), are given with the OESD capacity being 8.33 kWh. When the initial SOE of OESD is different, the optimal speed trajectory and the OESD discharging/charging strategy might change for adjusting their own operations to meet each other's constraints. In Figure 4.7 and Figure 4.8, for Scenario 4, the train speed trajectory with low initial SOE does not have notable change compared with Scenario 3 while the OESD is utilised for assisting the traction operation.

The speed trajectory changes noticeably when the initial SOE is higher, see Scenario 5 and Scenario 6 where both train's traction distances are lengthened significantly. Higher

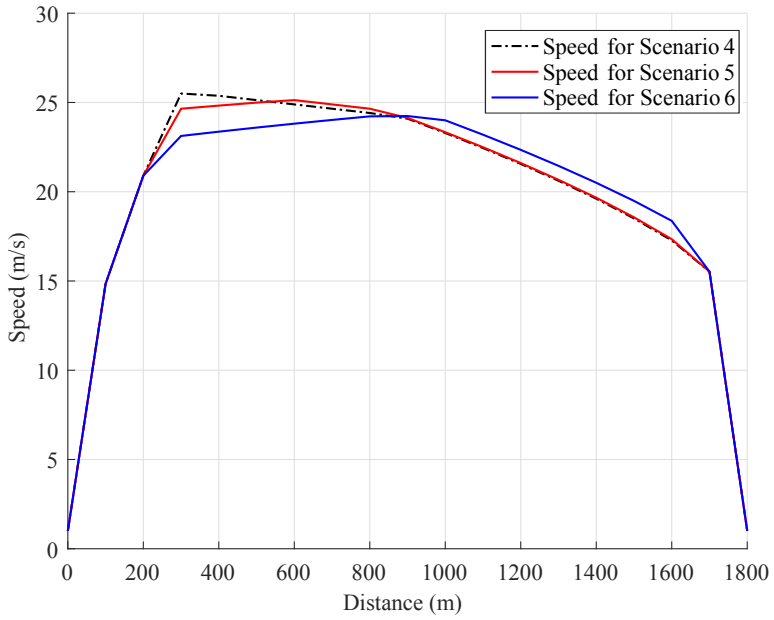

Figure 4.7: Optimal train speed trajectories for Scenario 4-6

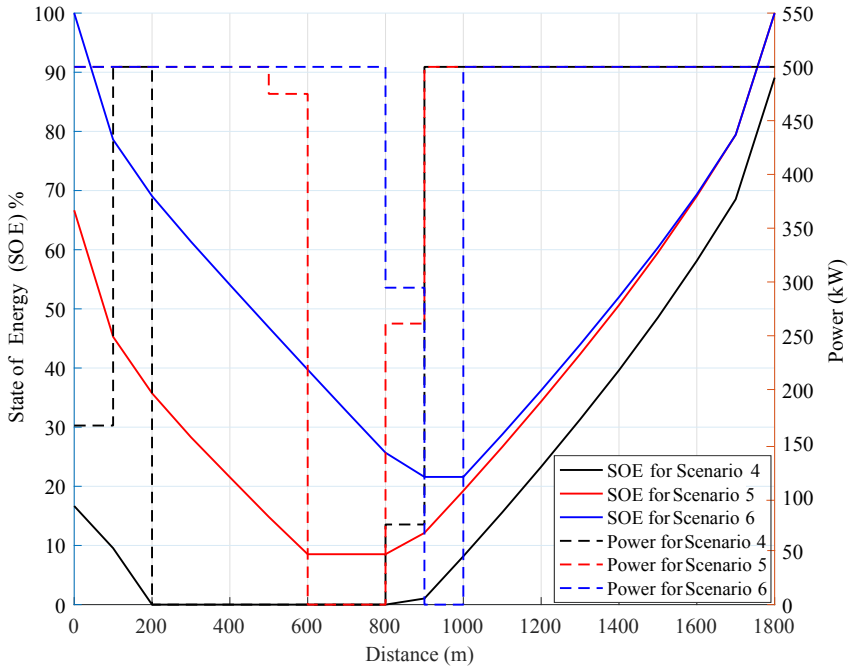

Figure 4.8: Optimal discharging and charging curves for Scenario 4-6

initial SOE results in longer traction distance (Figure 4.7) as well as more frequent discharging process (Figure 4.8). This might result from the different rechargeable

capability in OESD because for recovering more energy, the OESD needs to discharge first to make room for charging operation in the later braking operation of the train, which forces the train to conduct more traction operation.

However, it should be noticed that when introducing OESD with non-zero initial SOE, higher initial SOE is not always preferred as the net energy consumption could be raised. From Table 4.5 it is easily noted that the traction distances and initial SOE both see increase while the net energy consumption see an interesting trend, which firstly falls and then rises. Excessive initial SOE is observed to reduce OESD's capability of recapturing regenerative energy due to a reduction of the rechargeable room during the braking operation of the train. More details about this trend are illustrated in Figure 4.9. It implies that there is an unique optimal initial SOE value and a corresponding optimal train speed trajectory which is able to jointly achieve the minimum net energy consumption in a specific inter-station journey.

Table 4.5: Results of Scenario 4-6

Scenario	Initial SOE (%)	Traction Distance (m)	Net Energy Consumption (kWh)
4	16.7	300	13.42
5	66.7	600	13.13
6	100	900	13.62

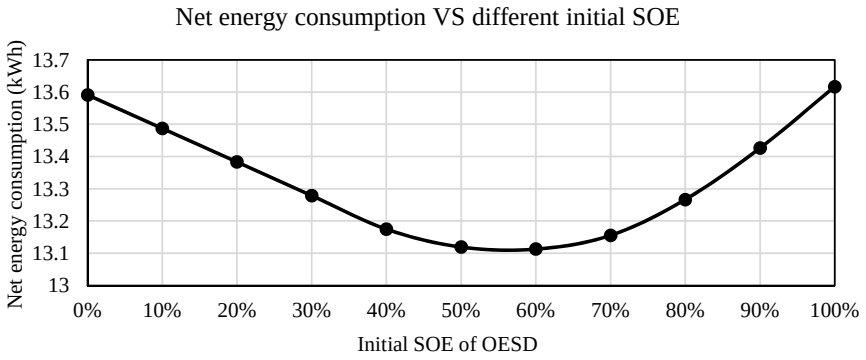

Figure 4.9: Relationship between net energy consumption and initial SOE

The optimisation results of the Scenario 4-6 tells that with different initial SOE, both of the train operation and discharging/charging strategy of the OESD are observed a necessity of trade-off and significant change to adjust themselves as much as possible for saving energy. The OESD with non-zero SOE has enhanced energy-saving potential whereas the initial energy in it should not be excessively high, otherwise the advantage

of the OESD is undermined.

4.3.4 Scenario with Speed Limits and Gradient Constraints

The scenarios above are all under the assumption that the gradient and the speed limits do not exist. However, when the train runs in different zones of an inter-station section, it might be constrained by speed limits resulted from the specific safety or operational requirements. Additionally, normally the gradients would not be zero in the entire journey. Therefore, introducing speed limits and gradients constraints into the model is rational and makes the model more adaptable in the practical operation.

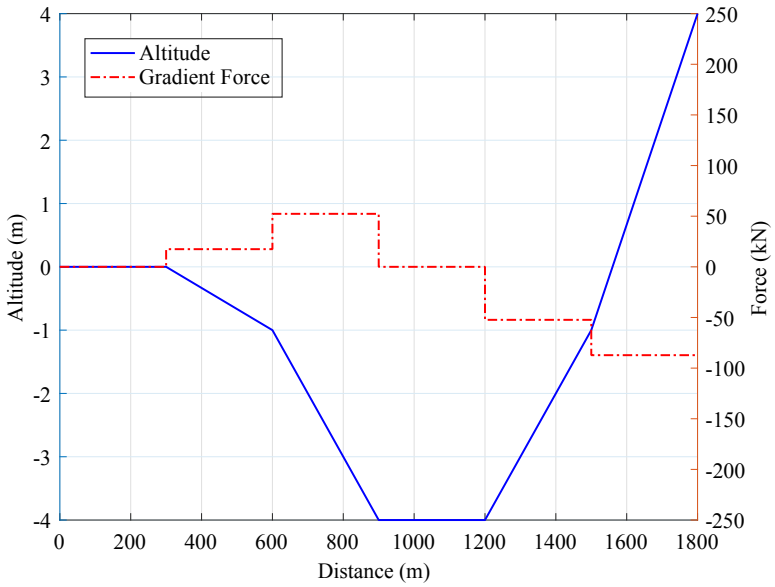

Figure 4.10: Altitude and corresponding gradient force in each segment

In the model, the influence of the height difference between two altitude switching points can be converted to the change of potential energy of the train caused by gradient force, which is the $(M_t + M_o)g\theta_i\Delta d_i$, see Figure 4.10. When the slope between two altitude points is larger, the gradient force thus the potential energy change is larger as well. Here Scenario 7 with general speed limits and gradients variation is shown.

The optimal train speed trajectory with OESD (SOE=0) under these constraints can be found by the model, which is plotted in Figure 4.11. Figure 4.12 shows the corresponding discharging and charging curves for OESD under these conditions. In Scenario 7, the running time is prolonged from 100 s to 110 s, and there are 5 speed limit zones with different gradients along with the whole travel distance. In each speed limit zone, except of the one between 600 m and 1300 m, the train takes cruising operations

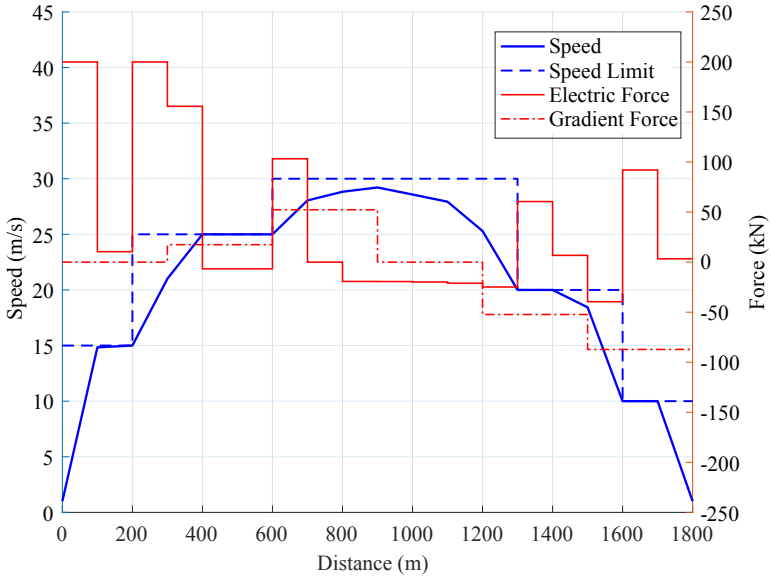

Figure 4.11: Optimal train speed trajectory for Scenario 7

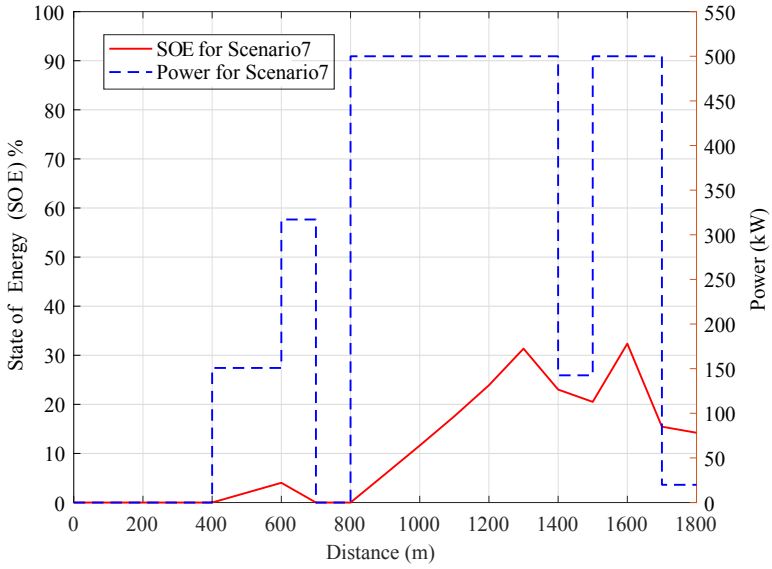

Figure 4.12: Optimal discharging and charging curve for Scenario 7

or nearly cruising operations for not exceeding the limit values of speed. It is not as same as the former scenarios that, with these constraints introduced, the OESD is not only allowed to discharge but also to be charged during the acceleration period because under both the speed limit and gradient force, the train needs to brake in order to maintain a constant speed or a slowly-increasing speed to satisfy the constraints of

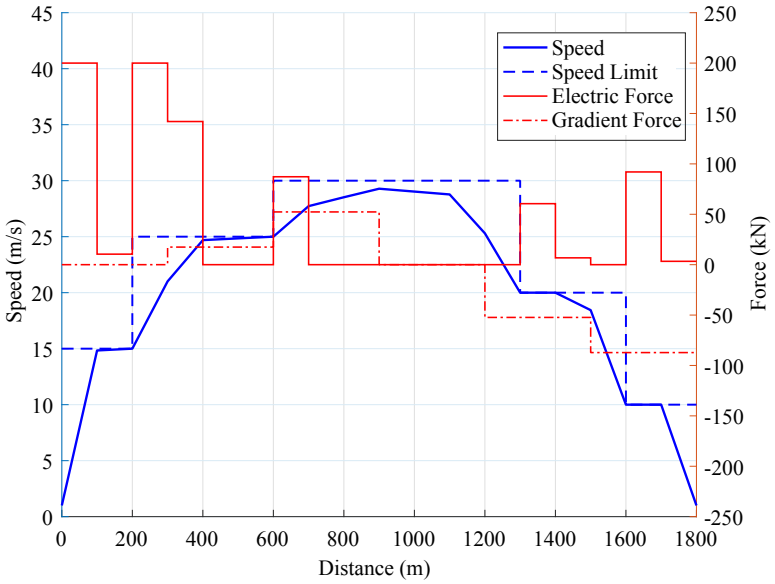

Figure 4.13: Optimal train speed trajectory for Scenario 8

running time. Similarly, the OESD is permitted to not only be charged during the deceleration period since the train need to conduct traction to climb the slope, which is able to utilise both the energy from catenary/third rail or OESD.

Although the constraints of travel distance, running time, speed limits and gradients all exert on the train operation, which means that the speed trajectory should not be easily changed due to smaller search space of solutions, the difference of optimal operation with and without OESD still exists, see Figure 4.11 and Figure 4.13. Figure 4.13 shows the Scenario 8 which is without the OESD under same speed limits and gradient constraints. In the speed limit zone from 600 m to 1300 m, the different operation occurs when compared with the Scenario 7. From 800m to 1300m, the train in Scenario 7 conducts braking to generate more regenerative braking energy whereas the train in Scenario 8 conducts coasting from 700 m to 1300 m to reduce energy loss from braking. Due to the frequent discharging and charging process during the journey in Scenario 7, a notable reduction rate of the net energy consumption, i.e. 11.6%, is achieved, as shown in Table 4.6.

4.3.5 A Glimpse of Degradation of the OESD

In real operation, after frequent discharging and charging process for a long period of use, the OESD would suffer from degradation such as the decreased dishchargeable/chargeable capability, decreased discharging/charging power etc., leading to a lower

Table 4.6: Results of Scenario 7-8

Scenario	E_{cap} (kWh)	Initial SOE (%)	Net Energy Consumption (kWh)
7	8.33	0	24.61
8	/	/	27.86

discharging/charging efficiency which undermine its energy-saving potential. Thus, it is an important parameters to be considered in train operation with OESD.

In the proposed MILP model, degradation of the OESD can also be considered from the perspective of energy conversion. Since the degradation mainly results in the low efficiency of usage of the OESD, thus, for each time when the OESD is charged or discharging, both process will have an extra cost which can be expressed by a penalty C_{deg} [112] and [113] as in (4.21).

$$C_{deg} = \frac{C_c}{E_t} \cdot k \tag{4.21}$$

where C_c is the OESD's capital cost in \$, E_t is the total dischargeable/chargeable energy per life cycle of the OESD in kJ, and k is a price-to-energy conversion ratio in kJ/\$.

Therefore, in each Δd_i a new term $\Delta E_{i,deg}$ which represents this extra energy cost is introduced, and it can be formulated in (4.22).

$$\Delta E_{i,deg} = C_{deg} \cdot (\Delta E_{i,dch} + \Delta E_{i,ch}) \tag{4.22}$$

The objective of the model considering OESD degradation is also to achieve the minimum net energy consumption, thus can be written as (4.23)

$$\min \quad \sum_{i=1}^{N} (\Delta E_{i,s} + \Delta E_{i,dch} - \Delta E_{i,ch} + \Delta E_{i,deg}) \tag{4.23}$$

Here Scenario 7 are taken as an example to see how the change in the C_{deg} influences the optimal discharging/chraging strategy of OESD. In Scenario 7, degradation of the OESD is not considered thus its C_{deg} is 0. When its C_{deg} is changed to be 0.5 (Scenario 7'), it is found that the optimal speed trajectory and the optimal discharging/charging strategy are both influenced by the degradation of OESD, see Figure 4.14 (The force, speed limits and gradients are removed in the figure for a clear demonstration) and Figure 4.15. From 600 m to 900 m, the optimal speed trajectory of Scenario 7' is lower than that of Scenario 7 while from 900 m to 1200 m the trend is inverse. The OESD

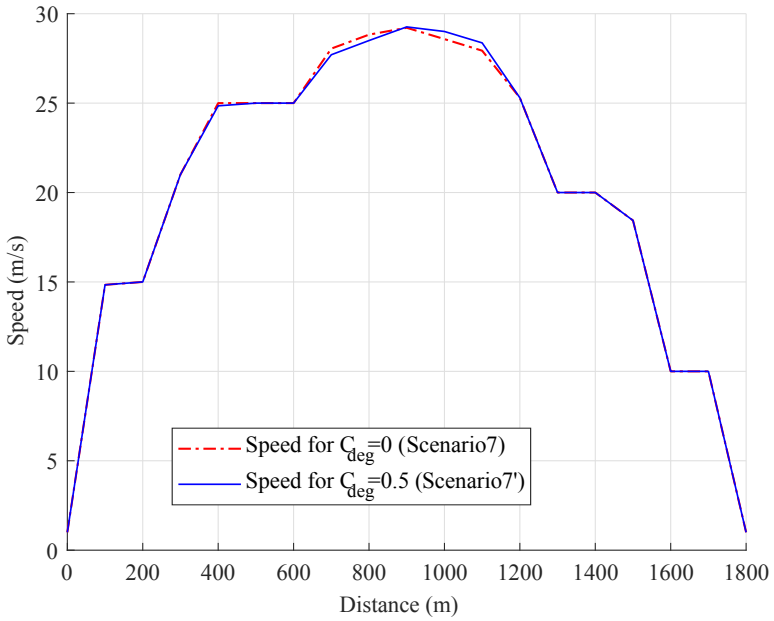

Figure 4.14: Comparison of the optimal speed trajectories with different C_{deg}

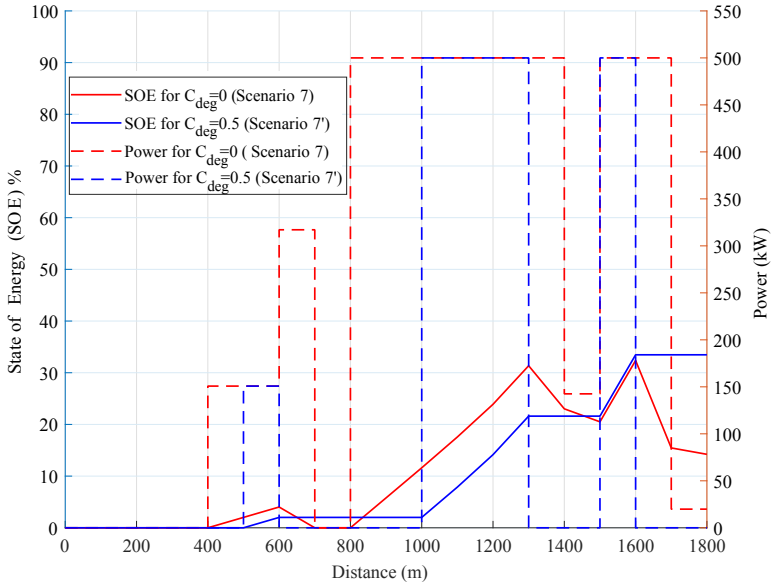

Figure 4.15: Comparison of the optimal discharging/charging strategies of OESD with different C_{deg}

discharging and charging frequencies are reduced to be 0 times and 5 times respectively, and the discharging/charging behaviour is avoided to some extend, as shown in Figure 4.15, to reduce energy loss due to degradation.

The change of OESD optimal discharging/charging strategy also implies the reason for the change of the optimal speed trajectory. In Scenario 7, the discharging behaviour of OESD from 600 m to 700 m assists the train's traction operation and raises the average speed of the distance from 600 m to 900 m, resulting in a higher speed trajectory. The charging frequency in Scenario 7 is more than that in Scenario 7' between 800 m to 1300 m, which leads to more braking operations and reduces the average speed in this zone, yielding a lower speed trajectory.

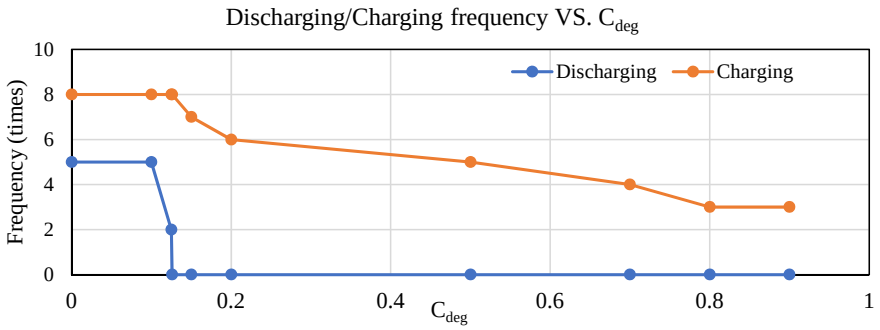

Figure 4.16: Relationship between discharging/charging frequency and degradation

Furthermore, the sensitivity of the OESD discharging/charging strategy with respect to degradation can be explored by replacing different value of C_{deg} in the optimisation process. The result is shown in Figure 4.16, and it indicates that with the increase of degradation rate, both of discharging and charging frequencies decrease whereas discharging frequency drops with a faster pace than charging frequency, showing that the discharging process is more sensitive. With C_{deg} increased to 0.126, the discharging frequency decreases to 0 times as discharging energy from OESD has no advantages over getting energy from the substation. This is because for a given energy consumption ΔE_k, its corresponding energy provided by the substation will be $\Delta E_k/\eta_s$ =1.25ΔE_k while the energy provided by the OESD will be $\Delta E_k/\eta_o \cdot (1+C_{deg}) = 1.2511\Delta E_k$, which is higher than the one directly obtained from the substation.

Energy-Saving potential of the OESD lies more on the charging process, especially when the OESD is not necessary to discharge itself to create rechargeable capacity. As a result, reducing discharging frequency is preferred rather than reducing charging one as the energy can still be recovered through charging process to achieve the optimal energy-saving operation although with some extra cost caused by degradation. A trade-off between discharging and charging process should be achieved when rechargeable capacity needs to be increased through discharging. Therefore, it can be concluded that when the OESD suffers degradation, the train operation will not be the optimal

energy-saving one if the initial solution is still followed. Both the train operation and discharging/charging strategy of the OESD need adjustments to make the most of the degraded device.

4.4 Summary

This chapter aims at obtaining the optimal train operation with OESD to achieve a minimisation of the net energy consumption by employing the MILP. Compared with previous literature [89] and [106], the results demonstrated in this chapter, however, show that the train speed trajectory and OESD can be linearised in an integrated optimisation model, which also indicates that both of the OESD and train operation would influence each other significantly.

In this chapter, different OESD capacity and initial SOE as well as degradation are considered in the proposed model. The constraints of different capacity and initial SOE of OESD lead to corresponding adjustments of the traction distance, coasting distance and braking distance, which brings a notable change in optimal train speed trajectory and a significant decrease of net energy consumption. In addition, the net energy consumption is reduced by 11.6% when introducing OESD with on-route constraints to model the real-world scenario. All in all, the research results present that after introducing the OESD, both of the train and the OESD need to do trade-offs during the running in order to further reduce energy consumption, and the OESD is also found to be with a substantial energy-saving potential when integrated in the optimisation of train operation.

Based on the proposed MILP model, degradation of the OESD is also studied, and the results of which show that the occurrence of degradation changes both the original optimal train operation and discharging/charging strategy of the OESD. Both discharging and charging frequencies are reduced while it gives priority to reducing discharging ones.

Chapter 5

Intelligent Train Operation with OESD in a Service Cycle

The main content of this chapter is from the author's published articles in a version with minor reconfiguration to fit the structure and context of this thesis. The published articles are:

C. Wu, S. Lu, F. Xue, L. Jiang, and J. Yang, "Optimization of Speed Profile and Energy Interaction at Stations for a Train Vehicle with On-board Energy Storage Device," in *2018 IEEE Intelligent Vehicles Symposium (IV)*, 2018, pp. 1-6.

C. Wu, S. Lu, F. Xue, L. Jiang, M. Chen and J. Yang, "A Two-Step Method for Energy-Efficient Train Operation, Timetabling, and On-Board Energy Storage Device Management," *IEEE Transactions on Transportation Electrification*, vol. 7, no. 3, pp. 1822-1833, 2021.

5.1 Introduction

This chapter mainly discusses the optimisation problem on the train operation with OESD in service cycles containing multiple inter-station sections. Different from Chapter 4, in this chapter, the scope of the research is expanded from single inter-station section to an increasing number of inter-station sections, which gives the opportunities of further applications of the OESD in railway systems.

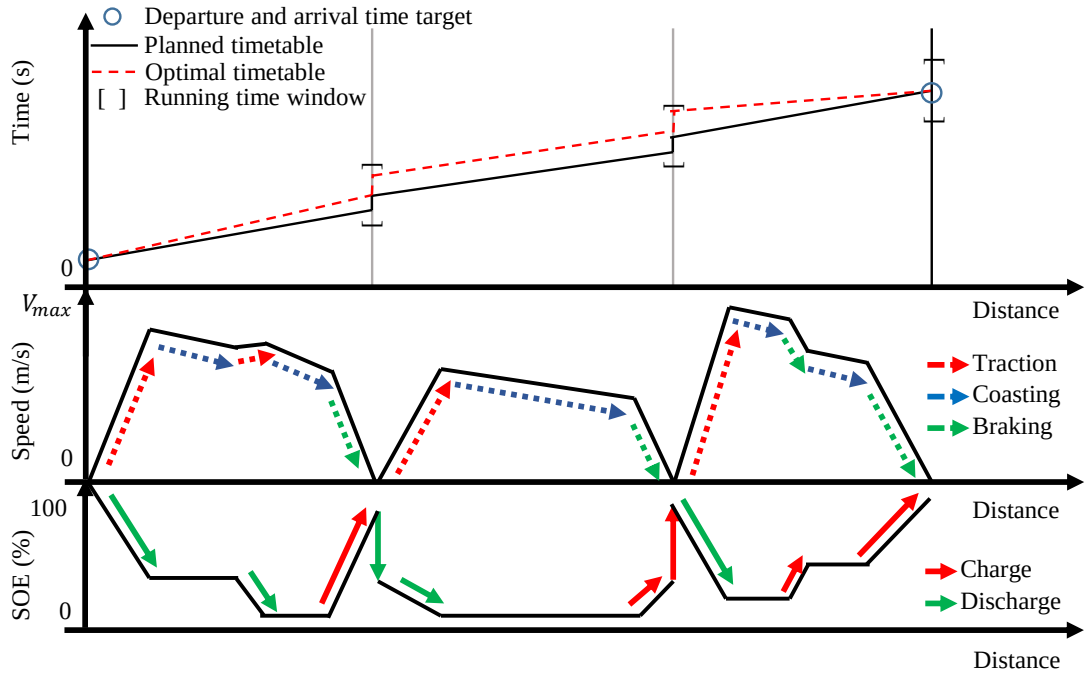

Figure 5.1: Illustration of the expected optimised timetable, train operation and OESD management with a 4-station simple case. The speed trajectory and SOE profiles at the bottom indicate that the OESD is closely interacting with the train speed trajectories and timetable. OESD supports the traction and receives the regenerative energy for each inter-station journey and it takes an active charging and discharging control on the SOE when the train dwells at each station

In Chapter 4, the optimal train speed trajectory and OESD discharging/charging strategy in two adjacent stations are obtained based on the proposed MILP model. However, OESD not only should be utilised when the train runs in the inter-station section but also should be used freely when the train dwells at the station as long as the reduction of net energy consumption can be achieved. Therefore, this chapter aims to concurrently find the the optimal train speed trajectory, timetable and discharging/charging strategy of the OESD during running in inter-station sections as well as dwelling at intermediate stations, the expected results of which is shown in Figure 5.1. The proposed methods are based on MILP by extending the proposed single-inter-station model in Chapter 4 and convex optimisation, in which the OESD is given the freedom to interact with power system when the train dwells at the station and the OESD can charge or discharge according to different demand for achieving an energy-efficient operation of the whole system. The main contributions of this chapter

are listed as follows:

- The MILP model proposed in Chapter 4 dealing with the optimisation problem of the train operation with OESD in single inter-station section is extended into multi-station scenario, where the OESD is given the freedom to discharge/be charged when the train is dwelling. The results shows that the proper adjustment of the energy status of OESD will reduce the net energy consumption of the whole journey.
- The drawbacks of the extended MILP method is then found, and a two-step method based on convex optimisation is proposed combined with the MILP model in Chapter 4. The two-step method can concurrently find the optimal train speed trajectory, the train timetable discharging/charging strategy of the OESD during the running and at each station for a entire service cycle with large number of inter-station sections with fast computing speed.

5.2 Optimising Multi-Station Operation with MILP

Notation of variables	
v_i^2	Square of train speed in the position of $\sum_1^{i-1} \Delta d_i$ [m^2/s^2]
$\Delta E_{i,s}$	Energy from the substation in Δd_i [kJ]
$\Delta E_{i,dch}$	Energy discharged from the OESD in Δd_i [kJ]
$\Delta E_{i,ch}$	Energy charged to the OESD in Δd_i [kJ]
$\Delta E_{i,r}$	Energy transmitted to the resistor from the motor in Δd_i [kJ]
$\Delta E_{s,dch}$	Energy discharged from the OESD at s^{th} station [kJ]
$\Delta E_{s,ch}$	Energy charged to the OESD at s^{th} station [kJ]
λ_i	Binary variables to determine the train operation mode in Δd_i
ϵ_s	Binary variables to determine the OESD operation mode at s^{th} station
$\alpha_{i,j} \in [0,1]$	SOS2 variable set for linearisation of nonlinear speed-related constraints
$\beta_{i,j} \in [0,1]$	SOS2 variable set for linearisation of nonlinear speed-related constraints
$\mu_{i,j}^{\alpha}$	Binary variables used in SOS2 variable set
$\mu_{i,j}^{\beta}$	Binary variables used in SOS2 variable set
Assumption	

(Continued from last page)

The regenerative braking energy can only be recovered by OESD or dissipated by resistors but cannot be fed back to the substation or used by other trains during the running.

5.2.1 OESD Discharging/Charging Process at Stations

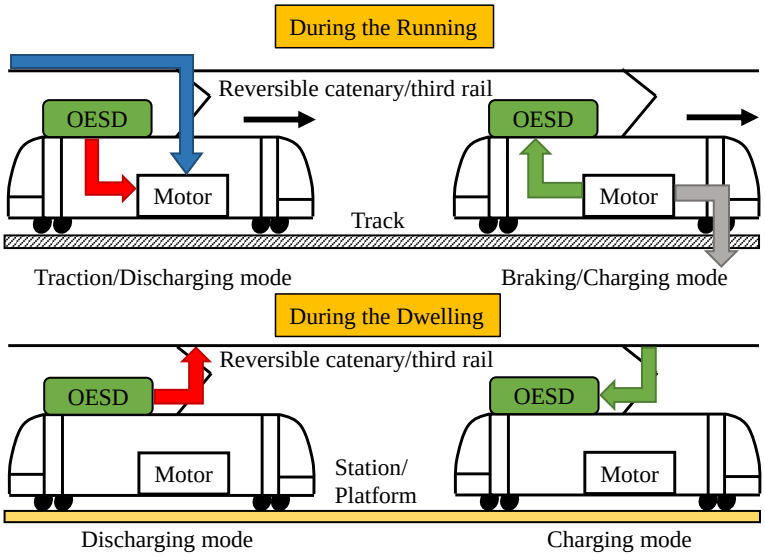

Figure 5.2: Schematic of the energy flow for a typical train with OESD considering reversible catenary/third rail

Here the catenary/third rail is enabled to receive the regenerative braking energy. When the train dwells at the station, the dwell time is given for passengers to board and alight. During the dwelling, the OESD is given the time to interact with reversible catenary/third rail, namely discharges to catenary/third rail or being charged from catenary/third rail, as shown in Figure 5.2. The discharging/charging process of the OESD cannot exist simultaneously, thus the discharging and charged energy of the OESD at s^{th} station can be shown as (5.1) and (5.2).

$$\Delta E_{s,dch} \leq \epsilon_n L, \quad \forall s = 1, 2, ..., S \tag{5.1}$$

$$\Delta E_{s,ch} \leq (1 - \epsilon_n) L, \quad \forall s = 1, 2, ..., S \tag{5.2}$$

where ϵ_s is the binary variables to help select the OESD operation at s^{th} station, S is the total number of the stations, and L is a sufficient large number, the modelling

method is based on the formulation of Either-Or conditions (see Section 3.5.1). When ϵ_s=1, discharging process is enabled, otherwise, charging process is enabled.

At the station, the charging/discharging time cannot exceed the dwell time at s^{th} station, $T_{s,d}$, thus the (5.3) should be imposed to limit the maximum discharging energy and maximum charged energy of OESD during the dwelling.

$$\frac{\Delta E_{s,ch}}{\eta_{s,ch}} \leq \overline{P_o} T_{s,d}, \quad \Delta E_{s,dch} \cdot \eta_{s,dch} \leq \overline{P_o} T_{s,d}, \quad \forall s = 1, 2, ..., S \tag{5.3}$$

where $\eta_{s,ch}$ and $\eta_{s,dch}$ is the charging efficiency and discharging efficiency of the OESD at n^{th} station.

Different from the proposed method in Chapter 4, the running time constraint here is extended to be limited by the total running time for the train to run from 1^{th} station to S^{th} station, with the given dwell time at each station, the constraint can be written as (5.4)

$$\sum_{i=1}^{N} \Delta t_i + \sum_{s=1}^{S} T_{s,d} = T_t, \quad \forall i = 1, 2, ..., N, \quad \forall s = 1, 2, ..., S \tag{5.4}$$

The net energy consumption caused by the discharging/charging process of the OESD at each station is the transmission loss, and they are easily obtained as $\Delta E_{s,ch} \cdot (1 - \eta_{s,ch})/\eta_{s,ch}$ for charging process and $\Delta E_{s,dch} \cdot (1 - \eta_{s,dch})$ for discharging process. As a result, the objective of the model considering operation with multiple stations can be formulated as (5.5)

$$\min \quad \underbrace{\sum_{i=1}^{N} (\Delta E_{i,s} + \Delta E_{i,dch} - \Delta E_{i,ch})}_{\text{Inter-Station net energy consumption}} + \underbrace{\sum_{s=1}^{S} ((1 - \eta_{s,dch}) \Delta E_{s,dch} + \frac{1 - \eta_{s,ch}}{\eta_{s,ch}} \Delta E_{s,ch})}_{\text{At-Station Net energy consumption}} \tag{5.5}$$

The model minimises the net energy consumption of traction, maximises the recovered regenerative braking energy, and minimises the extra energy consumption of charging/discharging process of at station, resulting in a minimisation on the net energy consumption of the whole journey from 1^{th} station to the S^{th} station. In addition, the running time of each inter-station section are also optimised with the constraint of the total running time from 1^{th} station to the S^{th} station.

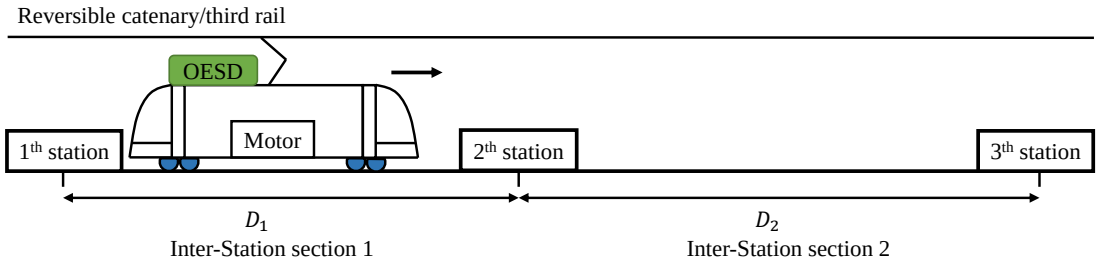

Figure 5.3: Track condition for a three-station route

5.2.2 Simple Test on A 3-Station Route

In this test, the parameters are set according to Table 4.1 in Section 4.3 with the value for both newly added parameters $\eta_{s,dch}$ and $\eta_{s,ch}$ being 0.9. The track condition of the journey is shown in Figure 5.3 and the simple service cycle for the train is assumed to cover three stations and two inter-station sections with no gradient variation. D_1 is 1800 m and D_2 is 2200 m, and the whole track length is 4000 m. T_1 and T_2 is the journey time for inter-station section 1 and section 2 respectively. Thus, journey time from the initial station to terminal station is $\sum_{i=1}^{N} \Delta t_i = T_1 + T_{2,d} + T_2 = 210$ s with $T_{2,d}$ given as 30 s for the 2^{th} station. The capacity of the OESD is 8.33 kWh, initial SOE when the train departs at the 1^{st} station is set to be 0, and the charging/discharging power of it at each station is fixed to be the maximum value 500 kW.

For a clear demonstration on how the discharging/charging process of OESD at stations changes the optimal train speed trajectory, running time allocation and discharging/charging strategy of the OESD to reduce the net energy consumption of the whole journey, two scenarios are given as follows:

- Scenario 1: Discharging/Charging process of OESD at stations are allowed.
- Scenario 2: Discharging/Charging process of OESD at stations are not allowed ($\Delta E_{s,dch}$ and $\Delta E_{s.ch}$ are both fixed to be 0).

The results of two scenarios are shown in Figure 5.4 and Figure 5.5, where red lines are for scenario 1 and blue lines are for scenario 2. The optimal running time allocation is T_1=82.5 s and T_2=97.5 s with the sum being 180 s, which guarantees the total running time of this service cycle. Since the discharging/charging process of OESD at each station is allowed, as long as this process contributes to the reduction of net energy consumption of the whole journey, the specific discharging/charging process will be given and observed. For instance, in scenario 1 when the train stops at the station, there is a gap between the final SOE of OESD for the operation of inter-station section

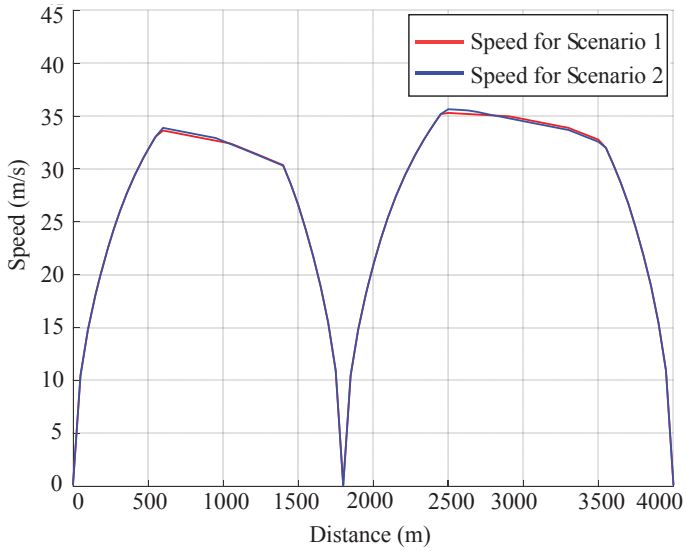

Figure 5.4: Optimal train speed trajectory for the two scenarios

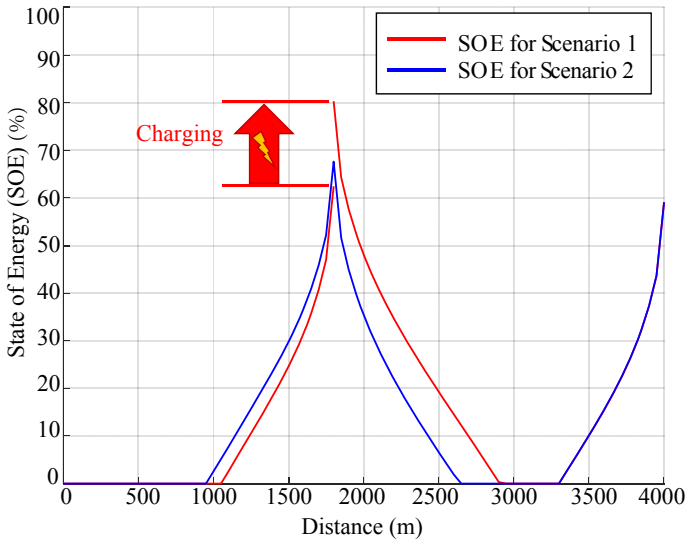

Figure 5.5: Optimal discharging/charging strategy of OESD for the two scenarios

1 and the initial SOE of OESD for the operation of inter-station section 2. It means that the OESD is charged to raise its SOE from 62.4% to 80.3%. The time consumed on charging process at 2^{th} station is 10.7 s, which is less than the given dwell time $T_{2,d}$ and the net energy consumption of this journey is 53.51 kWh. The net energy consumption of scenario 2 is 56.63 kWh, which is 0.2% higher than that of scenario 1, showing that adjusting properly the SOE of OESD at station is able to reduce net

energy consumption of the service cycle, though with an extra energy loss when OESD is charged at station. The optimal he train speed trajectory of 2 scenarios are obtained and it sees changes with different behaviours of OESD at stations. It can be seen that when OESD is charged at station, the braking distance of the train is shortened in the first inter-station section while its traction distance in the second inter-station section is lengthened.

5.2.3 Soaring Problem Size and Sub-Optimum

It can be found that though the model extended based on MILP is able to deal with the optimal train operation with OESD in a service cycle by adjusting the train speed trajectory, running time allocation and discharging/charging strategy of the OESD, the limitations of it are also evident, which are summarised as follows:

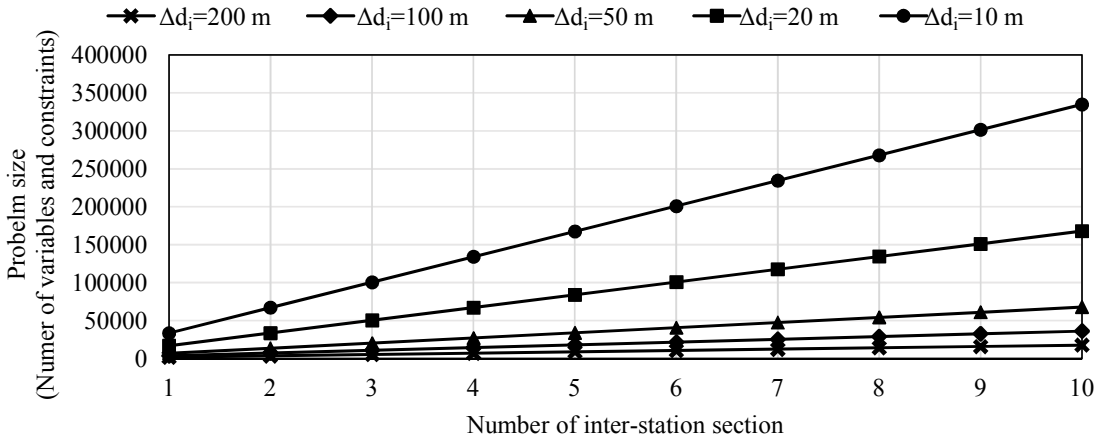

Figure 5.6: Problem size (number of variables and constraints) of different number of inter-station section involved with different Δd_i

- The first limitation is the size of the MILP problem when dealing with the multi-station operation. With the increasing number of the inter-station sections, the variables to be optimised and the constraints imposed will also increase significantly. Here 10 inter-station sections with track length being 2000 m are used as example, and the results are plotted in Figure 5.6. It is observed that the problem size increases when Δd_i becomes smaller, as well as when more inter-section sections are involved. Due to the soaring problem size, the computation time of the model grows exponentially, or the problem directly becomes unsolvable due to the memory overflow, which can be seen in Figure 5.7. This leads to the extremely

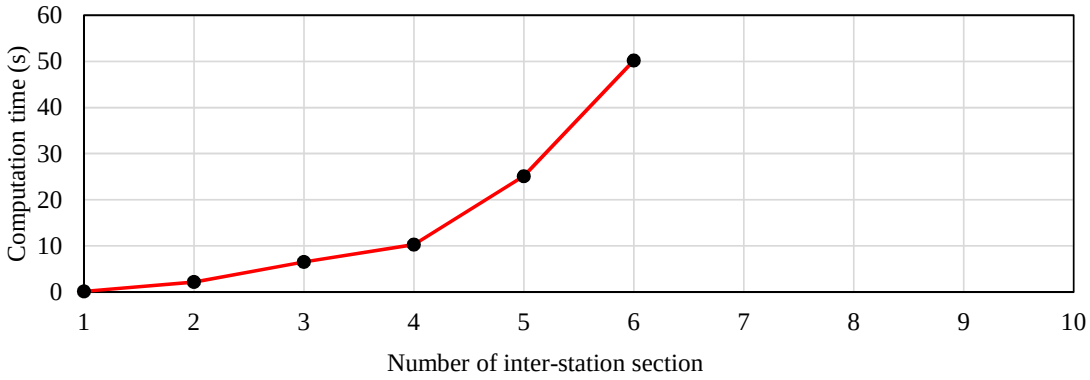

Figure 5.7: Computation time of different number of inter-station section when different Δd_i =100 m

limited number of inter-station operations to be optimised, which is not practical in the real applications with the increasing number of larger railway networks with dozens or hundreds of stations.

- The second limitation is the sub-optimum brought by the proposed method. It can be seen from the simple test in above Section 5.2.2, the initial energy status of the OESD is still a parameters given before optimisation process. This still leaves a question that when dealing with the multi-station operation, if the freedom of discharging/charging process are given at each station, what is the optimal initial energy status for OESD when the train departs at each station? A more intelligent model should tell the railway operator the best way to operate the OESD at each station, even at the initial departure station.

Due to limitations of only applying MILP in solving the optimisation problem for the train operation with OESD in service cycles, it is concluded that a more efficient way is needed and essential.

5.3 Minimum Net Energy Consumption Approximation and Modelling

5.3.1 Approximating Function Formulation

Here a special case is used to show the key deduction of the proposed approach by applying the MILP model in Chapter 4 in single inter-station scenario. In the case the parameters follow the Table 4.1, where the track length is 3000 m, train mass is 178 t,

OESD capacity and mass is 8.33 kWh (30 MJ) and 1.6 t, maximum traction/braking force and power is 200 kN and 5000 kW, maximum acceleration/deceleration is 1.2 m/s^2 and running time window is from 110 s to 210 s. The results are shown in Figure 5.8 and Figure 5.9. Noted that initial SOE of the OESD is shortened as the ISOE hereafter.

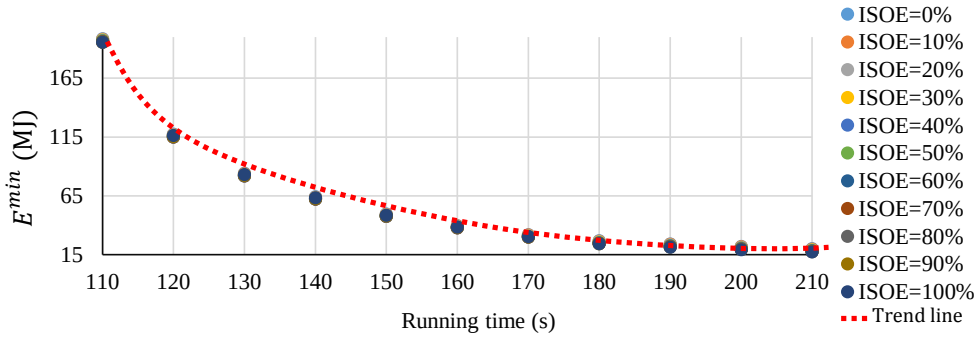

Figure 5.8: The minimum net energy consumption based on different running time in a specific inter-station section. The trend line shows minimum net energy consumption are all monotonically decreasing under different given ISOE

When the running time increases, the minimum traction energy consumption of the train drops, which has been commonly recognised in the field of study [7, 70]. In the research outcome based on the model proposed in Chapter 4, it is also found that even with the OESD, the minimum net energy consumption will be reduced significantly when the running time in a specific inter-station section increases. The minimum net energy consumption is denoted as E^{min} and Figure 5.8 demonstrates the change of it resulted from different running time under specific ISOE of the OESD. As a result, the relationship between E_i^{min}, which is the minimum net energy consumption for specific inter-station section i, and running time T can be firstly approximated to be in inverse proportion with some modifications as function f_i in (5.6), thus it has:

$$E_i^{min} \approx f_i(T) = P_{1,i} + \frac{P_{2,i}}{T + P_{3,i}} \tag{5.6}$$

where $P_{1,i}$, $P_{2,i}$ and $P_{3,i}$ are the constant for specific inter-station section i.

In a specific inter-station operation, the variation of minimum net energy consumption ΔE^{min} with respect to different given ISOE under certain running time is investigated. From Figure 5.9 it is found that when ISOE changes from 0% to 100%, the ΔE^{min} is always negative and decreases first then rises again, the same results can be found in Figure 4.9 in Section 4.3.3. This is also found in the simulation of the operation of the train equipped with on-board batteries [91]. For all the running time

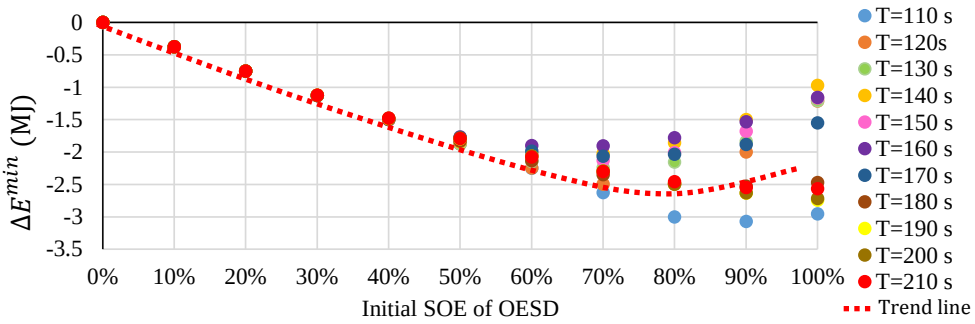

Figure 5.9: The variation of minimum net energy consumption based on different ISOE in a specific inter-station section. The trend line shows that these variations drop first then rise for different given running time

assigned in this specific inter-station operation, this trend remains similar though with slight discrepancies. As a result, the trend is approximated by a quadratic function, as the red dash line in Figure 5.9. Therefore, the relationship between the ΔE_i^{min}, which is the variation of minimum net energy consumption for a specific inter-station section i, and ISOE of OESD under different running time satisfies the following function g_i in (5.7):

$$\Delta E_i^{min} \approx g_i(ISOE) = P_{4,i} \times ISOE + P_{5,i} \times ISOE^2 \tag{5.7}$$

where $P_{5,i}$ is the constant parameters for linear term and quadratic term respectively for a standard quadratic function form in specific inter-station section i. The approximating function has no parameter of zero order because when $ISOE = 0$, ΔE_i^{min} is normally 0.

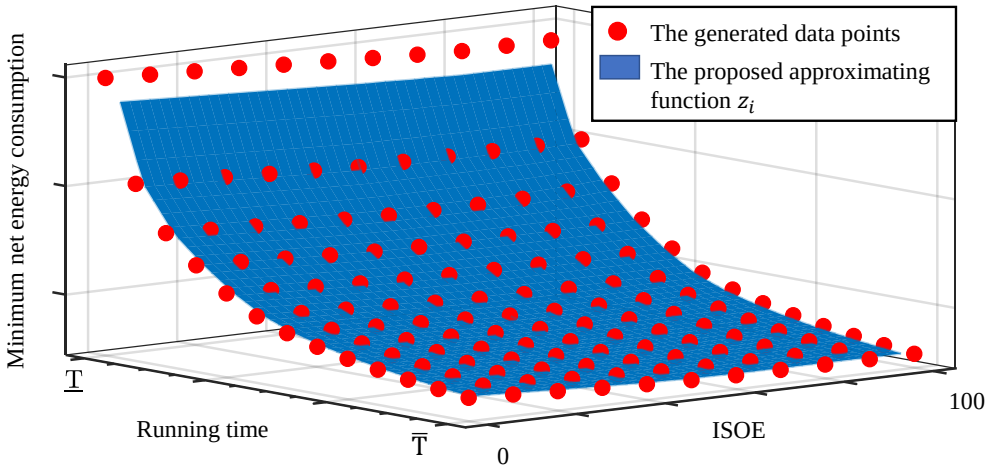

Figure 5.10: An illustration of data points generated and the proposed approximating function $z_i(T, ISOE)$ in the form of (5.8)

Figure 5.8 and Figure 5.9 are two projected planes from the direction of x-axis being the running time T and y-axis being the ISOE of OESD for specific inter-station operation, and the data group (E^{min}, T, $ISOE$) in general situation with the running time window ($\underline{T}$, $\overline{T}$) is shown in Figure 5.10. To find the approximating function $z_i(T, ISOE)$ to fit the data group, (5.6) and (5.7) are summed up directly to do the reformulation of the function, as shown in (5.8).

$$z_i = P_{1,i} + \frac{P_{2,i}}{T + P_{3,i}} + P_{4,i} \times ISOE + P_{5,i} \times ISOE^2 \tag{5.8}$$

where $P_{1,i}$, $P_{2,i}$, $P_{3,i}$, $P_{4,i}$ and $P_{5,i}$ need to be calibrated in data fitting process using the results of specific inter-station section i.

The reason for forming (5.8) is that the E_i^{min} for one specific running time T while ISOE=0 is regarded as the basis, when the value of ISOE is changed, it is easy to observe that the corresponding negative ΔE_i^{min} can be simply added to E_i^{min}, showing that the sum of $f_i(T)$ and $g_i(ISOE)$ can approximate the minimum net energy consumption.

5.3.2 Verification of the Proposed Approximation

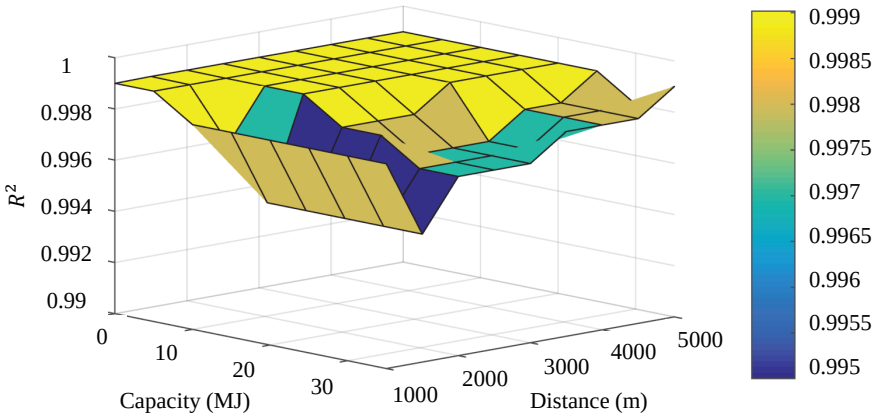

Figure 5.11: The performance of the proposed approximating function when given different OESD capacity and different track length. The minimum value of R^2 is observed to be 0.995

Since only a specific inter-station section and fixed OESD properties are used to show the deduction of the approximating function (5.8), verification of the proposed approximation function is needed. For doing this, 9 different distances of inter-station journey from 1000 m to 5000 m with an increment step of 500 m and different OESD capacity from 1 MJ to 35 MJ with an increment step of 5 MJ as two components are

selected. Different running time windows are also given to different track length.

By employing the MILP model in Section 4 based on the above different inter-station information and energy storage information, the performance of the approximating function can be obtained followed by the data fitting process. Figure 5.11 shows the coefficient of determination R^2 of the verification with the minimum value of 0.995 and maximum value of 0.999. It means that though it is with some minor fluctuation of R^2, using function (5.8) to approximate the relationship among minimum net energy consumption, running time and ISOE of OESD is reasonable, feasible and with a satisfactory modeling precision.

5.3.3 Convexity Proof of the Proposed Approximation

In the above sections, it has been demonstrated that by using data fitting, the approximating function z_i can be built up. In this section, a proof of convexity of z_i will be conducted by using basic mathematical theory. The proof of convexity will directly lead to the global optimum of the results to be achieved by convex programming.

The Hessian matrix or Hessian is a square matrix of second-order partial derivatives of a scalar-valued function, or scalar field. It describes the local curvature of a function of many variables. The Hessian matrix is often used to determine the convexity of the given functions, which is presented in Section 3.7. A function $f(x)$ is strictly convex if or only if its Hessian matrix H is positive definite for all of the x in the domain, see Section 3.7. The Hessian matrix of the approximating function $z = z(x, y) = P_1 + \frac{P_2}{x+P_3} + P_4 \times y + P_5 \times y^2$ is shown as below:

$$H_z = \begin{bmatrix} \frac{2P_2}{(x+P_3)^3} & 0 \\ 0 & 2P_5 \end{bmatrix}$$

The Hessian matrix is positive definite if and only if its n leading principal minors are greater than 0, which means that the components in the matrix need to satisfy the three conditions shown in (5.9).

$$\begin{cases} \dfrac{2P_2}{(x+P_3)^3} > 0 \\ 2P_5 > 0 \\ \dfrac{2P_2}{(x+P_3)^3} \times 2P_5 - 0 > 0 \end{cases} \tag{5.9}$$

From the property of the inversely proportional function in relationship between E_i^{min} and T, it can be deduced that the parameter P_2 is positive. The reason for this is

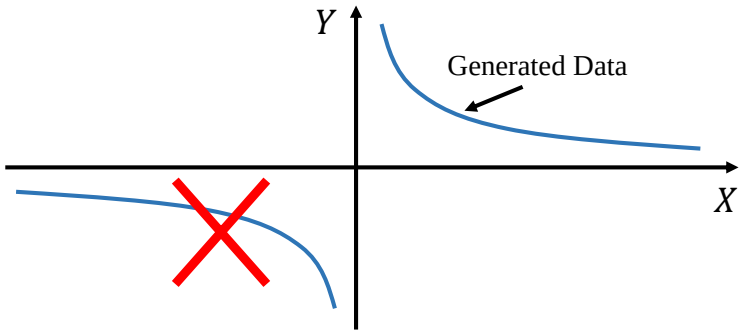

Figure 5.12: The property of relationship between running time and minimum energy consumption extracted by the generated data. The generate data can only form the curve in first quadrant but not the curve in third quadrant

because the inversely proportional function is a strictly monotone decreasing function, the first-order derivative of it should greater then 0:

$$\because \frac{\partial z}{\partial x} = -\frac{P_2}{(x+P_3)^2} < 0$$
$$\therefore P2 > 0$$

In addition, another important property of the inversely proportional function is that it contains a pair of centrosymmetric curves, as the blue curves shown in Figure 5.12. If $Y = y - P_1$ and $X = x + P_3$, under the realistic train operation, the fitting curve representing the relationship between running time and minimum energy consumption can only form the right-sided curve located in the first quadrant but not the left-sided curve located in the third quadrant (Figure 5.12), thus it has:

$$\because X > 0, Y > 0$$
$$\therefore x + P_3 > 0, y - P_1 > 0$$
$$\therefore (x + P_3)^3 > 0$$

On the other hand, it is easily known that P_5 is always greater than 0 because the ΔE_i^{min} sees a decrease trend first then rises again (Figure 5.9), which means that this parameter for the quadratic function is positive. As a result, H_z is positive definite, which means the proposed approximating function z_i is strictly convex. In addition, one of a very important properties of convex function is that if z_1, z_2, ... z_n are all convex, the sum of them $\sum_{i=1}^{n} z_i$ is convex as well, and the convexity of the function also tells

that this function has global minimum point (see Section 3.7).

5.4 A Two-Step Approach combining MILP and Convex Optimisation

Notation of variables	
T_i	The running time of inter-station section i [s]
$ISOE_i$	The initial SOE of the OESD for the train's journey of inter-station section i
Assumptions	
	1. The regenerative braking energy can only be recovered by OESD or dissipated by resistors but cannot be fed back to the substation or used by other trains during the running. 2. The energy losses caused by the discharging/charging process of the OESD at stations are ignored.

5.4.1 Step 1: Preprocessing Step

The proposed approach consists of two steps, one is the preprocessing step (Step 1) and the other is the solving step (Step 2), as shown in Figure 5.13. Step 1 is the bottom level which generates, collects the data and builds the approximating functions to describe the relationships between the minimum net energy consumption, running time and ISOE of OESD. Since each inter-station section has its own route conditions e.g. speed limits or gradient information which usually stay fixed once the construction and rolling stock is finished and confirmed. By inputting different journey time T from the lower boundary $\underline{T}$ to the upper boundary $\overline{T}$ with a preset step length e.g. 5 s and different ISOE from 0 to 100% with a preset step length e.g. 10% in the MILP model proposed in Chapter 4 repeatedly, the minimum net energy consumption data group (E_k^{min}, T_k, $ISOE_k$) for specific inter-station section i can be generated and collected. After having the data group for each inter-station operation, the data fitting can be applied by using the proposed approximating function form shown in (5.8). The data fitting process is repeated until this work for all of the inter-station sections are finished then all of the approximating functions z_i are obtained.

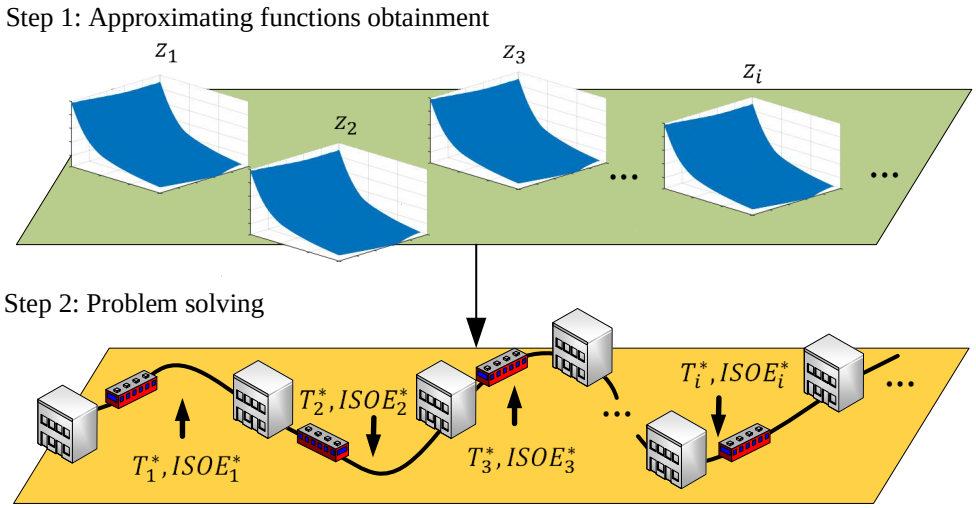

Figure 5.13: The schematic of the proposed two-step method. In Step 1, the approximating functions z_i of all the studied inter-station operations are obtained. In Step 2, convex optimisation problem is established and solved to obtain the optimal running time allocation and ISOE of each inter-station journey $(T_i^*, ISOE_i^*)$

5.4.2 Step 2: Solving Step

After the procedure in Step 1, when the approximating functions z_i for all of the inter-station sections of the studied railway line are obtained, procedure of Step 2 is conducted. In Step 2, allocation of the running time for each inter-station operation and management of the ISOE of OESD of each inter-station operation with relevant constraints arising from the operation of OESD and the train can be conducted. The total operation time from the initial station to the terminal station needs to be determined to ensure sufficient service capacity in real operations, and assuming that there are totally N inter-station sections thus the constraint of which is added as (5.10)

$$\sum_{i=1}^{N} T_i = T_t, \quad \forall i = 1, 2, 3, ..., N \tag{5.10}$$

where n is the total number of the inter-station section of the whole journey, T_i is the running time for inter-station section i and T_t is the total running time for the whole journey. Additionally, the running time for each inter-station operation needs to be in a preset running time window, thus the constraint (5.11) is added as below.

$$\underline{T_i} \leq T_i \leq \overline{T_i}, \quad \forall i = 1, 2, 3, ..., N \tag{5.11}$$

where $\underline{T_i}$ and $\overline{T_i}$ are the lower and upper boundaries of the running time window for i^{th} inter-station run. Due to the capacity limit of the OESD, for each inter-station journey, the constraints (5.12) need to be satisfied.

$$0 \leq ISOE_i \leq 100\%, \quad \forall i = 1, 2, 3, ..., N \tag{5.12}$$

where $ISOE_i$ is the ISOE for inter-station operation i.

The target is to find out the optimal train speed profile, timetable and ISOE for each inter-station operation with minimised total net energy consumption of all the inter-station operations, Thus the optimisation problem is formulated as shown in (5.13):

$$\begin{aligned} \min \quad & \sum_{i=1}^{N} z_i \\ \text{s.t.} \quad & (5.10) - (5.12). \end{aligned} \tag{5.13}$$

Since both the objective function and constraints are all convex, a constrained convex optimisation problem will be formulated based on the outcomes of Step 1.

After optimisation in Step 2, a set of optimal (T_i^*, $ISOE_i^*$) can be obtained and allocated. Then (T_i^*, $ISOE_i^*$) can be substituted in the MILP model in Chapter 4 to obtain the detailed optimal train speed profile and optimal discharge/charge strategy for OESD of each inter-station section i.

5.5 Numerical Experiments

In this section, the proposed approach is firstly conducted on the general case to show the effectiveness and flexibility of the method. After the general case study, the method is applied on a real-world metro line: Beijing Yizhaung Line to show the robustness of the proposed model as well as to provide a detailed illustration on how to allocate the running time and manage the OESD well for energy reduction in a real-world case. Noted that the case studies are conducted by using Matlab R2018b and CPLEX 12.8.0 solver on a PC with Intel Core i5-6500 processor (3.20 GHz) and 8.00 GB RAM.

5.5.1 General Case Studies

The general case studies are to present the effectiveness of the proposed method on dealing with the optimisation problem under various conditions. The maximum traction/braking force and power of the train vehicle used in general case studies are

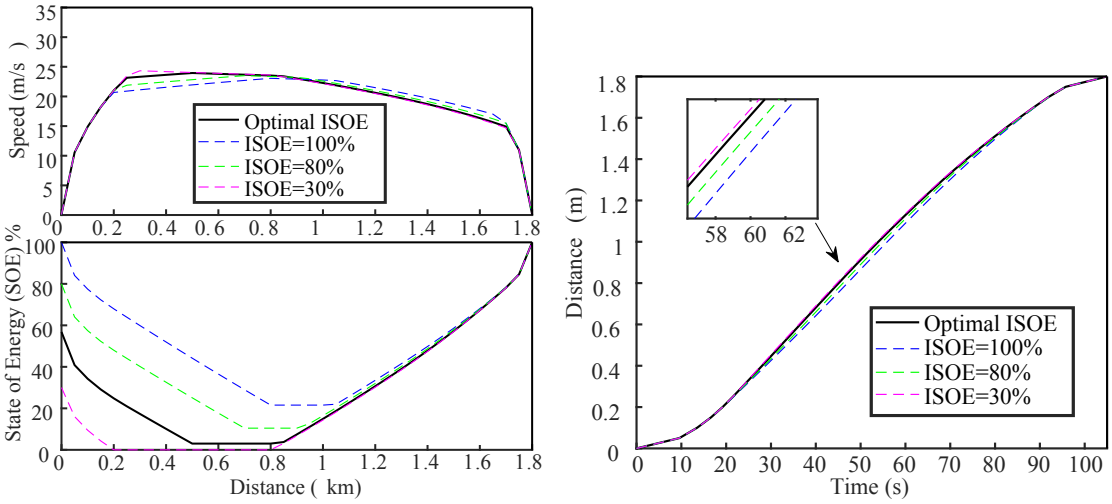

Figure 5.14: The optimal train speed trajectories, discharging/charging management and timetable for a general single inter-station operation

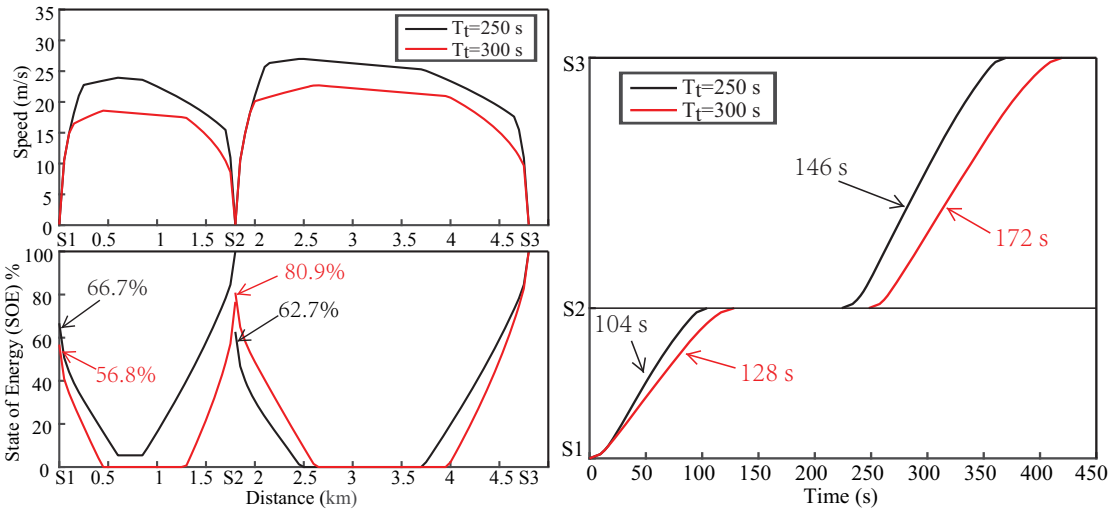

Figure 5.15: The optimal train speed trajectories discharging/charging management and timetable for a general 3-station route with different total running time T_t (The sudden change of the SOE at the station represents the adjustment of SOE at each station)

set to be 200 kN and 5000 kW with the OESD capacity being 8.33 kWh (30 MJ). The track is set to be flat without slope and speed limits.

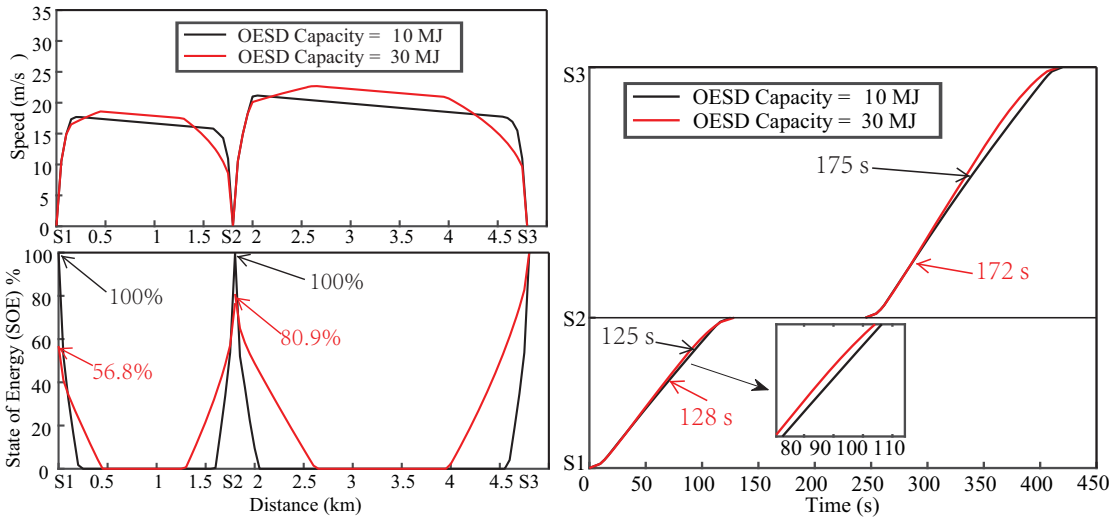

Figure 5.16: The optimal train speed trajectories, discharging/charging management and timetable for a general 3-station route with different OESD capacity (The sudden change of the SOE at the station represents the adjustment of SOE at each station)

Firstly, scenarios with different ISOE of the OESD, which are 30%, 80% and 100%, for a general inter-station operation, are conducted and compared, as shown in Figure 5.14. The running time for this case is 105 s and the track length is 1800 m. The black solid line is the optimal train speed trajectory obtained by using the proposed approach. It is easily observed that train speed trajectories and discharging/charging strategies of OESD are notably different due to the influence of the ISOE of OESD. The OESD should be charged to reach the optimal ISOE which is 57.0% before the train departs. When the train accelerates, the OESD is used to assist this motion, followed by slight acceleration motion until the OESD is fully utilised then the train starts to coast. The OESD is charged to be 100% when the train finishes the trip. As for the scenarios with respective ISOE, the train operations see different strategies, e.g. longest acceleration distance for case with ISOE=100% and longest braking distance for case with ISOE=30%. The discrepancies of the running time can also be observed when ISOE is different.

Normally different railway line has different operational requirement on timetable. In this case, here a general 3-station route with the total running time T_t set to be 250 s and 300 s respectively is investigated to understand how the model deal with different operational constraints. The results have been shown in Figure 5.15, and the optimal speed trajectories and the optimal ISOE for both journeys of both scenarios are

significantly different due to the change of T_t from the initial station to the terminal station. For instance, at the intermediate station, for scenario with $T_t = 250$ s the OESD needs to be discharged to decrease its SOE by 38.3% to reach the optimal ISOE for the next inter-station journey, which is 62.7%. For the scenario with $T_t = 300$ s the optimal solution is to charge the OESD and raises its SOE by 4.3% to reach the ISOE of 80.9%. The results indicate that different T_t brings different optimal strategies of both train operation and OESD management when the OESD is allowed to adjust its SOE during dwelling.

Different OESD specs will also lead to different optimal solutions, and the scenarios on the a general 3-station route with different capacities of OESD being 2.78 kWh (10 MJ) and 8.33 kWh (30 MJ) respectively are given to show this influence. The total running time T_t is fixed to be 300 s and the results are shown in Figure 5.16. It can be found that the optimal running time allocation, train operation and OESD operation are changed due to the influence of different OESD capacity. For the train equipped with OESD whose capacity is 2.78 kWh, the optimal ISOE of both inter-station operations are all 100% and at the end of the journey the OESD is fully charged by the regenerative energy. As a result, the OESD does not need to discharge or be charged at station 2.

In summary, the general case studies above show that the mutual influences among train operation, timetabling and OESD discharge/charge management exist. Additionally, it can also be told that the proposed method can deal with the systems with different parameters and specs, which shows the effectiveness and robustness of the approach.

5.5.2 Real-World Case: Beijing Yizhuang Line

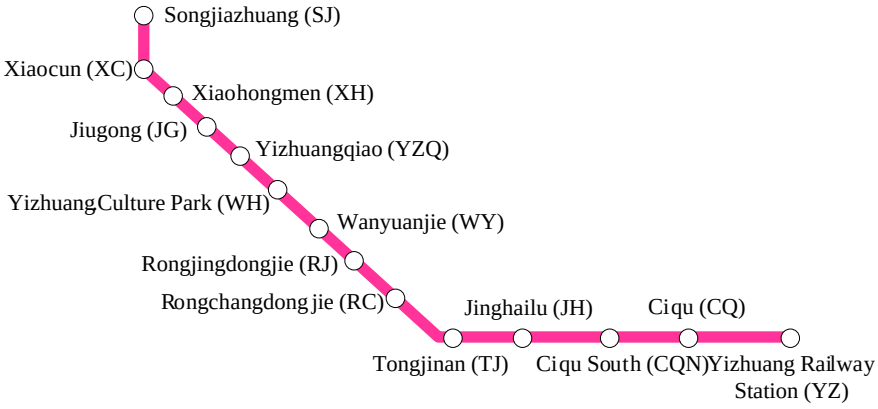

Figure 5.17: The route map of Beijing Yizhuang Line

Table 5.1: The operational information of Yizhuang Line

Start station	End station	Track length (m)	Running time windows (s)		Practical running time (s)	
			$\underline{T_I}$	$\overline{T_I}$	upline	downline
SJ	XC	2631	160	220	188	190
XC	XH	1274	82	138	106	103
XH	JG	2366	82	177	156	153
JG	YZQ	1983	117	152	133	133
YZQ	WH	992	68	120	84	84
WH	WY	1539	97	123	112	112
WY	RJ	1280	80	133	95	98
RJ	RC	1354	83	134	101	102
RC	TJ	2337	150	185	161	158
TJ	JH	2265	138	171	147	147
JH	CQN	2086	142	179	137	139
CQN	CQ	1287	80	132	98	98
CQ	YZ	1334	84	135	102	103
SUM		22728			1620	1620

Yizhuang Line has 14 stations, 1 depot and the total length of line is more than 22 km, see Table 5.1. For each inter-station section, the running time windows are different according to corresponding track length, system capacity and passenger demand, and the practical total running time for each direction, i.e. upline and downline, is 1620 s (27 minutes) respectively. The gradient change, speed limits, traction/braking force and train drag force are all are shown in Figure 5.18. Train mass is 194.3 t, maximum acceleration/deceleration rate is 1.2 m/s^2, OESD capacity is 11.1 kWh with a mass of 2.2 t and the maximum discharging/charging power being 500 kW. With the provided information above, the preprocessing in Step 1 will be conducted for all inter-station sections. It should be noticed that due to the different direction of movement of the train, the optimal train operation of each inter-station section on upline and downline will change due to different speed limits and gradients. This requires the preprocessing work to extend to 26 inter-station operations for both directions. Table 5.2 tabulates the results of the preprocessing work at Step 1 and the performances of the approximation for each inter-station operation of both direction are considered satisfactory with the minimum R^2 being 0.998 for inter-station operation YZQ-WH and WH-YZQ, which also shows the robustness of the proposed approximation in dealing with the real-world problem.

The optimal running time allocation for the whole line and the optimal ISOE of

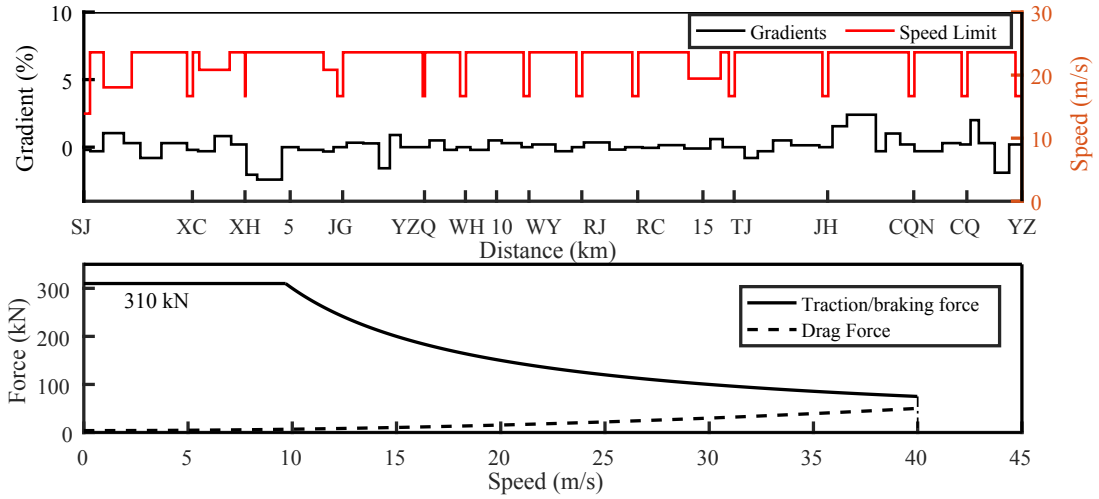

Figure 5.18: The route and traction/braking conditions of Yizhuang Line

OESD for each inter-station operation are listed in Table 5.3. It is easily observed that the optimal running time allocation yielded by the proposed approach has significant discrepancies when compared to the practical running time, and the offsets are also given in the parenthesis. The comparison between the optimal timetable and practical one are presented in Figure 5.19, showing that though the total running time for upline and downline is the same, the running time allocation is different. Similarly, the optimal ISOE for the same inter-station section is also different for upline and downline operation. After obtaining optimal solution of running time and ISOE for each inter-station operation, they can be used as input of MILP model in Chapter 4 to yield the optimal train speed trajectories, optimal discharging/charging curves of OESD as well as the minimum net energy consumption from the initial station to the terminal station.

The total CPU time for obtaining the optimal solution is the sum of the time consumed on finding optimal (T_i^*, $ISOE_i^*$) for each direction and the time consumed on finding the optimal speed profile for each inter-station operation based on the resulted (T_i^*, $ISOE_i^*$). The CPU time is 0.08+38.78 =38.86s for upline and 0.10+48.28=48.38 s for downline, which shows the high computational efficiency of the proposed approach. This is resulted from the proposed approach where solving step can significantly enhance computational efficiency with much fewer decision variables and much less complex modelling using the data from the preprocessing step. For instance, for each running direction the optimisation problem of this real-world case only consists of 26 variables (13 T_i and 13 $ISOE_i$) to be optimised in the objective function, 1 equality constraint

Table 5.2: The results of Step 1 for upline and downline of Yizhuang Line

Inter-Station section	P_1	P_2	P_3	P_4	$P_5(\times 10^{-4})$	R^2
SJ-XC	15.90	1470.42	-129.76	-0.06	2.15	0.999
XC-XH	4.33	613.92	-68.81	-0.05	3.85	0.999
XH-JG	4.97	2327.42	-94.88	-0.06	3.36	0.999
JG-YZQ	4.00	1747.21	-84.35	-0.06	4.01	0.999
YZQ-WH	0.37	548.51	-55.51	-0.04	3.48	0.998
WH-WY	-0.31	1283.22	-70.31	-0.06	4.12	0.999
WY-RJ	1.40	807.40	-64.97	-0.05	3.91	0.999
RJ-RC	1.88	869.05	-67.62	-0.05	3.97	0.999
RC-TJ	0.54	3208.89	-81.39	-0.06	3.31	0.999
TJ-JH	3.23	2552.20	-87.06	-0.06	3.44	0.999
JH-CQN	8.33	1710.89	-90.62	-0.06	3.64	0.999
CQN-CQ	1.22	826.23	-64.91	-0.05	3.92	0.999
CQ-YZ	1.32	879.97	-66.58	-0.05	3.95	0.999
YZ-CQ	0.95	891.92	-66.45	-0.05	3.92	0.999
CQ-CQN	1.27	824.89	-65.01	-0.05	3.91	0.999
CQN-JH	8.65	1658.26	-90.77	-0.06	3.69	0.999
JH-TJ	3.69	2174.83	-91.88	-0.06	3.48	0.999
TJ-RC	7.08	2139.44	-97.89	-0.06	3.17	0.999
RC-RJ	2.03	854.84	-67.89	-0.05	3.94	0.999
RJ-WY	1.41	804.72	-65.06	-0.05	3.88	0.999
WY-WH	-0.33	1286.04	-70.34	-0.06	4.13	0.999
WH-YZQ	0.21	558.43	-55.22	-0.04	3.43	0.998
YZQ-JG	3.72	1770.66	-84.09	-0.06	4.00	0.999
JG-XH	6.16	2181.99	-97.49	-0.06	3.31	0.999
XH-XC	4.18	612.30	-68.80	-0.05	3.83	0.999
XC-SJ	12.15	2064.00	-115.74	-0.06	2.72	0.999

ensuring the fixed total running time 1620 s and the lower/upper bounds of the variables guaranteeing their effective range, leading to a fast computing speed.

Figure 5.20 shows the optimal train speed trajectories and optimal discharging/charging strategy of OESD for upline and the Figure 5.21 shows the both optimal curves for downline, referring to the black solid line in the figure. The net energy consumption of each station and both directions are tabulated in Table 5.3. At each station, OESD needs to adjust its SOE, which has been shown as the gap of the SOE at each station in Figure 5.20 and Figure 5.21. The value for the gap is the difference between the terminal SOE of the last inter-station journey and the optimal ISOE of the next inter-station journey.

For showing the effectiveness of the proposed approach, three scenarios: "Fully

Table 5.3: The optimisation results for upline and downline of Yizhuang Line

Inter-Station section	T^* (s)	$ISOE^*$ (%)	E^* (kWh)
SJ-XC	176 (-12)	79.5	12.10 (+1.80[1], +0.67[2], -1.18[3])
XC-XH	99 (-7)	71.4	6.57 (+1.36[1], +1.28[2], -0.87[3])
XH-JG	151 (-5)	81.3	11.95 (+0.89[1], +0.56[2], -2.07[3])
JG-YZQ	140 (+7)	79.8	9.17 (-1.16[1], -1.23[2], -4.02[3])
YZQ-WH	85 (+1)	65.4	4.53 (-0.37[1], -0.31[2], -4.02[3])
WH-WY	120 (+8)	75.0	6.21 (-1.46[1], -1.44[2], -3.96[3])
WY-RJ	99 (+4)	70.5	6.51 (-1.11[1], -0.99[2], -3.28[3])
RJ-RC	104 (+3)	71.7	6.65 (-0.77[1], -0.69[2], -3.04[3])
RC-TJ	160 (-1)	81.5	10.57 (+0.13[1], +0.13[2], -2.70[3])
TJ-JH	143 (-4)	81.4	12.73 (+0.95[1], +0.89[2], -1.10[3])
JH-CQN	143 (+6)	81.4	10.63 (-0.99[1], -1.08[2], -3.81[3])
CQN-CQ	100 (+2)	70.6	6.46 (-0.45[1], -0.38[2], -2.66[3])
CQ-YZ	101 (-1)	72.0	6.99 (+0.16[1], +0.21[2], -2.09[3])
SUM	1620 (0)		111.35 (-1.00[1], -2.42[2], -64.08[3])
YZ-CQ	104 (+1)	77.9	6.21 (-0.24[1], -0.71[2], -2.58[3])
CQ-CQN	100 (+2)	76.3	6.29 (-0.62[1], -0.55[2], -2.86[3])
CQN-JH	143 (+4)	88.7	10.50 (-0.59[1], -0.62[2], -3.42[3])
JH-TJ	150 (+3)	88.7	11.19 (-0.51[1], -0.69[2], -3.53[3])
TJ-RC	155 (-3)	89.2	11.32 (+0.42[1], +0.28[2], -2.48[3])
RC-RJ	104 (+2)	77.4	6.70 (-0.43[1], -0.38[2], -2.75[3])
RJ-WY	100 (+2)	76.1	6.21 (-0.57[1], -0.51[2], -2.80[3])
WY-WH	115 (+3)	81.4	7.29 (-0.65[1], -0.64[2], -3.17[3])
WH-YZQ	84 (0)	70.4	4.71 (-0.17[1], -0.11[2], -2.24[3])
YZQ-JG	137 (+4)	86.7	9.69 (-0.63[1], -0.63[2], -3.49[3])
JG-XH	155 (+2)	89.0	11.34 (-0.32[1], -0.33[2], -3.45[3])
XH-XC	100 (-3)	76.3	6.20 (+0.64[1], +0.64[2], -1.73[3])
XC-SJ	172 (-18)	88.5	12.42 (+2.35[1], +1.95[2], -0.45[3])
SUM	1620 (0)		110.17 (-1.32[1], -2.31[2], -34.95[3])

[1] The difference between optimal strategy and fully charged strategy

[2] The difference between optimal strategy and no management strategy

[3] The difference between optimal strategy and situation without OESD

Charged", "No Management" and "No OESD", are selected to make comparison with the proposed optimal strategy based on this real-world metro line, the explanations of three scenarios are as follows:

- "Fully Charged" is to represent that the OESD is fully charged before the train departs from each station;
- "No Management" is to denote that OESD is empty at the first station and no

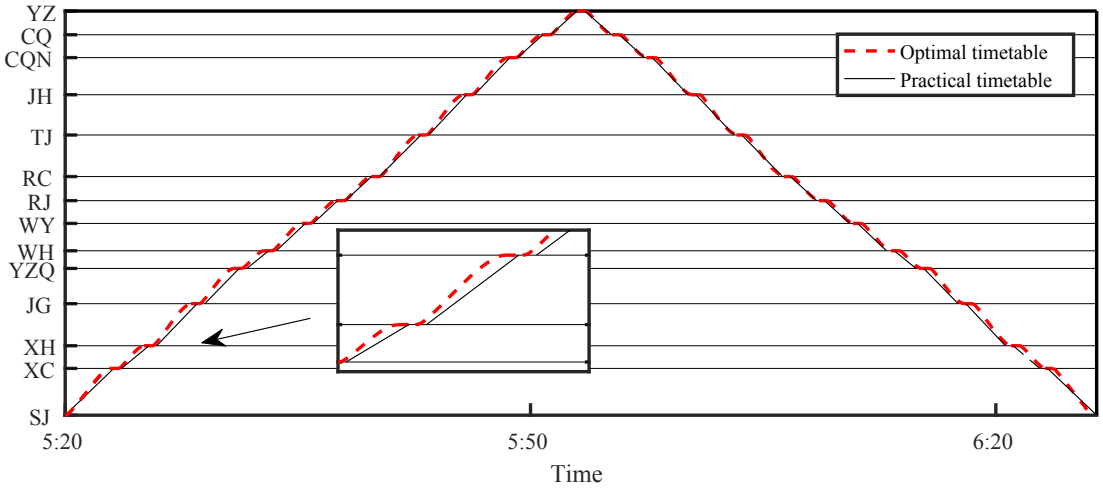

Figure 5.19: The comparison between the resulted optimal timetable and practical timetable of Beijing Yizhuang line for one service cycle from 5:20 am

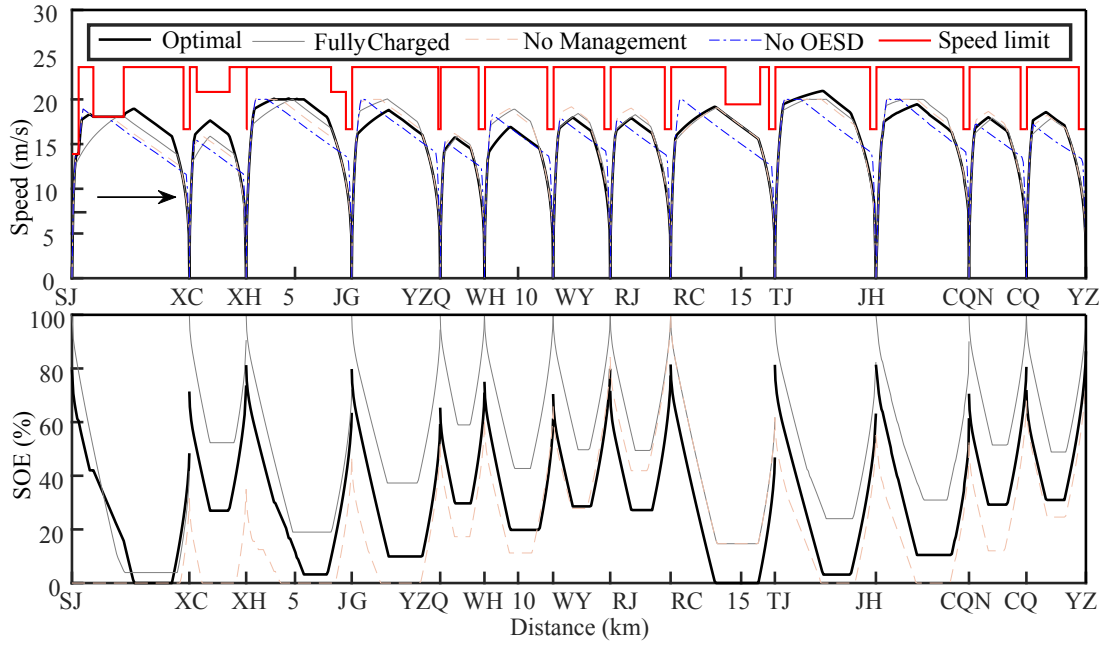

Figure 5.20: The optimal speed trajectories and discharging/charging management for upline operation (gap of the SOE represents the adjustment of SOE at each station)

discharging/charging behaviour are allowed when train dwells at station, thus the terminal SOE of the OESD is the ISOE of the next inter-station operation;

- "No OESD" is to denote the scenario that there is no OESD installed on the train.

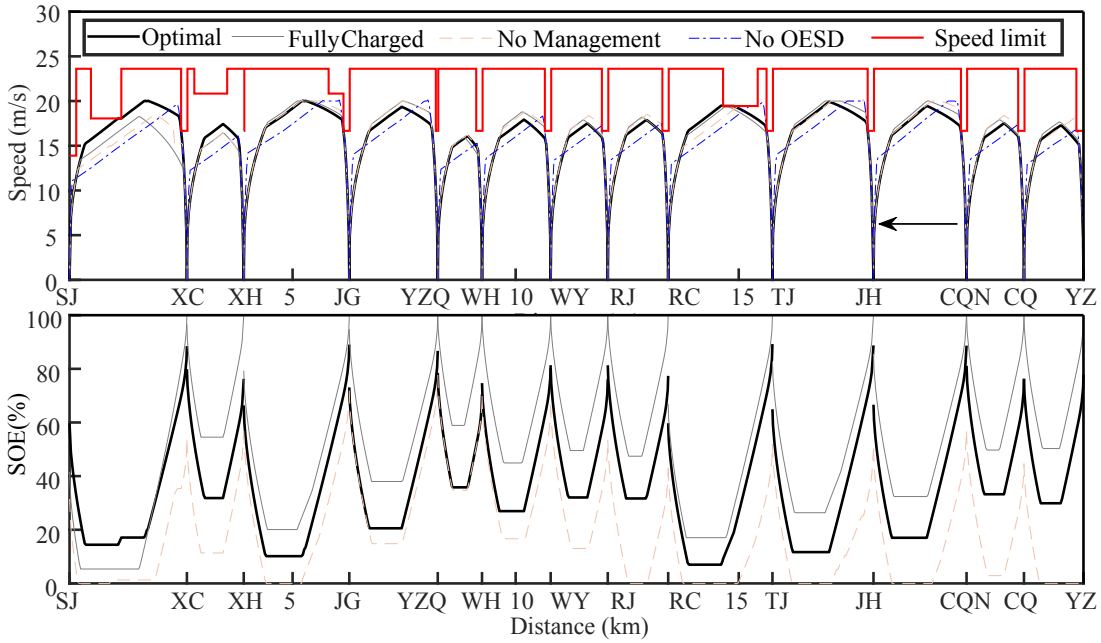

Figure 5.21: The optimal speed trajectories and discharging/charging management for downline operation (gap of the SOE represents the adjustment of SOE at each station)

Both scenarios involving OESD have been studied in previous research [114] and [93] and show good energy-saving performance. "Fully charged", "No Management" and "No OESD" scenarios are all conducted following the practical running time, the results of which are shown in Figure 5.20 and Figure 5.21, referring to the gray, brown and blue lines.. It is worth mentioning that for the "No OESD" scenario, the regenerative energy is not completely wasted but assumed to be utilised by the accelerating trains around, and the average recovering efficiency is set to be 30% according to the existing literature [7].

The speed trajectories and discharging/charging behaviours of these three scenarios and the optimal solution are significantly different. One thing should be noticed is that the optimal running time for WH-YZQ of the downline remains the same with the practical running time while the net energy consumption of the proposed optimal strategy is still lower than that of "Fully Charged" and "No Management" scenario, which shows the effectiveness of the proposed approach on OESD management to help reduce the energy consumption. Though for some inter-station operation, the proposed optimal strategy raises the net energy consumption, the total net energy consumption of each direction is minimised further, as shown in Table 5.3. For the upline the net energy consumption is reduced by 1.00 kWh, 2.42 kWh and 64.08 kWh, which is 0.89%,

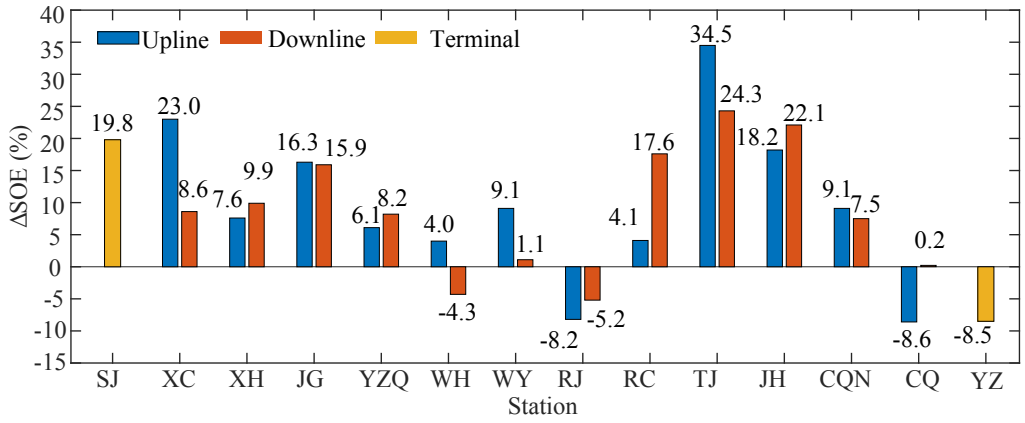

Figure 5.22: The optimal SOE adjustment value for OESD at each station, where the positive values mean that the OESD needs to charge the corresponding SOE when dwelling and negative values mean that the OESD needs to discharge the corresponding SOE

2.12% and 23.43%, and for the downline it is reduced by 1.32 kWh, 2.31 kWh and 34.95 kWh, which is 1.18%, 2.06% and 24.10% , compared to the "Fully charged", "No Management" and "No OESD" situations respectively. Therefore, for a service cycle of a single train, the net energy consumption can be saved by 1.04%, 2.09% and 23.77%. It can be seen that the energy consumption of the "No OESD" scenario is the highest among the optimal solution and other two scenarios, which implies that the installation of OESD has the most significant impact on the energy-saving effect. Also, by managing the ISOE and OESD power properly, the energy consumption can be reduced further by a relatively small but still effective value.

Figure 5.22 shows the adjustment value for the OESD at each station and it should be noticed that for upline and downline though at the same station it sees different management strategy i.e. charge by 4.0% SOE for upline operation and discharge by 4.3% for downline operation at RC, and different adjustment value i.e. charge by 34.5% SOE for upline operation and charge by 24.3% SOE for donwline operation at TJ. Additionally, it can be noticed that when each train begins the first service cycle from SJ the OESD needs to be charged to 79.5% of capacity assuming that the OESD is empty before the journey starts. Nevertheless, for the later service cycles, the OESD just needs to keep SOE to be 19.8% because the OESD has been charged by regenerative energy from the downline operation. Therefore, there are two special stations, SJ and YZ at both ends of the line, at which the OESD only has unique strategy regardless of the running directions.

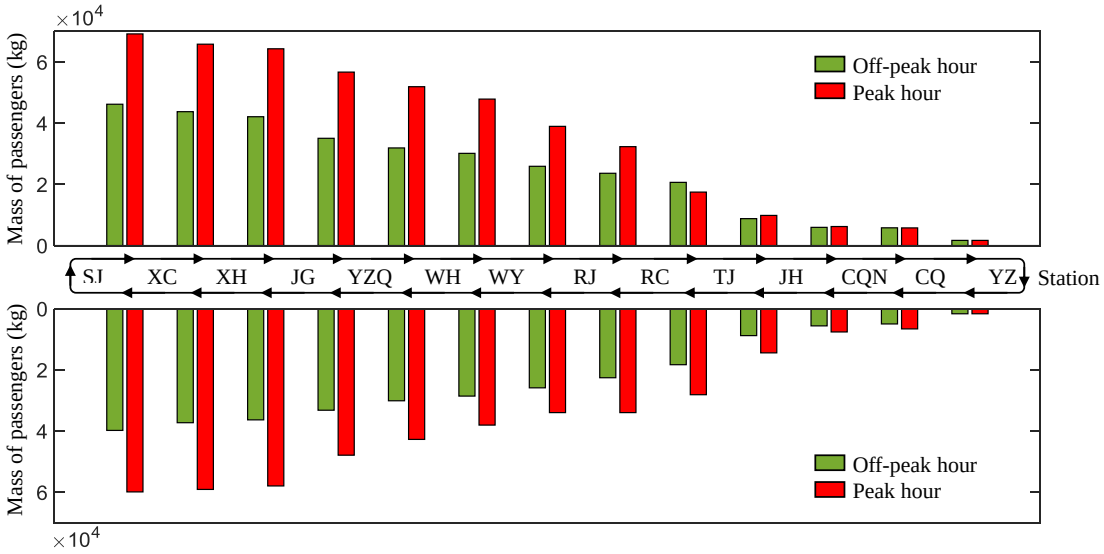

Figure 5.23: The average mass of the passengers for all of the inter-station sections during "off-peak hour" and "peak hour"

5.5.3 Considering Dynamic Passenger Demand

It can be observed that in real-world operations the passenger demand of the metro system is time-variant, which will lead to the different optimal solution for different time in one day. In the above case, only the optimal solution for off-peak time of Yizhuang Line from 5:20 am is investigated, for showing the flexibility and robustness of the proposed method, in this section the case with consideration of dynamic passenger demand is conducted.

It has been found that though the passenger demand of the metro system is time-variant in one day, its daily pattern is similar for each day, thus the real-world metro operation of one day will be divided into "peak-hour" and "off-peak hour" operations. As shown in Figure 5.23, the average mass of passenger for Yizhuang Line with respect to all of the inter-station sections are investigated [45], the data of which will be used in Step 1 of our proposed method to generate the approximations of energy consumption. As an example, Figure 5.24 illustrates the change of the approximation in different period for SJ-XC inter-station operation. It can be found that consideration of the passenger demand will not influence the proposed modelling and solving procedure, and the only difference for the approximation of "peak hour" and "off-peak hour" lies on increment of the minimum net energy consumption resulted from the varied total mass of the train with in-vehicle passengers.

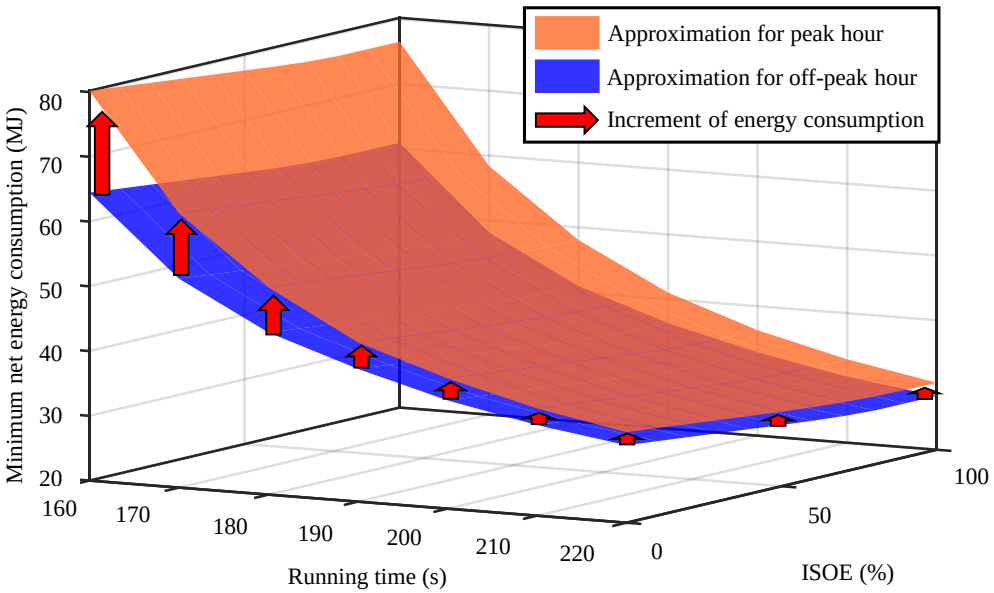

Figure 5.24: An SJ-XC example for showing the change of the approximation of minimum net energy consumption when considering the different passenger demand

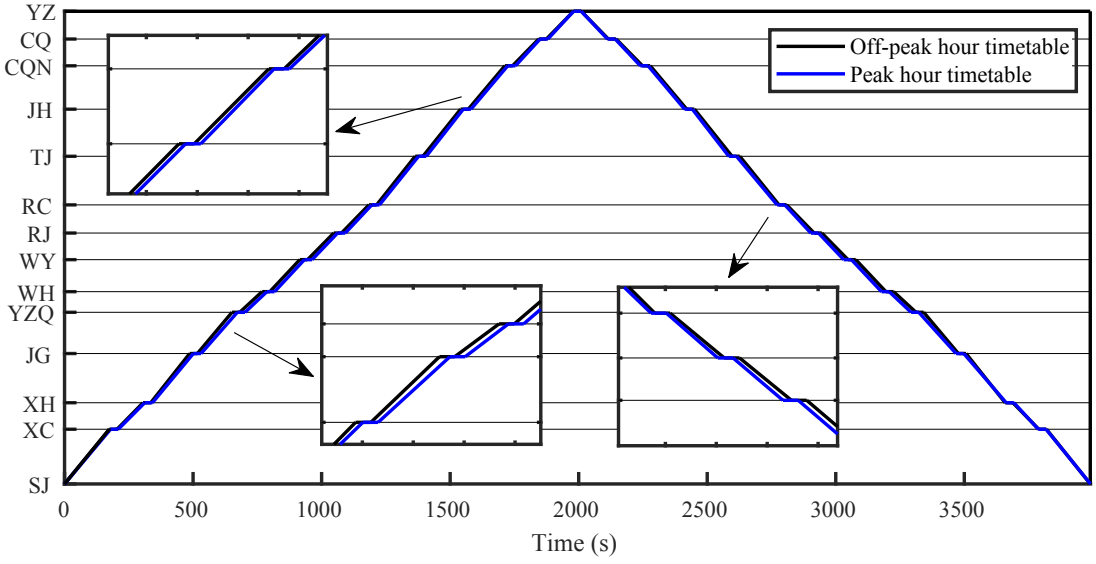

Figure 5.25: The optimal timetable for both "off-peak hour" and "peak hour" operations and the corresponding comparison for upline and downline

The optimal solution of the train timetable of the upline and downline, speed trajectories for each inter-station operation and OESD discharging/charging strategies during each inter-station journey/at each station are obtained for both "peak hour" and

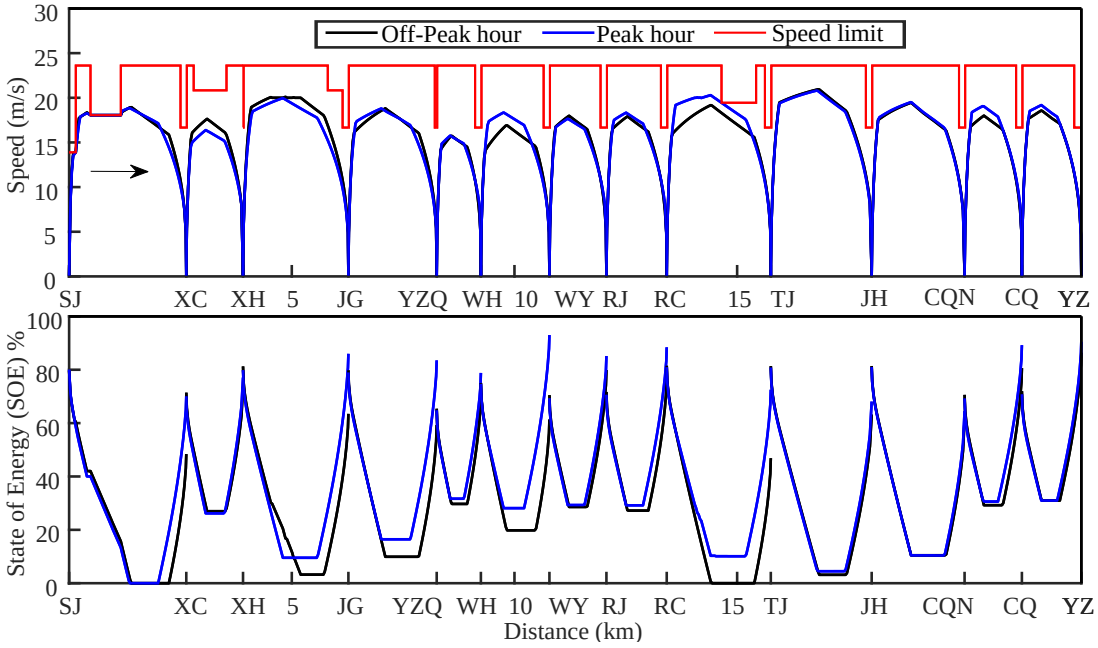

Figure 5.26: The optimal train speed trajectories and OESD discharging/charging management for both "off-peak hour" and "peak hour" operations and the corresponding comparison for upline

"off-peak hour" operations. Due to the difference of the passenger demand, the optimal solutions see difference in both period. The comparison between optimal timetable of each inter-station for "off-peak hour" and "peak hour" are presented in Figure 5.25, which shows that the proposed method reallocates the running time considering the impact of the passenger demand. Correspondingly, the optimal train speed trajectories for both directions and OESD discharging/charging strategies change as well when comparing both operation period, as illustrated in Figure 5.26 and 5.27.

The case shows the robustness of the proposed method when dealing with the dynamic passenger demand of the railway system, and the modelling and solving process of two steps guarantee the efficient and effective obtainment of the optimal solutions.

5.6 Summary

By extending the proposed model in Chapter 4, the optimal operation of the train with OESD for a service cycle is firstly studied in this chapter. From the perspective of energy interaction among train, substation and OESD, the energy-efficient management on energy stored in OESD and the optimal train speed trajectory can be integrated in

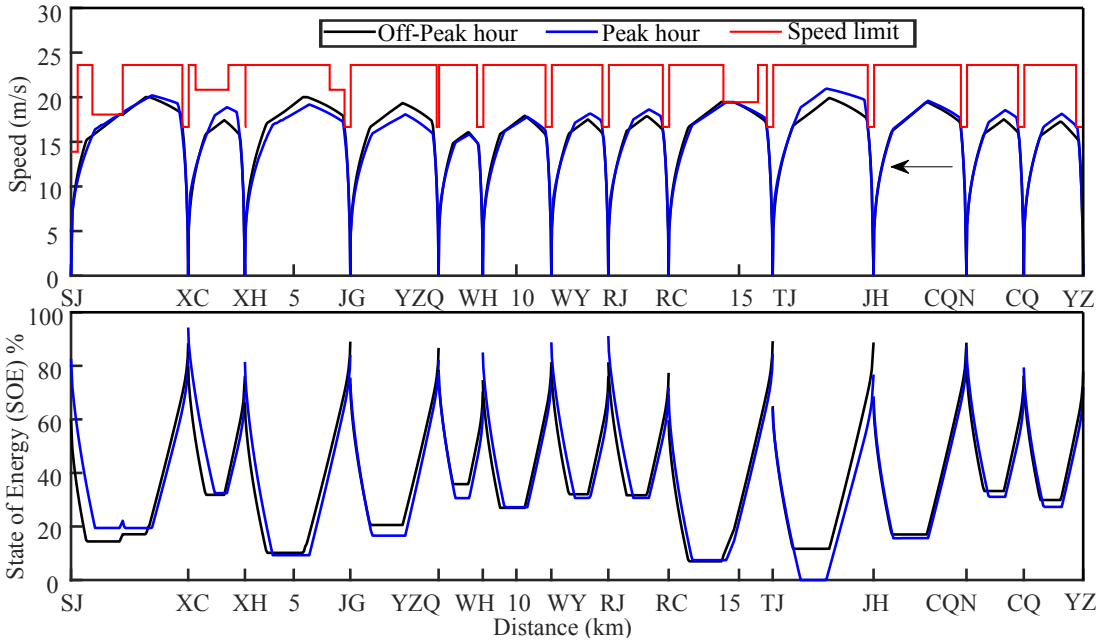

Figure 5.27: The optimal train speed trajectories and OESD discharging/charging management for both "off-peak hour" and "peak hour" operations and the corresponding comparison for downline

the optimisation process. A simple three-station route is used to test the method, and the results show that the method can concurrently optimise the train speed trajectory, timetable and OESD discharging/charging strategy during the running and at the stations.

However, the extended MILP method is found to be with serious limitations due to the soaring number of the variables and constraints when dealing with large number of inter-station operations, which implies that the new method needs to be adopted if the intelligent energy management of both the train and OESD are achieved in real-world railway systems with large number of stations.

Therefore, a two-step approach combining both of the MILP and convex optimisation to concurrently optimise the train speed, timetable and energy management strategy of the OESD to minimise the net energy consumption of the whole system is proposed. The drawbacks of the MILP are overcome by applying this new method, which is able to effectively address the up-rising challenging but also important issues when OESDs are deployed in the large-scale railway system operations. The real-world case, Beijing Yizhuang line, is adopted in case study by using the two-step approach, and the resulted optimal train operation, timetable and energy management strategy of OESD is found

to reduce the net energy consumption by 1.04%, 2.09% and 23.77% of a service cycle for a single train when compared to "Fully Charged", "No Management" and "No OESD" scenario respectively. The proposed approach is also computationally efficient since the CPU time for obtaining the optimal solution for multiple inter-station sections of the entire metro line is less than 1 min, namely 38.86 s for the upline and 48.38 s for the downline.

Chapter 6

Intelligent Train Operation with OESD in a Network

The main content of this chapter is from the author's submitted article in a version with minor reconfiguration to fit the structure and context of this thesis. The submitted article is:

C. Wu, S. Lu, Z. Tian, F. Xue and L. Jiang "Energy-Efficient Train Operation with Onboard Energy Storage Device considering Stochastic Regenerative Braking Energy," *under review*.

6.1 Introduction

This chapter aims to continuously extend the scope of the thesis, from the optimisation of operation in single inter-station section (Chapter 4), optimisation of operation in a service cycle (Chapter 5), to the optimisation of operation in the network (this chapter). In this chapter, the train operation with OESD is studied with the power network and train network involved.

It can be seen that some researchers have explored the area to optimise the train speed trajectory considering OESD and some have studied the utilisation of the regenerative braking energy by adjusting train timetable or operation mode. However, in the existing research the regenerative braking energy that cannot be recovered by the OESDs are assumed to be dissipated by the resistors as heat, as shown in Figure 6.1. Additionally, the regenerative braking energy utilisation is normally achieved by adjusting only the

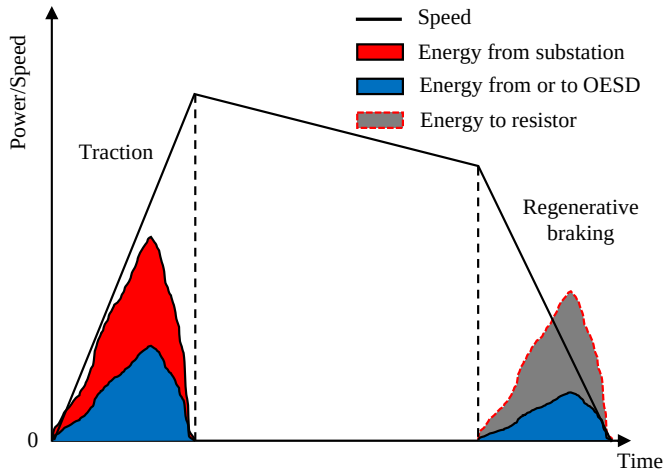

Figure 6.1: The schematic of the energy split for the train operation with OESD in the existing works

timetable or the train speed trajectory while the OESDs, as an efficient mean to absorb the regenerative braking energy, are not involved in these works. In this case, it can be found that these assumptions undermine the energy-saving potential of the OESD as well as the regenerative braking energy utilisation for the train with OESD, showing that the intelligent energy management of the train with OESD considering the utilisation of regenerative braking energy needs to be further explored.

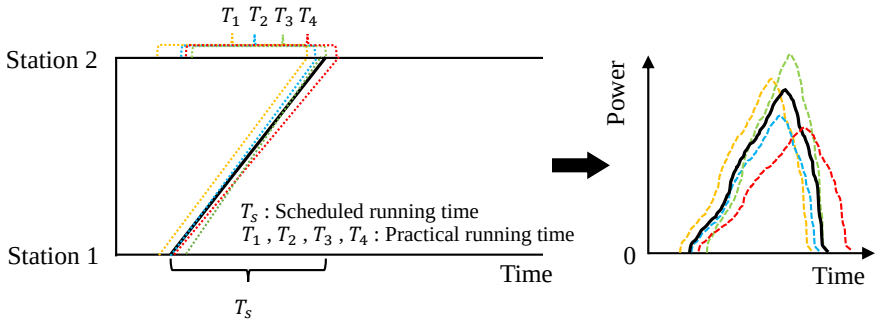

Figure 6.2: Relationship between various running time and the corresponding regenerative braking power in one inter-station operation

On the other hand, in real applications, uncertainties exist all the time, especially the stochastic train network with number of trains running at the same time across different power supply sections. One of the uncertainties is train's running time at each inter-station section, and the fluctuations of the train running time always occurs in the daily operations [117–120], as shown in Figure 6.2, which influences the regenerative

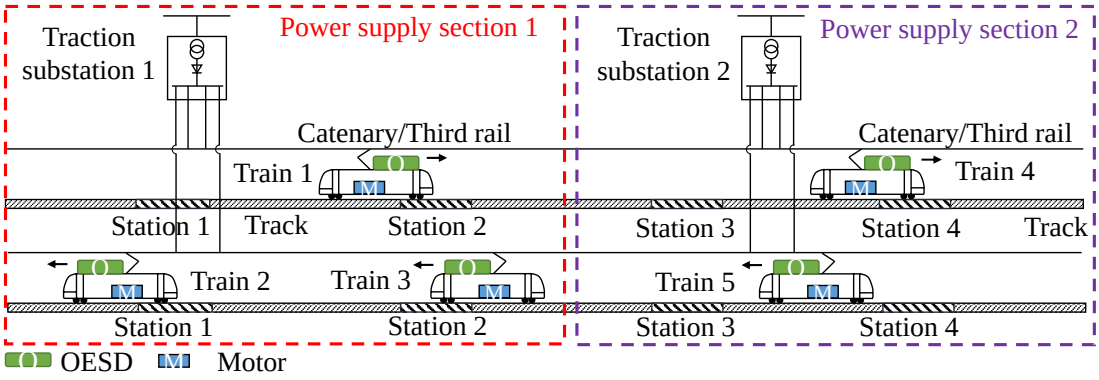

Figure 6.3: A schematic illustration of two power supply sections where the power is supplied from different traction substations. Most of power interaction is assumed to occur within one section, e.g. the regenerative braking energy generated in power supply section 1 can only be used by the trains running within the same section, i.e. Train 1, Train 2 and Train 3, but not by the trains running in other supply sections, i.e. Train 4 and Train 5 in power supply section 2 [57, 115, 116]

braking power in the environment of the power network. The uncertainty of the running time brings the stochastic characteristic on both the value and distribution of the regenerative braking energy in each power supply section (see Figure 6.3) along a period of time then the whole railway power network, which also leads to difficult applications of the solution given by the traditional timetable and trajectory optimisation methods based on deterministic parameters arising from static environment. Thus it can be seen that the stochastic characteristic of the system is not discussed yet by other relevant research in the field.

Given the above discussions, this chapter is mainly to tackle both of the problems related to the OESD's further applications in electrified railway systems as well as the utilisation of the stochastic regenerative braking energy in the environment. In this chapter, an agent-environment interface model as shown in Figure 6.4 is proposed to describe the relationship between the train and the network. Monte-Carlo simulation as the "perception" method is firstly applied to generate the expected regenerative braking power that cannot be absorbed by the OESDs from the viewpoint of long-term operation. This expectation is regarded as the environment to be perceived by each single train running in the network, as shown in Figure 6.4. Then based on the simulation results, an integrated MILP model is proposed to optimise the train trajectory with OESD to minimise the net energy consumption by taking into consideration of the stochastic regenerative braking energy in the railway power network. In summary, the main contributions are highlighted as follows:

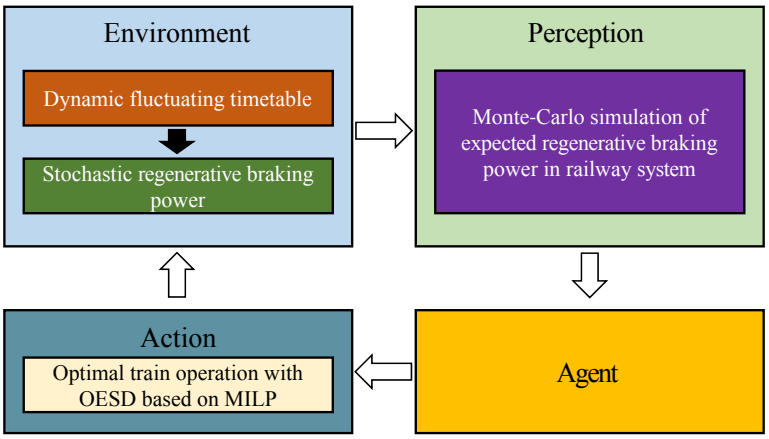

Figure 6.4: An agent-environment model between the train and railway power network. The train is the intelligent "agent" to perceive the environment using Monte-Carlo simulation to obtain the information of stochastic regenerative braking power and take optimal action to minimise the long-term expected energy cost via actuation such as ATO systems to offer an impact to the environment

- Different from most of the previous train operation optimisation methods depending on the deterministic information of power supply and precise control of multiple trains at the same time, including the proposed model in Chapter 4 and Chapter 5 in this thesis, this chapter adopts a agent-environment model and achieves the optimal solutions for each single-train operation in the network considering the environment information of other trains to realise a long-term expectation optimisation of the total energy cost.
- A new method is proposed to find the optimal train trajectory with OESD considering utilisation of regenerative braking energy, where the optimal catenary/third rail power, OESD power and utilised regenerative braking power is obtained to minimise the net energy consumption and maximise the expected utilisation of the available regenerative braking energy.

6.2 Trains with OESD in Stochastic Environment

Notation of variables	
v_i^2	Square of train speed in the position of $\sum_1^{i-1} \Delta d_i$ [m^2/s^2]
$\Delta E_{i,s}$	Energy from the substation in Δd_i [kJ]
$\Delta E_{i,dch}$	Energy discharged from the OESD in Δd_i [kJ]

(Continued from last page)	
$\Delta E_{i,ch}$	Energy charged to the OESD from motor in Δd_i [kJ]
$\Delta E_{i,r}$	Energy transmitted to the resistor from the motor in Δd_i [kJ]
$\Delta E_{i,reg,o}$	Energy transmitted to environment from the motor in Δd_i [kJ]
$\Delta \tilde{E}_{i,reg}$	Expected energy from the environment to the motor in Δd_i [kJ]
$\Delta \tilde{E}_{i,ch,reg}$	Expected energy from the environment to the OESD in Δd_i [kJ]
$\lambda_{i,1}, \lambda_{i,2}, \lambda_{i,3}$	Binary variables to determine the train operation mode in Δd_i
$t'_{i,x}$	Auxiliary variables to build the linear relationship of the expected regenerative braking power and time instant in Δd_i from t_x to t_{x+1}
α_x	Binary variables to build the linear relationship of the expected regenerative braking power and time instant in Δd_i from t_x to t_{x+1}
$\alpha_{i,j} \in [0,1]$	SOS2 variable set for linearisation of nonlinear speed-related constraints
$\beta_{i,j} \in [0,1]$	SOS2 variable set for linearisation of nonlinear speed-related constraints
$\mu^{\alpha}_{i,j}$	Binary variables in SOS2 variable set
$\mu^{\beta}_{i,j}$	Binary variables in SOS2 variable set
$y_{i,1}, y_{i,2}$	Auxiliary variables used in linearisation of the product of power and time in Δd_i
$\alpha^{y}_{i,j} \in [0,1]$	SOS2 variables used in linearisation of the product of power and time in Δd_i
$\beta^{y}_{i,j} \in [0,1]$	SOS2 variables used in linearisation of the product of power and time in Δd_i
$\sigma^{\alpha}_{i,j}$	Binary variables in SOS2 variable set
$\sigma^{\beta}_{i,j}$	Binary variables in SOS2 variable set
Assumptions	
	1. Running time variation follows a certain distribution based on the real data.
	2. Dwell time at each station follows the scheduled timetable without fluctuation.
	3. Energy interaction among trains can only happen when they are in the same power supply section.
	4. The expected available regenerative braking power is from all the trains in the network who are conducting the optimal speed trajectory with OESD.

In this section, the detailed procedure to optimise the train speed trajectory with OESD considering the stochastic regenerative braking power of the railway network is given. The Monte-Carlo simulation (see Section 3.8) is used to obtain the expected regenerative braking power distribution, the MILP model integrating the energy transmission among each resource and main objective of the proposed approach are elaborated.

6.2.1 Stochastic Time-Variant Regenerative Braking Power

Scenario Simulation of the Stochastic Running Time

For obtaining the expected regenerative braking energy distribution in the environment, the stochastic running time scenarios need to be found firstly. The detailed procedure has been shown as the flowchart in Figure 6.5. The running time for the certain run w of inter-station section s in one specific day q is denoted as $T_{w,s,q}$. Based on the data collected from the industry, running time between two adjacent stations are stochastic due to the unexpected influence of the status of passengers, operators or rolling stocks. In many papers related to the performance of the train timetable, most of the theoretical distribution models, such as Normal, Exponential, Weibull, and Log-normal distributions, have been used to fit statistical models to train running times [118–120]. In this case, the running time variation of each inter-station section s is assumed to follow specific distribution based on the performance analysis of the field running time data. In addition, it is assumed that there are totally S inter-station sections, W_S journeys for each inter-station s and Q days in the simulation of the studied railway network.

After the running time of all inter-station sections for Q days are obtained, the running time matrix for each day $\boldsymbol{T}^q$ can be constructed. Here the $\boldsymbol{T}^q$ with exact same elements are marked as a specific scenario γ with corresponding number of occurrence day q'_γ. The total number of the scenario is denoted as Γ, then scenario $\boldsymbol{T}^\gamma$ from 1 to Γ can be obtained. In this case, the probability π_γ of each specific scenario γ can be calculated by q'_γ over the total number of days Q, as presented in Figure 6.5.

Obtain the Expected Regenerative Braking Power

In the above running time simulation by using Monte-Carlo simulation, all scenario $\boldsymbol{T}^\gamma$ and the their corresponding probability π_γ from 1 to Γ have been obtained. Then the $\boldsymbol{T}^\gamma$ can be assigned to form the simulated timetable following the base timetable of the studied railway system, as shown in Figure 6.6-(a). Note that in the research the departure headway for the first train of initial station and the dwell time at each station

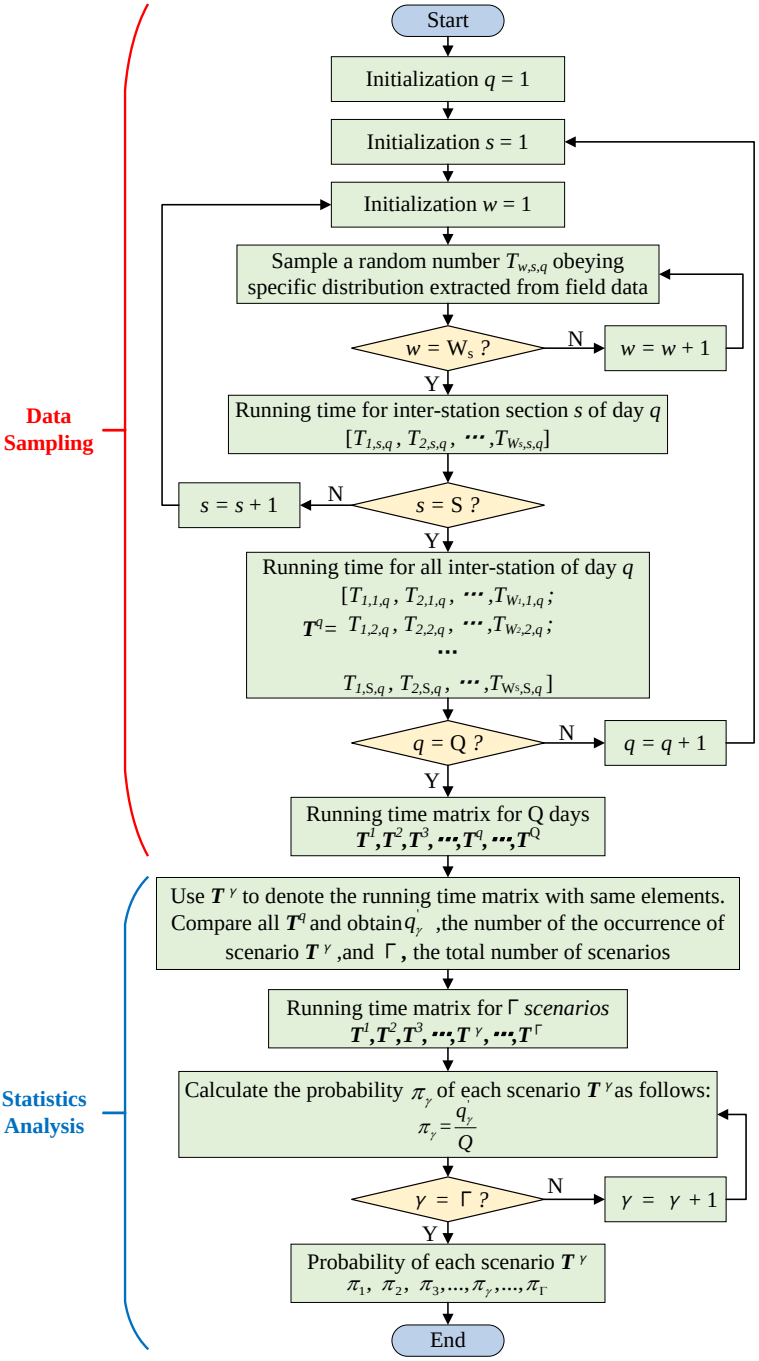

Figure 6.5: The flowchart of the Monte-Carlo simulation by sampling the running time for all of the inter-station operations and conducting the statistics analysis of the generated scenarios

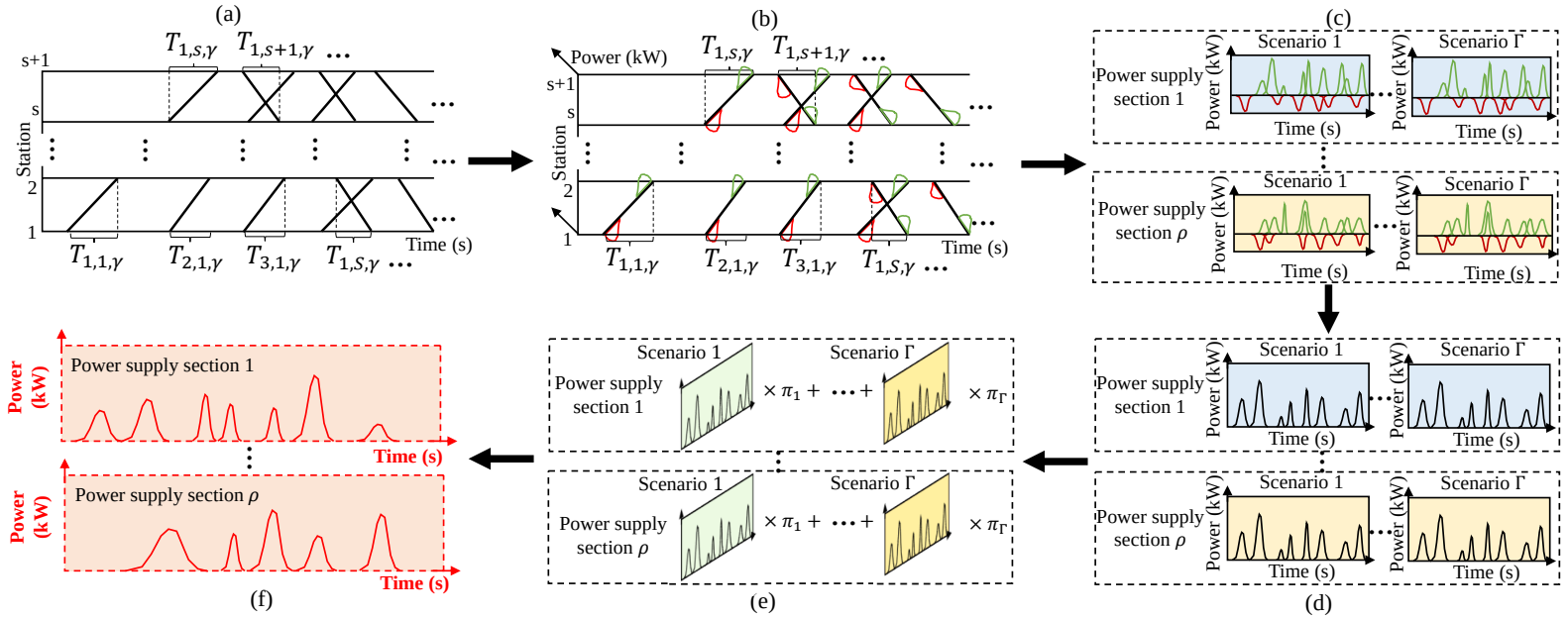

Figure 6.6: The procedure to obtain the expected time-variant regenerative braking power distribution of the railway system: (a) Simulate the timetable of each scenario using $\boldsymbol{T}^{\gamma}$ following the base timetable of the studied system; (b) Simulate the power distribution of each scenario of the studied system; (c) Calculation of the time-variant net power values of all scenarios for all power supply sections; (d) Time-variant available regenerative barking power distribution of all scenarios for all power supply sections; (e) Calculation of the expected value based on all scenarios for all power supply sections; (f) Expected time-variant available regenerative braking power distribution for all power supply sections

are assumed to remain unchanged as the scheduled base value. After the simulated timetable of all scenarios are made, the power distribution of each scenario can be produced by using the model proposed in Chapter 4 based on each $\boldsymbol{T}^{\gamma}$, as illustrated in Figure 6.6-(b). The model proposed in Chapter 4 is able to obtain the traction power outstripping the OESD discharging power and the regenerative braking power outstripping the OESD charging power. Here the regenerative braking energy is positive and the traction power is negative. Assuming ρ is used to index each power supply section in the studied railway system, as shown in Figure 6.6-(c), the time-variant net power distribution can be obtained by summing all of the negative and positive power on same time instant in same power supply section since some released regenerative braking energy would be used instantly by the train in traction mode. By eliminating the negative part of the net power distribution, the rest of the regenerative braking power forms the time-variant available regenerative braking power distribution $P_{reg,\gamma,\rho}$ in the environment for each scenario in each power supply section, as presented in Figure 6.6-(d). As shown in Figure 6.6-(e), the next step is to calculate the expected value by multiplying the power distribution of each scenario with its corresponding probability π_{γ}, then the expected available regenerative braking power for each power supply section $\tilde{P}_{reg,\rho}$ can be gained, as presented in Figure 6.6-(f).

6.2.2 Energy Transmission in Stochastic Environment

During the journey, the train can consume the energy from the substation $\Delta E_{i,s}$, the energy discharged by the OESD $\Delta E_{i,dch}$ and the expected regenerative braking energy from other trains $\Delta \tilde{E}_{i,reg}$ when the train is in traction mode. Here the work of the train motor, denoted as $\Delta E^{+}_{i,m}$, can be expressed in (6.1).

$$\Delta E^{+}_{i,m} = \Delta E_{i,s}\eta_s + \Delta E_{i,dch}\eta_o + \Delta \tilde{E}_{i,reg}\eta_r, \quad \forall i = 1, 2, 3, ..., N \tag{6.1}$$

where η_s, η_o and η_r is the energy transmission and conversion efficiency for the corresponding energy supply source.

When the train is braking, the motor is in braking mode and part of the energy can be delivered to the OESD, which is denoted as $\Delta E_{i,ch}$ here. Some of the energy will be transmitted to other trains through catenary/third rail, denoted as $\Delta E_{i,reg,o}$, and the rest of the energy will be dissipated by resistor, denoted as $\Delta E_{i,r}$. Thus, during the

braking mode, the work of the train motor, denoted as $\Delta E^{-}_{i,m}$, is represented in (6.2).

$$\Delta E^{-}_{i,m} = -\frac{\Delta E_{i,ch}}{\eta_o} - \Delta E_{i,reg,o} - \Delta E_{i,r}, \quad \forall i = 1, 2, 3, ..., N \tag{6.2}$$

According to the law of conservation of the energy, the conversion of the energy can be expressed in (6.3).

$$\Delta E^{+}_{i,m} - \Delta E^{-}_{i,m} - \frac{1}{2}(M_t + M_o)(v^2_{i+1} - v^2_i) - R_i \Delta d_i - (M_t + M_o) g \theta_i \Delta d_i - \Delta E_{i,r} = 0, \quad \forall i = 1, 2, ..., N \tag{6.3}$$

Since the OESD is able to receive the regenerative braking energy from the environment all the time, variables $\Delta \tilde{E}_{i,ch,reg}$ is used to represent the expected regenerative braking energy charged to the OESD from other trains. Additionally, the train cannot conduct traction and braking at the same time, the traction energy in (6.1) and regenerative energy in (6.2) of the train cannot exist simultaneously in one Δd_i. Similarly, OESD cannot discharge or be charged at the same time but the OESD can receive the regenerative braking energy in the environment whenever the train is running on the track, just as shown in Figure 6.3. In this case, the binary variables $\lambda_{i,1}$, $\lambda_{i,2}$, $\lambda_{i,3}$ and a large number L need to be imposed into the model to determine the train and OESD operation mode in each Δd_i, as shown in (6.4) - (6.8).

$$0 \leq \Delta E_{i,s} \leq \lambda_{i,1} L, \quad 0 \leq \Delta \tilde{E}_{i,reg} \leq \lambda_{i,1} L, \quad \forall i = 1, 2, 3, ..., N \tag{6.4}$$

$$0 \leq \Delta E_{i,ch} \leq (1 - \lambda_{i,1}) L, \quad \forall i = 1, 2, 3, ..., N \tag{6.5}$$

$$0 \leq \Delta \tilde{E}_{i,ch,reg} \leq (1 - \lambda_{i,2}) L, \quad \forall i = 1, 2, 3, ..., N \tag{6.6}$$

$$0 \leq \Delta E_{i,dch} \leq \lambda_{i,3} L, \quad \forall i = 1, 2, 3, ..., N \tag{6.7}$$

$$\lambda_{i,3} \leq \lambda_{i,1}, \quad \lambda_{i,3} \leq \lambda_{i,2}, \quad \lambda_{i,3} \geq \lambda_{i,1} + \lambda_{i,2} - 1, \quad \forall i = 1, 2, 3, ..., N \tag{6.8}$$

To make it clearer, the value selection of these 3 binary variables and the resulted train operation mode with different energy flow have been shown in Table 6.1. It can be seen that when $\lambda_{i,1}$=1, the substation, OESD and regenerative braking energy in the environment can be transmitted to the train jointly. At the same time, if $\lambda_{i,2}$=1, then $\lambda_{i,3}$=1, the train is in traction mode and discharging process of the OESD is able to happen; if $\lambda_{i,2}$=0, then $\lambda_{i,3}$ =0, discharging process of OESD does not happen and it

Table 6.1: The value selection of the binary variables $\lambda_{i,1}$, $\lambda_{i,2}$ and $\lambda_{i,3}$ and the resulted train operation mode with corresponding energy flow illustration

Value selection	Operation mode	Energy flow illustration
$\lambda_{i,1}$=1, $\lambda_{i,2}$=1, $\lambda_{i,3}$=1.	Traction	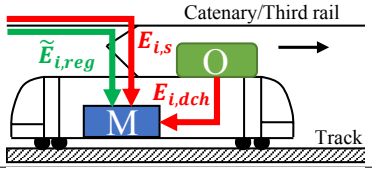
$\lambda_{i,1}$=1, $\lambda_{i,2}$=0, $\lambda_{i,3}$=0.	Traction	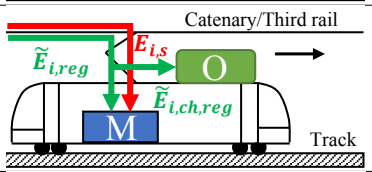
$\lambda_{i,1}$=0, $\lambda_{i,2}$=1, $\lambda_{i,3}$=0.	Braking	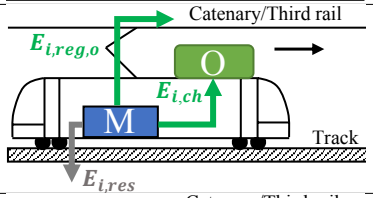
$\lambda_{i,1}$=0, $\lambda_{i,2}$=0, $\lambda_{i,3}$=0.	Braking	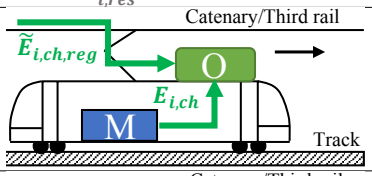
$\lambda_{i,1}$=1, $\lambda_{i,2}$=0, or $\lambda_{i,3}$=0. $\lambda_{i,1}$=0, $\lambda_{i,2}$=0, $\lambda_{i,3}$=0.	Coasting	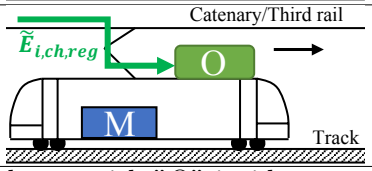

*In all of the figures in the table, the green boxes with "O" inside represent OESDs, and the blue boxes with "M" inside represent motors.

represents 2 possible scenarios: (1) the train is in traction mode and the regenerative braking energy in the environment can be charged into the OESD during the traction; (2) the train is coasting and the regenerative braking energy in the environment can be charged into the OESD when energy from substation and environment to motor are both assigned to be 0. Contrarily, when $\lambda_{i,1}$=0, then $\lambda_{i,3}$ is always 0, ensuring that the discharging process would not happen at the same time. The train motor is enabled to regenerate the energy, and the OESD can receive the energy from the motor and environment. At this time, if $\lambda_{i,2}$=1, the train is braking, and the OESD can only be charged by the regenerative braking energy from the train's own motor; if $\lambda_{i,2}$=0, it represents two possible scenarios: (1) the train is braking, and the OESD

can be charged by the regenerative braking energy from the train's own motor and the environment together; (2) the train is coasting and the regenerative braking energy in the environment can be charged into the OESD when energy from train's own motor is assigned to be 0.

As the the motor has its own traction/braking characteristics, thus, in each Δd_i, the maximum force the motor can conduct should follow the limitation of its maximum traction force $\overline{F_t}$ and maximum braking force $\overline{F_b}$. Also, it needs to be limited by the maximum traction power $\overline{P_t}$ and maximum braking power $\overline{P_b}$. Thus, these can be expressed as shown in (6.9) and (6.10).

$$0 \leq \Delta E_{i,m}^{+} \leq \overline{F_t} \Delta d_i, \quad 0 \leq \Delta E_{i,m}^{-} \leq \overline{F_b} \Delta d_i, \quad \forall i = 1, 2, 3, ..., N \tag{6.9}$$

$$0 \leq \Delta E_{i,m}^{+} \leq \overline{P_t} \Delta t_i, \quad 0 \leq \Delta E_{i,m}^{-} \leq \overline{P_b} \Delta t_i, \quad \forall i = 1, 2, 3, ..., N \tag{6.10}$$

For OESD, the discharged and charged energy cannot exceed the maximum value determined by the maximum charge and discharge power P_o, as expressed in (6.11).

$$0 \leq \Delta E_{i,dch} \leq \overline{P_o} \Delta t_i, \quad 0 \leq \Delta E_{i,ch} + \tilde{E}_{i,ch,reg} \leq \overline{P_o} \Delta t_i, \quad \forall i = 1, 2, 3, ..., N \tag{6.11}$$

There are $N + 1$ SOE_i during the journey with N Δd_i. SOE for OESD when the train passes Δd_i, denoted as SOE_{i+1}, can be expressed in (6.12).

$$0 \leq SOE_{i+1} = SOE_1 + \frac{-\sum_1^i \Delta E_{i,dch} + \sum_1^i \Delta E_{i,ch} + \sum_1^i \Delta \tilde{E}_{i,ch,reg}}{E_{cap}} \leq 100\%, \quad \forall i = 1, 2, 3, ..., N \tag{6.12}$$

where SOE_1 is the initial stored energy in OESD, and E_{cap} is the capacity of the OESD.

The relationships among the speed-related variables, v_i, v_i^2, $v_{i,ave}^2$ and $1/v_{i,ave}$, are not linear. These relationships can be linearised by using the proposed method discussed in Chapter 4. The riding comfort of the passengers and the operational limit of the train can follow the constraints of maximum allowed acceleration/deceleration maximum given in Chapter 4. Similarly, the punctuality can be ensured by adding the constraint of total journey, see Chapter 4 also.

6.2.3 Modelling the Utilisation of Regenerative Braking Energy

As shown in Figure 6.7-(a), the black solid line is the gained expected available time-variant regenerative braking power distribution in power supply section ρ, and it can be

expressed with the function shown in (6.13).

$$\tilde{P}_{reg,\rho} = f(t) \tag{6.13}$$

where t is the time instant in one day.

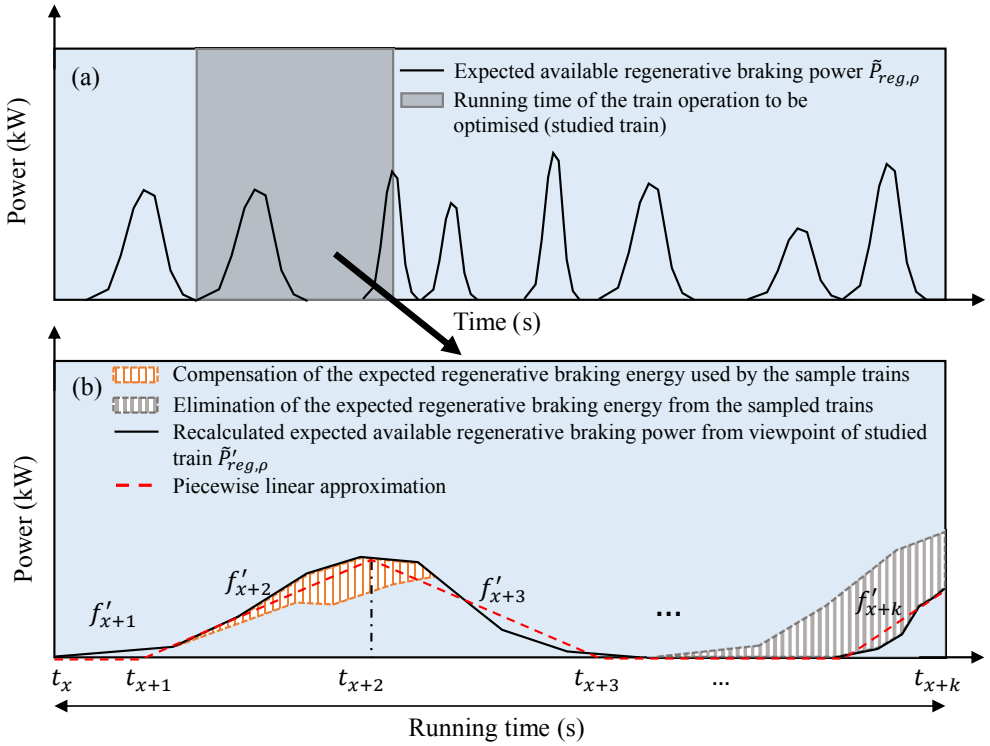

Figure 6.7: (a) The obtained expected time-variant available regenerative braking power in the environment formed by the sampled trains; (b) The piecewise linear approximation of the recalculated expected available regenerative braking power from the viewpoint of the studied train by compensating and eliminating the expected regenerative braking power affected by the sampled trains

It needs to be clarified that $\tilde{P}_{reg,\rho}$ is formed by the trains following simulated timetables (Referred to as the "sampled trains" below). In order to integrate $\tilde{P}_{reg,\rho}$ with the proposed single-train model above, the available regenerative braking energy that can be utilised by single train operation need to be extracted. The gray square in Figure 6.7-(a) represents the running time of a specific inter-station train service to be optimised (Referred to as the "studied train" below). In this running time horizon, the expected generated and consumed regenerative braking energy by sample trains serving the same inter-station section for same service cycle as the studied train need

to be deducted from/compensated back to the $\tilde{P}_{reg,\rho}$ as these sampled trains are not supposed to directly contribute to the environment from the viewpoint of the studied train and their impacts need to be off-set by the deduction or compensation procedure as demonstrated by Figure 6.7-(b).

As shown in Figure 6.7-(b), $\tilde{P}_{reg,\rho}$ excludes the expected used regenerative braking power by the sampled trains, thus this part needs to be compensated to the environment since the studied train can still use it, shown as the orange area in Figure 6.7-(b). In addition, $\tilde{P}_{reg,\rho}$ also contains the expected regenerative braking power from the sampled trains, this part should be eliminated since the studied train cannot use it, as the gray area shown in Figure 6.7-(b). After the recalculation procedure of the expected regenerative braking power distribution in the environment from the viewpoint of studied train, $\tilde{P}'_{reg,\rho}$, can be obtained. Then the piecewise linear approximation is introduced, shown as the red dashed lines in the figure, to approximate $\tilde{P}'_{reg,\rho}$. Assuming that there are K piecewise linear sections for the approximation, thus it can be represented by using (6.14).

$$\tilde{P}_{reg,\rho} \approx \begin{cases} f'_1(t) = a_1 t + b_1, & \text{for} \quad t_0 \leq t \leq t_1 \\ f'_2(t) = a_2 t + b_2, & \text{for} \quad t_1 \leq t \leq t_2 \\ \vdots & \\ f'_x(t) = a_x t + b_x, & \text{for} \quad t_{x-1} \leq t \leq t_x \\ \vdots & \\ f'_K(t) = a_K t + b_K, & \text{for} \quad t_{K-1} \leq t \leq t_K \end{cases} \tag{6.14}$$

where t_0, t_1, t_2, ... , t_x, ... , t_K are the time instant for the piecewise linear sections, f_1, f_2, ... , f_x, ... , f_K are the approximated linear functions, a_1, a_2, ... a_x, ... , a_K and b_1, b_2, ... b_x, ... , b_K are the coefficient for the piecewise functions.

As the approximation of expectation of the regenerative braking power are obtained, the utilisation of it through adjusting the train operation can be conducted. The gray square in Figure 6.7-(a) represents the running time of a specific inter-station operation to be optimised, which is also enlarged in Figure 6.7-(b). In one specific inter-station, except the energy from the traction substation and OESDs, the regenerative braking energy can also be used by the train. The expected regenerative braking power has been approximated by several time-variant piecewise linear functions, $k-1$ piecewise sections, from time instant t_x to t_{x+k} with the corresponding linear functions f'_{x+1} to f'_{x+k}, are assumed to be covered by the running time of the studied train operation.

The expected regenerative braking power the train can utilise in each Δd_i depends

on the corresponding time instant. Due to the discretisation of the proposed model, the time instant, denoted as t'_i, of the train from departure to any Δd_i can be calculated using (6.15).

$$t'_i = t_x + \sum_{1}^{i-1} \Delta t_i + \frac{1}{2}\Delta t_i, \quad \forall i = 1, 2, 3, ..., N \tag{6.15}$$

Here the $\frac{1}{2}\Delta t_i$ is the midpoint of the elapsed time of each Δd_i that is used to approximate the time instant together with the accumulated value of the previous journey. It can be observed that this approximation is more accurate with the shorter Δd_i.

Here $\tilde{P}'_{i,reg,\rho}$ is used to represent the maximum expected regenerative braking power that can be used by the train in each Δd_i in certain power supply section ρ. To piecewisely linearise the relationship between $\tilde{P}'_{i,reg,\rho}$ and time instant, the binary variables α_x, and the auxiliary variables $t'_{i,x}$ are introduced to reformulate the original functions as shown in (6.16) - (6.19).

$$\tilde{P}'_{i,reg,\rho} = \sum_{x}^{x+k} a_x t'_{i,x} + b_x \alpha_x, \quad \forall i = 1, 2, 3, ..., N \tag{6.16}$$

$$\alpha_x t_x \leq t'_{i,x} \leq \alpha_{x+1} t_{x+1}, , \quad \forall x = x, x+1, ..., x+k, \quad \forall i = 1, 2, 3, ..., N \tag{6.17}$$

$$\sum_{x}^{x+k} \alpha_x = 1 \tag{6.18}$$

$$t'_i = \sum_{x}^{x+k} t'_{i,x}, \quad \forall i = 1, 2, 3, ..., N \tag{6.19}$$

(6.16) - (6.19) are used to build the linear relationship of the time-variant expected regenerative braking power and time instant by introducing the logical determination process, as shown in Section 3.5.2. It can be observed that in each Δd_i, the corresponding t'_i will be automatically allocated to a certain piecewise linear section.

In this case, the expected regenerative braking energy utilised by the studied train operation in each Δd_i depends on the product of $\tilde{P}'_{i,reg,\rho}$ and Δt_i which is expressed by (6.20).

$$0 \leq \Delta \tilde{E}_{i,reg} + \Delta \tilde{E}_{i,ch,reg} \leq \tilde{P}'_{i,reg,\rho} \Delta t_i, \quad \forall i = 1, 2, 3, ..., N \tag{6.20}$$

In (6.20) the product of the power and time can be linearised by conducting the method in Section 3.5.3. The auxiliary variables $y_{i,1}$ and $y_{i,2}$ are introduced, as shown

in (6.21).

$$y_{i,1} = \frac{1}{2}(\tilde{P}'_{i,reg,\rho} + \Delta t_i), \quad y_{i,2} = \frac{1}{2}(\tilde{P}'_{i,reg,\rho} - \Delta t_i), \quad \forall i = 1, 2, 3, ..., N \tag{6.21}$$

In this case, it has the relationships represented by (6.22).

$$\tilde{P}'_{i,reg,\rho}\Delta t_i = y_{i,1}^2 - y_{i,2}^2, \quad \forall i = 1, 2, 3, ..., N \tag{6.22}$$

Here one preset series of piecewise points Y_j is used to represent $y_{i,1}$ and $y_{i,2}$. In this case, (6.22) can be reformulated into (6.23).

$$\tilde{P}'_{i,reg,\rho}\Delta t_i = \sum_{j=1}^{J} Y_j^2 \alpha_{i,j}^y - \sum_{j=1}^{J} Y_j^2 \beta_{i,j}^y, \quad \forall i = 1, 2, 3, ..., N \tag{6.23}$$

where $\alpha_{i,j}^y$ and $\beta_{i,j}^y$ are 2 sets of SOS2 variables for each type of OESD in Δd_i, and J is the number of the corresponding piecewise points. As a result, they also need to follow the (6.24).

$$\sum_{j=1}^{J} \alpha_{i,j}^y = 1, \quad \sum_{j=1}^{J} \beta_{i,j}^y = 1, \quad \forall i = 1, 2, 3, ..., N \tag{6.24}$$

To ensure that only the adjacent $\alpha_{i,j}^y$ and $\beta_{i,j}^y$ can be nonzero and their sum being 1, binary variables $\sigma_{i,j}^\alpha$ and $\sigma_{i,j}^\beta$ need to be imposed, as shown in (6.25) and (6.26).

$$\alpha_{i,j}^y + \alpha_{i,j+1}^y - \sigma_{i,j}^\alpha \geq 0, \quad \beta_{i,j}^y + \beta_{i,j+1}^y - \sigma_{i,j}^\beta \geq 0, \quad \forall i = 1, 2, 3, ..., N \tag{6.25}$$

$$\sum_{j=1}^{J-1} \sigma_{i,j}^\alpha = 1, \quad \sum_{j=1}^{J-1} \sigma_{i,j}^\beta = 1, \quad \forall i = 1, 2, 3, ..., N \tag{6.26}$$

6.2.4 Objective of the Proposed Model

The optimisation objective of the proposed model is to minimise the net energy consumption of the train operation from the energy sources, substation, OESD and other trains in the network. The net energy consumption can be expressed by the difference of the traction energy consumption and the recovered energy by OESD, which can be formulated as (6.27).

$$\min \quad \sum_{i=1}^{N} (\underbrace{\Delta E_{i,s} + \Delta E_{i,dch} + \Delta \tilde{E}_{i,reg}}_{\text{Energy consumed for traction}} \underbrace{- \Delta E_{i,ch} - \Delta \tilde{E}_{i,ch,reg}}_{\text{Energy recovered by OESD}}) \tag{6.27}$$

By conducting the optimisation, it can be seen that the traction energy consumption, $\Delta E_{i,s} + \Delta E_{i,dch} + \Delta \tilde{E}_{i,reg}$, can be minimised with support of the energy from OESD and expected utilisation of regenerative braking energy, and the expected recovered energy $\Delta E_{i,ch}$ and $\Delta \tilde{E}_{i,ch,reg}$ by OESD can be maximised.

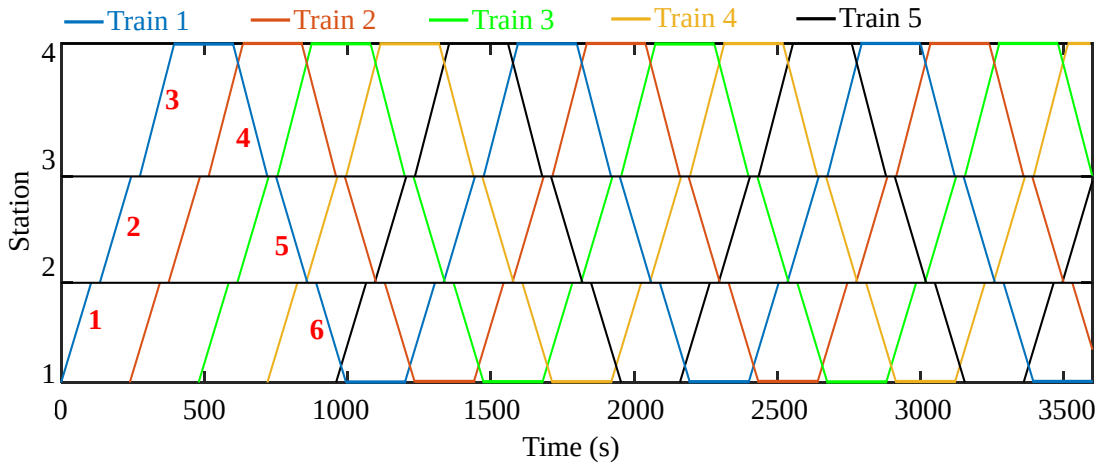

Figure 6.8: The first-hour scheduled timetable of the railway system used in the numerical experiment. There are four stations with six inter-station operations (red solid lines) in total

6.3 Numerical Experiments

In the above sections, detailed simulation methods for obtaining the expected available regenerative braking power of the railway network and the MILP model for train operation optimisation are both proposed and integrated. In this section, the proposed method is tested to show its feasibility.

6.3.1 Parameters Set-Up

Here a generic railway network with four stations supplied by one traction substation are used in the numerical experiment. Since there are 4 stations in the studied railway system, the number of the inter-station operation is six including both the up-directional and down-directional ones, as shown in Figure 6.8 with its first hour's timetable. The scheduled headway is set to be 240 s for each run thus there would be 15 runs for each inter-station per hour since its first train service. The track length and scheduled running time for each inter-station operation are listed in Table 6.2. Assuming there are 18 hours' operation for a day q, the total number of the operations W_S is $15 \times 18 = 270$.

Table 6.2: The parameters for the studied route

Inter-station section	Track length (m)	Scheduled running time (s)	W_S	Q	(μ_s, σ_s^2)
1	1500	105	270	365	$(105, 4.4^2)$
2	1600	110	270	365	$(110, 4.4^2)$
3	2000	120	270	365	$(120, 4.4^2)$
4	2000	120	270	365	$(120, 4.4^2)$
5	1600	110	270	365	$(110, 4.4^2)$
6	1500	105	270	365	$(105, 4.4^2)$

Table 6.3: The parameters for the rolling stock and the OESD used in the numerical experiment

Parameter	Value/Type
Train mass (t)	176
Max traction/braking force (kN)	310
Max traction/braking power (kW)	4000
R_0 (kN)	2.0895
R_1 (kN·s/m)	0.0098
R_2 (kN·s^2/m^2)	0.0065
Max acceleration/deceleration (m/s^2)	1.2
η_s	0.81
η_o	0.90
η_r	0.85
OESD type	Maxwell® 125V HEAVY TRANSPORTATION MODULE
OESD max power (kW)	1034
OESD mass (t)	0.61
OESD capacity (kWh)	1.4

The running time variation for each inter-station operation is assumed to obey the normal distribution $Nor(\mu_s, \sigma_s^2)$, and the mean value μ_s and the variance σ_s^2 of each inter-station operation are also preset in Table 6.2. μ_s is assumed to be the scheduled running time of each inter-station operation, and σ_s^2 is assumed to make the most of running time variation range from -10 s to 10 s. The parameters for the train vehicle and OESD used in both simulation and optimisation are tabulated in Table 6.3. The size of the OESD follows the similar value used in [93, 109]. Additionally, though the proposed model is flexible enough to take into consideration of the varied slope and speed limit of the journey, the track of this numerical experiment is set to be flat, and there is no speed limit for all of the inter-station sections in order to avoid the interference of other

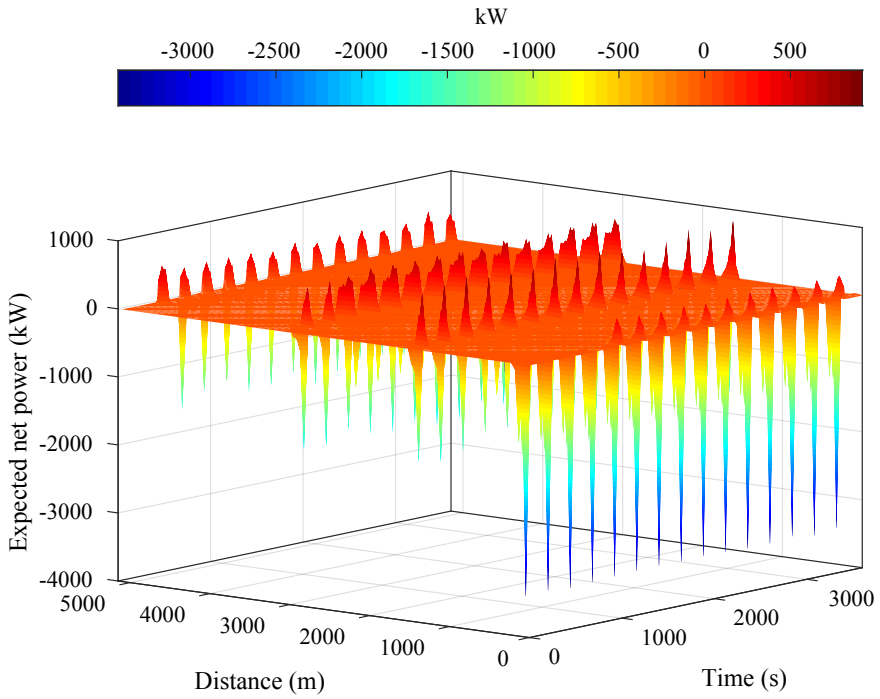

Figure 6.9: The heat map of the expected net power for the first hour in the studied railway system after the Monte-Carlo simulation. The sparks, including both positive and negative ones, in the figure represent the expected net power that accumulated due to departure or arrival following the stochastic timetable

factors and highlight the direct influence of the energy interaction among train, OESD and regenerative braking energy in the environment on train trajectory changes in the later sections.

Following the parameters shown in Chapter 4 and Chapter 5, the energy transmission efficiency from substation to the motor is set as 90% due to a 10% average energy loss and the energy conversion efficiency of electric motor is set as 90% for most typical engineering applications [111]. Therefore, the approximated value for η_s is 81% = 90% $\times$ 90% in this study. On the other hand, energy can be directly transmitted between the motor and OESD with a negligible transmission loss [8], thus, the value for η_o is set as 90% considering only the discharging/charging efficiency resulted from the OESD's internal resistance. From [35] and [116], the efficiency for the utilisation of the regenerative braking energy from other trains ranges from 0.65 for inter-city railway systems and 0.95 for urban rail transit systems, thus here η_r in this study is set as 85%. These three values can be modified according to the field data collected from different types of power supply system, different rolling stocks and different types of OESD.

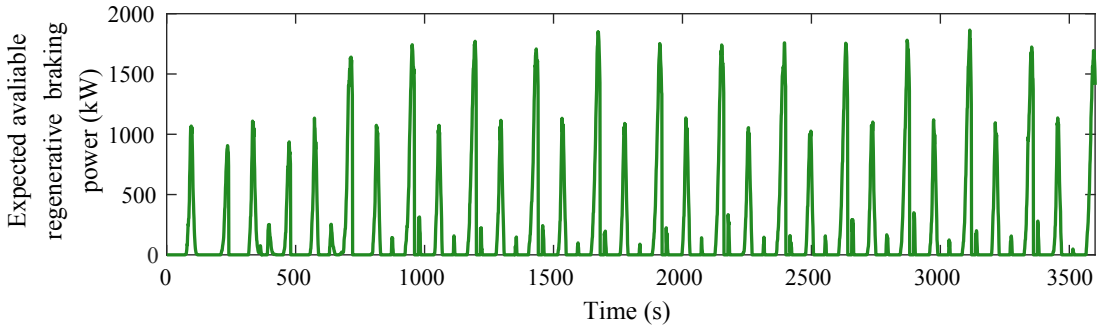

Figure 6.10: The expected available regenerative braking power distribution in the first hour of the studied railway system based on the results of Monte-Carlo simulation. Similar pattern can be found when the train services become stable

Note that this experiment is conducted by using Matlab R2020a® and Gurobi® 9.0.1 solver on a PC with Intel Core® i5-6500 processor (3.20 GHz) and 8.00 GB RAM.

6.3.2 Monte-Carlo Simulation of the Regenerative Braking Power

As shown in Figure 6.11, the running time distribution for all the inter-station sections is generated based on the information listed in Table 6.2 and Table 6.3.Since Q is set to be 365 to represent the 365 days in one year, the total running time generated for each inter-station operation is $15 \times 365 = 5475$. Due to difference of the service cycle for each train, some of the inter-station sections see less than 15 operations in the first hour since the first train departs from the initial station, e.g. inter-station section 3 with 14 operations, inter-station section 4 with 13 operations, inter-station section 5 with 12 operations and inter-station section 6 with 12 operations, which is usual in daily operations and does not influence the results of the proposed method.

Due to the fluctuation of the running time of each inter-station operation, the practical timetable for any day in a year is different. This leads to the number of scenarios being 365 and the same probability for each scenario being 1/365=0.0027. Based on the simulation results, the heat map for the expected net power of the studied railway network with regard to the distance and time is shown in Figure 6.9. It can be seen from the figure that the value of the net power is different at different position and time instant. The heat map looks like a timetable since only when the train is braking can the regenerative braking power be generated, and this normally happens near the arrival station. The more trains are braking at the same time, the higher regenerative braking power in this power supply section it will be at that moment. Figure 6.10 shows the time-variant expected available regenerative braking power in

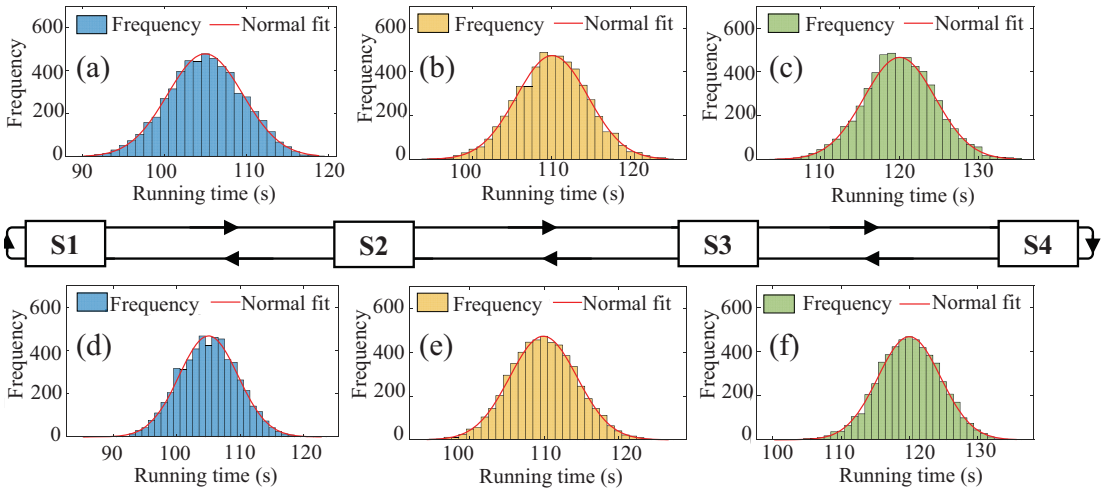

Figure 6.11: The sampled running times for inter-station sections 1-6 of the first hour of the studied railway system, where (a) is the sampling histogram for inter-station section 1, (b) for inter-station section 2, (c) for inter-station section 3, (d) for inter-station section 6, (e) for inter-station section 5 and (f) for inter-station section 4

the environment. Though the practical timetable is stochastic and fluctuated, it can be seen that the expected available regenerative braking power in the first hour's operation follows similar patterns with respect to the time when the train service cycles are stable.

6.3.3 Train Speed Trajectory Optimisation

After the obtainment of the expected available regenerative braking power in the environment, each of the specific inter-station operation can be optimised by using the proposed MILP model. Here the service cycles for Train 1 (see Figure 6.8) in the first hour from the initial station to the terminal station are selected to show the optimisation results. The running time for each inter-station is fixed to be scheduled running time, as shown in Table 6.2.

The results are illustrated in Figure 6.12 and Figure 6.13 which show the approximation of the expected available regenerative braking power in the environment, optimal train speed trajectories, power profiles and OESD discharging/charging profiles for the 1^{st} and 2^{nd} service cycles of Train 1. From the figures it can be observed that the energy from substation, OESD and regenerative braking energy from other trains are all utilised during one service cycle, shown as the red, blue and green dashed lines. The train speed trajectories for all of the inter-station operation are obtained, and the OESD discharging/charging power profiles also change frequently and notably, which

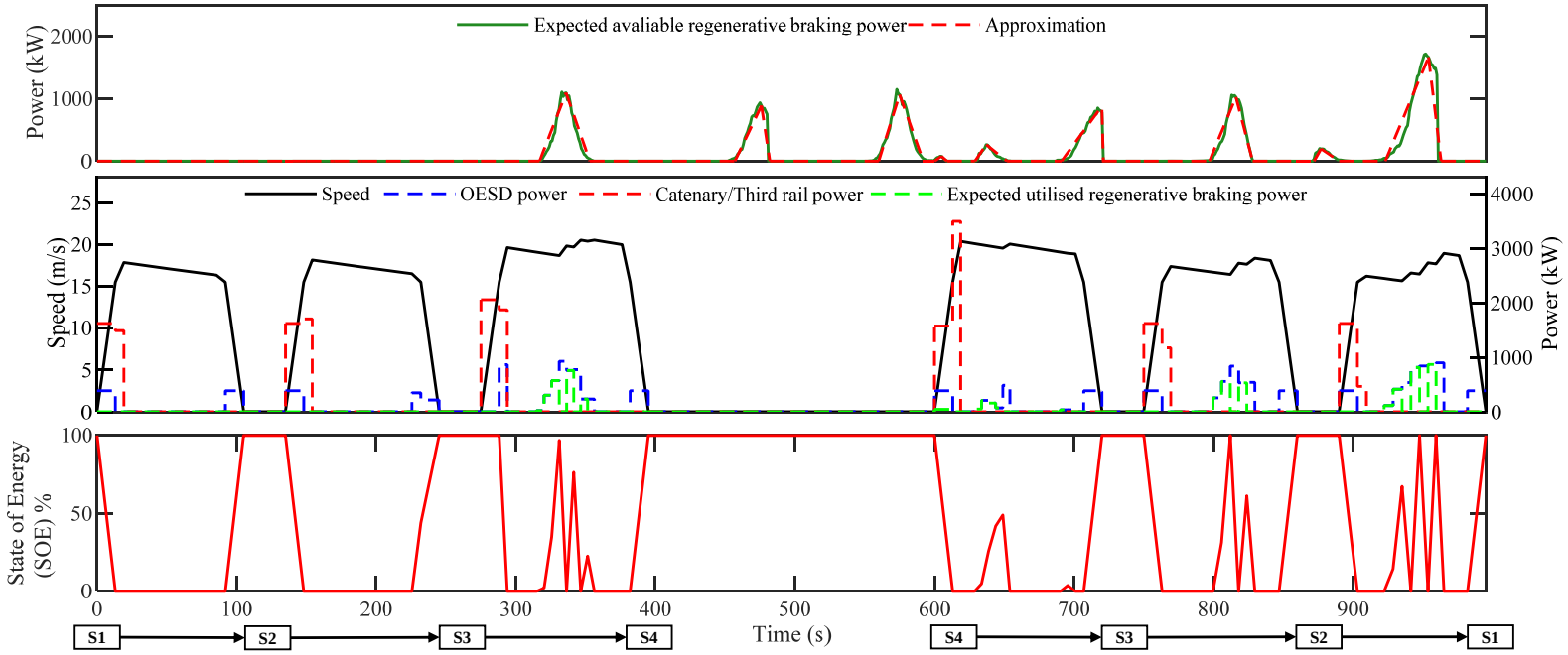

Figure 6.12: The optimal train speed trajectory, catenary/third rail power, OESD power and expected utilised regenerative braking power from other trains for the 1^{st} service cycle of Train 1

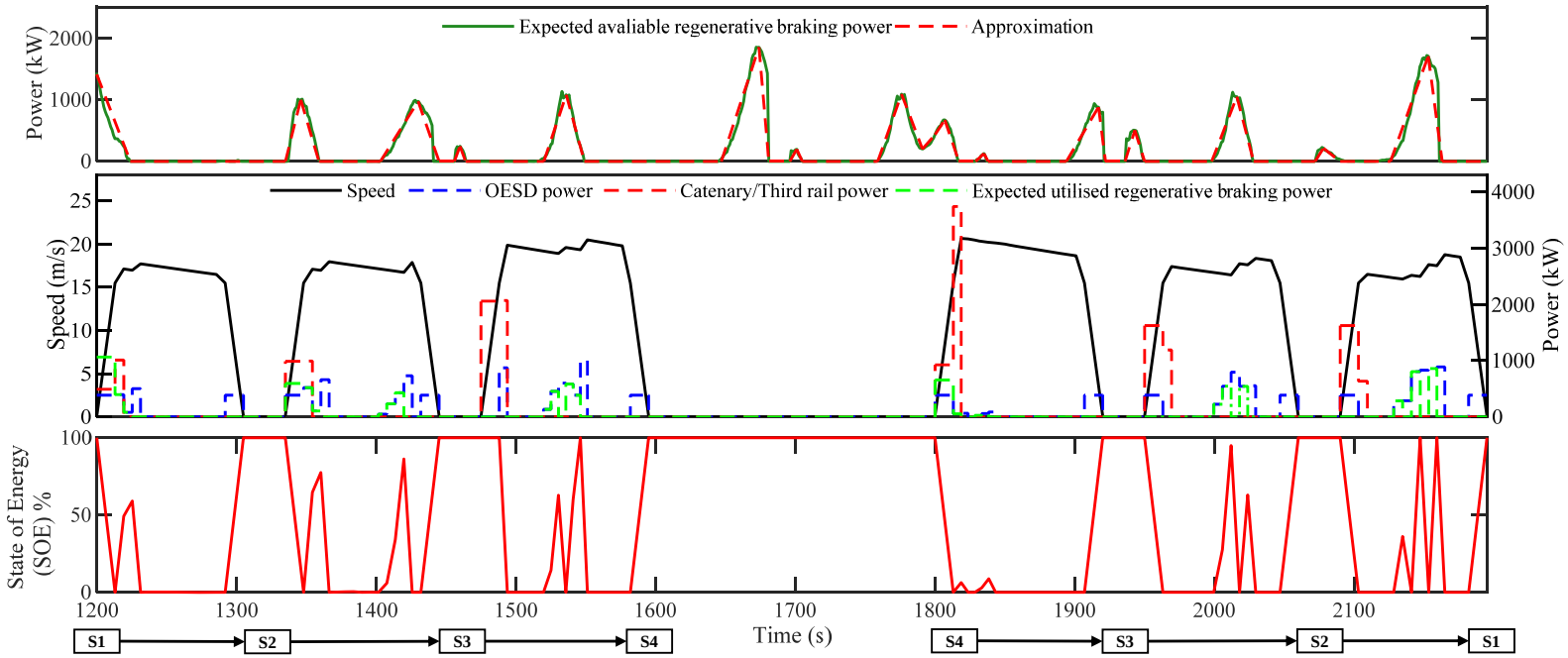

Figure 6.13: The optimal train speed trajectory, catenary/third rail power, OESD power and expected utilised regenerative braking power from other trains for the 2^{nd} service cycle of Train 1

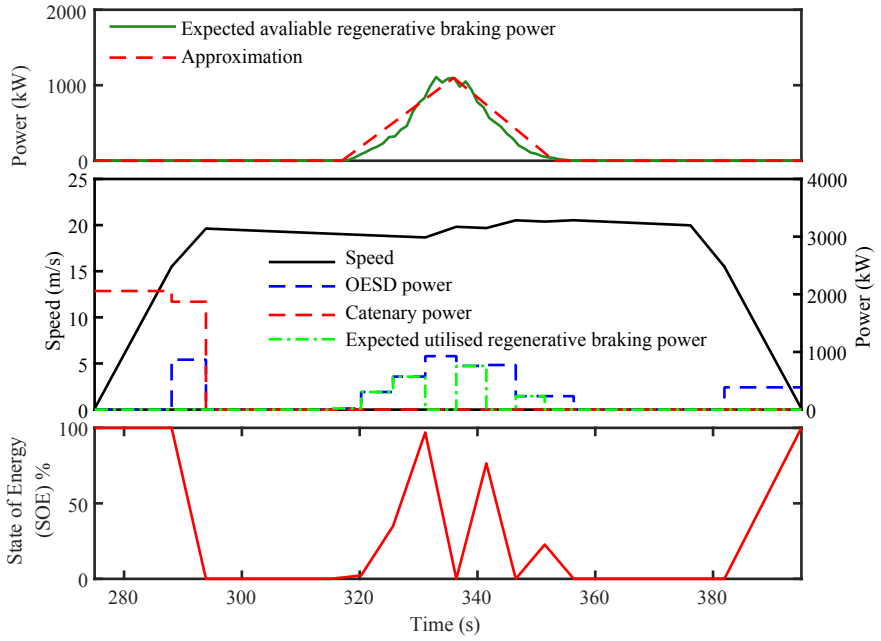

Figure 6.14: The optimal train speed trajectory, catenary/third rail power, OESD power and expected utilized regenerative braking power from other trains for the inter-station operation 3 of the 1^{st} service cycle of Train 1

shows the OESD releases the energy or receives energy from the studied train and the other trains. Since the track is flat and there is no speed limit, the optimal train speed trajectory between two adjacent stations of its both directions (inter-station section 1 and 6, 2 and 5 and 3 and 4) should be the same. However, due to the influence of the regenerative braking energy in the environment, the train speed trajectory for each inter-station section changes accordingly to adjust the train operation status, which results in the different adaptive train speed trajectories. For instance, the train speed trajectory for the inter-station section 1 is less fluctuated than that for the inter-station section 6 since the regenerative braking energy from other trains in the environment is less. Similar observations can also be found when comparing the train speed trajectories for inter-station section 2 and 5 and 3 and 4. On the other hand, when comparing the running in same inter-station section in different time, the influence of the regenerative braking power in the environment on the the optimal train operation, referring to the optimal speed trajectories for inter-station section 1, 2 and 4 in two service cycles in both Figure 6.12 and Figure 6.13.

To clearly demonstrate how the energy interaction happen among the train, OESD and the available regenerative braking energy in the environment, the optimal solutions

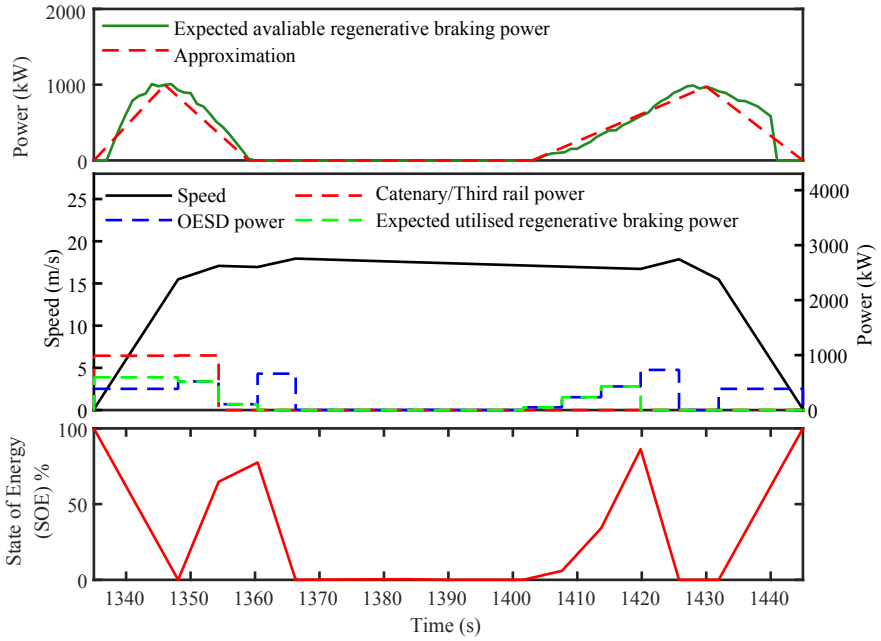

Figure 6.15: The optimal train speed trajectory, catenary/third rail power, OESD power and expected utilised regenerative braking power from other trains for the inter-station operation 2 of the 2^{nd} service cycle of Train 1

for inter-station operation 3 in Figure 6.12 and the inter-station operation 2 in Figure 6.13 are enlarged here as examples for a more detailed discussion.

Figure 6.14 presents the optimal solution of the inter-station section 3 of the 1^{st} service cycle of Train 1, and it can be seen that the train firstly uses the energy from the traction substation and the energy stored in the OESD to support its traction at the beginning of the journey. After the traction, the train begins to coast, and during the coasting, the regenerative braking energy from other trains is charged into the OESD, which raises its SOE to nearly 100%. Then the train begins to conduct traction again and only uses the energy from the OESD. The OESD's process of receiving the regenerative braking energy from the environment and releasing the energy occurs back and forth during the journey, showing the effectiveness of the proposed method on utilisation of the available regenerative braking energy by adjusting both the train and OESD operations accordingly. It can also be observed that the OESD power equals to the expected regenerative braking power when charging, and it rises first as the expected regenerative braking power rises as well.

Figure 6.15 presents the optimal solution of the inter-station section 2 of the 2^{nd} service cycle of Train 1. It can be found that due to the occurrence of the regenerative

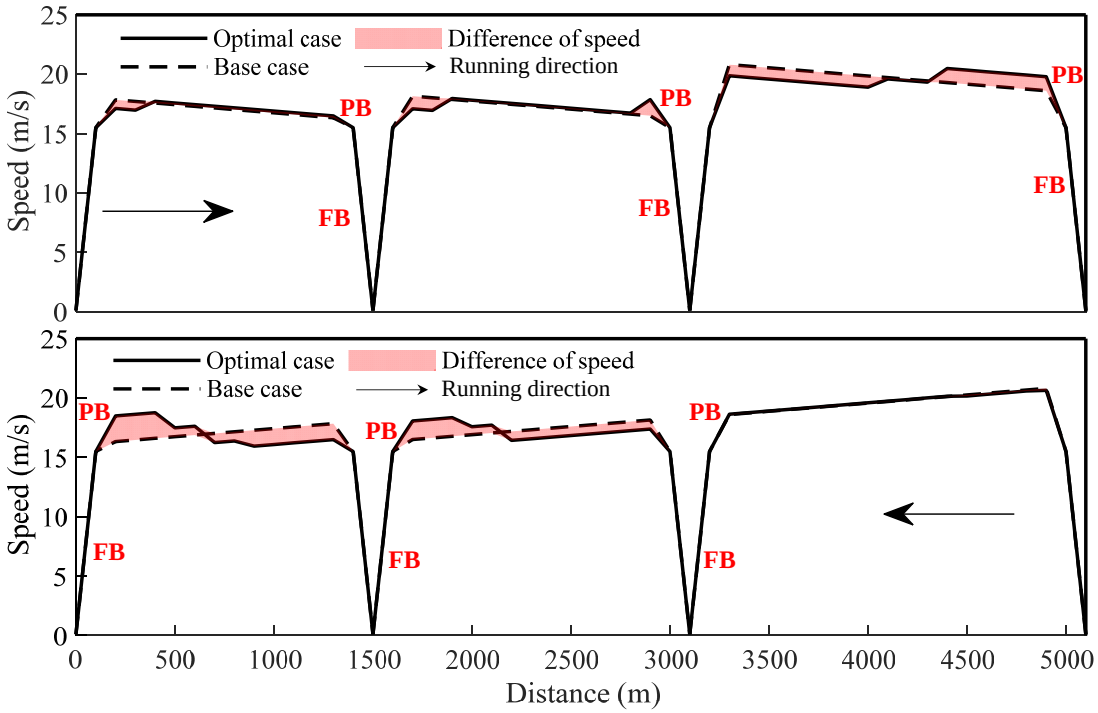

Figure 6.16: The comparison between the optimal speed trajectory resulted by the proposed method (Optimal case) and the base trajectory from the case without utilisation of regenerative braking energy of other trains (Base case)

braking energy from other trains at the beginning of the journey, the studied train utilises the energy from substation, OESD and other trains together in its traction process. During the traction mode of the train (from 1335 s to 1366 s), the available regenerative braking energy in the environment can be used to charge the OESD and replace part of the energy from substation. It is observed that during the later period of the traction mode, regenerative braking energy becomes the main power source of the train. The change of the expected utilised regenerative braking power follows the trend of the variation of the power in the environment, which illustrates the proposed method can help utilise the energy from other trains as much as possible.

Figure 6.16 compares the difference between the optimal train speed trajectory with OESD taking into account the expected available regenerative braking energy in the environment (Optimal case) and optimal train speed trajectory with OESD but without regenerative braking energy in the environment (Base case). It can be found the train speed trajectories for both situations are significantly different. For the base case, fewer fluctuation of the speed trajectory is found, and more coasting is preferred to save energy

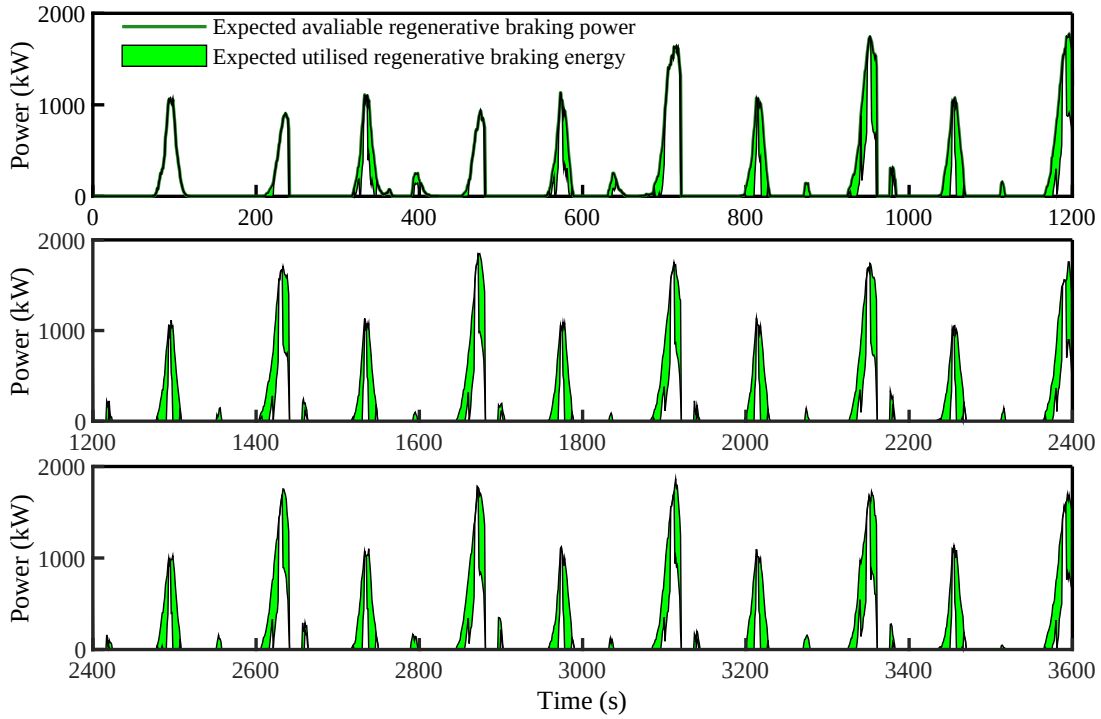

Figure 6.17: The expected utilisation of the available regenerative braking power in the environment for the studied railway system after the application of the proposed method in the first hour

consumption. While for the optimal case obtained in this study, slight acceleration with lower speed at the beginning of the journey and traction process in the middle of the journey happen frequently. The traction phase is observed to be postponed to the later operation stages, in order to adapt the expected time of the occurrence of regenerative braking energy from other trains to utilise more of it. It also should be noted that the optimal results does not impose much impact on the obtained expected regenerative braking energy as the same full braking operation ("FB" in Figure 6.16) occurs only at the end of each inter-station section, which keeps the same trend with the base case, before some slightly different or even same partial braking operation ("PB" in Figure 6.16) compared with base case. This indicates that the proposed method does not generate much new regenerative braking energy to the environment.

6.3.4 Energy-Saving Performance

Following the optimisation method mentioned in the above sections, the optimal train operations for the whole one hour's time can be obtained, and the performance of which

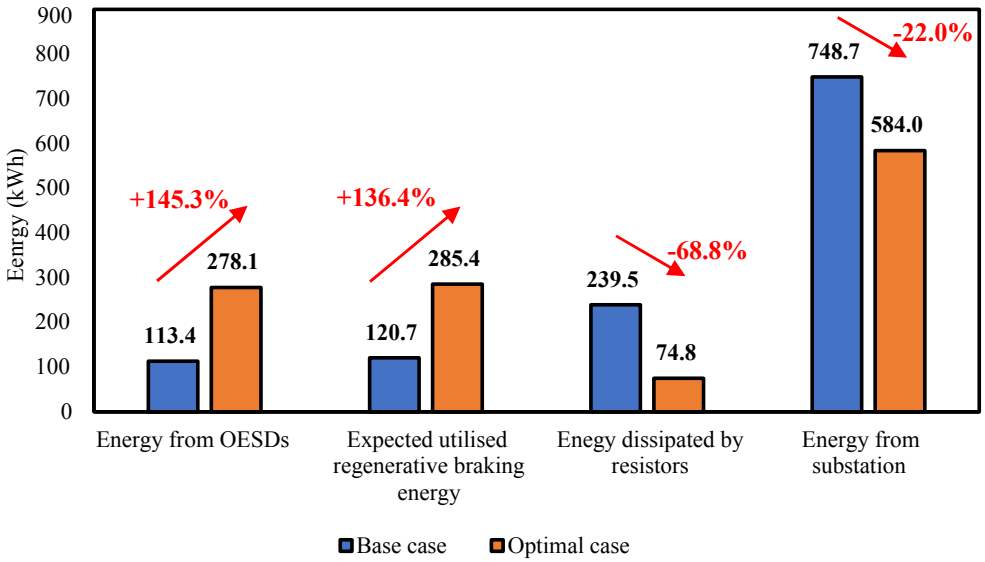

Figure 6.18: The energy consumption comparison between the base case and optimal case. The energy from traction substation is expected to be significantly reduced by 22%

is demonstrated by using the expected utilised regenerative braking power in Figure 6.17. The figure presents the expected utilised regenerative braking power in one hour's time horizon, and it can be found that at most of the time the regenerative braking energy in the environment is expected to be fully utilised, and 68.8% of available regenerative braking energy is expected to be utilised by using the OESD and adjusting train speed trajectory following the optimal solution.

Figure 6.18 shows the energy-saving rate of the optimal train speed trajectory resulted from the proposed method (optimal case) and its comparison with the solution without the consideration of the regenerative braking energy utilisation (base case). It can be seen that the energy released by the OESD during each journey of the optimal case reaches 278.1 kWh, which is the 145.3% of that of the base case (113.4 kWh). The reason for this large discrepancy is that for the base case without consideration of the regenerative braking energy utilisation, the OESD is normally used at the beginning and the end of the journey without the discharge/charge processes back and forth like the optimal case in the middle of the journey. When the OESD is able to receive the energy from the environment, it can support the train repeatedly, making the most of the OESD and available regenerative braking energy together. As a result, it can be seen that the regenerative braking energy utilisation rate is expected to see an 136.4% increase compared with the base case, and the energy dissipated by resistors is expected

to drop by 68.8%. The energy from traction substation is expected to see a 22.0% reduction, showing the energy-saving potential of the proposed approach.

6.4 Summary

By adopting an agent-environment model, this chapter proposes a new approach to optimise the train speed trajectory with OESD taking into account the utilisation of the regenerative braking energy in the environment of the network i.e. train network and power network.

Different from most of previous studies to simultaneously optimising the operation of all trains in the network, this chapter considers the stochastic available regenerative braking energy as the environment information to be fed into the smart decision making process using MILP for each single-train operation in the network. By employing the Monte-Carlo simulation based on the field data of the stochastic timetable, the expected time-variant available regenerative braking power in the environment can be obtained. Then, by integrating the energy support from substation, OESD and regenerative braking energy from other trains, a MILP model combined with the uncertain network information is established to find the optimal train speed trajectory with the objective of minimising the expected net energy consumption.

A generic railway system with four stations in one power supply section is used in the numerical experiments in the chapter, and the results show that the proposed method can give an optimal solution on minimising the expected net energy consumption by adjusting the train speed trajectory and the operation of the OESD to make the most of available regenerative braking energy. In this case, from the results it can be seen that the energy consumption from substation is expected to be reduced by 22.0%, and 68.8% of regenerative braking energy in the environment is expected to be further utilised for one hour's operation by applying the optimal solution.

Chapter 7

Impacts of Different Types of OESD on Train Operations

The main content of this chapter is from the author's published article in a version with minor reconfiguration to fit the structure and context of this thesis. The published article is:

C. Wu, B. Xu, S. Lu, F. Xue, L. Jiang and M. Chen, "Adaptive Eco-Driving Strategy and Feasibility Analysis for Electric Trains with On-Board Energy Storage Devices," *IEEE Transactions on Transportation Electrification*, vol. 7, no. 3, pp. 1834-1848, 2021.

7.1 Introduction

This chapter mainly aims to discuss the impact of the different types of OESD on train operation, including the optimal speed, energy consumption and the advantages/disadvantages of each type of energy storage when involving energy-saving operations. Three main types of OESD, supercapacitors, flywheels and Li-ion batteries are investigated in this chapter based on the proposed mathematical model. The research does not focus on specific product in each energy storage type, but in an average level to represent the average influence and performance of different types of OESD applied.

In the previous chapters of this thesis, Chapter 4, Chapter 5 and Chapter 6, general models of train operation with OESD are established to study the optimal running and discharging/charging strategy of OESD in different scopes from small scale to large

scale. However, the OESD involved is regarded as a general energy supplier and receiver without dynamic characteristics resulted by the specific energy storage type, which undermines the practicality of the model.

In fact, the discharging/charging process of different types of OESD is strongly shaped by their own dynamic power limits which is related to their current status [128]. Figure 7.1 shows the dynamic power limits of the three main types of OESD. It can be noted that the discharging/charging power limits of different types of OESD are closely related to their energy status (for supercapacitors and electrochemical batteries) and motion status (for flywheels), but few reports can be found in the literature. In the literature review (Chapter 2), it can be seen that train operation problem with supercapacitors as OESD have been studied by some researchers [89, 93, 95, 109, 129] while flywheels and electrochemical batteries are still rarely investigated. A systematic study and comparison on the influence of different types of energy storage devices on the train operation and its comparison is still missing. Also, in the existing works the dynamic discharging/charging characteristics of the OESD are not considered, which undermines the models' applicability in real-world applications. Since these dynamic discharging/charging power limits may have further influences on the optimal train operation and result in different control strategies for both train and OESD, a systematic investigation is needed. In this case, this chapter aims to develop a new MILP model to find the optimal driving strategy, namely the speed trajectory, of the train equipped with three popular types of OESD, i.e. supercapacitor, flywheel and Li-ion battery to minimise the net energy consumption by taking into account their corresponding dynamic discharge/charge limits. The contributions of the chapter are outlined as follows:

- This chapter provides a comprehensive comparative study on the energy-saving performance of three popular types of OESD considering the investment constraints and dynamic power limits using the proposed MILP model. It is an extension of the model proposed in Chapter 4.
- The optimal driving strategy of the train and the discharging/charging behavior for three types of OESDs are located, where the corresponding train speed, SOE and power of OESD are all obtained.
- The optimal train operation with OESD on fully electrified railways, discontinuously electrified railways and catenary-free railways are found, and insightful comparisons of the energy-saving and feasibility of different types of OESD are given.

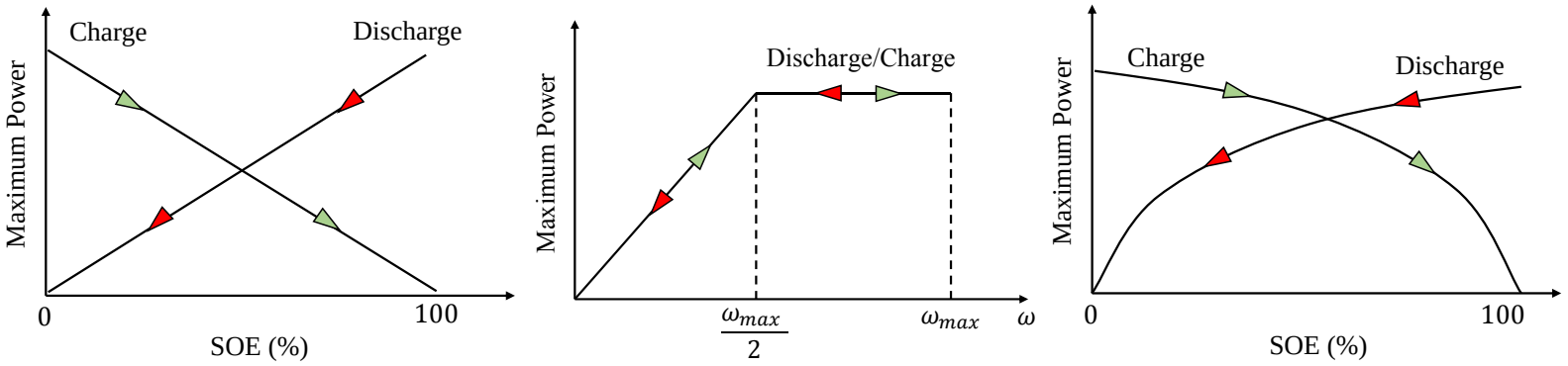

Figure 7.1: The illustration of the maximum discharge/charge power for (a) supercapacitors, (b) flywheels and (c) Li-ion batteries. **For the supercapacitor**, the maximum discharge/charge power limit of it has linear relationship with its real-time energy status, namely state of energy (SOE), where the maximum discharge power decreases linearly from SOE being 100% to 0 and maximum charge power also decreases linearly from SOE being 0 to 100% [121, 122]. **As for the flywheel**, its maximum discharge/charge power increase linearly with its angular speed ω until ω reaches the half of the maximum angular speed ω_{max} then becomes a constant value [123, 124]. **For the electrochemical batteries**, such as lead-acid batteries, Ni-Cd batteries, NiMH batteries, Li-ion batteries and so on, the dynamic power limits of them is also related to its real-time SOE, where the maximum discharge power decreases with an increasing gradient from SOE being 100% to 0 and its maximum charge power decreases with an increasing gradient from SOE being 0 to 100% [125–127]

7.2 Train Operation with Different Types of OESD

Notation of variables	
v_i^2	Square of train speed in the position of $\sum_1^{i-1} \Delta d_i$ [m^2/s^2]
$\Delta E_{i,s}$	Energy from the substation in Δd_i [kJ]
$\Delta E_{i,dch}^k$	Energy discharged from the k-type OESD in Δd_i [kJ]
$\Delta E_{i,ch}^k$	Energy charged to the k-type OESD from motor in Δd_i [kJ]
$\Delta E_{i,r}$	Energy transmitted to the resistor from the motor in Δd_i [kJ]
λ_i	Binary variables to determine the train operation mode in Δd_i
$\alpha_{i,j} \in [0,1]$	SOS2 variable set for speed-related constraints linearisation
$\beta_{i,j} \in [0,1]$	SOS2 variable set for speed-related constraints linearisation
$\mu_{i,j}^{\alpha}$	Binary variables in SOS2 variable set
$\mu_{i,j}^{\beta}$	Binary variables in SOS2 variable set
$y_{i,1}^k, y_{i,2}^k,$ $y_{i,3}^k, y_{i,4}^k$	Auxiliary variables for product linearisation on discharging/charging process of k-type OESD in Δd_i
$\alpha_{i,j}^{k,ch} \in [0,1]$	SOS2 variables for product linearisation on charging process of k-type OESD.
$\beta_{i,j}^{k,ch} \in [0,1]$	SOS2 variables for product linearisation on charging process of k-type OESD.
$\alpha_{i,j}^{k,dch} \in [0,1]$	SOS2 variables for product linearisation on discharging process of k-type OESD.
$\beta_{i,j}^{k,dch} \in [0,1]$	SOS2 variables for product linearisation on discharging process of k-type OESD.
$\mu_{i,j}^{k,ch_\alpha}$	Binary variables for product linearisation on charging process of k-type OESD.
$\mu_{i,j}^{k,ch_\beta}$	Binary variables for product linearisation on charging process of k-type OESD.
$\mu_{i,j}^{k,dch_\alpha}$	Binary variables for product linearisation on discharging process of k-type OESD.
$\mu_{i,j}^{k,dch_\beta}$	Binary variables for product linearisation on discharging process of k-type OESD.
u_j^k	Binary variables for piecewise linearisation of the relationship between maximum discharging/charging power and SOE for k-type OESD.

(Continued from last page)	
$SOE_{i,j}^{k}$	Auxiliary variables to represent the SOE in different piecewise sections for k-type OESD.
Assumptions	
	1. The regenerative braking energy can only be recovered by OESD or dissipated by resistors but cannot be fed back to the substation or used by other trains. 2. The long-term or life-cycle factors that might influence the performance of OESD are ignored.

7.2.1 Approximating OESD Dynamic Power Limits

In this chapter, three different types of energy storage devices, namely the supercapacitor (k=1), flywheel (k=2) and Li-ion battery (k=3) as OESD are modelled. From [8,130,131], the energy and power density and capital cost of each type of OESD can be obtained, as shown in Table 7.1. From Table 7.1 the average capital cost of three OESD types can be calculated to be 200 \$/kW for supercapacitor, 300 \$/kW for flywheel and 1875 \$/kW for Li-ion battery respectively. For making a general comparison, a constant investment for each OESD is set to be 150 k\$. As a result, the maximum power of each OESD can be obtained and shown in Table 7.2, where the capacity and mass for OESD with corresponding maximum power are also tabulated. In this chapter, the listed OESD will be adopted for our case study.

Table 7.1: The energy density per unit mass/volume, power density per unit mass and capital cost per unit power for three types of OESD [8, 130, 131]

OESD type	Energy density		Power density	Capital cost
	(kWh/t)	(kWh/m^3)	(kW/t)	(\$/kW)
Supercapacitor	2.5-15	10-30	500-5000	100-300
Flywheel	5-100	20-80	1000-5000	250-350
Li-ion battery	75-200	150-500	100-350	1200-4000

As shown in Figure 7.1, the dynamic discharging/charging power limits of the OESD is mainly determined by its current SOE and motion status during the whole journey. There are $N+1$ SOE_i^k during the journey with N Δd_i. SOE for k-type OESD when

Table 7.2: The maximum power, capacity and weight of the adopted OESD with an investment of 150 k$

OESD type	Maximum power (kW)	Capacity (kWh)	Mass (t)
Supercapaitor	750	1.87	0.85
Flywheel	500	3.50	0.50
Li-ion battery	80	13.88	0.08

the train passes Δd_i, denoted as SOE^k_{i+1}, can be expressed in (7.1).

$$0 \leq SOE^k_{i+1} = SOE^k_1 + \frac{-\sum_1^i \Delta E^k_{i,dch} + \sum_1^i \Delta E^k_{i,ch}}{E^k_{cap}} \times 100\% \leq 100\%, \quad \forall i = 1, 2, 3, \cdots, N \tag{7.1}$$

where SOE^k_1 is the initial stored energy in k-type OESD.

Supercapacitor

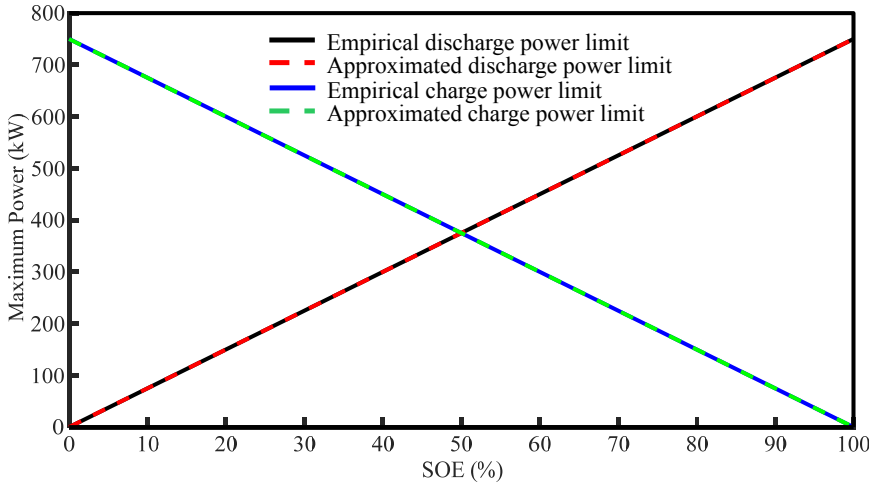

Figure 7.2: The empirical and linear approximation of the relationship between the power limits and SOE of the adopted supercapacitor, where the maximum power is 750 kW for both discharging and charging and power limits change linearly with respect to SOE

For supercapacitor, from [121,122] it is shown that the empirical real-time maximum power and SOE is linear correlated, as shown in Figure 7.2. The maximum discharging power and the maximum charging power for each Δd_i, denoted as $\overline{P^1_{i,dch}}$ and $\overline{P^1_{i,ch}}$, can

be expressed by (7.2) and (7.3).

$$\overline{P^1_{i,dch}} = c^1_1 SOE^1_i + b^1_1, \quad \forall i = 1, 2, 3, \cdots, N \tag{7.2}$$

$$\overline{P^1_{i,ch}} = c^1_2 SOE^1_i + b^1_2, \quad \forall i = 1, 2, 3, \cdots, N \tag{7.3}$$

Flywheel

For flywheel, since it is known from [123, 124] that in theory its maximum discharging/charging power increase linearly with its angular speed ω until it reaches the half of the maximum angular speed ω_{max}, then it becomes a constant value. Thus, in each Δd_i, the relationship between flywheel's maximum discharging/charging power $\overline{P^2_{i,dch}}/\overline{P^2_{i,ch}}$ and its current angular speed ω_i can be shown in (7.4).

$$\overline{P^2_{i,dch}} = \overline{P^2_{i,ch}} = \begin{cases} c\omega_i & 0 \le \omega_i \le \omega_{max}/2 \\ c\omega_{max}/2 & \omega_{max}/2 \le \omega_i \le \omega_{max} \end{cases}, \quad \forall i = 1, 2, 3, \cdots, N \tag{7.4}$$

where c is the parameter for the linear relationship before the ω_i reaches $\frac{1}{2}\omega_{max}$.

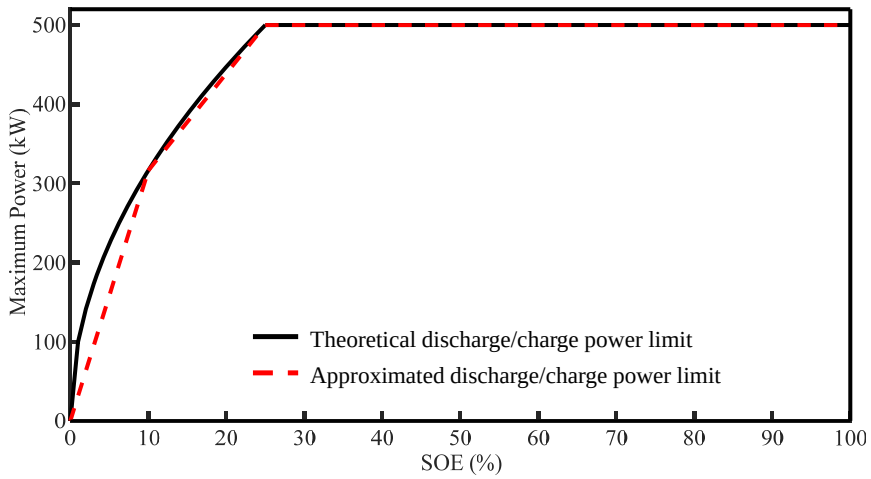

Figure 7.3: The theoretical and linear approximation of the relationship between the power limits and SOE of the adopted flywheel, where the maximum power is 500 kW for both discharging and charging and power limit is pieced into three linear sections with respect to SOE

Since the flywheel transforms the electrical energy to kinetic energy, the real-time

energy status can be expressed by using (7.5).

$$SOE_i^2 E_{cap}^2 = \frac{1}{2} M_o^2 q \omega_i^2, \quad \forall i = 1, 2, 3, \cdots, N \tag{7.5}$$

Thus, the relationship between the discharging/charging power limits of flywheel and its SOE can be established in (7.6).

$$\overline{P_{i,dch}^2} = \overline{P_{i,ch}^2} = \begin{cases} c\sqrt{\frac{2 \times SOE_i^2 E_{cap}^2}{M_o^2 q}} & 0 \leq SOE_i^2 \leq 25\% \\ \frac{c\omega_{max}}{2} & 25\% \leq SOE_i^2 \leq 100\% \end{cases}, \quad \forall i = 1, 2, 3, \cdots, N \tag{7.6}$$

It can be easily observed that when the flywheel stores one-fourth (25%) the maximum capacity, it would reach the maximum discharging/charging power limitations, as illustrated in Figure 7.3.

To approximate this relationship, the curve is pieced into three parts, a shown in Figure 7.3, where the breakpoints are chosen to be $SOE_i^2 = 10\%$ and $SOE_i^2 = 25\%$. As a result, (7.6) can be reformulated in (7.7).

$$\overline{P_{i,dch}^2} = \overline{P_{i,ch}^2} = \begin{cases} c_1^2 SOE_i^2 + b_1^2 & 0 \leq SOE_i^2 \leq 10\% \\ c_2^2 SOE_i^2 + b_2^2 & 10\% \leq SOE_i^2 \leq 25\% \\ c_3^2 SOE_i^2 + b_3^2 & 25\% \leq SOE_i^2 \leq 100\% \end{cases}, \quad \forall i = 1, 2, 3, \cdots, N \tag{7.7}$$

Li-ion Battery

According to [125–127], it is shown that Li-ion batteries' discharging/charging power limits are related to its current SOE as well, but it performs quite differently with the supercapacitors and flywheels, where the charging power limit decreases when SOE increases while its discharging power limit decreases as SOE decreases. This relationship of the adopted Li-ion battery in this chapter is shown in Figure 7.4. To model this feature with the approximation, similar as the flywheel, the dynamic power limits for both discharging and charging process, $\overline{P_{i,dch}^3}$ and $\overline{P_{i,ch}^3}$, are segmented into three parts respectively, and the formulations of which are shown in (7.8) and (7.9).

$$\overline{P_{i,dch}^3} = \begin{cases} c_1^3 SOE_i^3 + b_1^3 & 0 \leq SOE_i^3 \leq 15\% \\ c_2^3 SOE_i^3 + b_2^3 & 15\% \leq SOE_i^3 \leq 40\% \\ c_3^3 SOE_i^3 + b_3^3 & 40\% \leq SOE_i^3 \leq 100\% \end{cases}, \quad \forall i = 1, 2, 3, \cdots, N \tag{7.8}$$

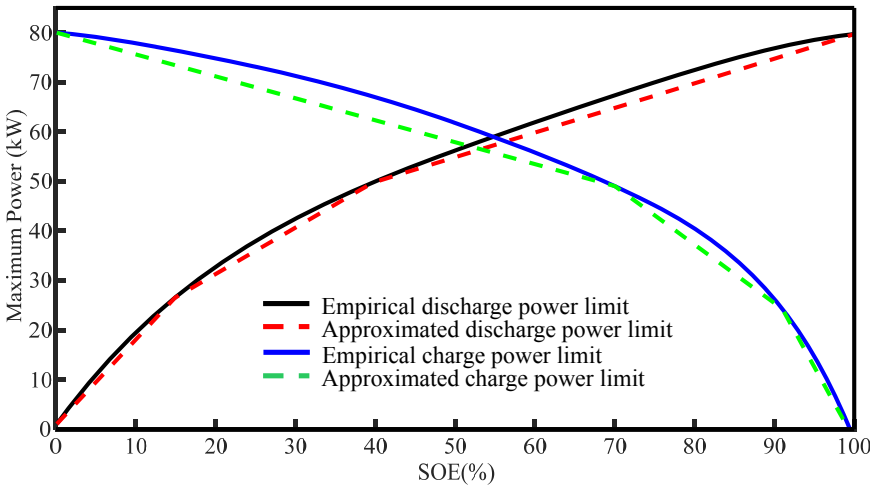

Figure 7.4: The empirical and linear approximation of the relationship between the power limits and SOE of the adopted Li-ion battery, where the maximum power is 80 kW for both discharging and charging and power limits are pieced into three linear sections with respect to SOE respectively

$$\overline{P^3_{i,ch}} = \begin{cases} c^3_4 SOE^3_i + b^3_4 & 0 \le SOE^3_i \le 70\% \\ c^3_5 SOE^3_i + b^3_5 & 70\% \le SOE^3_i \le 90\% \\ c^3_6 SOE^3_i + b^3_6 & 90\% \le SOE^3_i \le 100\% \end{cases}, \quad \forall i = 1, 2, 3, \cdots, N \tag{7.9}$$

From the above modelling process, it can be seen that the parameters (c^k_j, b^k_j) for the linear approximation of the power limits curve needs to be calibrated, especially for flywheel and Li-ion battery, and the results of which are tabulated in Table 7.3.

Table 7.3: The parameter (c^k_j, b^k_j) calibration of the approximation for three types of OESD adopted in this study

Piece-wise section	Discharge		
	Supercapacitor	Flywheel	Li-ion battery
1	(7.5, 0)	(31.62, 0)	(1.768, 0)
2	/	(12.25, 193.67)	(0.93, 12.58)
3	/	(0, 500)	(0.50, 29.58)
	Charge		
1	(-7.5, 750)	(31.62, 0)	(-0.44, 80)
2	/	(12.25, 193.67)	(-1.24, 135.85)
3	/	(0, 500)	(-2.425, 242.5)

7.2.2 Modelling OESD Dynamic Power Limits

As in Section 7.2.1 the dynamic discharging/charging characteristics of three types of OESD, supercapacitor, flywheel and Li-ion battery, have been approximated and elaborated, this section is aimed at discussing the linearisation of the relevant relationships among variables by using SOS2 as well as the binary variables.

In (7.7), the relationship between the power limits and SOE of the flywheel has been formulated into a piecewise function with three parts. To control the SOE in each piecewise part, in each Δd_i, binary variables are imposed to linearise these functions (see Section 3.5.2), as shown in (7.10) - (7.12).

$$\overline{P^2_{i,dch}} = \overline{P^2_{i,ch}} = c_1^2 SOE^2_{i,1} + b_1^2 u^2_{i,1} + c_2^2 SOE^2_{i,2} + b_2^2 u^2_{i,2} + c_3^2 SOE^2_i + b_3^2 u^2_{i,3}, \quad \forall i = 1, 2, 3, \cdots, N \tag{7.10}$$

$$\begin{cases} 0 \le SOE^2_{i,1} \le 10\% u^2_{i,1}, \\ 10\% u^2_{i,2} \le SOE^2_{i,2} \le 25\% u^2_{i,2}, \\ 25\% u^2_{i,3} \le SOE^2_{i,3} \le 100\% u^2_{i,3} \end{cases}, \quad \forall i = 1, 2, 3, \cdots, N \tag{7.11}$$

$$u^2_{i,1} + u^2_{i,2} + u^2_{i,3} = 1, \quad \forall i = 1, 2, 3, \cdots, N \tag{7.12}$$

where $SOE^2_{i,1}$, $SOE^2_{i,2}$ and $SOE^2_{i,3}$ are the auxiliary variables to represent the SOE^2_i in three piecewise sections.

In (7.8) and (7.9), the relationships between the discharging/charging power limits and SOE of the Li-ion battery has been formulated into a piecewise function with three parts respectively. Similarly, to control the SOE in each piecewise part, in each Δd_i, integer logical variables are imposed to linearise these functions, as shown in (7.13) - (7.18) for discharging power limits.

$$\overline{P^3_{i,dch}} = c_1^3 SOE^3_{i,1} + b_1^3 u^3_{i,1} + c_2^3 SOE^3_{i,2} + b_2^3 u^3_{i,2} + c_3^3 SOE^3_{i,3} + b_2^3 u^3_{i,3}, \quad \forall i = 1, 2, 3, \cdots, N \tag{7.13}$$

$$\overline{P^3_{i,ch}} = c_4^3 SOE^3_{i,4} + b_4^3 u^3_{i,4} + c_5^3 SOE^3_{i,5} + b_5^3 u^3_{i,5} + c_6^3 SOE^3_{i,6} + b_6^3 u^3_{i,6}, \quad \forall i = 1, 2, 3, \cdots, N \tag{7.14}$$

$$\begin{cases} 0 \le SOE^3_{i,1} \le 15\% u^3_{i,1}, \\ 15\% u^3_{i,2} \le SOE^3_{i,2} \le 40\% u^3_{i,2}, \\ 40\% u^3_{i,3} \le SOE^2_{i,3} \le 100\% u^3_{i,3} \end{cases}, \quad \forall i = 1, 2, 3, \cdots, N \tag{7.15}$$

$$\begin{cases} 0 \leq SOE^3_{i,4} \leq 70\%u^3_{i,4}, \\ 70\%u^3_{i,4} \leq SOE^3_{i,4} \leq 90\%u^3_{i,4}, \\ 90\%u^3_{i,5} \leq SOE^2_{i,5} \leq 100\%u^3_{i,5} \end{cases}, \quad \forall i = 1, 2, 3, \cdots, N \tag{7.16}$$

$$u^3_{i,1} + u^3_{i,2} + u^3_{i,3} = 1, \quad \forall i = 1, 2, 3, \cdots, N \tag{7.17}$$

$$u^3_{i,4} + u^3_{i,5} + u^3_{i,6} = 1, \quad \forall i = 1, 2, 3, \cdots, N \tag{7.18}$$

where $SOE^3_{i,1}$, $SOE^3_{i,2}$ and $SOE^3_{i,3}$, $SOE^3_{i,4}$, $SOE^3_{i,5}$ and $SOE^3_{i,6}$ are the auxiliary variables to represent the SOE^3_i in three piece-wise sections for discharging behaviour and charging behaviour respectively.

In each Δd_i, the maximum discharged or charged energy of each type of OESD, $\overline{\Delta E^k_{i,dch}}$ and $\overline{\Delta E^k_{i,ch}}$, should follow the limitation of its maximum discharge and charge power and the elapsed running time. Thus, it can be expressed as shown in (7.19).

$$\overline{\Delta E^k_{i,dch}} = \overline{P^k_{i,dch}}\Delta t_i, \quad \overline{\Delta E^k_{i,ch}} = \overline{P^k_{i,ch}}\Delta t_i, \quad \forall i = 1, 2, 3, \cdots, N \tag{7.19}$$

It is easily observed that that the maximum discharged/charged energy of OESD is determined by a product of two variables, $\overline{P^k_{i,dch}}$ (and $\overline{P^k_{i,ch}}$) and Δt_i. In this case, the linearisation on this product needs to be conducted and the method can be found in Section 3.5.3. The auxiliary variables $y^k_{i,1}$, $y^k_{i,2}$, $y^k_{i,3}$ and $y^k_{i,4}$ are introduced, as shown in (7.20) and (7.21).

$$y^k_{i,1} = \frac{1}{2}(\overline{P^k_{i,dch}} + \Delta t_i), \quad y^k_{i,2} = \frac{1}{2}(\overline{P^k_{i,dch}} - \Delta t_i), \quad \forall i = 1, 2, 3, ..., N \tag{7.20}$$

$$y^k_{i,3} = \frac{1}{2}(\overline{P^k_{i,ch}} + \Delta t_i), \quad y^k_{i,4} = \frac{1}{2}(\overline{P^k_{i,ch}} - \Delta t_i), \quad \forall i = 1, 2, 3, ..., N \tag{7.21}$$

In this case, it has the relationships as shown in (7.22) and (7.23).

$$\overline{\Delta E^k_{i,dch}} = \overline{P^k_{i,dch}}\Delta t_i = (y^k_{i,1})^2 - (y^k_{i,2})^2, \quad \forall i = 1, 2, 3, ..., N \tag{7.22}$$

$$\overline{\Delta E^k_{i,ch}} = \overline{P^k_{i,ch}}\Delta t_i = (y^k_{i,3})^2 - (y^k_{i,4})^2, \quad \forall i = 1, 2, 3, ..., N \tag{7.23}$$

Here 2 series of piecewise points $Y^{k,dch}_j$ and $Y^{k,ch}_j$ are used to represent $y^k_{i,1}$, $y^k_{i,2}$, $y^k_{i,3}$ and $y^k_{i,4}$. In this case, (7.22) and (7.23) can be reformulated into (7.24) and (7.25).

$$\overline{\Delta E^k_{i,dch}}' = \sum_{j=1}^{J_2}(Y^{k,dch}_j)^2\alpha^{k,dch}_{i,j} - \sum_{j=1}^{J_2}(Y^{k,dch}_j)^2\beta^{k,dch}_{i,j}, \quad \forall i = 1, 2, 3, ..., N \tag{7.24}$$

$$\overline{\Delta E_{i,ch}^{k}}' = \sum_{j=1}^{J_3}(Y_j^{k,ch})^2\alpha_{i,j}^{k,ch} - \sum_{j=1}^{J_3}(Y_j^{k,ch})^2\beta_{i,j}^{k,ch}, \quad \forall i = 1,2,3,...,N \tag{7.25}$$

$\alpha_{i,j}^{k,dch}$, $\beta_{i,j}^{k,dch}$, $\alpha_{i,j}^{k,ch}$ and $\beta_{i,j}^{k,ch}$ are 4 sets of SOS2 variables for each type of OESD in Δd_i, and J_2 and J_3 are the number of the corresponding piece-wise points. As a result, they also need to follow the (7.26) - (7.29).

$$\sum_{j=1}^{J_2}\alpha_{i,j}^{k,dch} = 1, \quad \sum_{j=1}^{J_2}\beta_{i,j}^{k,dch} = 1, \quad \forall i = 1,2,3,...,N \tag{7.26}$$

$$\sum_{j=1}^{J_3}\alpha_{i,j}^{k,ch} = 1, \quad \sum_{j=1}^{J_3}\beta_{i,j}^{k,ch} = 1, \quad \forall i = 1,2,3,...,N \tag{7.27}$$

$$0 \le \alpha_{i,j}^{k,dch} \le 1, \quad 0 \le \beta_{i,j}^{k,dch} \le 1, \quad \forall i = 1,2,3,...,N \tag{7.28}$$

$$0 \le \alpha_{i,j}^{k,ch} \le 1, \quad 0 \le \beta_{i,j}^{k,ch} \le 1, \quad \forall i = 1,2,3,...,N \tag{7.29}$$

To ensure that only the adjacent $\alpha_{i,j}^{k,dch}$, $\beta_{i,j}^{k,dch}$, $\alpha_{i,j}^{k,ch}$ and $\beta_{i,j}^{k,ch}$ can be nonzero and their sum being 1, 0-1 variables $\mu_{i,j}^{k,dch_\alpha}$ and $\mu_{i,j}^{k,dch_\beta}$, $\mu_{i,j}^{k,ch_\alpha}$ and $\mu_{i,j}^{k,ch_\beta}$ need to be imposed, as shown in (7.30) - (7.33).

$$\alpha_{i,j}^{k,dch} + \alpha_{i,j+1}^{k,dch} - \mu_{i,j}^{k,dch_\alpha} \ge 0, \quad \beta_{i,j}^{k,dch} + \beta_{i,j+1}^{k,dch} - \mu_{i,j}^{k,dch_\beta} \ge 0, \quad \forall i = 1,2,3,...,N \tag{7.30}$$

$$\alpha_{i,j}^{k,ch} + \alpha_{i,j+1}^{k,ch} - \mu_{i,j}^{k,ch_\alpha} \ge 0, \quad \beta_{i,j}^{k,ch} + \beta_{i,j+1}^{k,ch} - \mu_{i,j}^{k,ch_\beta} \ge 0, \quad \forall i = 1,2,3,...,N \tag{7.31}$$

$$\sum_{j=1}^{J_2-1}\mu_{i,j}^{k,dch_\alpha} = 1, \quad \sum_{j=1}^{J_2-1}\mu_{i,j}^{k,dch_\beta} = 1, \quad \forall i = 1,2,3,...,N \tag{7.32}$$

$$\sum_{j=1}^{J_3-1}\mu_{i,j}^{k,ch_\alpha} = 1, \quad \sum_{j=1}^{J_3-1}\mu_{i,j}^{k,ch_\beta} = 1, \quad \forall i = 1,2,3,...,N \tag{7.33}$$

7.2.3 Energy Transmission with Different Types of OESD

During the journey, the train can consume the energy from the substation $\Delta E_{i,s}$ and energy discharged by the OESD $\Delta E_{i,dch}^{k}$ when the train is in traction mode, thus it has (7.34).

$$\Delta E_{i,m}^{+} = \Delta E_{i,s}\eta_s + \Delta E_{i,dch}^{k}\eta_k, \quad \forall i = 1,2,3,...,N \tag{7.34}$$

where η_k is the efficiency of k-type OESD.

When the train is braking, the motor is in regenerative braking mode and part of

the energy can be delivered to the OESD. Thus, the energy that can be charged to OESD, demoted as $\Delta E^k_{i,ch}$, is represented in (7.35).

$$\Delta E^-_{i,m} = \frac{\Delta E^k_{i,ch}}{\eta_k} + \Delta E_{i,r}, \quad \forall i = 1,2,3,...,N \tag{7.35}$$

Since the train cannot conduct traction and braking at the same time, the traction energy in (7.34) and regenerative energy in (7.35) of the train cannot exist simultaneously in one Δd_i. In this case, the 0-1 variables λ_i need to be imposed into the model to determine the train operation mode in each Δd_i, as shown in (7.36) - (7.37).

$$0 \le \Delta E_{i,s} \le \lambda_i L, \quad 0 \le \Delta E^k_{i,dch} \le \lambda_i L, \quad \forall i = 1,2,3,...,N \tag{7.36}$$

$$0 \le \Delta E^k_{i,ch} \le (1-\lambda_i) L, \quad 0 \le \Delta E_{i,r} \le (1-\lambda_i) L, \quad \forall i = 1,2,3,...,N \tag{7.37}$$

It can be seen that when λ_i is 1, the train is in traction mode and the OESD and substation can supply the train together. In contrast, when λ_i is 0, the train is braking and the OESD can be charged to recover the regenerative energy.

According to the law of conservation of the energy, the conversion of the energy can be expressed in (7.38).

$$\Delta E^+_{i,m} - \Delta E^-_{i,m} - \frac{1}{2}(M_t + M^k_o)(v^2_{i+1} - v^2_i) - R_i \Delta d_i - (M_t + M^k_o) g \theta_i \Delta d_i - \Delta E_{i,r} = 0, \quad \forall i = 1,2,3,...,N \tag{7.38}$$

In addition, the power limit of the motor and OESD should be added as the constraints respectively. For the motor, (7.39) - (7.40) are used to ensure the force and power that the motor supplies in both traction mode and braking mode does not exceed the maximum allowed value.

$$\Delta E_{i,s}\eta_s + \Delta E^k_{i,dch}\eta_k \le \overline{F_t}\Delta d_i, \quad \Delta E_{i,s}\eta_s + \Delta E^k_{i,dch}\eta_k \le \overline{P_t}\Delta t_i, \quad \forall i = 1,2,3,...,N \tag{7.39}$$

$$\frac{\Delta E^k_{i,ch}}{\eta_k} \le \overline{F_b}\Delta d_i, \quad \frac{\Delta E^k_{i,ch}}{\eta_k} \le \overline{P_b}\Delta t_i, \quad \forall i = 1,2,3,...,N \tag{7.40}$$

For k-type OESD, the discharged and charged energy cannot exceed the maximum value determined by the maximum charge and discharge power, as expressed in (7.41).

$$\Delta E^k_{i,dch} \le \overline{\Delta E^k_{i,dch}}', \quad \Delta E^k_{i,ch} \le \overline{\Delta E^k_{i,ch}}', \quad \forall i = 1,2,3,...,N \tag{7.41}$$

The objective functions of the model for all three OESDs are the same but with different constraints. The objective function is defined to minimise the net energy consumption which is the total traction energy consumption deducted by the total regenerative energy received by OESDs. Here the models for finding the optimal driving strategy for the train with supercapacitor, flywheel and Li-ion battery are given in (7.42).

$$\min \quad \sum_{i=1}^{N}(\Delta E_{i,s} + \Delta E_{i,dch}^{k} - \Delta E_{i,ch}^{k}), \quad \forall k = 1, 2, 3 \tag{7.42}$$

The proposed MILP model can be solved by a commercial solver e.g. CPLEX®, Lingo® or Gurobi® etc. to efficiently determine the optimal driving strategy of the train with OESD. The optimal speed trajectory can be chosen by the model itself when inputting the relevant parameters of the railway system and OESD used as the constraints. In this case, the speed trajectory, including traction/coasting/braking behaviours, can be chosen freely as long as the net energy consumption is minimised for the whole journey.

7.3 Numerical Experiments

In this section, the case studies for various scenarios are conducted by using the proposed model. There are four scenarios in the case studies and listed as following:

- Train operation with OESDs without the varied route conditions (runs on flat track and no speed limits).
- Train operation with OESDs with the varied route conditions (runs on sloping track and varied speed limits).
- Train operation with OESDs on partial discontinuously electrified railway.
- Train operation with OESDs on catenary-free railways.

The results of these case studies show the adaptive eco-driving strategy of the train with different types of OESD adopted in the research, as well as their respective influence on train operations. In the case studies, mainly the generic urban railway systems, e.g. metro systems, tram systems with relatively short distance and short journey time between adjacent stations, are used to test the proposed model. However, the journey

time or track length can also be prolonged according to the real operational requirement, such as the metro ad tram systems with short-time operation or even the high-speed railways with long time operation.

The train traction/braking characteristics and the drag force used in the case studies are shown in Table 4.1. The mass of the train M_t in the case studies is 176 t without the OESD and the maximum acceleration $\overline{a}$ and deceleration $\underline{a}$ are both set to be 1.2 m/s^2. The track length D is equally divided to be 100 m for all of the scenarios. The average energy efficiency η_s and η_k can be set based on literature from long-term viewpoint. Specifically, the energy transmission efficiency from grid to the motor is set as 90% due to a 10% average energy loss and the energy conversion efficiency of electric motor is set as 90% for most typical engineering applications [111]. Therefore, the approximated value for η_s is 81% = 90% × 90% in this study. On the other hand, energy can be directly transmitted between the motor and OESD with a negligible transmission loss [8], thus, the value for η_k is set as 90% considering only the discharge/charge efficiency resulted from the OESD's own resistance. Both values can be modified according to the field data.

Note that the case studies are conducted by using Matlab R2020a® and Gurobi® 9.0.1 solver on a PC with Intel Core® i5-5200U processor (2.20 GHz) and 8.00 GB RAM.

7.3.1 Without/With Varied Route Conditions

Since the case study is for the train running between two adjacent stations, the track length is set to be 1800 m and the initial speed v_1 and the terminal speed v_{N+1} of the train should be 0. Each kind of OESD is assumed to be fully charged, namely SOE_{ini}= 100%, before the departure of the train.

Scenario 1 of the case study is to explore the optimal eco-driving strategy for train with different types of OESD on the flat track without speed limits, and the running time T is limited at 100 s. The optimal speed profiles, train operation mode, OESD power and SOE profiles are illustrated in Figure 7.5, and it is evident that the optimal eco-driving strategies of the train with different types of OESD are significantly different. For the train with supercapacitor, the SOE and power profiles show that its SOE and power limit drop/soar fast during the journey resulted from its highest maximum power and lowest capacity among the three types of OESD. This in turns results in the shortest motoring distance/braking distance and longest coasting distance. For the train with flywheel, the OESD always works at its power limits due to its larger capacity of

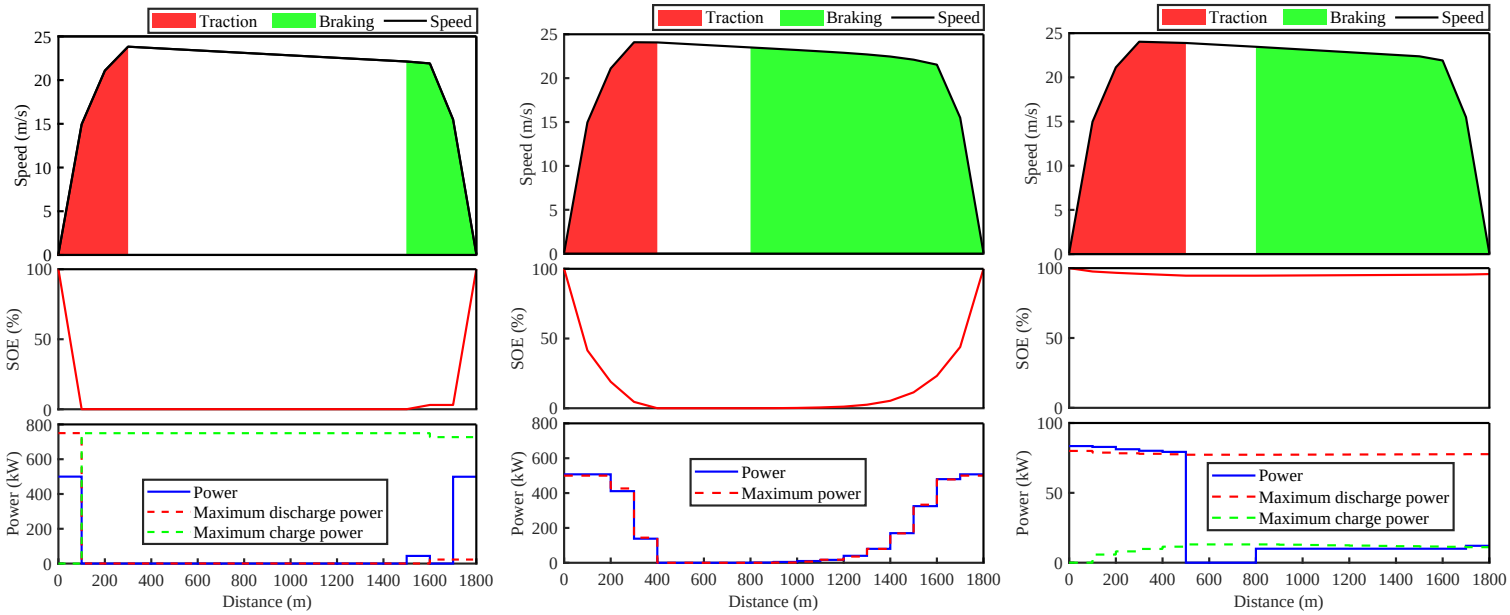

Figure 7.5: Scenario 1: The optimal train speed, OESD SOE and power profiles for the train with (a) supercapacitor, (b) flywheel and (c) Li-ion battery on a 1800-metre-long flat track without speed limits. Different traction and braking distribution resulted from different OESD, where 300-metre-long traction and braking distance for supercapacitor, 400-metre-long traction distance and 900-metre-long braking distance for flywheel and 500-meter-long traction distance and 900-metre-long braking distance for Li-ion battery. Also, the OESD power is limited by their own dynamic power limits with a slight violation due to the modelling precision, which is to be explained in Section 7.3.4

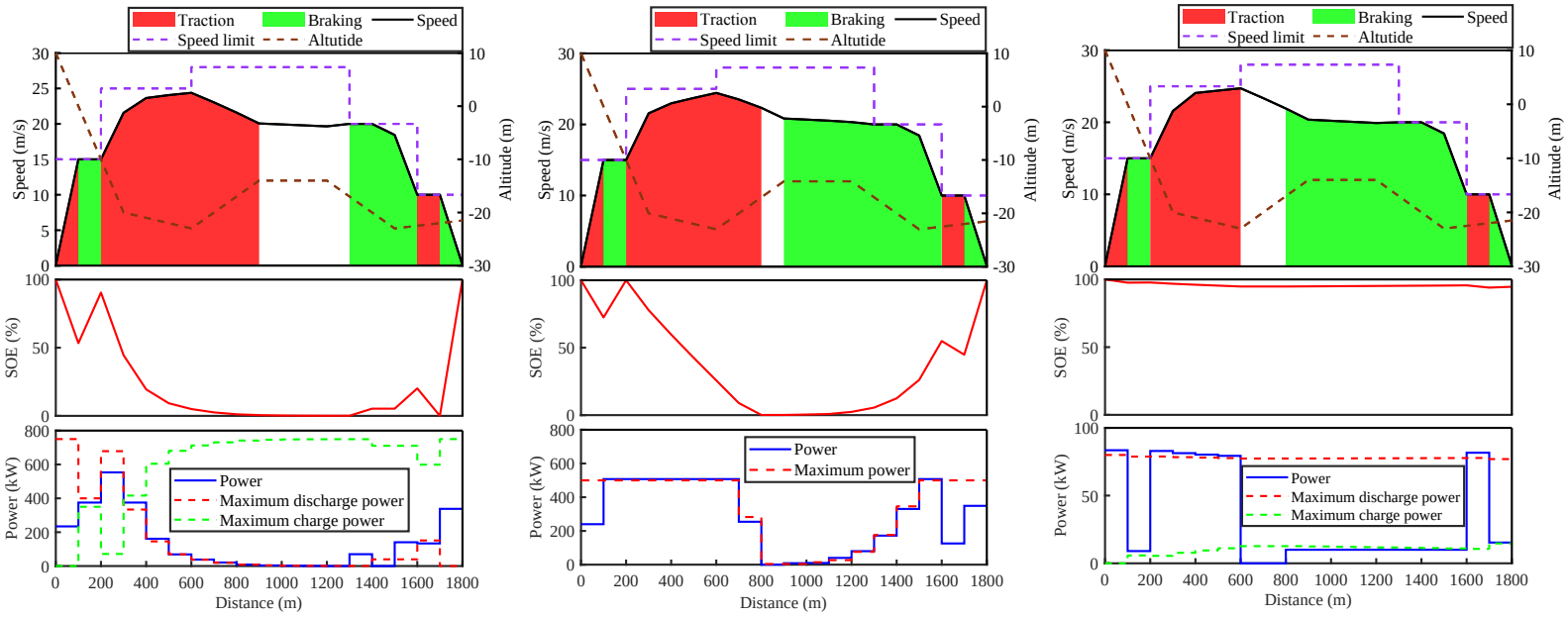

Figure 7.6: Scenario 2: The optimal train speed, OESD SOE and power profiles for the train with (a) supercapacitor, (b) flywheel and (c) Li-ion battery on a 1800-metre-long sloping track with speed limits. Different traction and braking distribution resulted from different OESD, both of the optimal speed and OESD discharging/charging power are limited by the speed limits and dynamic power limits respectively during the journey

and lower maximum power, leading to the longer discharge/charge process and longer traction/braking distance than supercapacitor. As for the train with Li-ion battery, due to its largest capacity and lowest maximum power, the discharge/charge process of it is the most frequent among the three, leading to the constant traction/braking to make the OESD release and recover as mush energy as possible.

Scenario 2 is to see the flexibility of the proposed method, where the varied route conditions e.g. gradient change and speed limits are introduced to make the case studies more practical, and the running time T is prolonged to be 120 s here since the maximum train speed is constrained by speed limits. The results are shown in Figure 7.6, which shows that due to the introduction of the complex route conditions the train speed, SOE and power profiles see significant difference compared to scenario 1. Different optimal eco-driving strategies for the train with different types of OESD can be found to meet the real operational requirements, where the discharging/charging process for three types of OESD still follow the corresponding dynamic power limit. Discharging/charging processes are more frequent than Scenario 1 resulted from the introduced route conditions. The train switches the traction and braking modes back and forth to finish the journey, where the SOE and power profiles for supoercapacitor and flywheel are more fluctuated than the Scenario 1 while SOE of Li-ion battery still changes mildly.

7.3.2 Discontinuously Electrified and Catenary-Free Railways

Though railway electrification prevails in some region and country in recent years, in some special locations, e.g. tunnel or bridges, installing the catenary or other power supply systems might be economically or technically impractical. On the other hand, some of the railway systems are too old to be fully electrified, e.g. the TransPennine route between Leeds and Manchester built in Victorian times [132]. In addition, the future projects should ensure that all options for traction power supplies are considered, including distribution and energy storage options on the discontinuous electrification, where the operating and maintenance costs and the resilience of the alternatives should also be considered [133]. When the train is equipped with OESD, if well designed, the train can always secure adequate energy supply and operate on railway sections without temporary or permanent electricity supply from substations. In this section, the potential of each types of OESD applied in discontinuously-electrified and catenary-free railways is investigated. In Scenario 3, the train is running on a 2000-m track with a non-zero initial speed and a 1000 m non-electrified section at the beginning. The

total running time T is assumed to be 160 s and the new speed limits and gradients information are also introduced. In scenario 3, the initial speed v_1 and the initial SOE of OESD SOE_1^k when entering the non-electrified section is assumed to be 15 m/s and 60% respectively.

Since the train running in the first 1000 meters cannot be powered by the substation, thus, the 1^{st} to 10^{th} $E_{i,s}$ need to be set as 0. The results of scenario 3 are shown in Figure 7.7, it can be observed that the train can safely passes the non-electrified section under the support of OESD, and the speed profiles with different types of OESD are noticeably different. The traction and braking process together with the discharging/charging process of OESD occur repeatedly along with the journey. In addition, it can also be noted that the SOE change of Li-ion battery is still much more mild than that of supercapacitor and flywheel.

On the other hand, trains running on the catenary-free railway is also common in city trams or light rail systems. The proposed method can be used to evaluate the feasibility of each type of OESD in catenary-free railway lines using time-saving driving strategy. To achieve this, scenario with the track length being 2500 m with speed limits and gradient information is given. The objective function of the model needs to be revised to be (7.43), with the constraint of the total running time relaxed and all of the $E_{i,s}$ set to be 0.

$$\min \quad \sum_{i=1}^{N} \Delta t_i \tag{7.43}$$

By changing the objective function to minimise the total running time, the time-saving potential of the train with each type of OESD can be obtained, and the optimal speed trajectory, SOE profile, OESD power profile and corresponding time-distance paths are shown in Figure 7.8. It can be noted from the results that the train with flywheel can run faster than the other two because it makes the shortest total running time. Though with the highest maximum power, the small capacity of the supercapacitor undermines its time-saving driving strategy very much, resulting in the longest running time among the three. On contrary, due to the largest capacity of the Li-ion battery, the train with it can have constant but lowest power supply. This ensures that the train with it can constantly motor to accelerate for reducing the journey time, just as shown in Figure 7.8-(c). Also, from the change of the SOE and OESD power profile, though each of the 3 sees significant difference, the similar trend is to power the train as much as possible to raise the speed rather than recovering the regenerative braking energy.

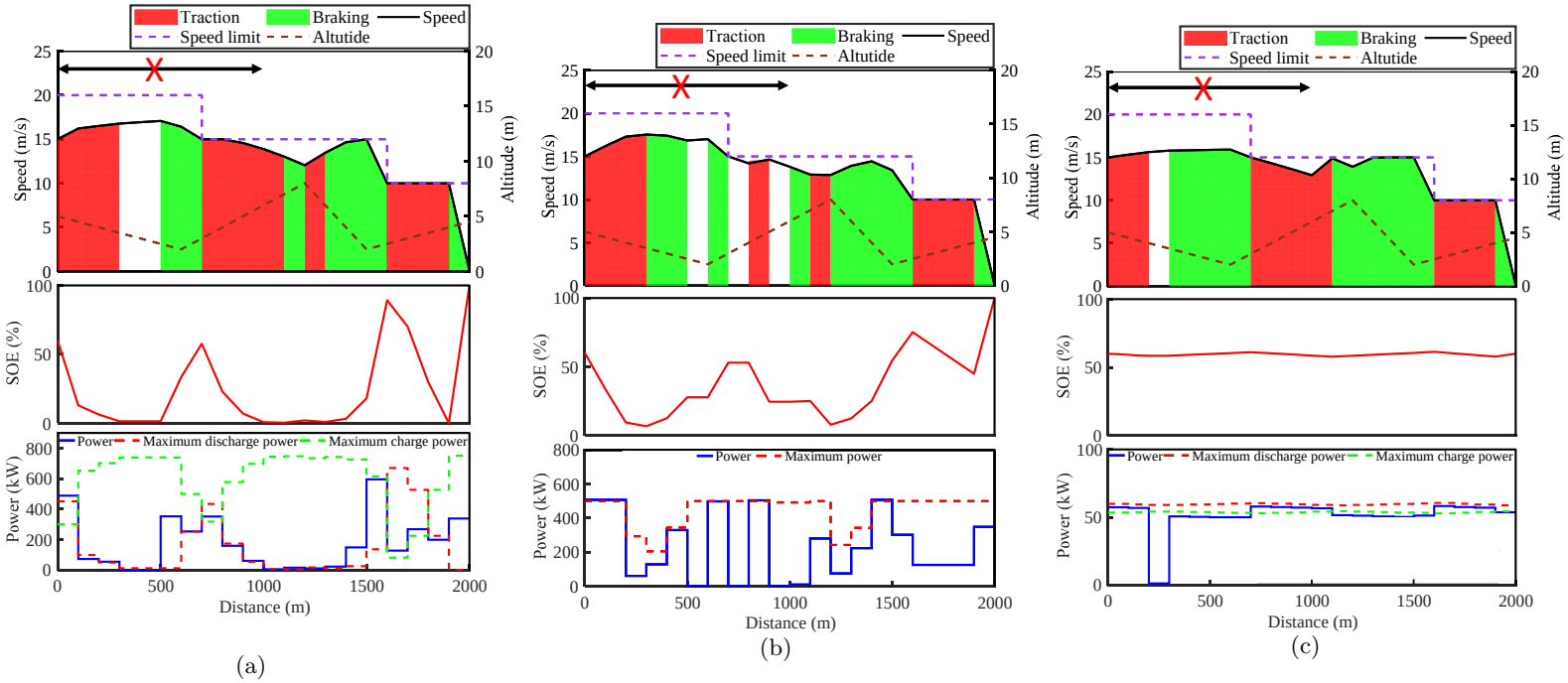

Figure 7.7: Scenario 3: The optimal train speed, OESDs' SOE and OESD power profiles for (a) supercapacitor, (b) flywheel and (c) Li-ion battery with non-electrified sections (The double arrow with "X" represents the non-electrified section). During the running in the non-electrified section, the train with different OESD conducts more traction than braking, e.g. 600-metre-long motoring VS 200-meter-long braking for supercapacitor, 400-meter-long traction VS 200-meter-long braking for flywheel and 500-meter-long traction VS 400-meter-long braking for Li-ion battery

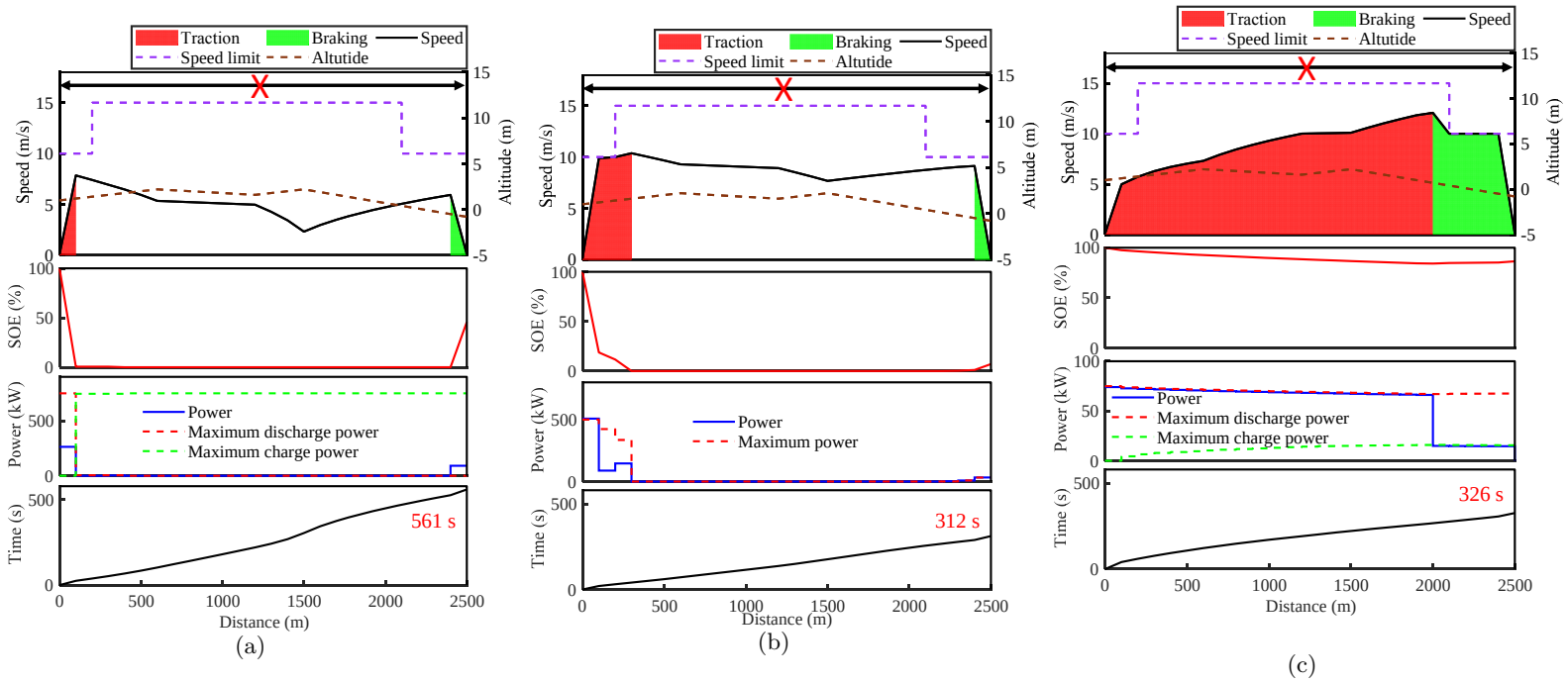

Figure 7.8: Scenario 4: The optimal train speed profile, SOE profile and OESD power profile and corresponding time-distance path for (a) supercapacitor, (b) flywheel and (c) Li-ion battery on the catenary-free railway section (The double arrow with "X" represents the non-electrified section). Different shortest journey time resulted from different OESD are shown, where the flywheel can bring the fastest arrival, Li-ion battery ranks the second and supercapacitor ranks the last

7.3.3 Results Comparison on Different Types of OESD

For a comprehensive evaluation and comparison, the net energy consumption, energy-saving rate and the energy-saving rate per k$ for all scenarios are given in Table 7.4. Noted that the unit in kWh is used to reduce the digit numbers when using unit kJ of the variables. From the result of scenario 1, it can be seen that except of Li-ion battery, both supercapacitor and flywheel have ran out of their stored energy since their supplied energy equal to their capacity. For scenario 2 and scenario 3, due to the more frequent discharge/charge process during the journey resulted by the more complex route conditions, the supplied energy and recovered energy by supercapacitor and flywheel are higher than their capacity. The net energy consumption of scenario 3 for both supercapacitor and flywheel is negative. This is resulted from the non-zero initial speed of the journey, where the energy consumption of the previous running is not counted in the results, and also due to the more energy recovered than energy supported of both type of OESD in this journey.

It can be seen that from Scenario 1 to Scenario 3, the train with flywheel are always with minimum net energy consumption on the same route when compared to the train with the supercapacitor and Li-ion battery. Flywheel can also supply and recover the most energy during the journey, resulting in the least dissipated energy by resistor. On the other hand, the Li-ion battery brings the least energy-saving effect, with the highest net energy consumption from Scenario 1 to Scenario 3. Li-ion battery can only supply and recover few energy due to its limited power capability, resulting in the most dissipated energy among the three types of OESD.

For Scenario 4, it should be noted that the objective of it is not on energy saving but on feasibility analysis. With the catenary-free railways, it is observed that Li-ion battery supplies the most energy and recovers the most energy during the journey. This is resulted from its largest capacity which enables it to have continuous traction and braking to save the running time of the journey. In contrary, due to the smallest capacity of the supercapacitor, though it can supply the highest power in short time, the train still has limited traction ability which undermines the time-saving effect.

In summary, based on the optimisation results of the 4 scenarios shown above, the technical advantages of these three types of OESD can be analysed on the average term. From the results tabulated in Table 7.4, it can be seen that the flywheel can bring the least energy consumption from substation and net energy consumption with the highest energy-saving rate, ranging from 22.32% to 129%, and also the most cost-effective for its highest energy-saving rate per k$. Though the supercapacitor and the Li-ion

Table 7.4: Results of the case studies

OESD type	Energy supplied by OESD (kWh)	Energy recovered by OESD (kWh)	Energy dissipated by resistor (kWh)	Energy from substation (kWh)	NEC* (kWh)	Energy-Saving rate (%)	Energy-Saving rate per k$ (%/k$)
Scenario 1: without varying route conditions (1800-metre-long track and 100-second journey time)							
S	1.87	1.87	9.60	15.76	15.76	13.55	0.09
F	3.50	3.50	8.18	14.46	14.46	22.32	0.15
L	0.16	0.75	10.63	18.64	18.05	0.99	0.01
Scenario 2: with varying route conditions (1800-metre-long track and 120-second journey time)							
S	2.94	2.94	14.24	2.49	2.49	59.24	0.39
F	4.82	4.82	12.93	1.42	1.42	76.76	0.51
L	0.22	0.97	15.95	6.58	5.83	4.58	0.03
Scenario 3: partially electrified railway (2000-metre-long track and 160-second journey time)							
S	3.86	4.61	2.17	0	-0.75	115	0.77
F	4.54	5.94	1.29	0	-1.40	129	0.86
L	1.15	1.16	5.89	2.91	2.90	39.71	0.26
Scenario 4: catenary-free railway (2500-metre-long track)							
S	1.87	0.86	0	0	1.01	/	/
F	3.50	0.24	1.89	0	3.25	/	/
L	5.35	0.96	2.73	0	4.38	/	/

S: Supercapacitor; F: Flywheel; L: Li-ion battery. NEC*: Net energy consumption.

battery bring less energy-saving rate than the flywheel, under the same capital cost the supercapacitor can provide the highest power output in a short time while the Li-ion battery is with the largest capacity for the long-term operation. It also implies that the proper combination of them will make the most of each type of OESD, which might help reduce more energy consumption.

7.3.4 Error Analysis of the Proposed Model

In this section, the error analysis of the proposed method is elaborated by focusing on power limits $\overline{P^k_{idch}}$ and $\overline{P^k_{ich}}$ and the running time T based on the results of the case studies.

In section 7.2, linear approximation of the train movement and the dynamic power characteristics of three types of OESD are conducted, which leads to the difference between the approximated value and actual value. This can be observed in the results that there are slight discrepancies between the OESD power profile and the corresponding power limits. For scenario 1, in Figure 7.5-(c), it can be seen that the discharge power of Li-ion battery slightly exceeds its power limits. For scenario 2, it can be observed in Figure 7.6-(a) and Figure 7.6-(c) that the discharging and charging power for both supercapacitor and Li-ion battery are slightly higher than their respective limits in some Δd_i. Also, the discharge power of supercapacitor in scenario 3, as shown in Figure 7.7-(a), sometimes goes beyond the power limits a bit during the journey.

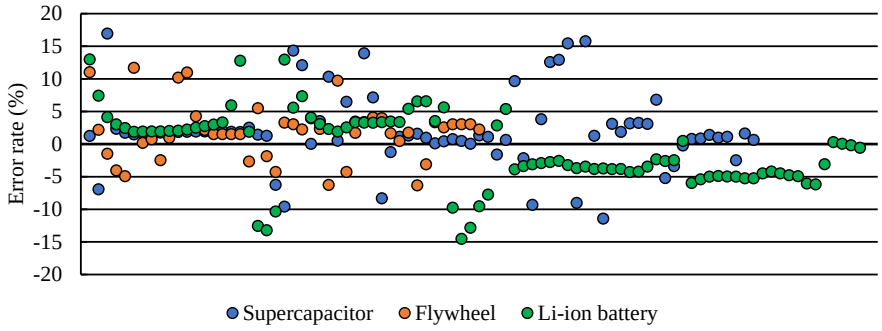

Figure 7.9: The error rate for dynamic power limits approximation of each types of OESD from the case studies

The dynamic power limits with respect to the current SOE of OESD for different types of OESD are approximated by using piece-wise linearisation and SOS2 method in the modelling process. As a result, the error analysis of it is needed to see the performance of the proposed approach. The error rate of the discharge/charge power

limit, $e_{i,P}^{dch}$ and $e_{i,P}^{ch}$, can be obtained by using (7.44).

$$e_{i,P}^{dch} = \frac{\overline{\frac{\Delta E_{i,dch}^{k}}{\Delta t_i}}' - \overline{P_{i,dch}^{k}}}{\overline{P_{i,dch}^{k}}} \times 100\%, \quad e_{i,P}^{ch} = \frac{\overline{\frac{\Delta E_{i,ch}^{k}}{\Delta t_i}}' - \overline{P_{i,ch}^{k}}}{\overline{P_{i,ch}^{k}}} \times 100\% \tag{7.44}$$

Note that the error data when $\overline{P_{i,dch}^{k}}$ or $\overline{P_{i,ch}^{k}}$ equals to 0 are eliminated in the results due to the infeasible calculation. The results of the error rate is plotted in Figure 7.9. From the figure, it can be seen that the most of the points are located between ±5% in error rate data for all of the Δd_i of the case studies. Additionally, the average error rate for supercapacitor, flywheel and Li-ion battery is 2.04%, 1.84% and -0.71% respectively, showing that the proposed method preforms satisfactorily on modelling the dynamic power limits of each types of OESD.

On the other hand, the relationships among the speed-related variables are linearised by using SOS2, and the approximated values $\frac{1}{v'_{i,ave}}$ but not the real reciprocal of average speed of each Δd_i are used in calculating the running time T, which influences the accuracy of it. Since punctuality is important in real operation, the accuracy of it in the proposed model is also essential, which indicates that the error analysis of the running time is necessary. Here the error rate of the running time T is denoted as e_T, and it can be calculated by dividing the difference of the approximated values and real values by the real values, as shown in (7.45).

$$e_T = \frac{T - (\sum_{i=1}^{N} \frac{\Delta d_i}{\sqrt{v_i^2 + \sqrt{v_{i+1}^2}}})}{\sum_{i=1}^{N} \frac{\Delta d_i}{\sqrt{v_i^2 + \sqrt{v_{i+1}^2}}}} \times 100\% \tag{7.45}$$

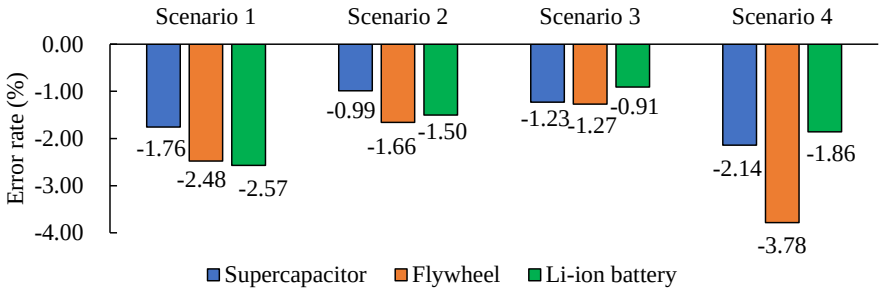

Figure 7.10: The error rate for running time modeling for each OESD in various case studies

Based on the obtained optimal speed trajectories, the e_T for 4 scenarios of these

three types of OESD can be calculated, the results of which are illustrated in Figure 7.10. It can be observed that the error rates of the running time for 4 scenarios of three types of OESD are all small, the range of which are only between -0.91% and -3.78%, while the average error rate being -1.8%. This error rate is relatively small when comparing with the error rate 5% in [134] and 2% in [34] dealing with the train speed optimisation using mathematical programming. This confirms the acceptable modelling accuracy of our method on controlling the running time of the journey.

7.4 Summary

This chapter investigates the optimal driving strategy of the train equipped with three popular types of OESD: supercapacitors, flywheels and Li-ion batteries, to minimise the net energy consumption by taking into account their corresponding dynamic discharging/charging characteristics.

The dynamic power limits of different types of OESD of the fixed investment cost together with the train operation are formulated as a MILP problem. The case studies are conducted by using the proposed method to investigate the train operation on fully electrified railways, partially electrified railways and catenary-free railways. Based on the results, insightful comparisons of the speed trajectories, SOE and power profiles of OESDs and energy-saving effect for the train with different type of OESD are given. It can be seen from the results that flywheel offers the best performance on saving the energy consumption with the highest energy-saving rate ranging from 0.15 %/k$ to 0.86 %k/$ under various scenarios. Supercapacitor ranks the second and can save the energy consumption from 0.09 %/k$ to 0.77 %/k$. Li-ion battery sees the poorest performance since it can only bring a energy-saving rate from 0.01 %/k$ to 0.26 %/k$ for all of the scenarios. In addition, from the error rate analysis it can be told that the proposed method can solve the problem with acceptable modelling accuracy, which shows the effectiveness and practicality of the approach.

Chapter 8

Choosing Right Size of OESD-A Data-Based Method

The main content of this chapter is from the author's published article in a version with minor reconfiguration to fit the structure and context of this thesis. The published article is:

C. Wu, S. Lu, F. Xue, L. Jiang and M. Chen, "Optimal Sizing of On-Board Energy Storage Devices for Electrified Railway Systems," *IEEE Transactions on Transportation Electrification*, vol. 6, no. 3, pp. 1301-1311, 2020.

8.1 Introduction

This chapter discusses the optimal sizing problem of the OESD for energy-saving train operations. In Chapter 4, it is found that the excessive capacity of the OESD will not bring more energy reduction, but might lead to the increase of the energy consumption due to the heavier mass, see Figure 4.6. Therefore, based on the characteristics of the train operation, finding out the best capacity of the used OESD will effectively guide the operators to do the smart decision on selecting the most suitable OESD to achieve the best energy-saving performance as well as reduce the unnecessary capital cost.

Locating the suitable capacity for energy storage systems has been a popular research topic in the field of electrical engineering, and it has been investigated in the microgrid (MG) [135–137] and electric vehicle (EV) applications [138–140]. The main focuses of these papers are to determine the appropriate size of the energy storage systems

to reduce or minimise the system's operating cost and investment cost of the energy storage devices. On the other hand, sizing problem of the energy storage in electrified railway systems is still a new research direction for both stationary energy storage and OESD [11]. Optimal sizing problem for stationary and substation-based energy storage has been studied with no constraints on weight and volume of the energy storage devices. In [13], energy storage technologies for Auxiliary-Battery-Based Substations are investigated, in which a Techno-economic model for battery sizing, locating and controlling are proposed to minimise the system's operating cost. For recuperation of the regenerative energy, study on the optimal sizing problem of a stationary hybrid energy storage system combining the batteries and supercapacitors is conducted [141], where the train power profiles, battery cycles and depth of discharge (DOD) are considered. To minimise the trade-off between stationary energy storage capacity and charging power, a sizing methodology is proposed and a barrier method combined with a Newton's method is applied to find the optimal solution [142].

Along with the stationary energy storage systems, OESDs on the other hand are also fast developing and widely applied in railway transportation. It has been argued that oversizing of the OESD might unnecessarily increase mass and volume of the system, whereas undersizing might lead to considerable energy waste [8]. By developing a specific simulation tool to simulate the train vehicle movements, power profiles and OESD control, the OESD sizing problem taking into account the railway traffic volumes is studied in [143], which helps shave peak power, reduce voltage drop and line losses. In [144], the numerical simulations and experimental tests are conducted to investigate the problem, where the size of the OESD is reduced to help shave the voltage peak of the overhead contact line as well as to save the energy consumption. In [145], the optimal sizing problem for a light railway vehicle with an OESD combining batteries and supercapacitors are studied by applying GA. The target of it is to minimise the cost of the energy from catenary as well as the initial investment and cycling cost of OESD. It is noted that the above optimal sizing studies are conducted by using simulations, hardware experiments and heuristic algorithms, which would result into an issue of sub-optimum and undermine the energy-saving potential of OESD.

It can be found that further studies are still needed on the optimisation method to address the OESD's optimal sizing problem considering both characteristics of OESD and train operations. In this case, this chapter aims to develop a mathematical model to be solved to determine the optimal capacity of different types of OESD which minimises the energy consumption for practical electrified railway operations. The contributions of the chapter are outlined as follows:

- three types of popular energy storage, supercapacitors, Li-ion batteries and flywheels, are investigated. The characteristics of OESD e.g. power density and energy density, and the industry-concerned factors e.g. capital cost and volume, are all taken into account in the model.
- By modelling the energy flow of the traction system, the discharging/charging process of the OESD, train operation status, complex route conditions and engineering properties of OESD are formulated into a mathematical programming model, in which the global optimal capacity of OESD can be obtained.
- The real-world train operation data from Beijing Changping line is adopted in this chapter, which shows the effectiveness of the proposed method in real application. Comprehensive compare and contrast studies are performed between different types and different size of OESD based on the results of the model, offering an inside view on their influences on energy-saving effect to the train operation.

8.2 Data-Based Modelling

Notation of variables	
E_{cap}	Capacity of the OESD [kJ]
$\Delta E_{i,j,s}$	Energy from the substation in $\Delta d_{i,j}$ [kJ]
$\Delta E_{i,j,dch}$	Energy discharged from the OESD in $\Delta d_{i,j}$ [kJ]
$\Delta E_{i,j,ch}$	Energy charged to the OESD in $\Delta d_{i,j}$ [kJ]
$\Delta E_{i,j,r}$	Energy transmitted to the resistor from the motor in $\Delta d_{i,j}$ [kJ]
$\lambda_{i,j}$	Binary variables to determine the train operation mode in $\Delta d_{i,j}$
Assumptions	
	1. The regenerative braking energy can only be recovered by OESD or dissipated by resistors but cannot be fed back to the substation or used by other trains. 2. The long-term or life-cycle factors that might influence the performance of OESD are ignored.

8.2.1 Data Collection from the Discretised Route

The inter-station sections in railway line are separated by different stations along with the whole track. The track length D_i for i^{th} inter-station section is first discretised and divided into several distance segments with the value $\Delta d_{i,j}$ respectively, the sum of

which satisfies (8.1).

$$\sum_{j=1}^{N_i} \Delta d_{i,j} = D_i \tag{8.1}$$

where N_i is the total amount of the divided distance segments for i^{th} inter-station section.

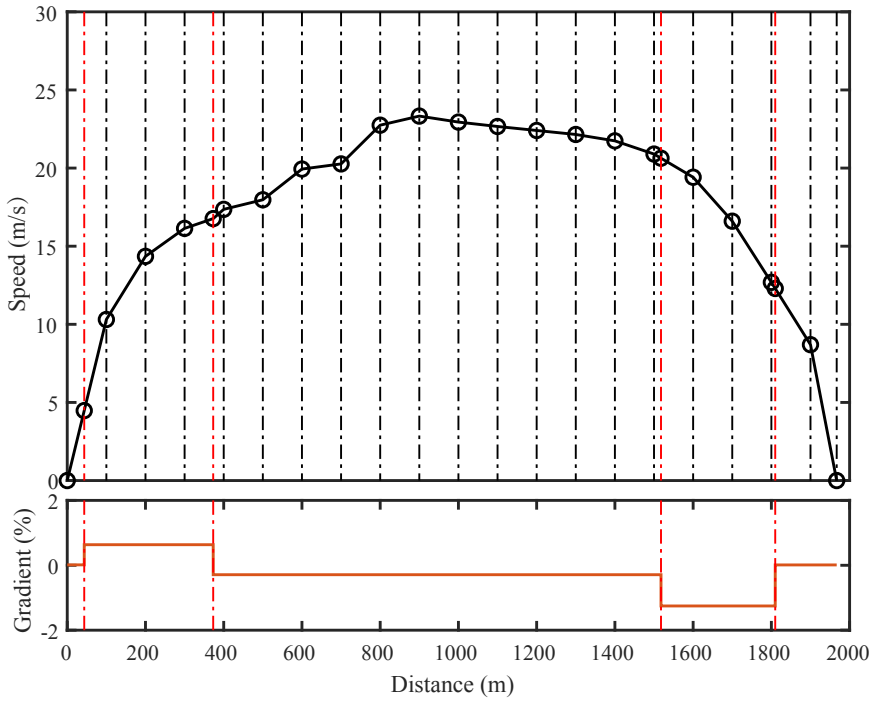

Figure 8.1: Schematic illustration of discretisation process of the one typical inter-station section. Black solid line is the practical train speed trajectory, black dash lines are the basic division without considering the gradients information, red dash lines are the division imposed by specific gradient change and circles are the corresponding speed points

$\Delta d_{i,k}$ can be modified with different value according to practical track conditions e.g. different track length and gradients so that the track length can be fitted. Within one distance segment, there is no change of the gradient. For example, as shown in Figure 8.1, the whole track length for the i^{th} inter-station journey is 1960 m and the gradient changes occur at 47 m, 380 m, 1510 m and 1805 m. D_i is first divided into 20 distance segments with 19 100-metre segments and 1 60-metre segment without considering the gradient information, shown as the black dash lines in Figure 8.1. This means that $\Delta d_{i,j}$ for $j = 1, 2, 3, ..., 19$ is 100 metres and $\Delta d_{i,20}$ is 60 metres in length.

Followed by this, we insert the division lines in gradient switching points mentioned above to do the reconfiguration of $\Delta d_{i,j}$, shown as the red dash lines in Figure 8.1. After the reconfiguration, the number of $\Delta d_{i,k}$ increases from 20 to 24 with $\Delta d_{i,1}$, $\Delta d_{i,2}$, $\Delta d_{i,3} \sim \Delta d_{i,4}$, $\Delta d_{i,5}$, $\Delta d_{i,6}$, $\Delta d_{i,7} \sim \Delta d_{i,17}$, $\Delta d_{i,18}$, $\Delta d_{i,19}$, $\Delta d_{i,20} \sim \Delta d_{i,21}$, $\Delta d_{i,22}$, $\Delta d_{i,23}$ and $\Delta d_{i,24}$ assigned with 47 m, 53 m, 100 m, 80 m, 20 m, 100 m, 10 m, 90 m, 100 m, 5 m, 95 m, 60 m respectively. Both D_i and $\Delta d_{i,j}$ have no minimum or maximum limits as they are determined by the studied railway systems and field data of the speed trajectories. Also, the shorter the $\Delta d_{i,j}$ is, the more speed data to be collected, and the more precise result it will be.

After the discretisation of the route, the practical train speed of both ends of each $\Delta d_{i,j}$ can be collected, shown as the circles in Figure 8.1. As there are N_i distance segment $\Delta d_{i,j}$, there will be $N_i + 1$ collected train speed points $V_{i,1}$, $V_{i,2}$,...,$V_{i,j}$,..., V_{i,N_1+1}. Therefore, the average speed $V_{i,j,ave}$ of each $\Delta d_{i,j}$ can be calculated by using the collected $V_{i,j}$ as shown in (8.2).

$$V_{i,j,ave} = \frac{V_{i,j} + V_{i,j+1}}{2}, \quad \forall j \in 1, 2, ..., N_i, \quad \forall i = 1, 2, ..., I \tag{8.2}$$

where I is the total number of the investigated inter-station sections.

After having the average speed for each $\Delta d_{i,j}$, the elapsed time $\Delta t_{i,j}$ for each $\Delta d_{i,j}$ for the inter-station journey can be calculated by using (8.3). Additionally, the drag force $R_{i,j}$ for each $\Delta d_{i,j}$ can be calculated by Davis equation as shown in (8.4).

$$\Delta t_{i,j} = \frac{\Delta d_{i,j}}{V_{i,j,ave}}, \quad \forall j \in 1, 2, ..., N_i, \quad \forall i = 1, 2, ..., I \tag{8.3}$$

$$R_{i,j} = R_0 + R_1 V_{i,j,ave} + R_2 V_{i,j,ave}^2, \quad \forall j \in 1, 2, ..., N_i, \quad \forall i = 1, 2, ..., I \tag{8.4}$$

As we can see, through collecting the practical train running speed based on route discretisation, the related parameters of this speed trajectory including running time and drag force can be obtained as well by simple calculation, which are the important inputs of the later modelling and optimisation process.

8.2.2 Relationship between OESD Capacity and Energy Conversion

It can be found in [8, 130] and [131] that the performance of the energy storage is commonly expressed by using energy density, power density, capital cost in the unit of "energy per unit mass", "energy per unit volume" and "power per unit mass". In this case, the linear relationships among the capacity, mass, maximum discharge/charge

power, volume of each type of OESD can be established. As a result, different capacity of the OESD E_{cap} leads to different mass of the OESD M_o, and the relationship between the capacity and the mass can be represented in (8.5).

$$M_o = \frac{E_{cap}}{X_m} \tag{8.5}$$

where X_m is the energy density with respect to the mass and it is a constant determined by the feature of different types of OESD.

Since in the Section 8.2.1 the $V_{i,j}$ are collected, the kinetic energy change $\Delta E_{i,j,k}$ of the train in each $\Delta d_{i,j}$ can be calculated by using (8.6).

$$\Delta E_{i,j,k} = \frac{1}{2}(M_t + M_o)(V_{i,j+1}^2 - V_{i,j}^2) = \frac{1}{2}(M_t + \frac{E_{cap}}{X_m})(V_{i,j+1}^2 - V_{i,j}^2), \\ \forall j = 1, 2, ..., N_i, \quad \forall i = 1, 2, ..., I \tag{8.6}$$

The work done by the drag force $\Delta E_{i,j,f}$ in each $\Delta d_{i,j}$ can also be obtained as shown in (8.7).

$$\Delta E_{i,j,f} = F_{i,j,drag} \Delta d_{i,j}, \quad \forall j = 1, 2, ..., N_i, \quad \forall i = 1, 2, ..., I \tag{8.7}$$

The potential energy change of the train $\Delta E_{i,j,p}$ resulted from the gradient change of the route is calculated by using (8.8).

$$\Delta E_{i,j,p} = (M_t + M_o) g \Delta d_{i,j} \theta_{i,j} = (M_t + \frac{E_{cap}}{X_m}) g \Delta d_{i,j} \theta_{i,j}, \\ \forall j = 1, 2, ..., N_i, \quad \forall i = 1, 2, ..., I \tag{8.8}$$

where $\theta_{i,j}$ is the gradient for the interval of $\Delta d_{i,j}$.

According to the law of conservation of the energy, the conversion of the energy can be expressed in (8.9).

$$\Delta E_{i,j,m}^+ - \Delta E_{i,j,m}^- - \Delta E_{i,j,k} - \Delta E_{i,j,f} - \Delta E_{i,j,p} - \Delta E_{i,j,r} = 0, \\ \forall j = 1, 2, ..., N_i, \quad \forall i = 1, 2, ..., I \tag{8.9}$$

where $\Delta E_{i,j,m}^+$ and $\Delta E_{i,j,m}^-$ are both extended from $\Delta E_{i,m}^+$ and $\Delta E_{i,m}^-$ in the previous chapters in order to deal with multiple inter-station sections. Since motoring and braking cannot occur at the same time, to distinguish different train operation modes, the binary variables $\lambda_{i,j}$ and large number L are introduced to ensure that when there are $\Delta E_{i,j,s}$ and $\Delta E_{i,j,dch}$, there is no $\Delta E_{i,j,ch}$ existing at the same time, and vice versa.

In addition to the energy restriction, the power limit of the motor and OESD should be added as the constraints respectively, and the work done by the motor also need to be restricted by the maximum traction force provided by the motor. Additionally, the maximum discharging and charging power $\overline{P_o}$ of OESD is related to the mass of it, thus we have the relationship as shown in (8.10).

$$\overline{P_o} = Y \times M_o = Y\frac{E_{cap}}{X_m} \tag{8.10}$$

where Y is the power density with respect to the mass and it is a constant determined by the feature of different types of OESD. Thus the power for the discharged and charged energy cannot exceed the maximum charge and discharge power.

$$\Delta E_{i,j,dch} \leq \overline{P_o}\Delta t_{i,j} = Y\frac{E_{cap}}{X_m}\Delta t_{i,j}, \quad \forall j = 1, 2, ..., N_i, \quad \forall i = 1, 2, ..., I \tag{8.11}$$

$$\Delta E_{i,j,ch} \leq \overline{P_o}\Delta t_{i,j} = Y\frac{E_{cap}}{X_m}\Delta t_{i,j}, \quad \forall j = 1, 2, ..., N_i, \quad \forall i = 1, 2, ..., I \tag{8.12}$$

The state of energy (SOE) defines the amount of stored energy relative to the capacity E_{cap} of the OESD, it is accumulated with the train's running from the first station. It can be expressed based on the proposed model in the study in the equation (8.13).

$$0 \leq SOE_{i,j} = \frac{E_{ini} - \sum_{j=1}^{J}\Delta E_{i,j,dch} + \sum_{j=1}^{J}\Delta E_{i,j,ch}}{E_{cap}} \times 100\% \leq 100\%, \quad \forall j = 1, 2, ..., N_i, \quad \forall i = 1, 2, ..., I \tag{8.13}$$

where E_{ini} is the initial available energy in the OESD when the train departs from the first station. In addition, $J = j$, when $i = 1$ for the running at the first inter-station journey; $J = N_1 + N_2 + ... + N_{i-1} + j$, when $i \geq 2$ since the status of the OESD in previous inter-station journeys needs to be accumulated together.

The objective function of the entire model is the net energy consumption which is the difference of the total traction energy consumption (The sum of total energy consumption from substation and total discharged energy from OESD) and the total regenerative energy received by OESD, as shown in (8.14). By conducting this optimisation to minimise the net energy consumption, energy consumption from the substation is also

minimised.

$$\min \quad \sum_{i=1}^{I}\sum_{j=1}^{N_i}(\Delta E_{i,j,s} + \Delta E_{i,j,dch} - \Delta E_{i,j,ch}), \tag{8.14}$$

8.3 Numerical Experiments

In this section, the effectiveness of the proposed approach is demonstrated by using a real case study based on the data from Beijing Changping line. The Changping line covers 21 kilometres distance and has 7 stations. The route map for the Changping line is shown in Figure 8.2 and Figure 8.3 illustrates the traction/braking characteristics, basic drag force of the train and gradient information of the route [146]. The practical train speed trajectory for each inter-station section of the Changping line and corresponding distance interval for speed data collection follow the literature [147]. These information has been integrated and tabulated in Table 8.1.

Figure 8.2: The route map for Beijing Changping line

Table 8.1: The inter-station length and the distance interval used in speed data collection for Beijing Changping line

Inter-Station section	Length (m)	Distance interval (m)
XRQ-LP	5441	200
LP-ZXZ	2368	100
ZXZ-GHC	3810	200
GHC-SH	2037	100
SH-SUP	1967	100
SUP-NS	5364	200

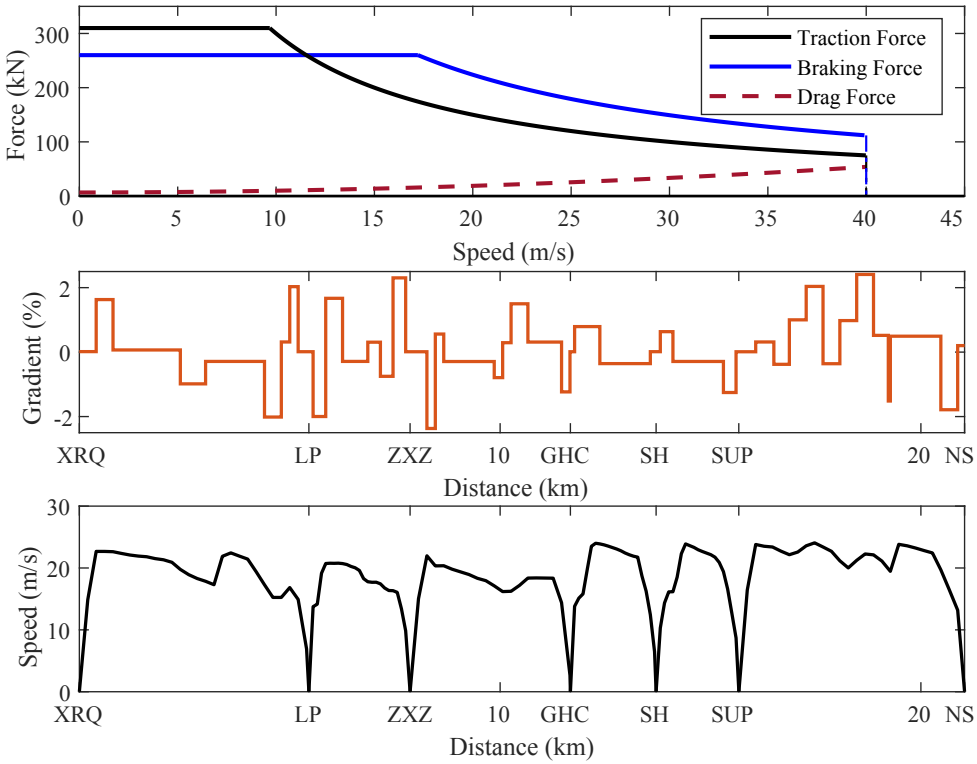

Figure 8.3: The traction/braking characteristics of the train motor, drag force, gradient information and practical train speed trajectory of the Changping line

Similar as Chapter 7, the case studies mainly focus on the three types of OESD, namely supercapacitor, battery and flywheel due to their most popular applications. In addition, Li-ion battery is selected to represent the other types of chemical battery. The OESD data used in the case studies can be found in Table 7.1 in Chapter 7. It should be noted that for the purpose of a general investigation, the halfway point of these ranges is selected e.g. the power density for supercapacitor used in the case studies is set to be $(500 + 5000)/2 = 2750$ kW/t. This halfway point value is considered as one of the reasonable presentations of the general characteristics of one type of energy storage. This value needs to be updated to reflect the technical development of energy storage technology and maintain a high level of modelling accuracy. With the fast development of energy storage technologies, the general performance of these three types of OESD will see substantial progresses and this halfway point will definitely change in the foreseeable future. The proposed model still can be used to obtain the corresponding new optimal size of the OESD based on the new values of these parameters.

Note that the case studies are conducted by using Matlab R2018b® and CPLEX®

12.8.0 solver on a PC with Intel Core® i5-6500 processor (3.20 GHz) and 8.00 GB RAM.

8.3.1 Without the Constraints of Capital Cost and Volume

This section introduces the optimal results regardless of the capital cost and volume of the OESD, and the reference train speed trajectories for the Changping line and its optimal discharge/charge curves represented by OESDs' SOE are shown in Figure 8.4. The optimal capacity of each type of OESD and respective energy consumption from substation are tabulated in Table 8.2, and the corresponding resulted volume, capital cost, maximum power and mass are also given in Table 8.3.

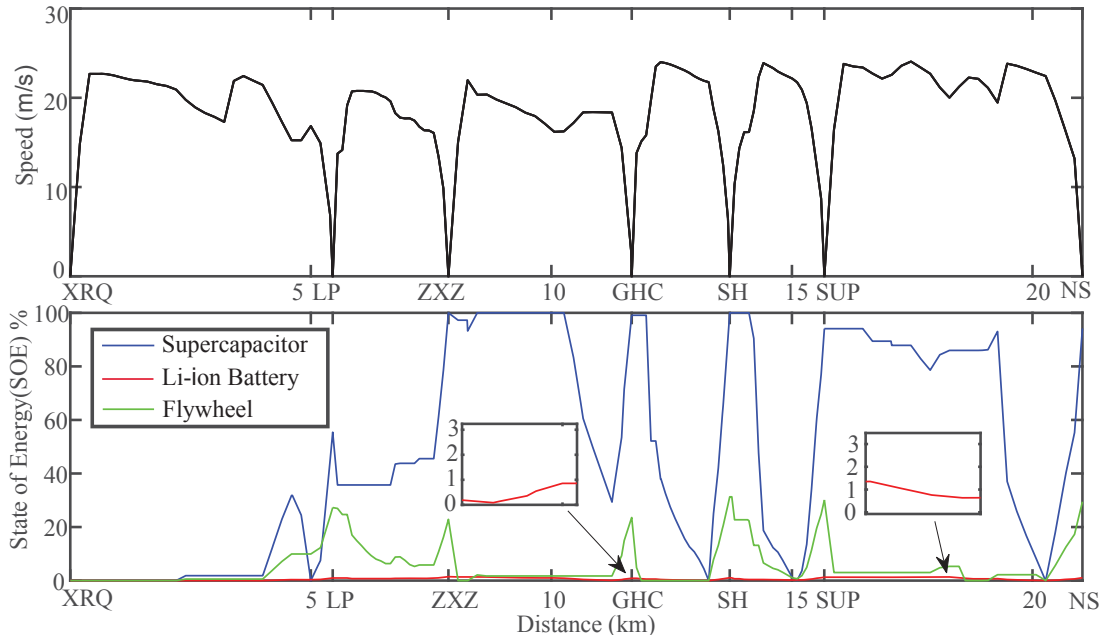

Figure 8.4: The reference train speed trajectories and discharging/charging curves for different optimally sized OESD without constraints of capital cost and volume

From the Table 8.2 it is observed that without any constraints on capital cost and volume, with the same reference speed trajectories, supercapacitor, Li-ion battery and flywheel with respective optimal capacity can bring the similar energy-saving effect, reducing energy consumption from substation by 23.6%, 22.9% and 23.7% respectively. However, the optimal OESD capacity sees substantial differences when compared among different types of OESD. For achieving the minimum energy consumption from substation, the optimal capacity for Li-ion battery is extremely high, which reaches 923.8 kWh, and for supercapacitor is the lowest being 10.1 kWh. In addition, results

Table 8.2: Optimisation results of energy consumption from substation and OESD capacity for case without constraints of capital cost and volume

OESD type	Optimal capacity (kWh)	Minimum energy consumption from substation (kWh)	Energy-saving rate* (%)
Supercapacitor	10.1	157.3	23.6
Li-ion battery	923.8	158.9	22.9
Flywheel	32.0	157.2	23.7

*The energy-saving rate of catenary energy consumption with optimally sized OESD in reference to the scenario without OESD.

Table 8.3: The volume, capital cost, maximum power and mass of the optimally sized OESDs for case without constraints of capital cost and volume

	OESD type		
	Supercapacitor	Li-ion battery	Flywheel
Volume (m^3)	0.5	2.8	0.6
Capital cost (k$)	11.6	1385.8	96.1
Maximum power (kW)	877.5	419.9	508.2
Mass (t)	0.32	1.87	0.17

shown in Table 8.3 also bring some valuable information about each OESD under this optimal capacity. For example, among the three types the Li-ion battery is the heaviest and the most space-consuming, which needs much space for installation even though its division into several sets, and flywheel is the lightest and supercapacitor is the most space-efficient in this case. Though the optimal capacity of Li-ion battery is the highest, maximum power of it is still the lowest among the three types, showing the low power support which is the commonly recognised drawback of the chemical battery. The capital cost for Li-ion battery becomes the most significant factor with an extremely high value of 1385.8 k$, which is also impractical in the real operation. In short, adoption of Li-ion battery demands higher economic cost and larger space to achieve the optimal capacity.

From Figure 8.4, it can also be seen that the discharge/charge curves for these three types of OESDs are also different. The maximum gradient of SOE curves for supercapacitor is much higher than the other 2 types of OESDs, depicting a much steeper curves than the other. The SOE curve for Li-ion battery is enlarged for a clear view in the figure since the change of it is hard to be observed. The maximum increment or decrement of SOE in each $\Delta d_{i,j}$, notated as $\Delta SOE_{i,j,max}$, is determined by the equation (8.15).

$$\Delta SOE_{i,j,max} = \overline{P_o} \Delta t_{i,j} / E_{cap} \tag{8.15}$$

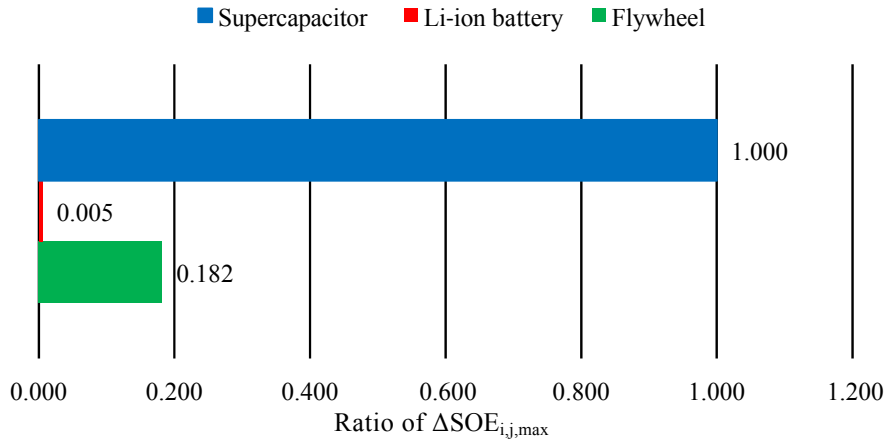

Figure 8.5: The ratio among $\Delta SOE_{i,j,max}$ of each type of OESD regarding supercapacitor as base value for the case without the constraints of capital cost and volume

Table 8.4: The energy-saving rate with respect to the capacity, volume and capital cost of optimally sized OESDs for case without constraints of capital cost and volume

	OESD type		
	Supercapacitor	Li-ion battery	Flywheel
Energy-saving rate per unit capacity (%/kWh)	2.35	0.02	0.74
Energy-saving rate per unit capital cost (%/k$)	2.05	0.02	0.25
Energy-saving rate per unit volume (%/m^3)	47.07	8.04	37.01

From Table 8.3 it is seen that supercapacitor is with the highest discharge/charge power, flywheel ranks the second and Li-ion battery is with the lowest maximum power while the trend for their respective capacity is exactly contrary. As a result, this leads to the different $\Delta SOE_{i,j,max}$ when different type of OESD is investigated. If the $\Delta SOE_{i,j,max}$ for supercapacitor is regarded as the base value, the ratio of $\Delta SOE_{i,j,max}$ for supercapacitor, Li-ion battery and flywheel can be obtained as 1: 0.005: 0.182, as shown in Figure 8.5, clarifying the reason for the significantly different discharging/charging curve for each type of OESD. It also should be noted that due to the low power density of the Li-ion battery, the obtained optimal solution results in a relatively high maximum power for it while with a extremely large capacity. In this case, though using Li-ion battery can bring the similar energy-saving effect as the supercapacitor and flywheel do, there is still more than 90% of the capacity of it not being used.

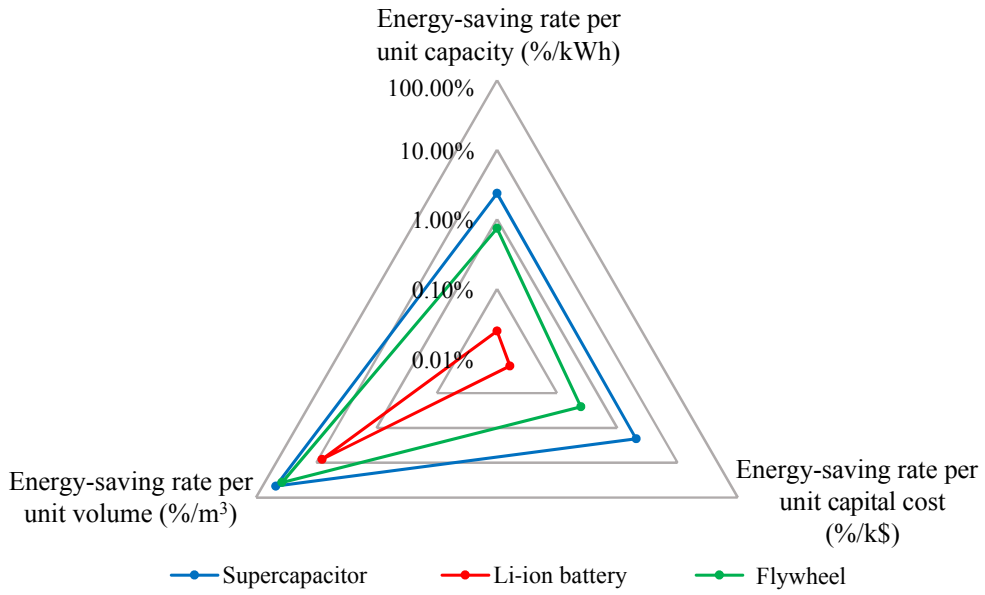

Figure 8.6: The radar chart for comparison among the energy saving rate with respect to the optimal capacity, volume and capital cost for the case without constraints of capital cost and volume

Since the optimal capacity, volume and capital cost of three types of OESD are obtained, the energy-saving efficiency from the industry viewpoint related to these three important factors can be studied. Here three terms, energy-saving rate per unit capacity in %/kWh, energy-saving rate per unit capital cost in %/k$ and energy-saving rate per unit volume in %/m^3, are proposed and obtained, as shown in Table 8.4. Additionally, the comparison among each value of them are made into a radar chart illustrated in Figure 8.6. From the figure, it can be observed that supercapacitor is the most efficient in reduction of energy consumption from substation in terms of the above three aspects while Li-ion battery seems to be with low efficiency to save energy consumption. In terms of energy-saving rate per unit volume, performance of flywheel is close to that of supercapacitor.

8.3.2 With the Constraints of Capital Cost and Volume

In Section 8.3.1, it can be found that without the constraint of capital cost ad volume, Li-ion battery, supercapacitor and flywheel can bring a very similar energy-saving effect through the optimised capacity. However, this also leads to an impractical capital cost for Li-ion battery and even for flywheel who reaches 96.1 k$. In addition, the resulted volume for Li-ion battery is also with large value. In real business, railway operators

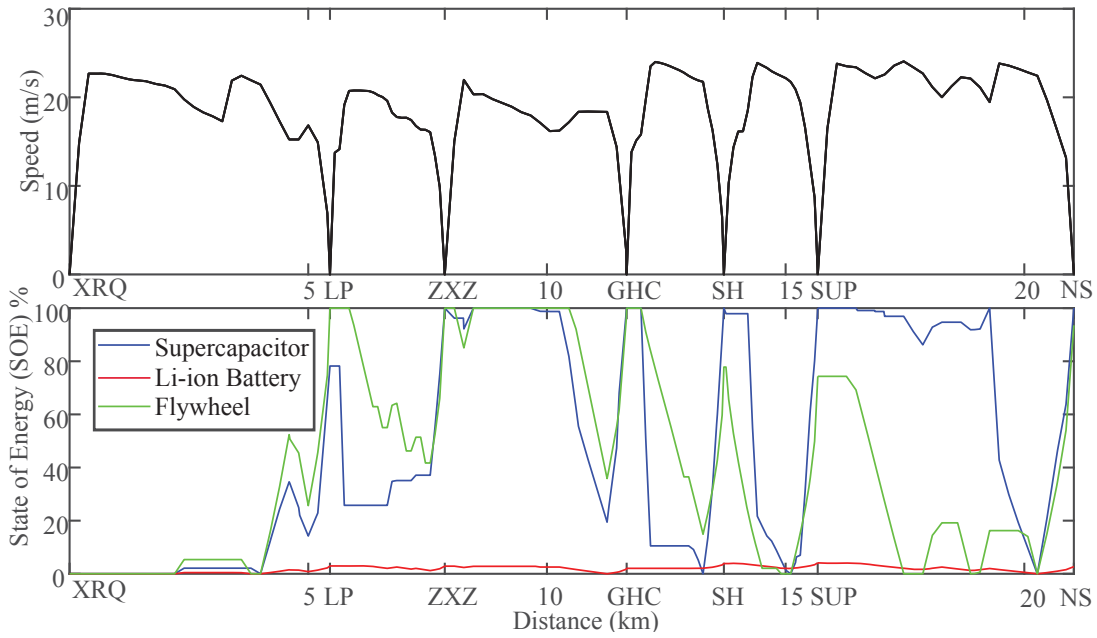

Figure 8.7: The reference train speed trajectories and discharging/charging curves for different optimally sized OESD with upper limit of capital cost being 10 k$

Table 8.5: Optimisation results of capacity, energy saving rate, volume, capital cost, maximum power and mass for different OESDs with an upper limit of capital cost of 10 k$

	OESD type		
	Supercapacitor	Li-ion battery	Flywheel
Optimal capacity (kWh)	8.7	6.7	3.3
Energy-saving rate (%)	22.5	0.5	8.3
Volume (m^3)	0.44	0.02	0.07
Capital cost (k$)	10	10	9.9
Maximum power (kW)	758.7	3.0	52.9
Mass (t)	0.28	0.01	0.02

need to take into account the company budget and left space on the rail vehicles when applying OESD, and normally different companies have different requirements. As a result, in this section the upper limits of the cost being 10 k$ and volume being 0.25 m^3 are selected firstly for showing the practicality and flexibility of the proposed method. This case study with the constraints of capital cost and volume shows that the proposed method can meet different needs of varies of operators with different investment and installation requirements.

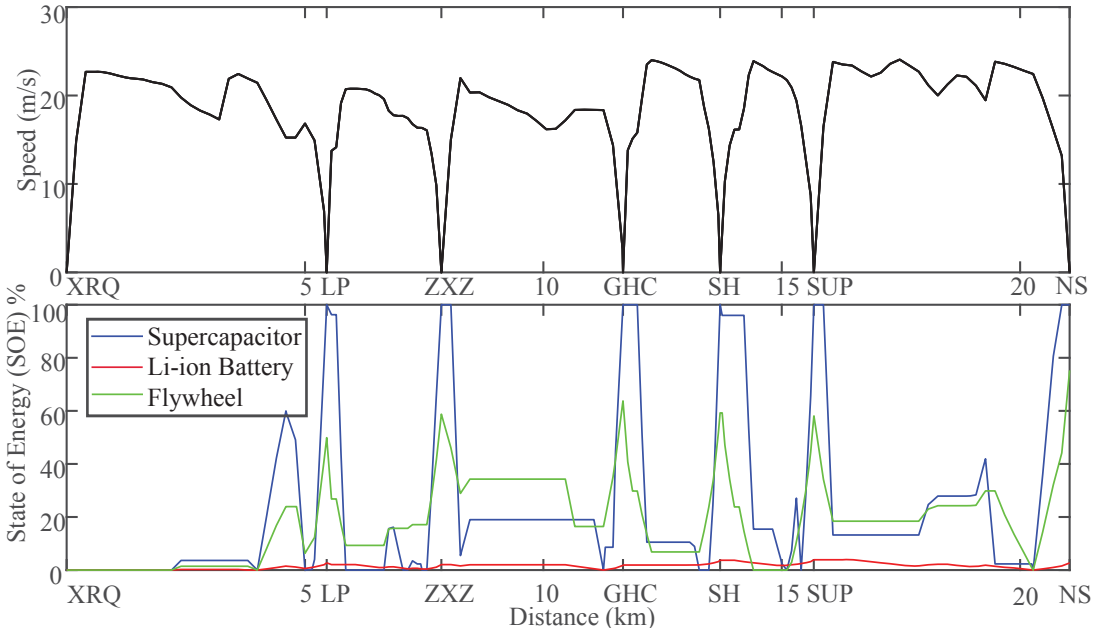

Figure 8.8: The reference train speed trajectories and discharging/charging curves for different optimally sized OESD with upper limit of volume being 0.25 m^3

Table 8.6: Optimisation results of capacity, energy saving rate, volume, capital cost, maximum power and mass for different OESDs with an upper limit of volume of 0.25 m^3

	OESD type		
	Supercapacitor	Li-ion battery	Flywheel
Optimal capacity (kWh)	5.0	81.3	12.5
Energy-saving rate (%)	16.9	5.8	19.9
Volume (m^3)	0.25	0.25	0.25
Capital cost (k$)	5.8	121.9	37.5
Maximum power (kW)	436.5	36.9	198.4
Mass (t)	0.16	0.16	0.07

The optimal results for both scenarios are tabulated in Table 8.5 and Table 8.6, and the discharge/charge curves are demonstrated in Figure 8.7 and Figure 8.8. It can be observed that when the upper limit of capital cost is set to be 10 k$, the most energy-saving OESD is supercapacitor as it has the highest optimal capacity and maximum discharging/charging power in this case. Li-ion battery sees the highest energy consumption from substation as well as with the low maximum power which is only 3.0 kW. Flywheel is with least optimal capacity since it is more expensive than

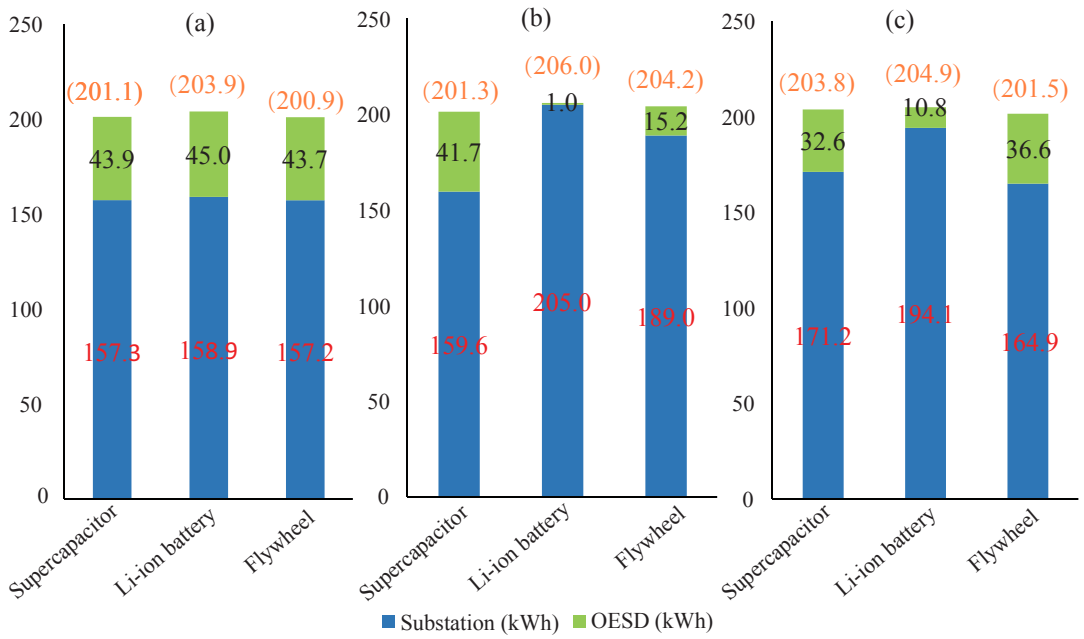

Figure 8.9: Traction energy supply split between substation and OESD in the optimisation results under different constraints. (a) No constraints of capital cost and volume imposed; (b) With a capital cost upper limit of 10 k$; (c) With a volume upper limit of 0.25 m^3 (The orange value in parentheses is the total traction energy consumption which is the sum of catenary energy consumption and discharged energy from OESD

other. When the upper limit of volume is 0.25 m^3, the most energy-saving OESD becomes flywheel which has the largest optimal capacity. Though Li-ion battery is still with the worst energy-saving effect, the optimal capacity is highest among the three, which indicates a high energy density of its kind. Supercapacitor is with the least optimal capacity, implying its low energy density with respect to the volume constraint. Similar to the case without the constraint of capital cost and volume, the change rate of discharging/charging curves for Li-ion battery in both scenarios here are not significant due to the relatively low maximum power and capacity.

The energy supply split for each type of OESD is shown in Figure 8.9, in which the scenarios investigated above are all compared and contrasted. From the figure, it is shown that in different scenario, the energy supply split varies. For the scenario without the constraints of capital cost and volume (Figure 8.9-(a)), it can be found that though the train equipped with Li-ion battery uses the most energy consumption rom substation, Li-ion battery supplies the most energy. From Figure 8.9-(b) for scenario with an upper limit of capital cost being 10 k$, it is clear that supercapacitor supplies

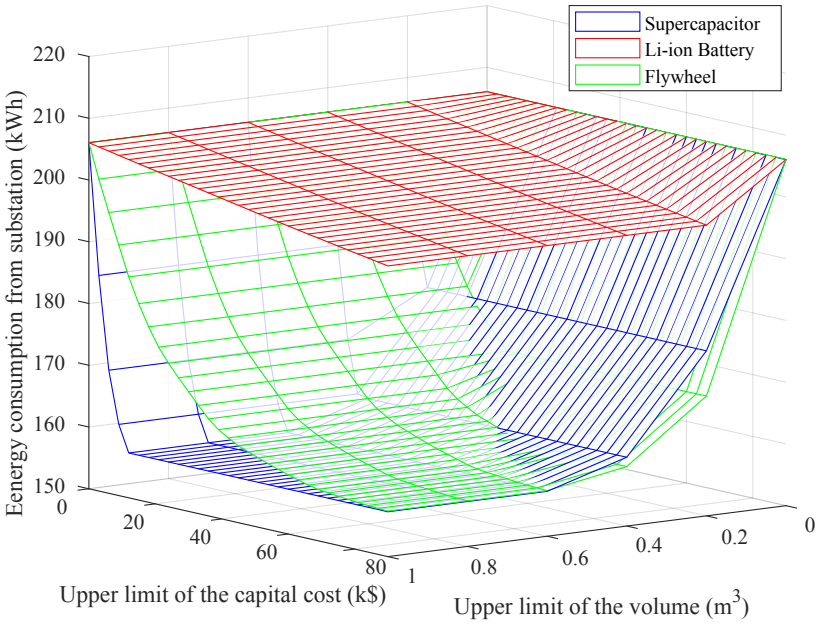

Figure 8.10: The energy consumption from substation for different types of OESD under varying upper limits of capital cost and volume

the most energy to train while Li-ion battery hardly support the train due to the low discharging/charging power. The performance of flywheel is also influenced passively by its low capacity. When given the upper limit of volume at 0.25 m^3, flywheel brings the most energy-saving effect and supply the most energy for traction, as shown in Figure 8.9-(c). The orange values in parentheses are their corresponding total traction energy consumption and it can be seen that in terms of one specific type of OESD, the more energy supplied by OESD, the less total traction energy consumed. This is due to the higher efficiency of using the energy supplied by OESD than using the energy from substation, which also cuts the energy consumption in turn.

Based on the proposed model, Figure 8.10 depicts further on the relationship between the energy consumption from substation and capital cost and space of OESD, which are industry-concerned factors. In Figure 8.10, the range of the upper limit for capital cost is from 0 to 90 k$ with an increment step of 3 k$ and the range of the upper limit for volume is from 0 m^3 to 1 m^3 with an increment step of 0.2 m^3. From the figure, it should be noted that Li-ion battery always gives the highest energy consumption from substation among the three. As for the supercapacitor, the energy consumption from substation for it is the most sensitive with respect to the upper limit of capital cost among the three since it can be noted from the figure that the energy consumption

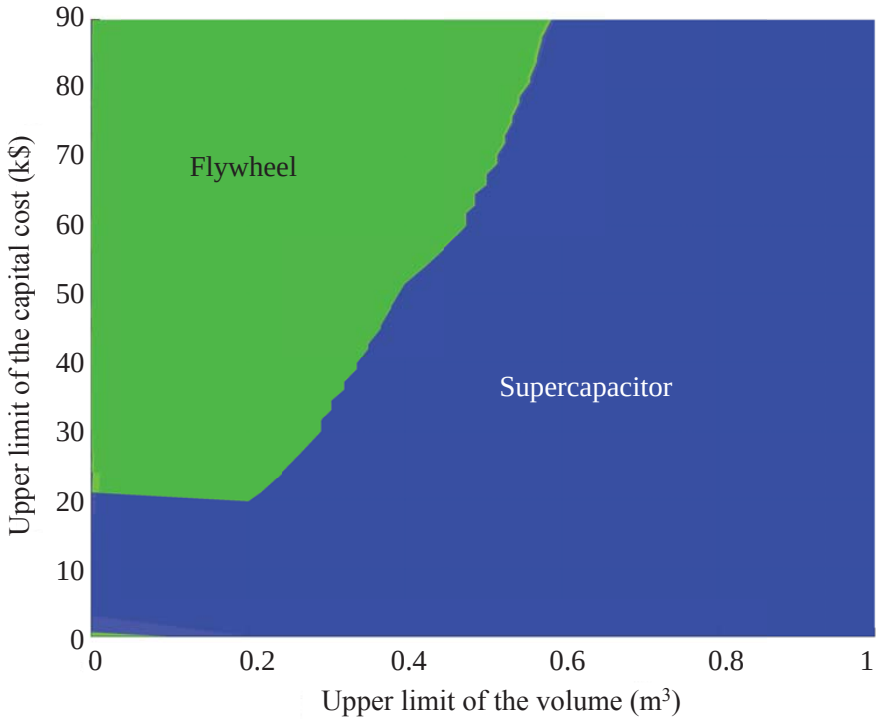

Figure 8.11: The different dominated area of minimum energy consumption from substation with respect to upper limits of volume and capital cost (The dominated area of both supercapacitor and flywheel is demonstrated on a projected plane of Figure 8.10 from the top with x-axis being the volume and y-axis being the capacity cost. By dominating area, it means that adoption of the specific type of OESD will consume the minimum energy consumption from substation among the three types)

from substation of it drops faster than others when upper limit of capital cost rises. The energy consumption from substation for flywheel is more sensitive and in some space it brings the least energy consumption. The dominated area for minimum energy consumption from substation of supercapacitor and flywheel with respect to capital cost and volume is illustrated in Figure 8.11 which is a projected plane of Figure 8.10 from the top. It can be told that with capital cost limited below 20 k$ and volume limitation relaxed to be higher than 0.6 m^3, supercapacitor with optimised capacity brings the minimum energy consumption from substation. When the upper limit of volume is set below 0.6 m^3 and maximum capital cost is allowed to go higher, flywheel with the optimised capacity saves the most energy consumption among the three types of OESD. This result clearly shows that when the installation room is limited, flywheel will be the better choice and if the limitation of the capital cost is tight, supercapacitor is more economic and able to achieve less energy consumption from substation. The result

provides a clear guide on how appropriate OESD can be selected for real engineering applications.

8.4 Summary

This chapter discusses the optimal sizing problem of the three popular types of energy storage, supercapacitors, flywheels and Li-ion batteries, as OESD in train operation. In Chapter 4 of this thesis, the energy consumption of train operation is found to drop firstly then increase when OESD capacity continuously increase, which also shows the existence of the optimal size of the OESD in train operation. Motivated by this finding, this chapter proposes a MILP model to optimise the capacity of the OESD to minimise the energy consumption from substation in train operation. three types of OESD, supercapacitor, Li-ion battery and flywheel, are investigated with different engineering characteristics including energy density, power density and capital cost.

From the results of the real-world case study, it is found that supercapacitor, Li-ion battery and flywheel can bring similar energy-saving effect, with a reduction rate of energy consumption from substation by 23.6%, 22.9% and 23.7% respectively, without the constraint of capital cost and volume. In cases with constraints on the capital cost and volume, it is found that the energy saving rate for Li-ion battery is significantly reduced compared with supercapacitor and flywheel. When the volume is limited below 0.6 m^3 and capital cost is allowed to be higher than 20 k$, optimally sized flywheel can bring the minimum energy consumption from substation. If the capital cost is constrained below 20 k$ while the volume can be relaxed beyond 0.6 m^3, supercapacitor with optimal capacity brings the most reduction of energy consumption. All in all, based on the proposed method, the optimal capacity of the OESD can be obtained to achieve the minimum energy consumption from substation, the industry-concerned factors that influence the reduction of energy consumption can also be studied, which reveals the impact of different types and different size of OESD on energy-saving effect in electrified railway systems.

Chapter 9

Conclusions and Future Works

9.1 Summary of the Thesis

On-Board energy storage device (OESD), as an emerging technologies utilised in modern railway systems in the few decades, has contributed much to the reduction of the energy consumption from the railway transportation, making the railway systems greener and more sustainable. When more subsystems are integrated in railway systems, it becomes important to locate the intelligent energy-saving solution by considering the cooperation of each subsystems with different engineering properties. By integrating train and OESD, this thesis proposes a series of methods to achieve intelligent train operation with OESD to reduce the energy consumption of the system from small scale (single inter-station section) operations to large scale (train network and power network) operations. In the thesis, the engineering characteristics of the train and OESD are all taken into account. General railway systems and specific real-world railway systems as case studies with multiple scenarios are all investigated in the numerical experiments of the thesis to show the effectiveness and robustness of the proposed methods.

The brief contents of each chapter are summarised as follows:

- Chapter 1 introduces the background of the research, where the current status of the carbon emission from the transportation sector, especially the railway transportation, is given followed by the introduction of the existing methods utilised to reduce energy consumption in railway systems. Moreover, the research motivation, objective and thesis outline are also presented.

- Chapter 2 gives the literature review regrading optimal train speed trajectory and timetabling, applications of different types of OESD in railway systems and the

integrated optimisation on train with OESD.

- Chapter 3 introduces the traditional energy-efficient train control model and the proposed discrete distance-based model. The utilised modelling, optimisation and simulation methods are also shown.

- Chapter 4 proposes an integrated mathematical model to optimise the train speed trajectory and OESD discharging/charging strategy in the scope of single inter-station section. MILP is applied in the chapter to find the optimal solution, based on which the influence of the OESD capacity, initial energy status and degradation on optimal train operation are presented.

- Chapter 5 firstly extends the MILP model in Chapter 4 to optimise the train speed trajectory, running time and OESD discharging/charging strategy (for both running and dwelling) in the scope of service cycles with multiple inter-station sections. Then a two-step method is proposed to solve the problem much more efficient by combining the MILP model and convex optimisation together. Beijing Yizhuang line as the case studies are given in this chapter.

- Chapter 6 proposes an agent-environment optimisation model to optimise the train speed trajectory with OESD in the scope of network considering stochastic train network and power network information. The stochastic regenerative braking energy from other trains in the network, formed as the expected parameters by using the Monte-Carlo simulation based on the MILP model in Chapter 4, can be utilised further by employing the optimised solution.

- Chapter 7 discusses the impact of the three popular types of energy storage, supercapacitors, flywheels and Li-ion batteries as OESD in train operation. A MILP model is proposed considering the dynamic power characteristics of each type of OESD, and the comparison is conducted on fully electrified railways, discontinuously electrified railways and catenary-free railways to show the difference of the energy-efficient operation strategies and the corresponding energy-saving performance.

- Chapter 8 discusses the optimal sizing problem of each type of energy storage as OESD in train operations to minimise the energy consumption. Sizing problem of the the supercapacitors, flywheels and Li-ion batteries are explored by the data-based method proposed in this chapter. Beijing Changping line as the real-world case studies are investigated in the chapter, in which the insightful comparison

of energy-saving and cost-saving performance of these three types of OESD are presented.

All in all, it can be easily observed that the main contents of the above chapters in this thesis all focus on the intelligent train operations with OESD from small scale operations to the large ones to reduce the energy consumption of the system. Finding the optimal train speed trajectory, timetable, energy management of the OESD and the optimal decision on selecting suitable type of energy storage for further energy saving form the skeleton of the whole thesis.

9.2 Main Conclusions and Findings

In thesis, a series of problems with train operation with OESD are explored by applying multiple mathematical modelling, optimisation and simulation methods together. Based on these approaches, the intelligent management of the train and OESD to achieve the minimum energy consumption can be conducted, the conclusions and findings of which are summarised as follows:

- **Intelligent Train Operation with OESD in an Inter-Station Section:** An integrated mathematical model is established based on MILP, where the engineering properties of both the train and OESD are considered with the objective to minimise the net energy consumption.
  - **MILP Model:** The relationship between the operation of the train and OESD in single inter-station section is formulated into the linear form by applying several approximating techniques, e.g., SOS2 and logic models. Based on the established linear relationship, the real-word and complex on-route constraints all can be involved in the model, and the case study for a general inter-station section show a 11.6% energy-saving rate compared with the train without OESD, presenting both the energy-saving potential of the OESD as well as the effectiveness of the proposed model.
  - **Influence of OESD Size:** Based on the proposed model, it is found that with the increase of OESD capacity (size), the net energy consumption decreases with a gradually-reduced changing rate. This implies that when the OESD capacity reaches a certain value, the net energy consumption also reaches the minimum value that cannot be reduced anymore. If the capacity of the OESD increases continually, the net energy consumption even

raises slightly due to the increase of the total mass resulted from the heavier OESD. This clearly indicates that with the given running time and travel distance, the optimal OESD capacity which brings the minimum net energy consumption is unique.

- **Influence of OESD Initial SOE:** Based on the proposed model, it is found that Excessive initial SOE is observed to reduce OESD's capability of recapturing regenerative energy due to a reduction of the rechargeable room during the braking operation of the train. It implies that there is an unique optimal initial SOE value and a corresponding optimal train speed trajectory which is able to jointly achieve the minimum net energy consumption in a specific inter-station journey.
- **Influence of OESD Degradation:** It is found that when the OESD suffers degradation, reducing discharging frequency is preferred rather than reducing charging one as the energy can still be recovered through charging process to achieve the optimal energy-saving operation although with some extra cost caused by degradation. A trade-off between discharging and charging process should be achieved when rechargeable capacity needs to be increased through discharging. The train operation will not be the optimal energy-saving one if the initial solution is still followed. Both the train operation and discharging/charging strategy of the OESD need adjustments to make the most of the degraded device.

- **Intelligent Train Operation with OESD in a Service Cycle:** The train operation with OESD for service cycles, i.e. multiple stations, are explored, where the optimal train speed trajectory, train timetable and discharging/charging strategy of the OESD during the running and dwelling are all obtained concurrently to minimise the net energy consumption.
  - **Building Convex Optimisation Problem:** Due to the limitations of the MILP methods in solving the train operation with OESD in service cycle scope, the convex function is used to fit the relationship among minimum energy consumption, running time and OESD initial SOE (ISOE). By building this convex relationship, the train operation with OESD in the scope of service cycle is formulated into a convex optimisation problem with high computational efficiency in finding the global optimum.
  - **OESD Discharging/Charging Process At Stations:** The optimisation considering the discharging/charging strategy of the OESD at each station is

conducted, where the OESD is allowed to discharge or be charged when the train dwells at each station to adjust its energy statues i.e. SOE during the multi-station operation in a service cycle. It is found that proper adjustment of the SOE at each station brings further energy saving due to the reconfiguration of the energy supply from each supplier during the running and at station through optimising the train operation, OESD operation and running time allocation of each inter-station section concurrently.

- **Further Reduced Energy Consumption:** The general cases and real-world case based on Beijing Yizhuang line is adopted in numerical experiments, and it is found that by applying the proposed method, the net energy consumption is further reduced when compared with three other scenarios, i.e., (1) OESD fully charged at each station, (2) No management and (3) No OESD. This shows the high energy-saving potential of the concurrent optimisation on train speed trajectory, timetable and OESD discharging/charging process.

- **Intelligent Train Operation with OESD in Network:** Train operation with OESD considering the network information is studied, where the stochastic characteristics of the train network, i.e., the uncertain running time for other trains, and power network, i.e., the uncertain regenerative braking energy in the environment, are integrated into the model to reduce the energy consumed from station and maximise the utilisation of the regenerative braking energy in the network.

  - **Stochastic Train Operation Environment:** In daily operations, trains face the uncertain environment due to the stochastic events. In this thesis, the expected regenerative braking energy in the environment can be found based on the stochastic train timetable extracted from the sampled running time data by using Monte-Carlo Simulation. It can be seen that the though the timetable is stochastic, the expected value of the regenerative braking energy released into the network follows a rather stable pattern with respect to time.
  - **Change of Optimal Train Operation:** Optimal case (case with network information) and base case (case without network information) are compared in the thesis. It can be found the train speed trajectories for both situations are significantly different. For the base case, fewer fluctuation of the speed trajectory is found, and more coasting is preferred to save energy consumption.

While for the optimal case obtained in this thesis, slight acceleration with lower speed at the beginning of the journey and traction process in the middle of the journey happen frequently.

- **Further Utilisation of OESD:** In the environment with available regenerative braking energy form other trains, the OESD is further utilised to recover the energy not only from the own motor but also from the environment (other trains). By using a general 4-station railway system in 1 power supply section, it can be found that at most of the time the regenerative braking energy in the environment is expected to be fully utilised, and 68.8% of available regenerative braking energy is expected to be utilised by using the OESD and adjusting train speed trajectory following the optimal solution.

- **Explorations on Different Types of OESD:** There are usually three types of energy storage, supercapacitors, flywheels and Li-ion batteries, used in modern railway systems as wayside/stationary energy storage device or OESD. The thesis explores the impact of these three types of energy storage as OESD on train operations.

  - **Adaptive Driving Strategy with Different Types of OESD:** Supercapacitors, flywheel and Li-ion batteries as OESD are investigated by taking into account their specific dynamic discharging/charging power limits. It is found from the numerical experiments that by applying different types of OESD, the optimal train speed trajectories will change accordingly to best fit each type's specific power capability. based on the optimisation results of the 4 scenarios shown above, the technical advantages of these three types of OESD can be analysed on the average term. it can be seen that the flywheel can bring the least energy consumption from substation and net energy consumption with the highest energy-saving rate, ranging from 22.32% to 129%, and also the most cost effective for its highest energy-saving rate per k$. Though the supercapacitor and the Li-ion battery bring less energy-saving rate than the flywheel, under the same capital cost the supercapacitor can provide the highest power output in a short time while the Li-ion battery is with the largest capacity for the long-term operation. It also implies that the proper combination of them will make the most of each type of OESD, which might help reduce more energy consumption.
  - **Optimal Sizing of OESD:** Since there exists the uniqueness of optimal OESD capacity to bring the minimum energy consumption, these three

types of energy storage as OESD are investigated with consideration of two industry-concerned factors: capital cost and volume of the OESD. It can seen from the numerical experiments that supercapacitor, Li-ion battery and flywheel can bring similar energy-saving effect, with a reduction rate of energy consumption from substation by 23.6%, 22.9% and 23.7% respectively, without the constraint of capital cost and volume. In cases with constraints on the capital cost and volume, it is found that the energy saving rate for Li-ion battery is significantly reduced compared with supercapacitor and flywheel. When the volume is limited below 0.6 m^3 and capital cost is allowed to be higher than 20 k$, optimally sized flywheel can bring the minimum energy consumption from substation. If the capital cost is constrained below 20 k$ while the volume can be relaxed beyond 0.6 m^3, supercapacitor with optimal capacity brings the most reduction of energy consumption.

9.3 Future Works

With the demand of more intelligence in transportation systems operation and smart energy management to deal with the energy exhaustion issue, energy-efficient train operation and OESD applications are expected to be the key roles to help reduce the energy consumption from the railway transportation. Based on the research outcome of this thesis, some recommendations for the future works are summarised as follows:

- **Optimal Solutions with Hybrid Energy Storage Systems:** In this thesis, though three main types of the OESD, supercapacitors, flywheels and Li-ion batteries, are investigated, the combination of them in railway systems can still be studied further. The combination of different types of the energy storage as OESD is expected to bring the promising energy-saving effect as it allows full play of different types of energy storage with specific dynamic characteristics to form the mutual cooperation when supporting the train's running and recovering the energy. This might leads to the change of the optimal train operation mode as well as the deployment/management of the OESD for railway operators, which is an interesting topic with both academic and industrial values.

- **Energy Transmission Efficiency Accuracy:** Energy transmission efficiency is a very important factor which influences the energy or power split hence the optimal solutions in the real railway system. In the thesis, the values for energy transmission efficiency of the among the train, OESD, substation and regenerative

braking trains in the network are set to be the long-term empirical constant, which leads to the accuracy issue of the model to simulate to real physical systems. In fact, these efficiencies is distance-variant or status-variant in real applications. In the future, the modelling process should take into account the more accurate approximation methods or utilise more advanced tool to obtain their dynamic values.

- **Timetabling for Trains with OESD in Network**: In this thesis, only the optimisation on speed trajectory for trains with OESD considering the regenerative braking energy in the network is conducted. This leads to a suboptimum since the timetable still follows the practical one but is not the variables to be optimised. In the future, the integrated optimisation to find the optimal train speed and timetable is necessary for further utilisation of the OESD and regenerative braking energy in the environment, achieving a more intelligent energy management of the railway system.

- **The City/Region-Wide Network Optimisation:** In this thesis, the largest scale for optimisation is the train network and power network in a single railway line. It is known that the main substations in a city or region supports several traction substations of different railway lines. This indicates that the energy consumption of the railway system contains the spatial and temporal information in the whole city/region-wide train network and power network containing multiple railway lines and substations. In the future, the wider scope can be explored since the railway network or metro systems should be studied as a whole, and the cooperation of the train operation, OESD and wayside/stationary energy storage devices might be achieved, which is likely to improve further the energy efficiency of the system in larger scale and management the operation of the train, OESD or other subsystems in a higher level.

- **Smart Grid Technologies in Train Operations:** Since the OESD is regarded a container for the train to store or release the energy during the running or dwelling at stations, it also enables the train to consume or supply other subsystems in the railway system or the systems beyond to management the energy to enhance the efficiency. The more energy interaction between difference kind of energy systems can be explored, and demand response operation can also be introduced into the railway system with OESD. Also, renewable energy utilisation can also be integrated to reduce the carbon intensity of both the train network and power

network.

- **Decentralised Operation Optimisation:** In recent years, the development of the artificial intelligence in railway operation and concept of decentralisation of the train control attract the attention of the academia and industry. Trains with OESD, to some extent, can also be regarded as a special Electric Vehicle (EV) or Electric Bus running on the track. In this case, how to management the train fleet with OESDs (EV fleet) to ensure the operation with high energy efficiency and safety might be a very interesting problem in the future.

Appendix A.

Publications

Published/Accepted Journal Articles:

1. M. Feng, **C. Wu**, S. Lu and Y. Wang " Notch-based Speed Trajectory Optimisation for High-Speed Railway Automatic Train Operation," *Proceedings of the Institution of Mechanical Engineers Part F: Journal of Rail and Rapid Transit*, accepted, 2021

2. **C. Wu**, S. Lu, F. Xue, L. Jiang, M. Chen and J. Yang, "A Two-Step Method for Energy-Efficient Train Operation, Timetabling and On-Board Energy Storage Device Management," *IEEE Transactions on Transportation Electrification*, vol. 7, no. 3, pp. 1822-1833, 2021.

3. **C. Wu**, B. Xu, S. Lu, F. Xue, L. Jiang and M. Chen, "Adaptive Eco-Driving Strategy and Feasibility Analysis for Electric Trains with On-Board Energy Storage Devices," *IEEE Transactions on Transportation Electrification*, vol. 7, no. 3, pp. 1834-1848, 2021.

4. Y. Guo, C. Zhang, **C. Wu** and S, Lu, "Multiagent System-Based Near Real-time Trajectory and Microscopic Timetable Optimization for Rail Transit Network", *Journal of Transportation Engineering, Part A: Systems*, vol 147, no.2, 2020.

5. R. Miao, **C. Wu**, K. Zhu, F. Xue, Z. Tian, S. Hillmansen, C, Roberts and S. Lu, "An Integrated Optimisation Model for Neutral Section Location Planning and Energy-Efficient Train Control in Electrified Railways," *IET Renewable Power Generation*, Accepted, 2020.

6. **C. Wu**, S. Lu, F. Xue, L. Jiang and M. Chen, "Optimal Sizing of On-Board Energy Storage Devices for Electrified Railway Systems," *IEEE Transactions on Transportation Electrification*, vol. 6, no. 3, pp. 1301-1311, 2020.

7. **C. Wu**, W. Zhang, S. Lu, Z. Tan, F. Xue and J. Yang, "Train Speed Trajectory Optimization with On-Board Energy Storage Device," *IEEE Transactions on Intelligent Transportation Systems*, vol. 20, no. 11, pp. 4092-4102, 2019.

8. Z. Tan, S. Lu, K. Bao, S. Zhang, **C. Wu**, J. Yang and F. Xue "Adaptive Partial Train Speed Trajectory Optimization," *Energies*, vol. 11, no. 12, p. 3302, 2018.

Working Journal Articles:

1. **C. Wu**, S. Lu, Z. Tian, F. Xue and L. Jiang "Energy-Efficient Train Operation with Onboard Energy Storage Device considering Stochastic Regenerative Braking Energy," *under review*

2. K. Zhu, **C. Wu**, F. Xue, S. Lu and J. Yang " A Passenger-Oriented Network-Wide Timetable Optimization Method for Urban Rail Transportation Systems," *under review*

3. **C. Wu**, B. Han, S. Lu, F. Xue and L. Jiang "Carbon-Efficient Timetable Optimization for Urban Railway Systems with Renewable Energy Resource," *manuscript in preparation*

4. G. Meng, **C. Wu** and S. Lu, "Minimizing the Net Hydrogen Consumption of Fuel-Cell Trains Using an Operation-Management Co-Optimization Model," *manuscript in preparation*

Invited Magazine Article:

1. "Optimising Operations with Onboard Energy Storage", *Railway Gazette International*, Oct, 2019

Published Conference Papers:

1. B. Xu, **C. Wu**, S. Lu and F. Xue, "Virtual-Coupling Operation for High-Speed Rail based on Following-Train Speed Profile Optimization," *32nd IEEE Intelligent Vehicles Symposium (IV' 21)*, Nagoya, Japan, accepted, 2021

2. M. Feng, **C. Wu** and S. Lu, "A New Operation-Oriented Mixed Integer Linear Programming Model for Energy-Efficient Train Operations," *2020 10th International Conference on Power and Energy Systems (ICPES)*, Chengdu, China, 2020, pp. 350-355

3. K. Zhu, **C. Wu**, F. Xue, J. Yang and S. Lu, "Network-wide Timetabling for Urban Railway Network based on Complex Network Theory: A Beijing Subway Case Study," in the *39th Chinese Control Conference*, 2020, pp. 5584-5589.

4. Z. Huang, **C. Wu**, S. Lu and F. Xue, "Hydrogen Consumption Minimization for Fuel Cell Trains based on Speed Trajectory Optimization," in *4th International Conference on Electrical Engineering and Information Technologies for Rail Transportation 2019 (EITRT2019)*, 2019. (Best Paper Award)

5. **C. Wu**, S. Lu, F. Xue, L. Jiang and Gong. G, "Smart Construction for Urban Rail Transit based on Energy-Efficient Bi-Directional Vertical Alignment Optimisation," in *2nd International Conference on Sustainable Buildings and Structures (ICSBS 2019)* , 2019, pp. 163–170.

6. R. Miao, **C. Wu**, S. Lu, F. Xue, Z. Tian and S. Hillmansen, "Optimization of Neutral Section Location on High-Speed Railways with Consideration of Train Operations," in *2nd International Conference on Sustainable Buildings and Structures (ICSBS 2019)*. 2019, pp. 171–177.

7. **C. Wu**, S. Lu, F. Xue, and L. Jiang, "Integrated Train Speed Profiles Optimization Considering Signaling System and Delay," in *2018 IEEE International Conference on Intelligent Rail Transportation (ICIRT)*, 2018.

8. **C. Wu**, S. Lu, F. Xue, and L. Jiang, "Earth Potential as the Energy Storage in Rail Transit System - on a Vertical Alignment Optimization Problem," in *2018 21st International Conference on Intelligent Transportation Systems (ITSC)*, 2018, pp. 2729 - 2734.

9. **C. Wu**, S. Lu, F. Xue, L. Jiang, and J. Yang, "Optimization of Speed Profile and Energy Interaction at Stations for a Train Vehicle with On-board Energy Storage Device," in *2018 IEEE Intelligent Vehicles Symposium (IV)*, 2018, pp. 1-6.

Bibliography

[1] I. T. Forum, *ITF Transport Outlook 2019*, 2019. (Cited on page 1.)

[2] F. Birol, "The future of rail opportunities for energy and the environment, france," *International Energy Agency (IEA)*, pp. 20–22, 2019. (Cited on pages ix, 2, and 4.)

[3] R. Salvucci and J. Tattini, "Global outlook for the transport sector in energy scenarios," *Transforming Urban Mobility*, p. 21, 2019. (Cited on page 2.)

[4] UIC-IEA, "Railway handbook 2017," 2017. (Cited on pages ix, 3, and 5.)

[5] Z. Yu, Y. Bai, Q. Fu, Y. Chen, and B. Mao, "An estimation model on electricity consumption of new metro stations," *Journal of Advanced Transportation*, vol. 2020, 2020. (Cited on page 4.)

[6] G. Alberto and C. H. Gabriel, "Technologies and potential developments for energy efficiency and co2 reductions in rail systems," *International Railways Union (UIC) Spanish Railways Foundation (FFE)*, 2016. (Cited on pages ix, 5, and 7.)

[7] X. Yang, X. Li, B. Ning, and T. Tang, "A survey on energy-efficient train operation for urban rail transit," *IEEE Transactions on Intelligent Transportation Systems*, vol. 17, no. 1, pp. 2–13, 2016. (Cited on pages 7, 16, 80, and 96.)

[8] A. González-Gil, R. Palacin, and P. Batty, "Sustainable urban rail systems: Strategies and technologies for optimal management of regenerative braking energy," *Energy conversion and management*, vol. 75, pp. 374–388, 2013. (Cited on pages xix, 8, 10, 27, 28, 57, 121, 136, 146, 159, and 162.)

[9] H. Douglas, C. Roberts, S. Hillmansen, and F. Schmid, "An assessment of available measures to reduce traction energy use in railway networks," *Energy Conversion and Management*, vol. 106, pp. 1149–1165, 2015. (Cited on page 10.)

[10] N. Ghaviha, J. Campillo, M. Bohlin, and E. Dahlquist, "Review of application of energy storage devices in railway transportation," *Energy Procedia*, vol. 105, pp. 4561 – 4568, 2017, 8th International Conference on Applied Energy, ICAE2016, 8-11 October 2016, Beijing, China. (Cited on pages 10, 16, 49, and 57.)

[11] T. Ratniyomchai, S. Hillmansen, and P. Tricoli, "Recent developments and applications of energy storage devices in electrified railways," no. September 2013, pp. 9–20, 2014. (Cited on pages 10, 29, 30, and 159.)

[12] G. M. Scheepmaker, R. M. Goverde, and L. G. Kroon, "Review of energy-efficient train control and timetabling," *European Journal of Operational Research*, vol. 257, no. 2, pp. 355–376, 2017. (Cited on pages 16 and 59.)

[13] G. Graber, V. Calderaro, V. Galdi, A. Piccolo, R. Lamedica, and A. Ruvio, "Techno-economic sizing of auxiliary-battery-based substations in DC railway systems," *IEEE Transactions on Transportation Electrification*, vol. 4, no. 2, pp. 616–625, 2018. (Cited on pages 16 and 159.)

[14] K. Ichikawa, "Application of optimization theory for bounded state variable problems to the operation of train," *Bulletin of Japan Society of Mechanical Engineers*, vol. 11, no. 47, pp. 857–865, 1968. (Cited on page 17.)

[15] V. Maksimov, "Optimal control of automatic subway trains," *Proceedings of Moscow Railway Engineering Institute*, vol. 388, pp. 103–114, 1971. (Cited on page 17.)

[16] H. Strobel and P. Horn, "On energy-optimum control of train movement with phase constraints," *Electric, Informatics and Energy Technique Journal*, vol. 6, pp. 304–308, 1973. (Cited on page 17.)

[17] I. Milroy, "Aspects of automatic train control," PhD thesis, Loughborough University, 1980. (Cited on pages 17 and 35.)

[18] I. Golovitcher, "An analytical method for optimum train control computation," *Izvestiya Vuzov Seriya Electrome Chanica*, vol. 3, pp. 59–66, 1986. (Cited on page 17.)

[19] P. Howlett, "An optimal strategy for the control of a train," *ANZIAM Journal (formerly J. Australian Math. Soc. Series B)*, vol. 31, pp. 454–471, 1990. (Cited on page 17.)

[20] J. Cheng and P. Howlett, "Application of critical velocities to the minimisation of fuel consumption in the control of trains," *Automatica*, vol. 28, no. 1, pp. 165 – 169, 1992. (Cited on page 17.)

[21] ——, "A note on the calculation of optimal strategies for the minimization of fuel consumption in the control of trains," *IEEE Transactions on Automatic Control*, vol. 38, no. 11, pp. 1730–1734, Nov 1993. (Cited on page 17.)

[22] P. Howlett and P. Pudney, *Energy efficient train control*, ser. Advances in Industrial Control, M. Grimble and M. Johnson, Eds. Springer, 1995. (Cited on pages 17 and 35.)

[23] P. Howlett, "Optimal strategies for the control of a train," *Automatica*, vol. 32, no. 4, pp. 519–532, 1996. (Cited on page 17.)

[24] P. G. Howlett and J. Cheng, "Optimal driving strategies for a train on a track with continuously varying gradient," *The Journal of the Australian Mathematical Society. Series B. Applied Mathematics*, vol. 38, no. 3, p. 388–410, 1997. (Cited on page 17.)

[25] J. Cheng, Y. Davydova, P. Howlett, and P. Pudney, "Optimal driving strategies for a train journey with non-zero track gradient and speed limits," *IMA Journal of Management Mathematics*, vol. 10, no. 2, pp. 89–115, 1999. (Cited on page 17.)

[26] P. Howlett, "The optimal control of a train," *Annals of Operations Research*, vol. 98, no. 1-4, pp. 65–87, 2000. (Cited on pages 17 and 20.)

[27] E. Khmelnitsky, "On an optimal control problem of train operation," *IEEE transactions on automatic control*, vol. 45, no. 7, pp. 1257–1266, 2000. (Cited on pages 17, 21, and 36.)

[28] R. R. Liu and I. M. Golovitcher, "Energy-efficient operation of rail vehicles," *Transportation Research Part A: Policy and Practice*, vol. 37, no. 10, pp. 917–932, 2003. (Cited on pages 17 and 21.)

[29] P. Howlett, P. Pudney, and X. Vu, "Local energy minimization in optimal train control," *Automatica*, vol. 45, no. 11, pp. 2692 – 2698, 2009. (Cited on page 17.)

[30] Z. Liang, Q. Wang, and X. Lin, "Energy-efficient handling of electric multiple unit based on maximum principle," in *Control Conference (CCC), 2014 33rd Chinese*. IEEE, 2014, pp. 3415–3422. (Cited on pages 17 and 21.)

[31] A. R. Albrecht, P. G. Howlett, P. J. Pudney, and X. Vu, "Energy-efficiency train control: From local convexity to global optimization and uniqueness," *Automatica*, vol. 49, pp. 3072–3078, 2013. (Cited on page 17.)

[32] A. Albrecht, P. Howlett, P. Pudney, V. Xuan, and P. Zhou, "The key principles of optimal train control—part 1: Formulation of the model, strategies of optimal type, evolutionary lines, location of optimal switching points," *Transportation Research Part B: Methodological*, vol. 94, pp. 482–508, 2016. (Cited on pages 17 and 21.)

[33] ——, "The key principles of optimal train control—part 2: The key principles of optimal train control—part 2: Existence of an optimal strategy, the local energy minimization principle, uniqueness, computational techniques," *Transportation Research Part B: Methodological*, vol. 94, no. 2, pp. 509–538, 2016. (Cited on pages 17 and 21.)

[34] Y. Wang, B. D. Schutter, T. J. van den Boom, and B. Ning, "Optimal trajectory planning for trains – a pseudospectral method and a mixed integer linear programming approach," *Transportation Research Part C: Emerging Technologies*, vol. 29, pp. 97 – 114, 2013. (Cited on pages 18, 21, and 157.)

[35] G. M. Scheepmaker and R. M. P. Goverde, "Energy-efficient train control including regenerative braking with catenary efficiency," in *2016 IEEE International Conference on Intelligent Rail Transportation*, 2016, pp. 116–122. (Cited on pages 18 and 121.)

[36] P. Wang and R. M. Goverde, "Multiple-phase train trajectory optimization with signalling and operational constraints," *Transportation Research Part C: Emerging Technologies*, vol. 69, pp. 255 – 275, 2016. (Cited on pages 18 and 21.)

[37] ——, "Multi-train trajectory optimization for energy efficiency and delay recovery on single-track railway lines," *Transportation Research Part B: Methodological*, vol. 105, pp. 340 – 361, 2017. (Cited on pages 18 and 22.)

[38] H. Ye and R. Liu, "Nonlinear programming methods based on closed-form expressions for optimal train control," *Transportation Research Part C: Emerging Technologies*, vol. 82, pp. 102–123, 2017. (Cited on page 18.)

[39] T. H. Cormen, C. E. Leiserson, R. L. Rivest, and C. Stein, *Introduction to algorithms*, 3rd ed. Massachusetts Institute of Technology Press, 2009. (Cited on page 18.)

[40] Y. V. Bocharnikov, A. M. Tobias, C. Roberts, S. Hillmansen, and C. J. Goodman, "Optimal driving strategy for traction energy saving on dc suburban railways," *IET Electric Power Applications*, vol. 1, no. 5, pp. 675–682, Sept 2007. (Cited on pages 19 and 21.)

[41] X. Li and H. K. Lo, "An energy-efficient scheduling and speed control approach for metro rail operations," *Transportation Research Part B: Methodological*, vol. 64, no. Supplement C, pp. 73 – 89, 2014. (Cited on pages 19 and 26.)

[42] N. Zhao, C. Roberts, S. Hillmansen, and G. Nicholson, "A multiple train trajectory optimization to minimize energy consumption and delay," *IEEE Transactions on Intelligent Transportation Systems*, vol. 16, no. 5, pp. 2363–2372, 2015. (Cited on pages 19 and 21.)

[43] F. Liu, J. Xun, and N. Bin, "An optimization method for train driving trajectory in urban rail systems," in *Chinese Association of Automation (YAC), Youth Academic Annual Conference of*. IEEE, 2016, pp. 413–418. (Cited on pages 19 and 21.)

[44] H. A. Hamid, G. L. Nicholson, H. Douglas, N. Zhao, and C. Roberts, "Investigation into train positioning systems for saving energy with optimised train trajectories," in *Intelligent Rail Transportation (ICIRT), 2016 IEEE International Conference on*. IEEE, 2016, pp. 460–468. (Cited on page 19.)

[45] X. Yang, A. Chen, B. Ning, and T. Tang, "A stochastic model for the integrated optimization on metro timetable and speed profile with uncertain train mass," *Transportation Research Part B: Methodological*, vol. 91, pp. 424 – 445, 2016. (Cited on pages 19 and 98.)

[46] N. Zhao, C. Roberts, S. Hillmansen, Z. Tian, P. Weston, and L. Chen, "An integrated metro operation optimization to minimize energy consumption," *Transportation Research Part C: Emerging Technologies*, vol. 75, pp. 168–182, 2017, integrated optimization between timetables and inter-station run. (Cited on page 19.)

[47] Z. Tian, P. Weston, N. Zhao, S. Hillmansen, C. Roberts, and L. Chen, "System energy optimisation strategies for metros with regeneration," *Transportation Research Part C: Emerging Technologies*, vol. 75, pp. 120–135, 2017. (Cited on pages 19, 23, and 24.)

[48] S. Lu, S. Hillmansen, T. K. Ho, and C. Roberts, "Single-train trajectory optimization," *IEEE Transactions on Intelligent Transportation Systems*, vol. 14, no. 2, pp. 743–750, 2013. (Cited on pages 19 and 21.)

[49] L. Zhou, L. C. Tong, J. Chen, J. Tang, and X. Zhou, "Joint optimization of high-speed train timetables and speed profiles: A unified modeling approach using space-time-speed grid networks," *Transportation Research Part B: Methodological*, vol. 97, pp. 157 – 181, 2017. (Cited on pages 20 and 26.)

[50] X. Li and H. K. Lo, "Energy minimization in dynamic train scheduling and control for metro rail operations," *Transportation Research Part B: Methodological*, vol. 70, no. Supplement C, pp. 269 – 284, 2014. (Cited on pages 20 and 26.)

[51] J. Yin, T. Tang, L. Yang, Z. Gao, and B. Ran, "Energy-efficient metro train rescheduling with uncertain time-variant passenger demands: An approximate dynamic programming approach," *Transportation Research Part B: Methodological*, vol. 91, pp. 178 – 210, 2016. (Cited on page 20.)

[52] J. T. Haahr, D. Pisinger, and M. Sabbaghian, "A dynamic programming approach for optimizing train speed profiles with speed restrictions and passage points," *Transportation Research Part B: Methodological*, vol. 99, pp. 167 – 182, 2017. (Cited on pages 20 and 21.)

[53] S. Lu, P. Weston, S. Hillmansen, H. B. Gooi, and C. Roberts, "Increasing the regenerative braking energy for railway vehicles," *IEEE Transactions on Intelligent Transportation Systems*, vol. 15, no. 6, pp. 2506–2515, 2014. (Cited on pages 20 and 21.)

[54] S. Lu, P. Weston, and N. Zhao, "Maximise the regenerative braking energy using linear programming," in *Intelligent Transportation Systems (ITSC), 2014 IEEE 17th International Conference on*. IEEE, 2014, pp. 2499–2504. (Cited on page 20.)

[55] S. Lu, M. Q. Wang, P. Weston, S. Chen, and J. Yang, "Partial train speed trajectory optimization using mixed-integer linear programming," *IEEE Transactions on*

Intelligent Transportation Systems, vol. 17, no. 10, pp. 2911–2920, 2016. (Cited on pages 20 and 21.)

[56] Z. Tan, S. Lu, F. Xue, and K. Bao, "A Speed Trajectory Optimization Model for Rail Vehicles Using Mixed Integer Linear Pragramming," *2017 IEEE 20th International Conference on Intelligent Transportation Systems (ITSC)*, pp. 1–6, 2017. (Cited on page 20.)

[57] X. Yang, A. Chen, X. Li, B. Ning, and T. Tang, "An energy-efficient scheduling approach to improve the utilization of regenerative energy for metro systems," *Transportation Research Part C: Emerging Technologies*, vol. 57, pp. 13–29, 2015. (Cited on pages xii, 22, 23, 24, and 105.)

[58] X. Xu, K. Li, and X. Li, "A multi-objective subway timetable optimization approach with minimum passenger time and energy consumption," *Journal of Advanced Transportation*, vol. 50, no. 1, pp. 69–95, 2016. (Cited on pages 22 and 24.)

[59] S. Binder, Y. Maknoon, and M. Bierlaire, "The multi-objective railway timetable rescheduling problem," *Transportation Research Part C: Emerging Technologies*, vol. 78, pp. 78–94, 2017. (Cited on pages 22 and 25.)

[60] J. Yin, L. Yang, T. Tang, Z. Gao, and B. Ran, "Dynamic passenger demand oriented metro train scheduling with energy-efficiency and waiting time minimization: Mixed-integer linear programming approaches," *Transportation Research Part B: Methodological*, vol. 97, pp. 182–213, Mar. 2017. (Cited on pages 22 and 24.)

[61] H. Sun, J. Wu, H. Ma, X. Yang, and Z. Gao, "A Bi-Objective Timetable Optimization Model for Urban Rail Transit Based on the Time-Dependent Passenger Volume," *IEEE Transactions on Intelligent Transportation Systems*, vol. 20, no. 2, pp. 604–615, Feb. 2019. (Cited on pages 22 and 24.)

[62] P. Mo, L. Yang, Y. Wang, and J. Qi, "A flexible metro train scheduling approach to minimize energy cost and passenger waiting time," *Computers & Industrial Engineering*, vol. 132, pp. 412–432, 2019. (Cited on pages 22 and 24.)

[63] H. Yeran, L. Yang, T. Tan, Z. Gao, and F. Cao, "Joint train scheduling optimization with service quality and energy efficiency in urban rail transit networks," *Energy*, vol. 138, no. 2, pp. 1124–1147, 2017. (Cited on pages 23 and 25.)

[64] X. Yang, J. Wu, H. Sun, Z. Gao, H. Yin, and Y. Qu, "Performance improvement of energy consumption, passenger time and robustness in metro systems: A multi-objective timetable optimization approach," *Computers & Industrial Engineering*, vol. 137, p. 106076, 2019. (Cited on pages 23 and 25.)

[65] J. Liao, F. Zhang, S. Zhang, G. Yang, and C. Gong, "Energy-saving optimization strategy of multi-train metro timetable based on dual decision variables: A case study of Shanghai Metro line one," *Journal of Rail Transport Planning & Management*, vol. 17, p. 100234, 2021. (Cited on pages 23 and 25.)

[66] H. Liu, M. Zhou, X. Guo, Z. Zhang, B. Ning, and T. Tang, "Timetable optimization for regenerative energy utilization in subway systems," *IEEE Transactions on Intelligent Transportation Systems*, vol. 20, no. 9, pp. 3247–3257, 2018. (Cited on pages 23 and 25.)

[67] H. Liu, B. Ning, T. Tang, and X. Guo, "Maximize Regenerative Energy Utilization Through Timetable Optimization in a Subway System," *2018 International Conference on Intelligent Rail Transportation (ICIRT)*, pp. 1–5, 2018. (Cited on pages 23 and 25.)

[68] P. Mo, L. Yang, A. D'Ariano, J. Yin, Y. Yao, and Z. Gao, "Energy-efficient train scheduling and rolling stock circulation planning in a metro line: a linear programming approach," *IEEE Transactions on Intelligent Transportation Systems*, vol. 21, no. 9, pp. 3621–3633, 2019. (Cited on pages 23 and 25.)

[69] S. Su, X. Wang, Y. Cao, and J. Yin, "An energy-efficient train operation approach by integrating the metro timetabling and eco-driving," *IEEE Transactions on Intelligent Transportation Systems*, vol. 21, no. 10, pp. 4252–4268, 2019. (Cited on pages 23 and 25.)

[70] S. Su, X. Li, T. Tang, and Z. Gao, "A subway train timetable optimization approach based on energy-efficient operation strategy," *IEEE Transactions on Intelligent Transportation Systems*, vol. 14, no. 2, pp. 883–893, 2013. (Cited on pages 26 and 80.)

[71] P. Wang and R. M. Goverde, "Multi-train trajectory optimization for energy-efficient timetabling," *European Journal of Operational Research*, vol. 272, no. 2, pp. 621–635, 2018. (Cited on page 26.)

[72] Z. Pan, M. Chen, S. Lu, Z. Tian, and Y. Liu, "Integrated timetable optimization for minimum total energy consumption of an ac railway system," *IEEE Transactions on Vehicular Technology*, vol. 69, no. 4, pp. 3641–3653, 2020. (Cited on page 26.)

[73] F. Häggström and J. Delsing, "Iot energy storage-a forecast," *Energy Harvesting and Systems*, vol. 5, no. 3-4, pp. 43–51, 2018. (Cited on page 26.)

[74] Z. Tehrani, D. Thomas, T. Korochkina, C. Phillips, D. Lupo, S. Lehtimäki, J. O'mahony, and D. Gethin, "Large-area printed supercapacitor technology for low-cost domestic green energy storage," *Energy*, vol. 118, pp. 1313–1321, 2017. (Cited on page 27.)

[75] M. Steiner and J. Scholten, "Energy storage on board of dc fed railway vehicles pesc 2004 conference in aachen, germany," in *2004 IEEE 35th Annual Power Electronics Specialists Conference (IEEE Cat. No. 04CH37551)*, vol. 1. IEEE, 2004, pp. 666–671. (Cited on page 27.)

[76] M. Steiner, M. Klohr, and S. Pagiela, "Energy storage system with ultracaps on board of railway vehicles," in *2007 European conference on power electronics and applications*. IEEE, 2007, pp. 1–10. (Cited on page 27.)

[77] B. Maher, "Ultracapacitors provide cost and energy savings for public transportation applications," *Battery Power Product & Technology*, vol. 10, no. 6, 2006. (Cited on page 27.)

[78] J.-P. Moskowitz and J.-L. Cohuau, "Steem: Alstom and ratp experience of supercapacitors in tramway operation," in *2010 IEEE Vehicle Power and Propulsion Conference*. IEEE, 2010, pp. 1–5. (Cited on pages 27 and 29.)

[79] U. Henning, F. Thoolen, M. Lampérth, J. Berndt, A. Lohner, and N. Jänig, "Ultra low emission vehicle–transport advanced propulsion," in *7th World Congress on Railway Research*, 2006. (Cited on page 28.)

[80] M. Ogasa, "Application of energy storage technologies for electric railway vehicles—examples with hybrid electric railway vehicles," *IEEJ Transactions on Electrical and Electronic Engineering*, vol. 5, no. 3, pp. 304–311, 2010. (Cited on pages 28 and 29.)

[81] F. L. ote, "Alstom : future trends in railway transportation," *Japan Railway Transport Review*, 2005. (Cited on page 28.)

[82] A. Rufer, "Energy storage for railway systems, energy recovery and vehicle autonomy in europe," in *The 2010 International Power Electronics Conference - ECCE ASIA -*, 2010, pp. 3124–3127. (Cited on page 29.)

[83] X. Liu and K. Li, "Energy storage devices in electrified railway systems: A review," *Transportation Safety and Environment*, vol. 2, no. 3, pp. 183–201, 2020. (Cited on page 29.)

[84] M. Meinert, "New mobile energy storage system for rolling stock," in *2009 13th European Conference on Power Electronics and Applications*, 2009, pp. 1–10. (Cited on pages 29 and 30.)

[85] O. Masamichi, "Onboard storage in japanese electrified lines," in *Proceedings of 14th International Power Electronics and Motion Control Conference EPE-PEMC 2010*, 2010, pp. S7–9–S7–16. (Cited on page 29.)

[86] M. Ogasa and Y. Taguchi, "Power electronics technologies for a lithium ion battery tram," *2007 Power Conversion Conference - Nagoya*, pp. 1369–1375, 2007. (Cited on page 29.)

[87] "Merseyrail class 777 arrives in liverpool," https://www.railwaygazette.com/uk/merseyrail-class-777-arrives-in-liverpool/55686.article, accessed: 2021-04-25. (Cited on page 30.)

[88] "Guangzhou huangpu tram line 1 is fully operational," https://www.seetao.com/details/54756.html, accessed: 2021-04-25. (Cited on page 30.)

[89] M. Miyatake and K. Matsuda, "Energy saving speed and charge/discharge control of a railway vehicle with on-board energy storage by means of an optimization model," *IEEJ Transactions on Electrical and Electronic Engineering*, vol. 4, no. 6, pp. 771–778, 2009. (Cited on pages 31, 49, 50, 70, and 133.)

[90] M. Miyatake and H. Haga, "Optimization of speed profile and quick charging of a catenary free train with on-board energy storage," in *Electrical Systems for Aircraft, Railway and Ship Propulsion*, 2010, pp. 1–6. (Cited on pages 31 and 49.)

[91] T. Sato and M. Miyatake, "A method of generating energy-efficient train timetable including charging strategy for catenary-free railways with battery trains," in *Rail-Norrköping 2019. 8th International Conference on Railway Operations Modelling and Analysis (ICROMA), Norrköping, Sweden, June 17th – 20th, 2019*, no. 69, 2019, pp. 995–1010. (Cited on pages 32 and 80.)

[92] W. Kampeerawar, T. Koseki, and F. Zhou, "Efficient urban railway design integrating train scheduling, onboard energy storage, and traction power management," in *2018 International Power Electronics Conference (IPEC-Niigata 2018 -ECCE Asia)*, 2018, pp. 3257–3264. (Cited on page 32.)

[93] Y. Huang, L. Yang, T. Tang, Z. Gao, F. Cao, and K. Li, "Train speed profile optimization with on-board energy storage devices: A dynamic programming based approach," *Computers Industrial Engineering*, vol. 126, pp. 149 – 164, 2018. (Cited on pages 32, 96, 120, and 133.)

[94] N. Ghaviha, M. Bohlin, and E. Dahlquist, "Speed profile optimization of an electric train with on-board energy storage and continuous tractive effort," in *2016 international symposium on power electronics, electrical drives, automation and motion (speedam)*. IEEE, 2016, pp. 639–644. (Cited on page 32.)

[95] Z. Xiao, X. Feng, Q. Wang, and P. Sun, "Eco-driving control for hybrid electric trams on a signalised route," *IET Intelligent Transport Systems*, 2019. (Cited on pages 32 and 133.)

[96] W. J. Davis, *The tractive resistance of electric locomotives and cars*. General Electric, 1926. (Cited on page 35.)

[97] I. Asnis, A. Dmitruk, and N. Osmolovskii, "Solution of the problem of the energetically optimal control of the motion of a train by the maximum principle," *USSR Computational Mathematics and Mathematical Physics*, vol. 25, no. 6, pp. 37–44, 1985. (Cited on page 36.)

[98] J. Bisschop, "Linear programming tricks," *AIMMS-Optimization Modeling*, pp. 63–75, 2006. (Cited on pages 41 and 44.)

[99] R. Sioshansi and A. J. Conejo, *Mixed-Integer Linear Optimization*. Cham: Springer International Publishing, 2017, pp. 123–196. (Cited on page 45.)

[100] S. Boyd and L. Vandenberghe, *Convex optimization*. Cambridge university press, 2004. (Cited on page 46.)

[101] C. Z. Mooney, *Monte carlo simulation*. Sage, 1997, no. 116. (Cited on page 46.)

[102] S. Raychaudhuri, "Introduction to monte carlo simulation," in *2008 Winter Simulation Conference*, 2008, pp. 91–100. (Cited on page 46.)

[103] F. Ciccarelli, A. D. Pizzo, and D. Iannuzzi, "Improvement of energy efficiency in light railway vehicles based on power management control of wayside lithium-ion capacitor storage," *IEEE Transactions on Power Electronics*, vol. 29, no. 1, pp. 275–286, Jan 2014. (Cited on page 49.)

[104] H. Xia, H. Chen, Z. Yang, F. Lin, and B. Wang, "Optimal energy management, location and size for stationary energy storage system in a metro line based on genetic algorithm," *Energies*, vol. 8, no. 10, pp. 11 618–11 640, 2015. (Cited on page 49.)

[105] H. Kobayashi, J. Asano, T. Saito, and K. Kondo, "A power control method to save energy for wayside energy storage systems in dc-electrified railway system," *Electrical Engineering in Japan*, vol. 196, no. 2, pp. 56–66, 2016. (Cited on page 49.)

[106] M. Dominguez, A. Fernandez-Cardador, A. P. Cucala, and R. R. Pecharroman, "Energy savings in metropolitan railway substations through regenerative energy recovery and optimal design of ato speed profiles," *IEEE Transactions on Automation Science and Engineering*, vol. 9, no. 3, pp. 496–504, July 2012. (Cited on pages 49, 50, and 70.)

[107] A. M. Gee and R. W. Dunn, "Analysis of trackside flywheel energy storage in light rail systems," *IEEE Transactions on Vehicular Technology*, vol. 64, no. 9, pp. 3858–3869, Sept 2015. (Cited on page 49.)

[108] R. Takagi and T. Amano, "Optimisation of reference state-of-charge curves for the feed-forward charge/discharge control of energy storage systems on-board dc electric railway vehicles," *IET Electrical Systems in Transportation*, vol. 5, no. 1, pp. 33–42, 2015. (Cited on page 49.)

[109] M. Miyatake and H. Ko, "Optimization of train speed profile for minimum energy consumption," *IEEJ Transactions on Electrical and Electronic Engineering*, vol. 5, no. 3, pp. 263–269, 2010. (Cited on pages 49, 120, and 133.)

[110] Y. Noda and M. Miyatake, "Methodology to apply dynamic programming to the energy-efficient driving technique of lithium-ion battery trains," in *2016 International Conference on Electrical Systems for Aircraft, Railway, Ship Propulsion and Road Vehicles International Transportation Electrification Conference (ESARS-ITEC)*, Nov 2016, pp. 1–6. (Cited on page 49.)

[111] A. González-Gil, R. Palacin, P. Batty, and J. Powell, "A systems approach to reduce urban rail energy consumption," *Energy Conversion and Management*, vol. 80, pp. 509–524, 2014. (Cited on pages 57, 121, and 146.)

[112] B. Han, S. Lu, F. Xue, L. Jiang, and X. Xu, "A Three-Stage Electric Vehicle Scheduling Considering Stakeholders Economic Inconsistency and Battery Degradation," *IET Cyber-Physical Systems: Theory & Applications*, pp. 1–9, oct 2017. (Cited on page 67.)

[113] W. Kempton and J. Tomić, "Vehicle-to-grid power fundamentals: Calculating capacity and net revenue," *Journal of Power Sources*, vol. 144, no. 1, pp. 268–279, jun 2005. (Cited on page 67.)

[114] M. Miyatake, H. Haga, and S. Suzuki, "Optimal speed control of a train with onboard energy storage for minimum energy consumption in catenary free operation," *13th European Conference on Power Electronics and Applications 2009 EPE 09*, pp. 1–9, 2009. (Cited on page 96.)

[115] X. Yang, X. Li, Z. Gao, H. Wang, and T. Tang, "A cooperative scheduling model for timetable optimization in subway systems," *IEEE Transactions on Intelligent Transportation Systems*, vol. 14, no. 1, pp. 438–447, 2012. (Cited on pages xii and 105.)

[116] X. Yang, B. Ning, X. Li, and T. Tang, "A two-objective timetable optimization model in subway systems," *IEEE Transactions on Intelligent Transportation Systems*, vol. 15, no. 5, pp. 1913–1921, 2014. (Cited on pages xii, 105, and 121.)

[117] T. Huisman and R. J. Boucherie, "Running times on railway sections with heterogeneous train traffic," *Transportation Research Part B: Methodological*, vol. 35, no. 3, pp. 271–292, 2001. (Cited on page 104.)

[118] J. Lessan, L. Fu, C. Wen, P. Huang, and C. Jiang, "Stochastic model of train running time and arrival delay: a case study of wuhan–guangzhou high-speed rail," *Transportation Research Record*, vol. 2672, no. 10, pp. 215–223, 2018. (Cited on pages 104 and 108.)

[119] F. Liu, R. Xu, W. Fan, and Z. Jiang, "Data analytics approach for train timetable performance measures using automatic train supervision data," *IET Intelligent Transport Systems*, vol. 12, no. 7, pp. 568–577, 2018. (Cited on pages 104 and 108.)

[120] P. Kecman and R. M. Goverde, "Predictive modelling of running and dwell times in railway traffic," *Public Transport*, vol. 7, no. 3, pp. 295–319, 2015. (Cited on pages 104 and 108.)

[121] F. Yang, L. Lu, Y. Yang, and Y. He, "Characterization, analysis and modeling of an ultracapacitor," *World Electric Vehicle Journal*, vol. 4, no. 2, pp. 358–369, 2010. (Cited on pages xv, 134, and 137.)

[122] D. Yan, L. Lu, F. Jiang, and M. Ouyang, "Comparing the performances of different energy storage cells for hybrid electric vehicle," in *EVS28 International Electric Vehicle Symposium and Exhibition*, 2015. (Cited on pages xv, 134, and 137.)

[123] N. Erd, X. Li, and A. Binder, "Power flow simulation of flywheel energy storage systems for tramways," *Renewable Energy and Power Quality Journal*, vol. 1, no. 15, pp. 149–153, 2017. (Cited on pages xv, 134, and 138.)

[124] X. Li, N. Erd, and A. Binder, "Design and calculation of a 130 kw high-speed permanent magnet synchronous machine in flywheel energy storage systems for urban railway application," in *2017 6th International Conference on Clean Electrical Power (ICCEP)*. IEEE, 2017, pp. 452–459. (Cited on pages xv, 134, and 138.)

[125] R. F. Nelson, "Power requirements for batteries in hybrid electric vehicles," *Journal of power sources*, vol. 91, no. 1, pp. 2–26, 2000. (Cited on pages xv, 134, and 139.)

[126] Y. Cao, S. Tang, C. Li, P. Zhang, Y. Tan, Z. Zhang, and J. Li, "An optimized ev charging model considering tou price and soc curve," *IEEE Transactions on Smart Grid*, vol. 3, no. 1, pp. 388–393, 2011. (Cited on pages xv, 134, and 139.)

[127] C. Z. El-Bayeh, I. Mougharbel, M. Saad, A. Chandra, D. Asber, and S. Lefebvre, "Impact of considering variable battery power profile of electric vehicles on the distribution network," in *2018 4th International Conference on Renewable Energies for Developing Countries (REDEC)*. IEEE, 2018, pp. 1–8. (Cited on pages xv, 134, and 139.)

[128] M. Ceraolo and G. Lutzemberger, "Stationary and on-board storage systems to enhance energy and cost efficiency of tramways," *Journal of Power Sources*, vol. 264, pp. 128 – 139, 2014. (Cited on page 133.)

[129] N. Ghaviha, M. Bohlin, C. Holmberg, and E. Dahlquist, "Speed profile optimization of catenary-free electric trains with lithium-ion batteries," *Journal of Modern Transportation*, Jan 2019. (Cited on page 133.)

[130] M. Aneke and M. Wang, "Energy storage technologies and real life applications – a state of the art review," *Applied Energy*, vol. 179, pp. 350 – 377, 2016. (Cited on pages xix, 136, and 162.)

[131] S. Koohi-Fayegh and M. Rosen, "A review of energy storage types, applications and recent developments," *Journal of Energy Storage*, vol. 27, p. 101047, 2020. (Cited on pages xix, 136, and 162.)

[132] J. Silmon, "Investigating discontinuous electrification and energy storage on the northern trans-pennine route," *IET Conference Proceedings*, pp. 13–13(1), January 2010. (Cited on page 149.)

[133] RIA (Railway Industry Association), "RIA electrification cost challenge," 2019. (Cited on page 149.)

[134] Y. Wang, B. De Schutter, B. Ning, N. Groot, and T. J. J. van den Boom, "Optimal trajectory planning for trains using mixed integer linear programming," in *2011 14th International IEEE Conference on Intelligent Transportation Systems (ITSC)*, vol. 19. IEEE, oct 2011, pp. 1598–1604. (Cited on page 157.)

[135] S. X. Chen, H. B. Gooi, and M. Q. Wang, "Sizing of energy storage for microgrids," *IEEE Transactions on Smart Grid*, vol. 3, no. 1, pp. 142–151, 2012. (Cited on page 158.)

[136] S. Bahramirad, W. Reder, and A. Khodaei, "Reliability-constrained optimal sizing of energy storage system in a microgrid," *IEEE Transactions on Smart Grid*, vol. 3, no. 4, pp. 2056–2062, 2012. (Cited on page 158.)

[137] T. K. Brekken, A. Yokochi, A. Von Jouanne, Z. Z. Yen, H. M. Hapke, and D. A. Halamay, "Optimal energy storage sizing and control for wind power applications," *IEEE Transactions on Sustainable Energy*, vol. 2, no. 1, pp. 69–77, 2011. (Cited on page 158.)

[138] E. Tara, S. Shahidinejad, S. Filizadeh, and E. Bibeau, "Battery storage sizing in a retrofitted plug-in hybrid electric vehicle," *IEEE Transactions on Vehicular Technology*, vol. 59, no. 6, pp. 2786–2794, 2010. (Cited on page 158.)

[139] M. Redelbach, E. D. Özdemir, and H. E. Friedrich, "Optimizing battery sizes of plug-in hybrid and extended range electric vehicles for different user types," *Energy Policy*, vol. 73, pp. 158–168, 2014. (Cited on page 158.)

[140] X. Hu, S. J. Moura, N. Murgovski, B. Egardt, and D. Cao, "Integrated Optimization of Battery Sizing, Charging, and Power Management in Plug-In Hybrid Electric Vehicles," *IEEE Transactions on Control Systems Technology*, vol. 24, no. 3, pp. 1036–1043, 2016. (Cited on page 158.)

[141] S. De La Torre, A. J. Sánchez-Racero, J. A. Aguado, M. Reyes, and O. Martínez, "Optimal Sizing of Energy Storage for Regenerative Braking in Electric Railway Systems," *IEEE Transactions on Power Systems*, vol. 30, no. 3, pp. 1492–1500, 2015. (Cited on page 159.)

[142] A. Ovalle, J. Pouget, S. Bacha, L. Gerbaud, E. Vinot, and B. Sonier, "Energy storage sizing methodology for mass-transit direct-current wayside support: Application to French railway company case study," *Applied Energy*, vol. 230, no. September, pp. 1673–1684, 2018. (Cited on page 159.)

[143] R. Barrero, X. Tackoen, and J. Van Mierlo, "Stationary or onboard energy storage systems for energy consumption reduction in a metro network," *Proceedings of the Institution of Mechanical Engineers, Part F: Journal of Rail and Rapid Transit*, vol. 224, no. 3, pp. 207–225, 2010. (Cited on page 159.)

[144] F. Ciccarelli, D. Iannuzzi, and P. Tricoli, "Control of metro-trains equipped with onboard supercapacitors for energy saving and reduction of power peak demand," *Transportation Research Part C: Emerging Technologies*, vol. 24, pp. 36–49, 2012. (Cited on page 159.)

[145] V. I. Herrera, H. Gaztañaga, A. Milo, A. Saez-De-Ibarra, I. Etxeberria-Otadui, and T. Nieva, "Optimal Energy Management and Sizing of a Battery-Supercapacitor-Based Light Rail Vehicle with a Multiobjective Approach," *IEEE Transactions on Industry Applications*, vol. 52, no. 4, pp. 3367–3377, 2016. (Cited on page 159.)

[146] Y. Huang, X. Ma, S. Su, and T. Tang, "Optimization of train operation in multiple interstations with multi-population genetic algorithm," *Energies*, vol. 8, no. 12, pp. 14 311–14 329, 2015. (Cited on page 165.)

[147] K. Huang, J. Wu, X. Yang, Z. Gao, F. Liu, and Y. Zhu, "Discrete train speed profile optimization for urban rail transit: A data-driven model and integrated

algorithms based on machine learning," *Journal of Advanced Transportation*, vol. 2019, 2019. (Cited on page 165.)